Twin-screw Melt Granulation as alternative Granulation Strategy

Dissertation

zur

Erlangung des Doktorgrades (Dr. rer. nat.)

der

Mathematisch-Naturwissenschaftlichen Fakultät

der

Rheinischen Friedrich-Wilhelms-Universität Bonn

vorgelegt von

Kristina Elena Steffens

aus

Marburg a.d.L.

Bonn 2021

Angefertigt mit Genehmigung der Mathematisch-Naturwissenschaftlichen
Fakultät der Rheinischen Friedrich-Wilhelms-Universität Bonn

Promotionskommission:

Erstgutachter:	Prof. Dr. Karl Gerhard Wagner
Zweitgutachter:	Prof. Dr. Alf Lamprecht
Fachnaher Gutachter:	PD Dr. Christian Tränkle
Fachfremder Gutachter:	Prof. Dr. Robert Glaum

Tag der Promotion:08.06.2021
Erscheinungsjahr: 2021

Danksagung

Die vorliegende Arbeit entstand unter der Leitung von Herrn Professor Dr. Karl Gerhard Wagner am Institut für Pharmazeutische Technologie und Biopharmazie der Rheinischen Friedrich-Wilhelms-Universität Bonn.
Meinem Doktorvater Herrn Prof. Wagner danke ich für die Aufnahme in seinen Arbeitskreis und die Vergabe eines spannenden Themas im Bereich der festen Arzneiformen. Ich danke ihm für die zahlreichen konstruktiven Gespräche und seine hilfreiche und intensive Unterstützung bei der Anfertigung dieser Arbeit.

Ich danke Herrn Professor Dr. Alf Lamprecht für die Übernahme des Zweitgutachtens, sowie Herrn Dr. Christian Tränkle und Herrn Professor Dr. Robert Glaum für Ihre Bereitschaft an der Prüfungskommission teilzunehmen.

Ich danke meinen Kollegen Esther Bochmann, Bernadette Kettel, Tim Lillotte, Simone Putzke, Maryam Shetab Boushehri und Pia Steinlein für die inspirierenden Gespräche und ihre stets aufmunternden Worte. Es war schön mit Euch ein Büro zu teilen und beim Christmas Decoration Award regelmäßig den Pokal zu holen. Ich werde mich noch lange und gerne an die unsere Zeit zurückerinnern.

Kai Berkenfeld, Esther Bochmann, Veronika Hagelstein, Simone Putzke, Fabian Simons und Pia Steinlein danke ich für eine außerordentlich kulturelle und kulinarische Reise durch Spanien. Ich werde unsere großartige Tour so schnell nicht vergessen.

Meinem Arbeitskreis danke ich für die herrlichen Ausflüge, Grillabende, Karnevalspartys und die gesellige Weihnachtszeit mit Weihnachtsmarkt und Käsespätzle. Unsere gemeinsame Zeit in Bonn, wird mir noch lange in Erinnerung bleiben.

Ein herzlicher Dank gilt auch Martina Gerlitz. Vielen Dank für die warmherzigen Gespräche und, dass Du immer eine offene Tür für uns hast und uns bei allen administrativen und bürokratischen Hürden unterstützt.

Ich möchte mich auch herzlich bei Jürgen Hohmann, Alexander Ramich, Thomas Vidua und Manfred Balkow für ihre technische Unterstützung und die kleinen und großen unersetzlichen Hilfen im Institutsalltag bedanken.

Ein ganz besonderer Dank gilt Esther Bochmann für ihr fleißiges Korrekturlesen und ihren Zuspruch. Du warst mir während der Zeit eine große Stütze und hast es immer geschafft mich zu motivieren.

Meiner Familie und meinen Freunden danke ich für ihre bedingungslose Unterstützung und ihre lieben Worte, die mich immer wieder in meinem Leben angespornt haben, nicht aufzugeben und an meine mich zu glauben. Ohne Euch wäre das nicht möglich gewesen.

Meiner Familie

Was wir wissen,
ist ein Tropfen,
was wir nicht wissen,
ein Ozean

Isaac Newton

TABLE OF CONTENTS:

1 Introduction and theoretical background

1.1 Granulation

Granulation is a routine procedure, where small particles are transformed into larger agglomerates, with the aim to increase flowability, compactibility, processability, dissolution, content uniformity or to reduce dust. The word “granule” is derived from the latin word: granulatum, meaning grained, because primary particles are still visible in the granulated material. Classically granulation can be divided into wet and dry granulation processes, where no liquid is used [1].

1.1.1 Melt Granulation

Melt granulation uses a molten liquid that solidifies at room temperature to form bridges between the primary particles. The binder has to be heated near or above its melting point to ensure a low viscosity and to achieve sufficient agglomeration. As no water or organic solvents need to be removed from the process, cost intensive drying steps are avoided. It makes the process more economic and environment-friendly than wet granulation processes. Furthermore, the “amount of liquid” can be controlled more precisely, especially when the binder is added as dry powder, resulting in highly reproducible granules [1]. Moreover, the process is suitable for moisture-sensitive active pharmaceutical ingredients (APIs) and it was seen to be beneficial for their production and stability [2].

In the past, melt granulation was used for both, the production of immediate and sustained release dosage forms [3]. The release profile can be controlled via the choice of binder [4]. Classic melt granulation was performed using high shear mixers (HSM), where hydrophilic substances like polyethylene glycols (PEG), polaxamers [3,5–9] or lipophilic waxes, glycerides, fatty acids or lipophilic polymers [10–14], were used as granulation liquid.

1.1.1.1 High-shear mixers

Since the 1970s, HSM have been used in the pharmaceutical technology for blending and granulation. With the use of vacuum and microwave drying systems, single-pot systems were developed especially designed for wet granulation techniques. An impeller rotates to mix and shear the mass, mounted as a top or bottom-drive system. The chopper has a much smaller diameter and can be mounted parallel from the top or on a vertical shaft. It rotates with much higher speeds than the impeller to cut lumps into smaller fragments. HSM are very useful for the granulation of cohesive and voluminous materials. Moreover, HSM offer the possibility of cleaning-in-place (CIP). Highly potent APIs can be formulated, due to the closed design of the HSM. However, the granulation process in high-shear mixers is sensitive to changes in process and machine variables, causing challenges in scale-up [15]. The bowl of the HSM is jacketed to enable cooling and heating of the process, making this equipment also usable for melt granulation processes. Process temperatures are limited. Hence, only binders with a melting temperature between 50-90°C are suitable [1]. The heat is not only introduced by the heated jacket, it is also generated by the agitation energy and friction, reducing the heating phase to a few minutes [10]. Pellets can be produced at high impeller speed and longer massing time [16–18]. However, due to the limited ratio of cooling transfer into the product, the long cooling phase to reduce product temperature results in long process times. Using an air-stripping system, cooling times can be shorten [1]. Nonetheless, it still may take hours to cool down the product strongly dependent on the batch-size. The following variables can be used to control the melt granulation process using high-shear mixers:

Process variables:

- Impeller rotation speed
- Chopper rotation speed
- Fill level (Load of the mixer)
- Temperature
- Processing time

1.1.1.2 Twin-screw-extruders

In recent years, screw extruders are gaining more and more attention. They consist of either one or two screws operating within a barrel. In the case of twin-screw extruders, screws can be either co- or counter-rotating, whereby, due to their mixing efficiency, co-rotating twin-screw extruders are the most commonly used type in the pharmaceutical field. In contrast to the classic melt extrusion process, the die at the end of the extruder is removed in the granulation processes to avoid unnecessary densification of the granules and further down-stream steps like milling [19,20]. This setup is also known as twin screw granulator (TSG).

Recently, it has been shown that the mechanisms of granule formation (immersion or distribution) underlying the melt granulation process, which were originally postulated for HSM (Fig.1.1), can be equally applied to TSG [21].

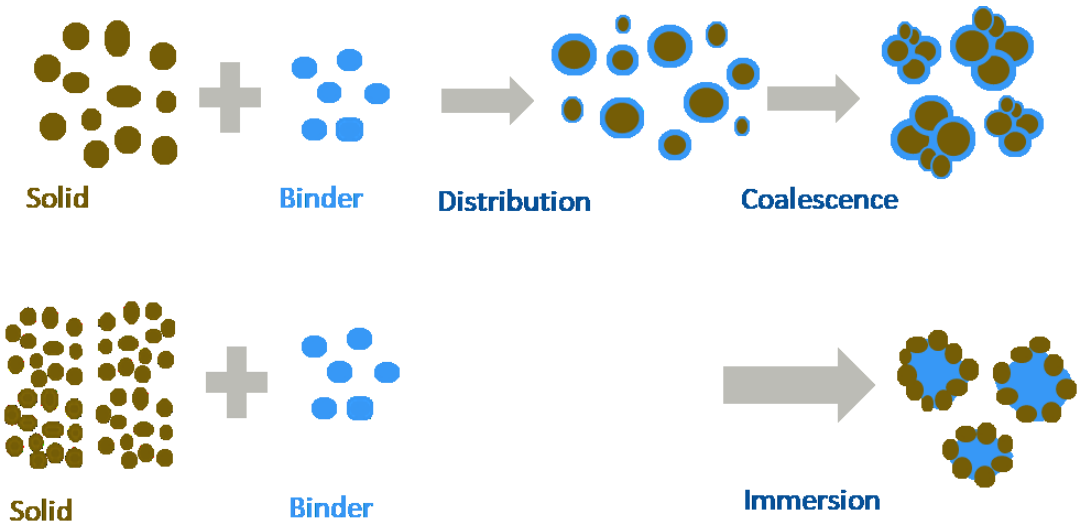

Fig. 1.1: Granulation mechanisms for granules produced via melt granulation according to Schaefer et al. [5].

Twin-screw extruders were introduced into pharmaceutical application by Gamlen and Eardley, who used the technique for the production of paracetamol extrudates with high drug loading [22].

Extruders are able to overcome limitations of HSM e.g. difficult product temperature control and long massing times, which might result in thermal degradation and uncontrolled granules growth, or the challenging end point determination [23]. Due to the small leakage of the extruder screws, the extruder has a high mixing efficiency and is therefore beneficial for both high- and low-drug loaded formulations, ensuring the content uniformity of the final product.

The high variability of screw-elements and screw speed makes it easier to control dispersive and distributive mixing during the granulation, which gives the opportunity to control the agglomeration process in terms of the resulting particle size. Different screw elements are available including conveying elements which simply transport the material from the inlet through the barrel without applying a lot of shear energy. They are defined by their pitch, which influences the product conveying speed. Mixing elements are star-shaped and still have conveying attributes while, applying a high level of mixing energy. Kneading elements are disc-shaped and their conveying character depends on the angle towards their neighboring element (30°>60°). If the angle is 90°C, only high shear energy is applied to the material. Due to the small leakage between the discs, these elements generate a high dispersive energy, which might result in breakage of brittle solid particles.

A further advantage of TSG are the reduced process times down to seconds, whereas in HSM it may take hours due to the long cooling periods. The mean process time and the exposure to heat of the material is defined by the mean residence time in the extruder. Short mean residence times reduce the risk of thermal degradation [24]. Hence, TSG opens the process of melt granulation even for thermolabile APIs.

Tab. 1.1: Comparison of high-shear mixers and twin-screw extruders.

High-Shear mixer	**Twin-Screw granulator**
Classical Batch Process	Feasible for continuous processing (PAT/RTR)
Long cooling periods	Short process and mean residence time (MRT)
Closed System	Containment necessary
Feasible for CIP	
Scale-up often empirical	Easy and rational scale-up
Rather inhomogeneous energy distribution →longer massing time: risk of over-granulation/pelletization	Homogenous energy distribution/ reproducible shear history
Long process time	Short mean residence time

Co-rotating intermeshing screws are self-cleaning and simultaneously reducing dead-zones during the process. It controls the residence time of the material in the extruder, which results in a very homogenous “shear-history” from batch to batch and finally reduces batch variability of the final product compared to HSM. The following process parameters can be varied in TSMG.

Process variables:

- Throughput
- Screw-speed
- Screw-design
- Temperature profile

1.1.1.2.1 Continuous manufacturing

Continuous processes are well established in the chemical, food processing and food technology industry. Due to the lack of batch definition and problems in transferring the cleaning-in-place (CIP) technology to continuous processing lines, which make batch processes very convenient in terms of product safety and quality assurance, the pharmaceutical industry remained long time on batch processing. Moreover, the production rates in the pharmaceutical industry are much smaller compared to chemical and food processing, which might have hindered a direct technology transfer [25]. Nevertheless, due to several advantages of continuous production as listed below, there is a high interest in continuous processing methods. Scale-up of HSG is often empirical and requires a large set of process equipment with a high footprint. Using extruders, scale-up can be simply performed by extending processing time, avoiding technology transfer from one equipment to another. As the energy introduction on a mass increment is homogeneous and easy to control in TSG, even scale-up to larger extruders is much more rational and might be assisted by process simulation [26,27]. Other reasons for continuous granulation are the ease of automation, less material handling and avoiding of process steps (e.g. weighing). Furthermore, less product waste is generated, if off-line analysis of the finished product fails the end-product specifications, as continuous production allows in-line control of the critical quality attributes (CQA) and fast control of the process parameters to meet product specifications, enabling real-time release (RTR) of the final product.[28].

With the introduction of new concepts as the quality by design (QbD) approach and the process analytical technology (PAT), stem from the international council of harmonization (ICH) guidelines (Q8, Q9 and Q10), continuous production is also of interest from a regulatory perspective. The regulatory agencies support the idea of QbD, which includes the definition of CQAs and a corresponding design space for the process, which already begins in pharmaceutical development. The CQAs should be monitored during production, e.g. by PAT, with the aim for RTR processes, potentially reducing production waste and time to final release.

Most research work on twin-screw extruders for granulation in a continuous processing line were done on wet granulation (TSWG) [19,29–35].

Several manufacturers offer a large range of equipment to support continuous processing. The ConsiGma™ system from GEA Pharma Systems was the first one, which incorporated an extruder for twin-screw granulation (TSG) as a continuous granulation module. ConsiGma™ is a complete continuous processing line enabling all process steps, such as TSWG, drying (semi-continuous, due to a six-chamber fluid-bed drying principle), milling and tableting, specifically designed for continuous wet granulation.

Glatt and Thermo Fisher Scientific developed a similar continuous processing line for wet-granulation. The MODCOS system provided by Glatt consists of a rotating circular arranged drying chamber, ensuring semi-continuous fluid-bed drying, with a precise residence-time.

The QbCon® 1 of Bohle simplifies continuous wet granulation, with a very narrow and controlled residence-time in the dryer, ensuring reproducible particle-size distribution and moisture content over long process times.

All these developments show the need for continuous reliable and reproducible drying methods in relation to wet granulation. As melt granulation avoids the need of this critical process step, it might be an interesting alternative technique, not only to ease processing of water-sensitive materials in a continuous processing line. Attention should be paid, when changing batch processes to continuous processing as this can have an impact on the product performance and might require adaptation measures. Until now, no comparison between TSMG and HSM exists for the production of melt granules.

1.1.1.2.2 The use of functional polymers

As higher temperatures can be applied in twin-screw extruders compared to HSM, a larger set of polymer based melt binders is available, including functional polymers to control product performance. A great number of polymers was recently screened for their performance to enhance tabletability of poorly compactable materials (Batra et al., 2017). The process and product performance strongly depends on the glass transition temperature (T_g) of the polymer used [37]. Polymers with higher T_g might result in unstable granulation processes, which require fine-tuning of the process (screw-speed, throughput or granulation temperature) to enable processing. The T_g of a polymer is directly linked to its melt viscosity [38]. The melt viscosity of the product plays an important role in classic extrusion processes and it is directly linked to the prediction of the optimal processing parameters. In general, the melt rheology of a polymer is influenced by heat and shear, which dictates the melt granulation processing window to obtain a stable and reproducible granule quality. During melt granulation, highly viscous polymers and high friction of non-molten particles might limit the granulation process and require high granulation temperatures or higher polymer contents. Subsequently, resulting in reduced drug loads and/or a higher risk of thermal degradation of the API.

However, functional polymers offer more advantages than higher granules strength and better tabletability. Additionally, they might be used to obtain a desired dissolution profile of the final product. As a result, the development of immediate release formulations is feasible [23], as well as the development of controlled release dosage forms [4,20,39], mainly in dependence of the polymer used and its dissolution characteristics.

Despite of the high number of potential polymeric melt binders their solubility and dissolution enhancing effects are still poorly understood.

1.2 Tablets:

From the pharmaceutical point of view, granules are mostly an intermediate in the production of tablets or capsules. Tablets are still the most accepted and commonly used dosage form. Due to their high dosage uniformity, low production costs and high stability, their market share on dosage forms administered to patients is around 80% [40].

The powder or granules need to fulfill several quality attributes to be processable at large and fast rotary presses or in a continuous processing line. For powder mixtures, flowability and compactibility is often limited, requiring the addition of excipients to improve these attributes and to make the API suitable for direct tableting [41]. A subsequent excipient level of more than 50% (w/w) is not uncommon [2], which might be critical when high doses and/or drug loads are required Granulation is often implemented as additional process step to enhance flowability or compressibility of the powders. Additionally, it improves content uniformity, since it can ensure dispersion of cohesive powders and it limits segregation or demixing of the formulation during production. Regarding the final drug product, tablets made of granules must withstand high mechanical forces during packing, transport and handling. Furthermore, if early onset of the therapeutic is required (immediate-release), the tablets must disintegrate and dissolve fast when in contact with aqueous media.

1.2.1 **The compaction process:**

Tablet manufacture can be regarded as the application of pressure to a population of particles in a confined space.

There are mainly three processes, which take place during compression: plastic deformation, elastic deformation and fragmentation.

Tablet mechanical strength mainly depends on the number of contact points and on the attraction forces between the particles [42]. Brittle materials are known to undergo fragmentation during compression. Fragmentation can improve tensile strength (TS), mainly due to the increase in available surface area for binding forces. Furthermore, a rough surface structure can increase the tablet strength. In the case of highly plastic materials, especially those with a rough surface, e.g. microcrystalline cellulose, TS can be substantially high. Nevertheless, elastic deformation during compaction might lower TS. To characterize the deformation process of the material during tableting compression models are often used. They describe the reduction of volume/porosity as a function of the compression force applied.

Force-displacement measurements are one of the most popular methods to study the compression behavior of materials during the tableting process. The measurement requires accurate determination of the force on the upper and lower punch and accurate recording of the displacement.

The Heckel equation (Eq. 1.1) is one of the most popular equations obtained from the porosity-pressure function, to describe the compression behavior. The displacement data, tablet weight and true density are used to calculate the porosity of the powder bed in-die at increasing compression pressure as described by Heckel (1961),

$$\ln\left(\frac{1}{1-SF}\right) = kP + A \qquad \text{(Eq.1.1)}$$

where *SF* is the relative density (solid fraction) at pressure *P*; *k* and *A* are material-dependent constants. This formula is valid for the linear part of the Heckel-plot (Fig.1.2). The length of the linear part varies with the compression behaviour of the material under investigation. The parameter *k* describes the slope of the linear part of the compression curve. The reciprocal of *k* is defined as the Yield Pressure (YP). This is theoretically the minimal pressure, at which plastic deformation and binding in the tablet occur. Extrapolating the linear part of the Heckel Plot to the y-axis, provides the

parameter *A*, which describes the corresponding solid fraction at which bonding is theoretically formed.

The compression properties of the material or the formulation allow the prediction of formulation properties (e.g. lubricant-sensitivity, speed-sensitivity) and are therefore of fundamental importance during formulation development. The initial curvature of the Heckel-Plot is used to describe particle rearrangement, packaging and fragmentation (Phase 1).

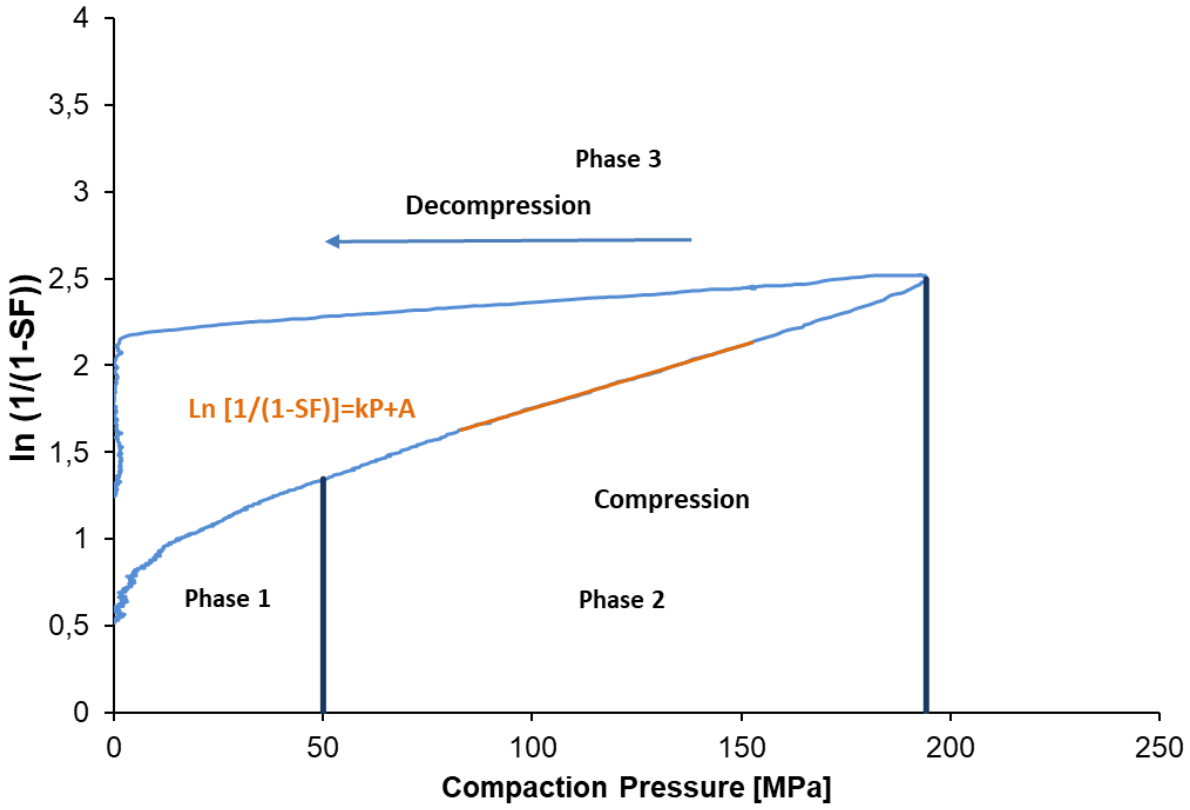

Fig. 1.2: Example of a Heckel plot.

The linear part of the compression phase is used to describe the deformation behavior (Phase 2). High YP indicates a more brittle deformation behavior, whereas a lower YP is typical for more plastic deforming materials. Overall, these parameters can be used to describe the deformation characteristics of granulated material. This is especially interesting in comparison to the ungranulated material. The difference in the obtained parameters (YP and *A*) for granulated and ungranulated (e.g. physical mixture) specimen is indicative for the impact of the granulation process on the deformation characteristics. Additionally, the decompression phase can be used to evaluate elastic

recovery (Phase 3). However, from this ejected tablet method, only conclusions on the total elastic recovery can be drawn. In general, one needs to keep in mind that the mean yield pressure (YP) depends on process parameters like punch velocity and accuracy of the displacement measurement. Hence, it is prone to errors and variability among research groups [44,45] . At high punch velocities the time dependent plastic flow might shift to a more ductile deformation behavior. Regarding brittle materials, they are less sensitive to punch velocity [45]. Furthermore, particle size and shape of the investigated material might significantly impact the results, since they have influence on the rearrangement phase during compression [46,47].

An alternative model to describe the volume reduction of a powder was developed by Kawakita.

The original Kawakita model [48] describes the volume reduction of a powder in a linearized form, were *P* is the applied pressure and *a* and *b* are constants (Eq.1.2).

$$\frac{P}{C} = \frac{P}{a} + \frac{1}{ab} \qquad \text{(Eq.1.2)}$$

C is the relative volume decrease, calculated from the initial volume V_0 and V_p, which is the volume under pressure *P*.

The constant *a* is identical to the minimum porosity of the powder bed prior to compaction, while *b* is the coefficient of compression and related to the materials plasticity. The reciprocal of b gives the pressure term (yield strength), which is the pressure P_k. It describes the necessary pressure to reduce the powder bed volume by 50%. The lower the P_k, the higher the degree of plastic deformation becomes [49]. The Kawakita model is the best applicable model systems for low applied pressures and high resulting porosities during compression [50]. Similar to the Heckel model, the Kawakita model is suitable to describe the deformation characteristics of the granules in relation to ungranulated material. Therefore, it can be used to evaluate the influence of the granulation process on the mechanical attributes of the drug product formulation.

1.2.2 **Immediate release formulations:**

The solid oral dosage forms may also be categorized by their release characteristics in immediate-release and modified release forms. Immediate-release tablets are designed to disintegrate and release their medication fast with no special rate-controlling features, such as special coatings and other techniques [51].

The process of drug product dissolution can be divided into several discrete steps (Fig. 1.3). The first step involves the wetting and penetration of the dissolution medium into the dosage form. The second step is the disintegration and/or disaggregation into granules or particles of the drug substance. The third step involves solubilization of the drug substance into solution. The drug dissolution rate increases when particle-size decreases. These steps can also occur simultaneously during the dissolution process [52].

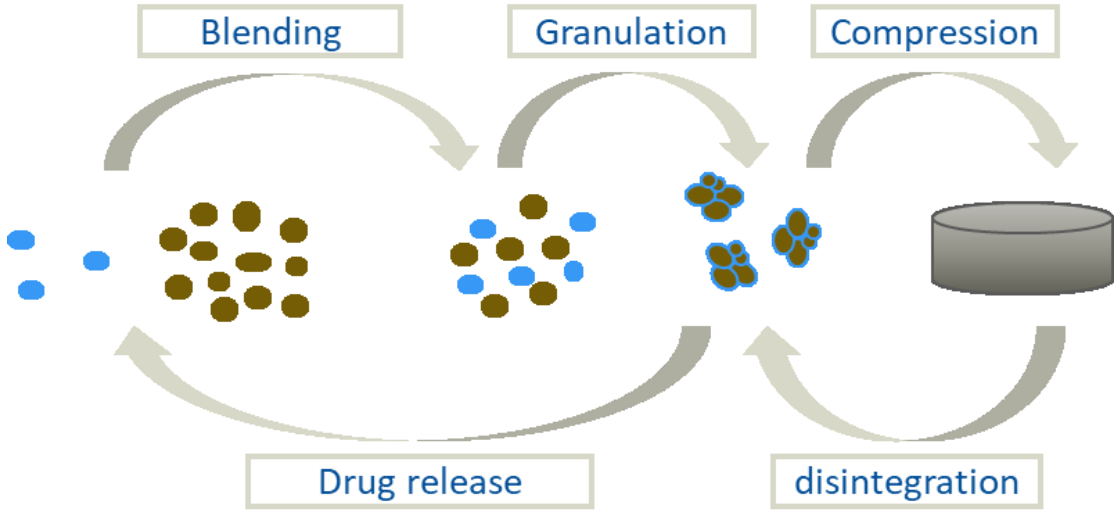

Fig. 1.3: Formulation from powder to compact and drug release modified from [53].

The dissolution rate of a drug is closely associated with the drug substance solubility. Compounds with high solubility generally exhibit significantly higher dissolution rates, described by the equation of Nernst-Brunner (Eq. 1.3),

$$\frac{dC}{dt} = \frac{DS}{Vh} * (C_s - C_t) \qquad \text{(Eq.1.3)}$$

where *dC/dt* is the dissolution rate over time, *D* is the diffusion coefficient, *S* is the surface area, *V* is the volume of the dissolution medium, *h* the thickness of the diffusion layer, $(C_s - C_t)$ is the concentration gradient between the diffusion layer and the bulk solution. The equation indicated that dissolution is affected by several factors, such as solubility, diffusivity, surface area, and solution hydrodynamics.

Superdisintegrants are excipients, which are added in small proportions to achieve a fast disintegration of the tablet. The most prominent disintegrants are crospovidone (CPV), croscarmellose sodium (CCS) and sodium starch glycolate (SSG). Different mechanisms for their way of action are postulated, including wicking, swelling and shape recovery. In wet granulation processes it is very common to add the disintegrant proportionally intra- and extra-granular to achieve a maximum of disintegration efficiency by, destroying the extra- and intra-granular bonds. This can minimize disintegration time and simultaneously results in a high surface area. The external addition of disintegrant after the granulation process is a crucial consideration in terms of continuous processing, as additional mixing steps might be integrated into the processing line.

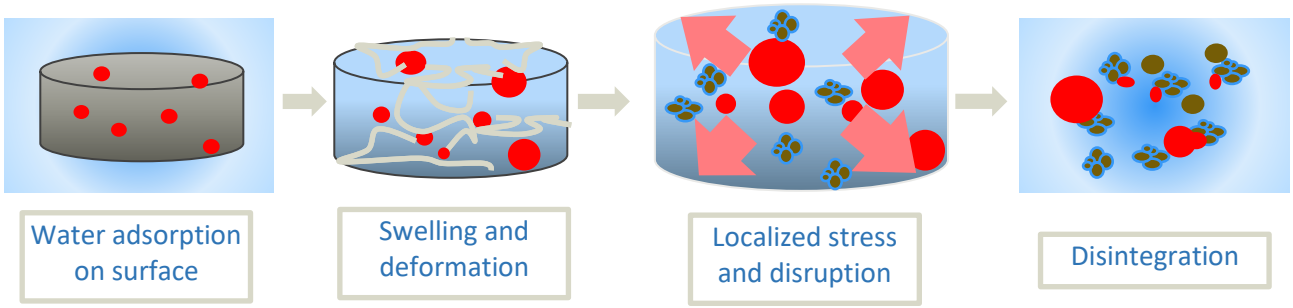

Fig. 1.4: Stages of tablets disintegration modified from [54].

Granules produced by melt granulation often exhibit a very high density, due to the absence of an additional drying step, which forms pores [5]. In contrast to comparable low densified granules produced by wet granulation, tablets produced from melt granules mostly achieve high SF and subsequently a high tensile strength in the pharmaceutical relevant pressure range [37,55]. Due to their poreless structure (high solid fraction), disintegration might be limited, requiring the addition of disintegrants to obtain immediate release dosage forms.

1.2.2.1 The biopharmaceutical classification system (BCS)

The BCS is a framework for classifying drug substances based on solubility and intestinal permeability. Among final product dissolution, these are the major factors governing rate and extent of absorption from immediate-release products [56]. The BCS classifies drug substances as:

- Class 1: high solubility and high permeability;
- Class 2: low solubility and high permeability;
- Class 3: high solubility and low permeability;
- Class 4: low solubility and low permeability.

A drug is classified as highly soluble when the highest dose strength is soluble in 250 ml or less of aqueous media over the pH range of 1.2 to 6.8 at 37°C. The volume estimate of 250 ml is derived from typical bioequivalence study protocols that prescribe administration of a drug product to fasted human volunteers with a glass of water.
Alternatively, drugs can be classified by their dissolution using USP Dissolution Apparatus 1 at 100 RPM or Apparatus 2 at 50 RPM in a volume of 900 ml or less. Different pH conditions should be included (pH 1.2, pH 4.5, and pH 6.8). A drug substances or formulation is classified as either very rapid dissolving (≥ 85 for the mean percent dissolved in ≤ 15 minutes) or rapid dissolving (≥ 85 for the mean percent dissolved in ≤ 30 minutes) [57].

A drug substance is classified as highly permeable when the extent of absorption in humans is 85% or more of the administered dose, based on a mass-balance determination or in comparison to an intravenous reference dose. Practically, the Caco-2 screening is the most popular in-vitro assay to classify the drug in intestinal permeability.

Nowadays, most new APIs belong to the BCS class II. Their oral bioavailability is limited due to their poor dissolution behavior. Melt granulation might be an alternative method to hot melt extrusion for processing formulations with both, high drug load and enhanced bioavailability. Using amorphous solid dispersions (ASDs), the drug load is often limited to 30 or 50% (w/w). Using melt granulation, drug loads up to 90% (w/w) might be achievable [2,4], which is an out-standing high drug load, making the technique even more attractive. The potential of melt granulation to enhance solubility of poorly soluble APIs is not proven, yet.

2 Aims and scope of work

Melt granulation is an interesting alternative technique to produce both, immediate and controlled-release final products using twin-screw extruders. It allows a continuous process from powder to tablet. One final product using this technique, is already on the market (metformin hydrochloride with vildagliptin (Eucrease® or Glavumet®; Novartis)). However, there is still a need for process understanding and impact factors (critical quality attributes) are still not fully examined.

The aim of this current work was to gain a deeper understanding of the granule's characteristic obtained from TSMG and their influence on further processing of these granules into tablets. Therefore, the following topics were investigated in this work:

- The role of binder distribution in the final tablets made of melt granules and their physical mixtures was examined and quantified via image analysis of energy dispersive X-ray maps. The influence of primary particle-size of both filler (non-molten phase) and binder (molten-phase) was systematically evaluated, regarding the compaction and compression performance. The obtained melt granules, where formed either by distribution or immersion mechanism (chapter 3).

- The compression behavior of granules i.e. mechanical characteristics and deformation behavior was precisely analyzed by out-of-die and in-die compression analysis. This increases knowledge of the granule's compression characteristics and is a helpful tool for QbD, if special drug product attributes are required. Furthermore it helps to define the optimal binder content for the formulation (chapter 4).

- Comparison of granules derived from twin-screw melt granulation and HSM process. Relevant CQAs were defined, including particle size distribution, yield (100-710 µm particle size), shape factor, bulk and tapped density as well as the compressibility index, porosity, specific surface area, flowability (mass flow), tabletability and binder distribution. This work aims to ease process adaptions needed, when changing from batch to continuous production (chapter 5).

- The suitability of TSMG to enhance the dissolution of poorly soluble APIs was investigated. Soluplus® and Kolliphor® P407 were chosen as functional melt binders and compared to the hydrophilic binder PEG 6000. Due to their amphiphilic structure, they enhance the wettability and dissolution of the lipophilic model API carbamazepine (chapter 6).

- Super-disintegrants were systematically evaluated to achieve immediate release formulation of the model drug paracetamol. The performance of croscarmellose sodium, crospovidone and sodium starch glycolate was tested intra- and extra-granular, which is a crucial point for continuous processing, as additional mixing steps might be needed in the processing-line (chapter 7).

3 Improvement of tabletability via twin-screw melt granulation: focus on binder distribution

Kristina E. Steffens; Karl G. Wagner

This part was published as:

Steffens, Kristina E., and Karl G. Wagner. "Improvement of tabletability via twin-screw melt granulation: Focus on binder distribution." International journal of pharmaceutics 570 (2019): 118649.

DOI:10.1016/j.ijpharm.2019.118649

3.1 Graphical abstract

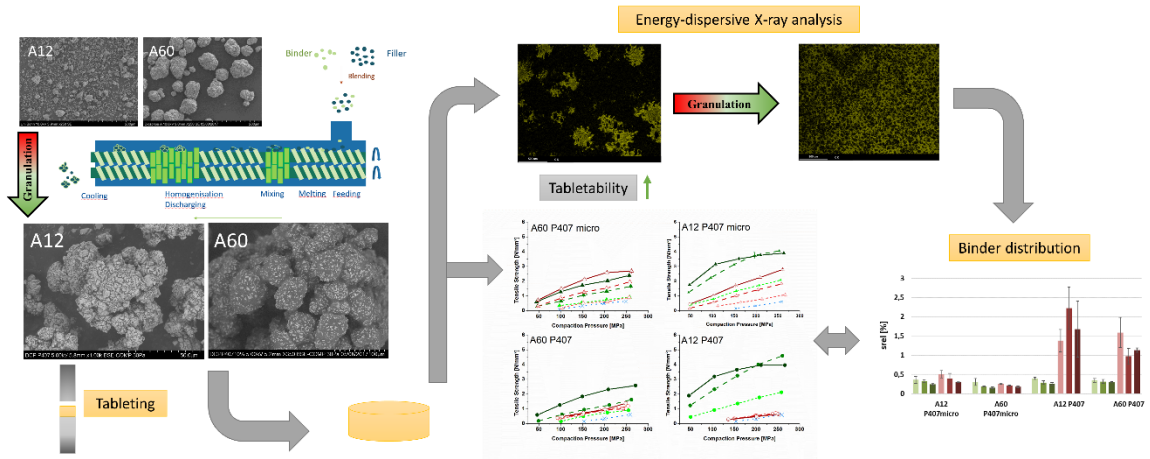

3.2 Abstract

In this study, the impact of binder distribution on the tabletability and compactibility of granules produced by twin-screw melt granulation was investigated. To this end, two grades of dicalcium phosphate anhydrous (fine and coarse) were used as model substances (filler) in combination with two grades of poloxamer (fine and coarse) as melt binder at three concentrations. For the fine filler, granule forming followed the immersion mechanism, whereas a distribution mechanism was observed in case of the coarse filler. Compared to the granules prepared with the coarse filler, the tabletability of granules prepared with the fine filler increased more pronouncedly compared to the corresponding physical mixtures (PM). In general, tabletability, compressibility and compactibility depended predominantly on the distribution of the binder in the tablet, and the homogeneity of distribution correlated with increased tensile strength. Binder distribution was analyzed using scanning electron microscopy combined with energy-dispersive X-ray analysis (SEM/EDX) and quantified by image-analysis of the tablet surface. PMs in general varied in tabletability. However, even at tabletability similar to the granules, all PMs suffered from poor flow and/or segregation.

3.3 Keywords

Twin-screw melt granulation; twin-screw extruder; tabletability; compactibility; binder distribution; energy dispersive X-ray analysis

3.4 Introduction

Granulation is a routine procedure in the pharmaceutical industry and used to overcome limitations such as insufficient processability, flowability, compactibility, content uniformity and dissolution of materials that are not suitable for direct tableting. Especially melt granulation, where the addition of aqueous and organic solvents can be avoided, is of interest for moisture sensitive active pharmaceutical ingredients (APIs). Due to this solvent-free process, subsequent solvent recovery or drying steps can be avoided, which in turn reduces the general effort and costs of manufacturing. A further advantage is the high drug load which can be achieved, since melt granulation requires only a small fraction of binder [2].

During melt granulation, the solid particles are bound together by agitation, kneading and layering in the presence of a molten binder. After the granulation process, the material is directly cooled down to room temperature, solidifies and forms dry agglomerates. The binder can either be added as a molten liquid, or as a dry powder, which melts as a result of the thermal processing (air or heat jacket) or the heat of friction during processing. To ensure handling and stability at room temperature, while avoiding high processing temperature, binders with melting points between 50°C and 80°C are commonly used [1].

Melt granulation processes are divided into low and high shear processing types, classically performed using fluid-bed agglomeration or high shear mixers. A further and continuous manufacturing opportunity for melt granulation is twin-screw extrusion, whereby ideally adjusted process conditions even allow the production of granules without any additional milling step [23,39]. In contrast to conventional melt extrusion, granules are obtained without a die plate at the end of the extruder, ensuring that the material is not densified, resulting in a discontinuous phase. The advantage of twin-screw extruders (TSEs) for melt granulation over high shear mixers is the homogeneous powder and energy distribution within the TSE resulting in a homogeneous binder distribution even at low binder level. At the same time, short process times and local heat transfer distances reduce the risk of thermal degradation and increase the energy efficiency. The high flexibility in screw configuration design, and hence various energy intake, allows the variation of distributive and dispersive mixing levels and the control of the degree of agglomeration, particle growth and homogenization [23].

The mechanisms underlying melt granulation are similar to those of wet granulation, being subcategorized as nucleation, coalescence and layering. With increasing binder addition, the liquid-bridging state changes from pendular to funicular and then to capillary state, leading to an uncontrolled granule growth. In general, granules obtained from melt granulation are denser compared to those obtained by wet granulation, since no pores are formed by solvent removal [1]. For describing the melt agglomeration process using high shear mixing, Schæfer (2001) proposed two elementary mechanisms, namely distribution and immersion. The former involves the distribution of the molten binder on the surface of the primary material, which can be followed by further agglomeration due to coalescence of the wetted nuclei. In the case of the immersion mechanism, nuclei are formed by immersion of the primary material on the surface of a molten binder droplet. Further densification of the material can lead to the coalescence of the formed particles. Depending on the relative particle size of filler to molten binder droplets and the molten binder viscosity, one of the two aforementioned mechanisms will be predominant. If the molten droplets are smaller than the filling material, the process will be mainly based on the distribution mechanism. Conversely, immersion will be paramount in the case that the filling material is smaller than the binder droplet size [58]. With respect to the relationship between binder viscosity and agglomeration mode, low viscosity binders can promote the distribution mechanism, whereas highly viscous binders induce agglomerate formation through immersion. Hence, it can be deduced that the agglomeration mechanism is influenced both by temperature and shear force.

Mu and Thompson (2012) examined the mechanism of granulation of lactose monohydrate with PEG as a model binder in a TSE, studying the influence of screw-design, binder content, binder molecular weight, process temperature and shear force. They showed that the mechanisms of melt granulation described for high shear mixers can be equally applied to an extruder [21]. Furthermore, tablets made of granules produced via melt granulation using TSEs often showed good compactibility [2,36,37,59,60]. Despite the enduring and variety of interest in melt granulation present in the literature, few studies have been dedicated to the comparison of simple physical mixtures (PM) to the granules with focus on the deformation behaviour.

The current study sought to compare PM and the resulting granules produced via twin-screw melt granulation using a poorly compactible material. This study was performed

to highlight the important role of the starting materials' particle size in determining the granulation mechanism, and the importance of binder-distribution to enhance tabletability of the brittle materials.

As model substance (filler), the dicalcium phosphate anhydrous DI-CAFOS A® with poor binding properties at low compaction pressures was used. It shows less fragmentation and binding capacity than other dicalcium phosphate grades and high residual porosity, when compressed into tablets [61]. A60 is a dicalcium phosphate anhydrous with a high bulk density and low specific surface area which was designed for direct tableting [62]. The obtained tableting properties (tabletability, compactibility and compressibility) were examined by means of changes in solid fraction (SF) and tensile strength (TS) over a pharmaceutically relevant pressure range. Binder distribution was quantified using SEM/EDX image analysis.

3.5 Material and methods

3.5.1 Material

Two different grades of dicalcium phosphate anhydrous with different particle sizes (DI-CAFOS® A12 and A60) were used as models for a filler material with low compactibility and high degradation temperature. Both DI-CAFOS® A12 and A60 were kindly donated by Chemische Fabrik Budenheim KG, (Budenheim, Germany). Kolliphor® P407 and P407 micro (melting point 56 °C [63]) were used as binding materials, which were kindly supplied by BASF (Ludwigshafen, Germany).

3.5.2 Methods

3.5.2.1 Physical mixtures

Both DI-CAFOS® types were formulated with the two binders in concentrations of 5, 10, and 15 % (w/w), resulting in 12 different blends (Tab. 3.1). These PM were prepared using a Turbula mixer (Willy A. Bachofen AG Maschinenfabrik, Switzerland), spinning at 50 rpm for 10 min. The batch size was 100 g. The obtained PMs were further used for twin-screw melt granulation.

Tab. 3.1 Formulations.

Substance	P407 micro % (w/w)			P407 % (w/w)		
A12	5	10	15	5	10	15
A60	5	10	15	5	10	15

3.5.2.2 Twin-screw melt granulation

Twin-screw melt granulation was performed using a co-rotating TSE (ZE12, Three-Tec GmbH, Seon, Switzerland) with a functional length of 25:1 L/D (length/diameter) and a 12 mm screw diameter. The extruder barrel consisted of five individually adjustable heating zones to ensure sufficient melting and distribution of the binder.

The process temperature was set up to 95 °C in the high shear regions of the extruder screws (zone 1: 30°-, 60°- and zone 2: 60°- and 90°-4-disc-kneading elements). At the terminal zone of the barrel, the temperature was reduced again to 55 °C to initiate solidification of the material.

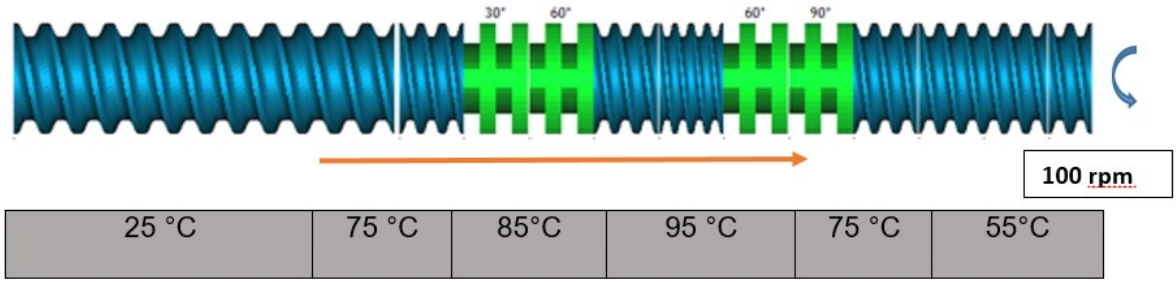

Fig. 3.1. Granulation conditions and screw configuration used (Ludovic® simulation software, Saint-Etienne, France).

In Fig. 3.1, the screw-configuration and the set temperature of each zone is depicted. During twin-screw melt granulation, the screw speed was set to 100 rpm and no die plate was mounted at the end of the extruder barrel. A volumetric feeder system ZD9 (Three-Tec GmbH, Seon, Switzerland) was used to enable a constant feed rate of 0.2 kg/h. Granules obtained were further hand-sieved by using a 2 mm sieve prior to compaction.

3.5.2.3 Particle size distribution

Particle size distribution was measured by laser diffraction using a Helos KF (Sympatec GmbH, Clausthal-Zellerfeld, Germany) with a helium-neon laser (λ = 632.8 nm) in combination with a multi-element detector. The samples were dry-dispersed using Rodos (Sympatec GmbH, Clausthal-Zellerfeld, Germany) at a pressure of 0.5 bar. Suitable lenses were chosen depending on the particle size. Particle size distribution was calculated according to Fraunhofer theory with the software Windox 4.2.1. All experiments were carried out in triplicate.

3.5.2.4 Flowability (mass flow)

Approximately 30 g of each sample was used to measure the flowability of the granules using an automatic test system (Erweka GT, Erweka GmbH, Heusenstamm, Germany). To this end, the powder was filled into a metal hopper, with an orifice of definite size (11.3 mm or 15.0 mm). With the help of an electronic balance, the time required for the sample to flow out was measured and reported as s/100g. The corresponding stirrer (level 3) was used if necessary. Measurements of the mass flow (MF) were done in triplicate.

3.5.2.5 Scanning electron microscopy (SEM)

A scanning electron microscope (SU 3500, Hitachi High Technologies, Krefeld, Germany), equipped with a backscattered electron detector (BSE) and an energy dispersive X-ray detector (EDX) (EDAX Element- C2B, Ametek, Weiterstadt, Germany) was used to elucidate the granule morphology and the distribution of the binder. BSE images were collected at an acceleration voltage of 5 kV at a variable pressure mode of 30 to 50 Pa. The samples were mounted using a conductive carbon paste (Leit-C-Plast, Plano GmbH, Wetzlar, Germany) and were not coated beforehand to ensure the visualization of material contrast. The intensity of the backscattered electrons correlates with the atomic weight of the samples. The micrographs were used to describe the granulation mechanism. For EDX-analysis, the samples were compressed with a pneumatic hydraulic tablet press (FlexiTab, Röltgen GmbH & Co. KG, Solingen, Germany) using 8 mm round flat-face tooling and a compaction pressure of 250 MPa to obtain a flat tablet surface. The tablets were further fixed on carbon paste and the analysis was performed without any coating. The surface of the tablets was mapped at high vacuum mode with an acceleration voltage of 10 kV and a magnification of 50x (total area: 5 mm^2). Working distance was kept constant at 10 mm ±0.5 mm.

3.5.2.6 Image analysis of SEM/EDX-maps

To parameterize the distribution of the binder, obtained micrographs from the EDX software containing the carbon signal only (512x400 pixels), were divided into 35 sub-frames (80x73 pixels), as schematically shown in Fig. 3.2. The percentage area of binder in each of the 35 sub-frames was calculated using image editing software ImageMagick 6.9 (ImageMagick Studio LLC). The relative standard deviation of the average area of the binder (carbon signal in yellow) from all 35 sub-frames was calculated. This relative binder variation (calculated as relative standard deviation (s_{rel})) was taken as a value for describing the binder distribution. Low levels indicate homogeneous binder distribution (Fig. 3.2b) while high levels would represent high variation of binder distribution within the 35 sub-frames, i.e. inhomogeneous binder distribution (Fig. 3.2a). For every formulation, three tablets were analysed in total for mean value and standard deviation calculation of this distribution value, defined as the binder variation.

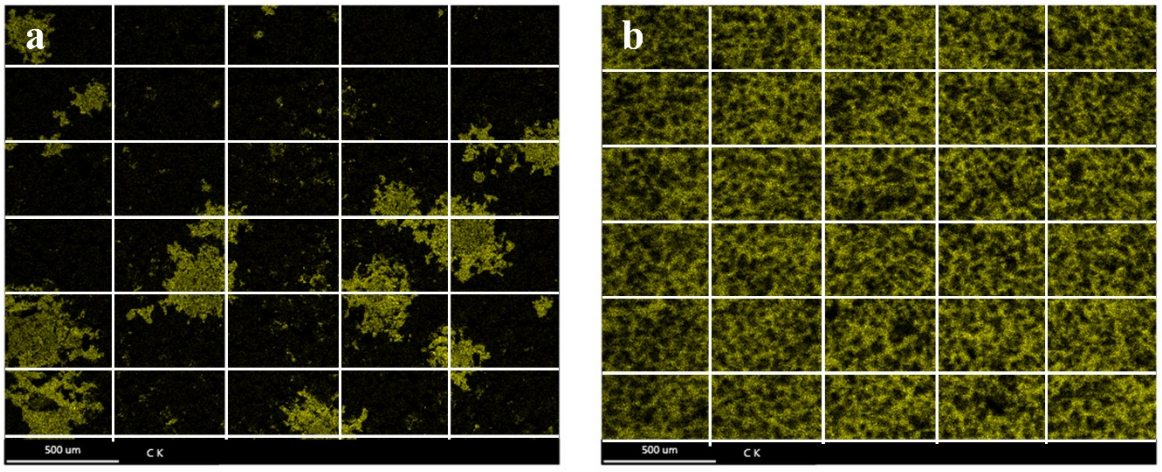

Fig. 3.2. Tablet surface SEM/EDX maps: (a): PM A60 P407 15 % (w/w); (b): granules A60 P407 15 % (w/w): Schematic diagram of the 35 frames taken for the calculation of the binder variation.

3.5.2.7 Density

Pycnometric density was measured for the pure materials, PM and granules using the AccuPyc 1330 helium pycnometer (Micromeritics GmbH, Aachen, Germany). The chamber was purged with 20 purge cycles prior measurement. A fill pressure of 136.86 kPa and an equilibration rate of 0.0345 kPa/min were used for analysis. Each measurement was repeated up to 25 times or until a standard deviation of 0.01 % was reached. The density was used for the calculation of the SF.

3.5.2.8 Tableting

Tablets (n = 5) were pressed on a single punch tablet press (StylOne Classic 105 ML, Medelpharm, Beynost, France/Romaco Kilian, Cologne, Germany) with a 8 mm flat-face tooling. Five compaction pressures from 50 MPa to 250 MPa were applied at constant tableting speed (dwell-time: 6-7 ms; compression time on average: 110 ms). The die was filled manually and lubricated externally if needed. After 24 h of storage, the tablets were analysed regarding their tablet weight (analytical balance, AG 204, Mettler Toledo GmbH, Gießen, Germany), thickness (Mitutoyo Absolute ID C125B, Mitutoyo Deutschland GmbH, Neuss, Germany), diameter and crushing strength (Erweka TBH 210, Erweka GmbH, Heusenstamm, Germany). TS (Eq. 3.1) and SF (Eq. 3.2, 3.3 and 3.4) were calculated from the data obtained. TS is the tablet crushing strength normalized by the dimension of the tablet and is therefore independent of its geometry [64],

$$TS = \frac{2F}{\pi dh} \qquad \text{(Eq. 3.1)}$$

where F is the crushing strength, d the diameter and h the thickness of the tablet.
SF represents the apparent density (P_{app}) of the compact calculated from tablet weight (m) and its volume relative to the true density (P_{true}) of the powder.

$$SF = \frac{Papp}{Ptrue} \qquad \text{(Eq. 3.2)}$$

$$Papp = \frac{m}{Vp} \qquad \text{(Eq. 3.3)}$$

$$Vp = \pi * \left(\frac{d}{2}\right)^2 * h \qquad \text{(Eq. 3.4)}$$

Where V_p is the volume of the compact calculated based on *d and h*, which describe the tablet diameter and thickness.

The above parameters were used to describe the tabletability, which is known as the ability of a powder to be transformed into tablets with a certain TS under the applied compaction pressure. Moreover, the parameters were used to plot the compressibility, which is defined as the ability of a powder to reduce volume under pressure (SF vs. applied compaction pressure). Additionally, the compactibility was evaluated, which describes the resulting TS as a function of SF, and is therefore also a descriptor for the number bonding points or the binding force formed during the tableting process.

3.6 Results and Discussion

3.6.1 Particle size distribution of the starting materials

Tab. 3.2 shows the d_{10}, d_{50} and d_{90} values of the starting materials. In the case of A60, a d_{50} value of 60 µm with a narrow particle size distribution was identified, whereas for A12 a larger content of fines was observed, resulting in a d_{50} of 10.6 µm. Kolliphor® P407 micro had a mean particle size of only 26 µm, whereas Kolliphor® P407 had a large mean particle size of 350 µm but it also contained very large ones around 500 µm.

Tab. 3.2 Particle size (d_{10}, d_{50}, d_{90}) and pycnometric density of the starting materials.

Substance	d_{10} [µm] ± SD	d_{50} [µm] ± SD	d_{90} [µm] ± SD	ρ [kg/m3] ± SD
A60	29.6 ± 1.4	60.4 ± 1.7	88.4 ± 0.8	2.8539 ± 0.0008
A12	1.2 ± 0.1	10.6 ± 0.7	37.7 ± 2.2	2.8932 ± 0.0003
P407 micro	7.7 ± 0.1	26.3 ± 0.1	60.0 ± 0.2	1.1758 ± 0.0015
P407	175.7 ± 35.9	342.8 ± 63.3	450.2 ± 57.9	1.0698 ± 0.0182

3.6.2 Density

Due to pronounced differences in density (Tab. 3.2) between dicalcium phosphate and the binding material, mass fraction (w/w) (Tab. 3.1) and volume fraction (V/V) (Tab. 3.3) differ approximately by the factor of two. The fraction of binder needed to produce adequate granules depends mostly on the binder volume and less on its mass fraction. Similar assumptions were made for mixing processes of components that differ in particle size and bulk volume [65]. This consideration is strongly evident when the differences in densities are as high as in this case. Regarding the percolation theory, the percentage (V/V) is more suitable, comparing the results to other materials, as the influence of a material is increasing with its volume fraction [66].

Nevertheless, the difference is not pronounced comparing the formulations under investigation (Tab. 3.3).

Tab. 3.3 calculated volume fraction in the tablet of the formulations under investigation.

Substance	P407 micro % (V/V)			P 407 % (V/V)		
	5 % (w/w)	10 % (w/w)	15 % (w/w)	5 % (w/w)	10 % (w/w)	15 % (w/w)
A12	11.47	21.47	30.27	12.46	23.11	32.31
A60	11.32	21.24	29.99	12.31	22.86	32.01

Density for the granules and the PM are given in Tab. 3.4. Density decreased with increasing polymer content due to the lower density of P407 compared to both grades of dicalcium phosphate under investigation. Overall, mixtures containing the same binder content, showed similar pycnometric density values. Values given in Tab. 3.4 were used for the calculation of the SF of the tablets produced from the corresponding materials.

Tab. 3.4 Measured density of the granules and PM under investigation.

Substance	Granules ρ [kg/m3] ± SD			PM ρ [kg/m3] ± SD		
	5 % (w/w)	10 % (w/w)	15 % (w/w)	5 % (w/w)	10 % (w/w)	15 % (w/w)
A12 P407 micro	2.7064 ± 0.0063	2.5548 ± 0.0039	2.3832 ± 0.0005	2.7142 ± 0.0008	2.5498 ± 0.0007	2.4050 ± 0.0009
A60 P407 micro	2.7060 ± 0.0017	2.5866 ± 0.0122	2.3822 ± 0.0129	2.7039 ± 0.0075	2.5343 ± 0.0012	2.3878 ± 0.0008
A12 P407	2.7090 ± 0.0102	2.5460 ± 0.0011	2.3728 ± 0.0051	2.6657 ± 0.0007	2.4420 ± 0.0045	2.2346 ± 0.0061
A60 P407	2.6764 ± 0.0007	2.5460 ± 0.0059	2.3525 ± 0.0103	2.7348 ± 0.0025	2.5551 ± 0.0020	2.3144 ± 0.0005

3.6.3 **Flowability (mass flow)**

Tab. 3.5: Mass flow of the formulations.

Formulation	Granules MF [s/100g] ± SD	PM MF [s/100g] ± SD
A12 P407 micro 5 % (w/w)	12.9 ± 0.8 (15.0 mm & stirrer)	N/A
A12 P407 micro 10 % (w/w)	7.1 ± 0.2 (11.3 mm)	N/A
A12 P407 micro 15 % (w/w)	5.5 ± 0.3 (11.3 mm)	N/A
A12 P407 5 % (w/w)	12.6 ± 0.6 (15.0 mm & stirrer)	N/A
A12 P407 10 % (w/w)	7.3 ± 0.6 (11.3 mm)	N/A
A12 P407 15 % (w/w)	5.4 ± 0.2 (11.3 mm)	N/A
A60 P407 micro 5 % (w/w)	5.5 ± 0.2 (11.3 mm)	7.0 ± 0.3 (11.3 mm)
A60 P407 micro 10 % (w/w)	7.2 ± 0.2 (11.3 mm)	3.3 ± 0.4 (15.0 mm & stirrer)
A60 P407 micro 15 % (w/w)	8.3 ± 0.5 (11.3 mm)	N/A
A60 P407 5 % (w/w)	4.0 ± 0.2 (11.3 mm)	3.2 ± 0.3 (11.3 mm)
A60 P407 10 % (w/w)	5.4 ± 0.1 (11.3 mm)	3.3 ± 0.2 (11.3 mm)
A60 P407 15 % (w/w)	8.1 ±0.4 (11.3 mm)	2.9 ±0.2 (11.3 mm)

Tab. 3.5 shows the results of the flowability analysis. PM of A12 did not flow at all indicating very poor flow properties. A60 itself, advertised as a direct compression excipient, showed improved flow properties compared to A12 [67], explaining the better flow properties of the PMs of A60 compared to A12. For the PMs containing A60, addition of Kolliphor P407 micro decreased the flow properties of A60, whereas P407 had no impact on the flowability of A60. Granules in general showed superior flowability compared to the PMs of A12, at increased flow with increasing binder content.

For A60, granulation decreased the flowability of A60 with increasing binder content (A60 P407 5% (w/w): 4.0 ± 0.2 and A60 P407 15%: 8.1 ± 0.4), which might be due to the more irregular shape of the granules compared to the spherical shape of unprocessed A60. However, all granules showed good flow properties, especially at binder levels of 10 % and above, enabling e.g. being processed on a commercial rotary tablet press.

3.6.4 **Scanning electron microscope images of the granules**

The predominant agglomeration process of the investigated mixtures is shown in the micrographs in Fig. 3.3. Using the backscattering detector, DI-CAFOS® appears brighter in the picture compared to the organic binder substances.

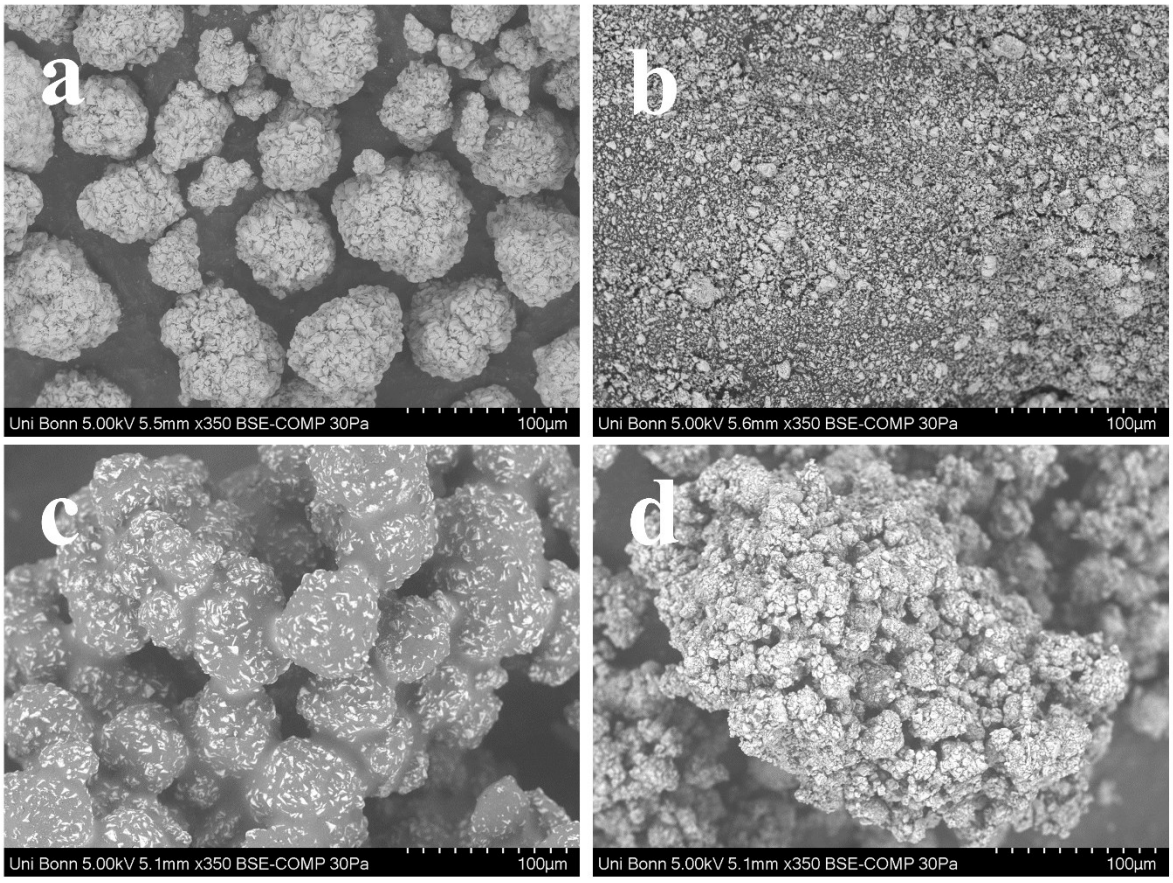

Fig. 3.3. SEM images using BSE-detector: (a) DI-CAFOS® A60; (b) DI-CAFOS® A12; (c) A60, Kolliphor® P407micro 10 % (w/w); (d) A12, Kolliphor® P407micro 10 %.

The intensity of the backscattered electrons, and therefore the brightness of the material, correlates with the atomic weight of the sample. In accordance with the primary particle size of the starting material DI-CAFOS® A, either the immersion (Fig. 3.3d) or the distribution mechanism (Fig. 3.3c) for granulation was predominant. For both types, the mechanism was independent of the binder's particle size (images not shown). In case of the larger primary particles (A60), the distribution mechanism has been predominant (Fig. 3.3c). When using A12, however, particles were rather located on the surface of the binder indicating a predominant immersion mechanism (Fig. 3.3d). For comparison, images of the starting materials A60 (Fig. 3.3a) and A12 (Fig. 3.3b) were added. In the case of A60 granules (Fig. 3.3c), bumps coming from the irregular surface structure of A60 are still appearing white, whereas the rest of the particle is coated with a thin layer of polymer. Using A12, small particles of dicalcium-phosphate are more located on the outside of the binder, indicating that immersion has taken place.

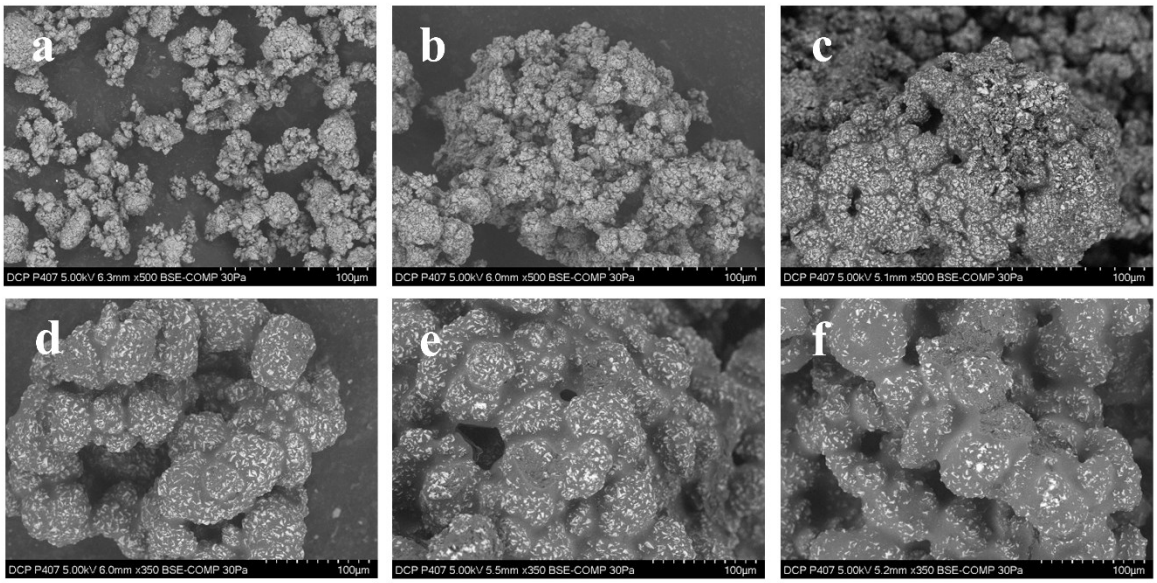

Fig. 3.4. SEM images using BSE-detector: (a) A12, Kolliphor® P407 5 % (w/w); (b) 10 % (w/w); (c) 15 % (w/w); (d) A60, Kolliphor® P407 5 % (w/w); (e) 10 % (w/w); (f) 15 (w/w).

The images comparing increasing binder content (Fig. 3.4) confirmed the previous finding for the predominant agglomeration mechanism. An increase in binder content was associated with a significant particle size enlargement during granulation. In the case of the immersion mechanism, particle size enlargement due to the formation of an increasingly greater continuous binder phase can be seen with increasing binder content (Fig. 3.4a, b, c). When using A60 (Fig. 3.4d, e, f), a size enlargement in accordance with the classical stages of wet granulation was observed. The stages changed from pendular at a weight fraction of 5 % (w/w) (Fig. 3.4d) to more funicular at 10 % binder (w/w) (Fig. 3.4e). At 15 % (w/w) binder, the capillary state was reached (Fig. 3.4f). This behaviour was also independent of the initial particle-size of Kolliphor® P407.

3.6.5 **Compression and Compaction Analysis**

In Fig. 3.5, the tabletability plots of the formulations investigated are shown. In most of the cases, the tablets made of granules (closed symbols) showed a higher TS than those produced from the respective PM (open symbols) with the exception of the combination of A60 and Kolliphor® P407 micro (Fig. 3.5a). Furthermore, tablets of A12 (Fig. 3.5b and d) generally showed higher TS in comparison to those of A60 (Fig. 3.5a and c). With increasing binder content, the TS of obtained tablets increased, too. This effect was more pronounced for the increase from 5 % to 10 % (w/w), than for 10 to 15 % (w/w) binder content when using A12 as filling material. An increase in binder weight fraction to 15 % for P407 and P407 micro in A12 did not improve the TS at higher compaction pressure (Fig. 3.5b and d), while 10 % (w/w) binder content resulted in increased TS values over the entire pressure range (Fig. 3.5b and d). Using a larger particle size of starting material (A60) resulted in lower TS (Fig. 3.5a and c). Only granulation with a binder content of 15 % (w/w) in the case of Kolliphor® P407 followed by a compaction with a pressure higher than 200 MPa resulted in TS greater than 2 N/mm².

Overall, the highest TS was reached when A12 was granulated with P407 or P407micro (Fig. 3.5b and d), resulting in a similar compaction profile. As expected, the resulting TS was not dependent on the initial particle size of the binder used for melt granulation. This finding was also the case for the A60 and both grades Kolliphor® P407 (Fig. 3.5a and c).

However, the enhancement in TS was never as high for A60 as in the case of A12. For A60 and Kolliphor® P407 micro, TS of the tablets prepared from the PM were similar to that of the tablets made of compressed granules (Fig. 3.5a). In contrast, using A12 (Fig. 3.5b) for granulation, a pronounced increase of tablet TS could be observed compared to tablet TS of the respective PMs.

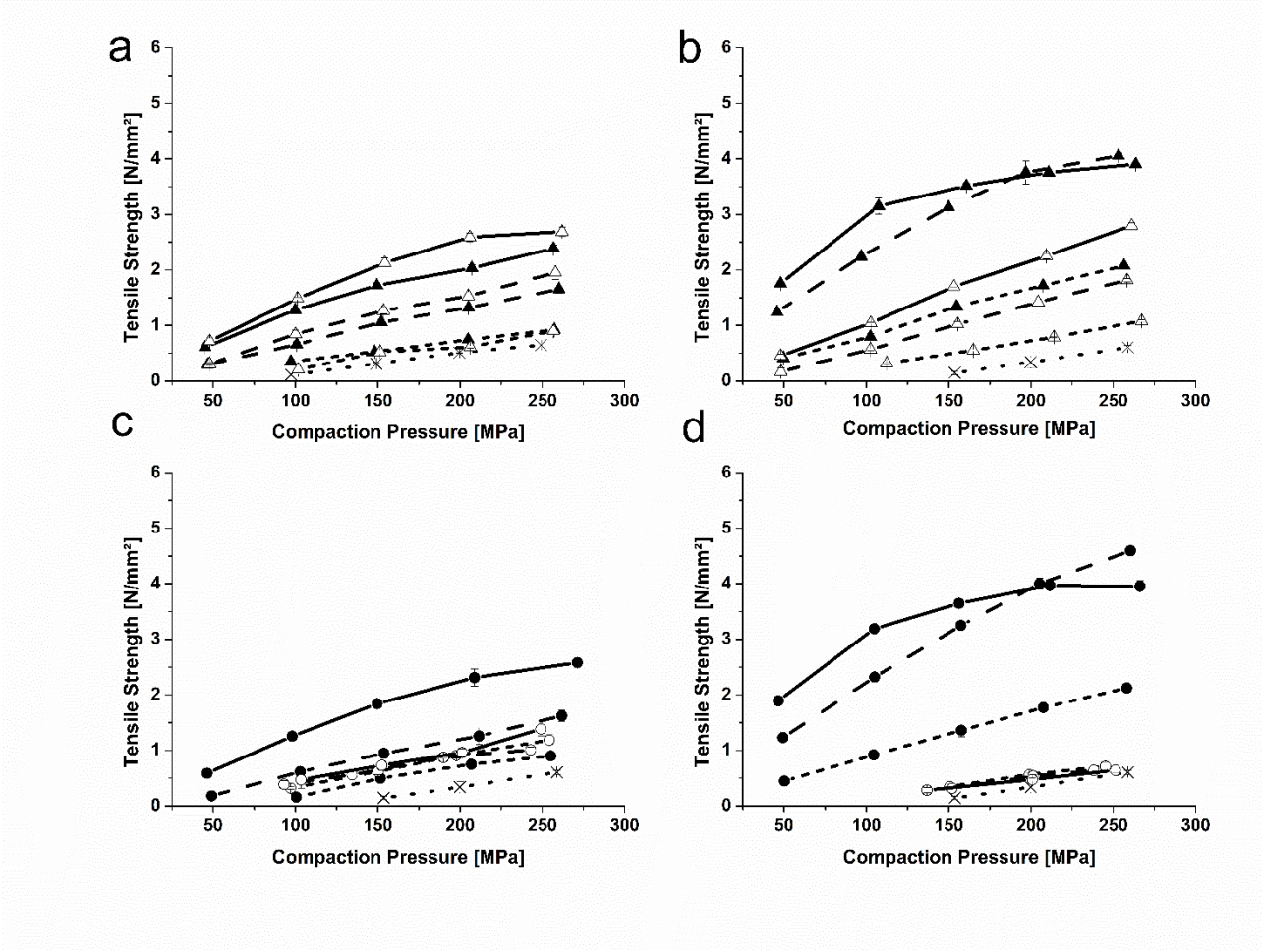

Fig. 3.5: Tabletability plots: (a, c) A60; (b, d) A12; (a, b) P407 micro; (c, d) P407; closed symbols: granules; open symbols: PM; cross: pure A12/ A60; dotted lines: 5 % (w/w), dashed lines: 10 % (w/w), solid lines: 15 % (w/w).

In the case of the PMs, Kolliphor® P407 did not substantially influence the TS compared to neat A12 (Fig. 3.5d). In contrast, PMs of A60 showed higher TS (5% (w/w): 0.91 ± 0.05; 10% (w/w): 0.87 ± 0.02 and 15% (w/w): 0.96 ± 0.07 at 200 MPa) compared to neat A60 (0.34 ± 0.11) independent of the binder concentration (P407) used (Fig. 3.5c).

However, this effect is difficult to evaluate as all PMs of coarse Kolliphor® P407 (d_{50} = 343 µm) and coarse filler (A60: d_{50} = 60 µm) showed strong segregation tendency. Using Kolliphor® P407 micro resulted in increasing TS with increasing binder concentration (Fig. 3.5a and b). For A12, the TS values of the PMs were always below the ones of the granules for equal binder concentration. However, for the combination of A60 and P407 micro (Fig. 3.5a), TS was higher for the PM (e.g. PM with 15% (w/w): 2.59 ± 0.08 and Gr with 15% (w/w) binder: 2.03 ± 0.06 at 200 MPa).
Compactibility plots (Fig. 3.6) showed increasing SF and increasing TS for the granules compared to the PM, except for the formulation containing A60 and P407 micro (Fig. 3.6a).
For granules of A12, a pronounced parallel shift in SF of approximately 0.05 comparing 10 % (w/w) binder content with 15 % (w/w) binder content (Fig. 3.6b and d) was observed. In case of the granules containing A12 and 15 % (w/w) of binder, a SF of approximately 1 is obtained, compared to the granules containing 10 % (w/w) of binder (Fig. 3.6b and d) and all granules produced with A60 (Fig.3.6a and c). The high SF of A12 granules at 15 % (w/w) of binder (Fig. 3.6b and d) explains the plateau of TS at 4.1 N/mm² and 4.0 N/mm² in the tabletability plot (Fig. 3.5b and d). In addition, high SF were achieved at low compaction pressure, resulting in a TS of 2 N/mm² at a compaction pressure even below 100 MPa for granules of A12 at a binder content of 10 % (w/w) and above (Fig. 3.5b and d).
Granules produced with A60 showed no pronounced shift in SF. Moreover, lower TS were achieved at similar SF ranges, when compared to the granules of A12.
Overall PMs showed lower TS and SF in the applied pressure range, except for the combination A60 and P407 micro (Fig. 3.6a), as mentioned above. However, TS and SF for PMs in general increased with increasing amounts of Kolliphor® P407 micro. This effect was more pronounced for A60 while A12 benefited more strongly from the granulation process (Fig. 3.5b). The use of Kolliphor P407 in PMs of A12 and A60 (Fig. 3.6c and d) resulted in a shift to higher SF without a great impact on the TS, indicating that bonding was not strongly influenced by using a coarse binder in the PM. High variability (SD) for PMs of P407 (Fig. 3.6c) were related to the high segregation tendency of the mixture containing A60 during die filling.

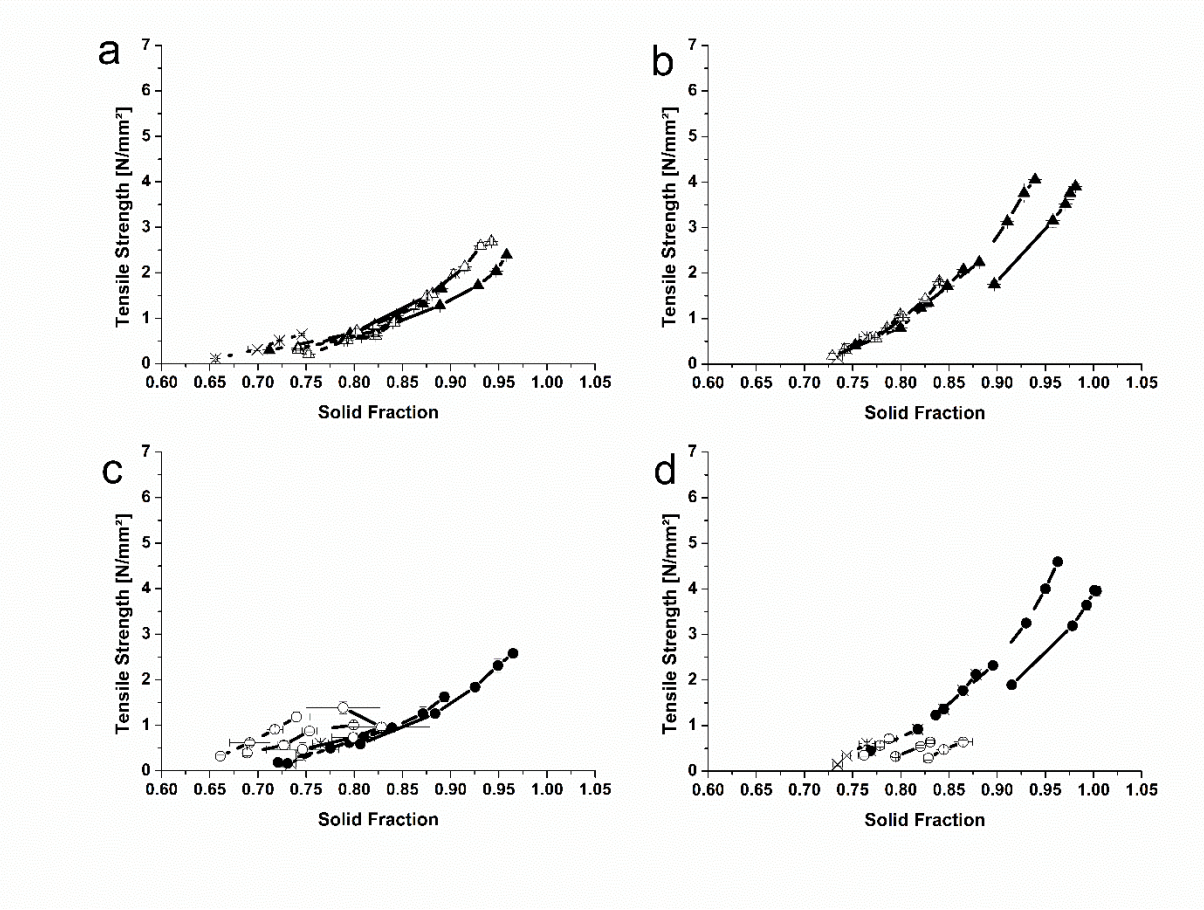

Fig. 3.6: Compactibility plots: (a, c) A60; (b, d) A12; (a, b) P407 micro; (c, d) P407; closed symbols: granules; open symbols: PM; cross: pure A12/ A60; dotted lines: 5 % (w/w), dashed lines: 10 % (w/w), solid lines: 15 % (w/w).

The compressibility plots for all formulations (PM and granules) are shown in Fig. 3.7. In general, SF increased with increasing binder content as already seen in the compactibility plots (Fig. 3.6), with the overall highest SF of approximately 1 resulting for granules containing A12 and 15 % (w/w) binder (Fig. 3.7b and d) and a SF of 0.96 already achieved at a pressure of 100 MPa.

In general, compared to the respective PM (below 0.85), granules exhibited a higher SF even at low compaction pressures, except for the combination of A60 and P407 micro shown in Fig. 3.7a. Here, granules and PM resulted in almost equal SF at the applied compaction pressure, indicating that granulation could not influence the compression behaviour of this mixture. However, granulation of the larger initial particle size of Kolliphor P407 (Fig. 3.7c) resulted in a similar compression profile to the granules produced from Kolliphor P407 micro (Fig. 3.7a).

Overall, granules comprising A60 had a lower SF, especially at lower compaction pressures compared to formulations containing A12. A SF of 0.96 was obtained at the maximum compaction pressure of 250 MPa for A60 granules with 15% (w/w) P407 and P407 micro. However, the SF was below 0.9 for these formulations when using a compaction pressure of 100 MPa. As described for the compactibility, the high variation (SD) of SF for the PM of A60 and P407 (Fig. 3.7c) can be explained by its high segregation tendency.

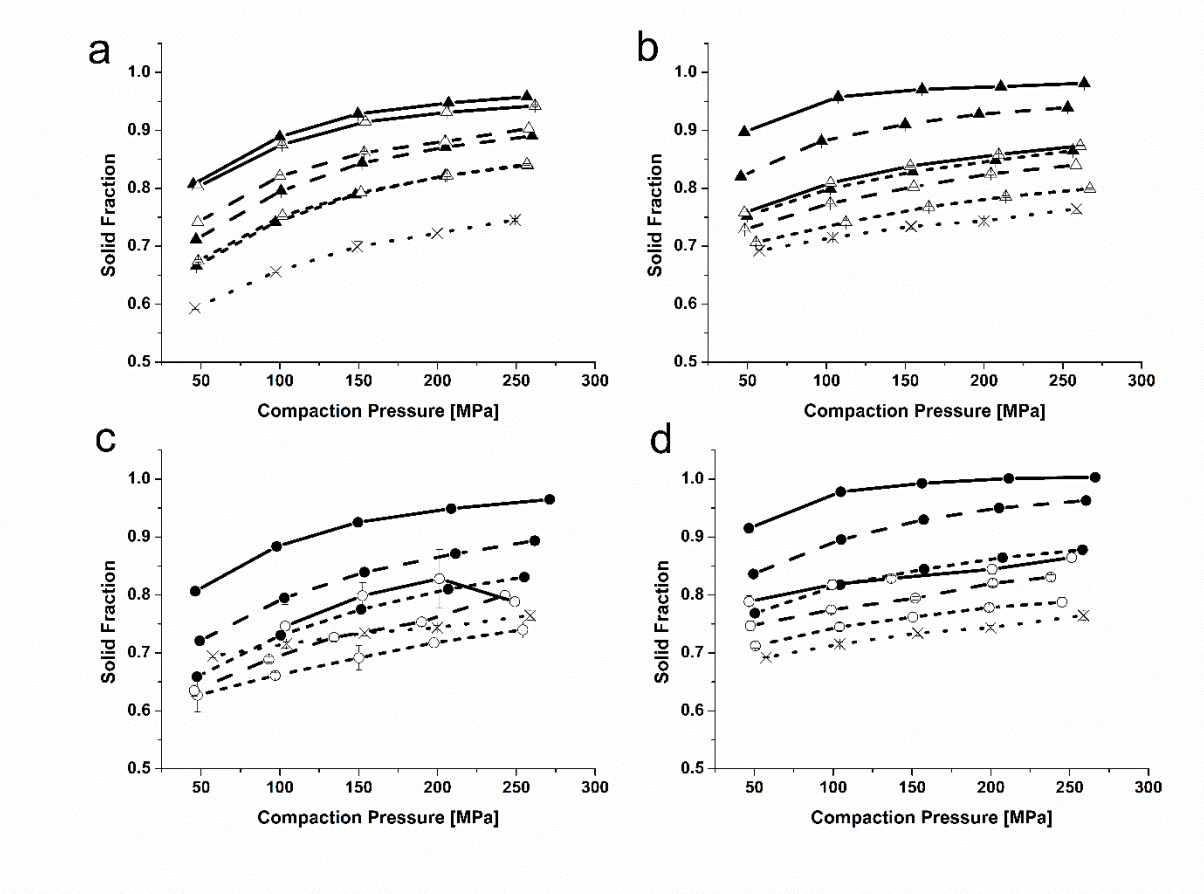

Fig. 3.7: Compressibility plots: (a, c) A60; (b, d) A12; (a, b) P407 micro; (c, d) P407; closed symbols: granules; open symbols: PM; cross: pure A12/ A60; dotted lines: 5 % (w/w), dashed lines: 10 % (w/w), solid lines: 15 % (w/w).

Compression and compaction analysis showed that using a small initial particle size of binder (Kolliphor P407 micro) and a large initial size of filler (A60) resulted in nearly equal TS and SF for the tablets produced of this combination.

Due to its small particle size, Kolliphor® P407 micro can be well distributed in the tablets when used as a part of the PM, and granulation had therefore almost no boosting effect on the TS or a change in SF in case of the coarse A60.

However, TS of the tablets produced from the granules with A12 were higher compared to those with the coarse filler A60. This effect could be explained by the smaller particle size of A12 compared to A60. Correspondingly, the larger specific surface are of A12 (1.25 m²/g) compared to A60 (0.25 m²/g) [67], resulted in a larger number of bonding points, as was already described for different particle sizes of sodium chloride and microcrystalline cellulose [68,69]. The difference in specific surface area explains the enhancement in TS for A12 granules when using the small binder Kolliphor P407 micro for granulation compared to the simple PMs, whereas for the coarse filler A60, no enhancement in TS was achieved. In case of the PM of A60 and P407 micro, the binder could be well distributed on and between the A60 particles by using only a simple mixing process. Similar effects were seen for different particle size fractions of methylcellulose as binding material and paracetamol [70].Further, only lower binder concentrations were necessary to “coat” the smaller surface of A60 and to reach a homogenous distribution compared to a material with a smaller particle size and larger specific surface area, like A12, where granulation could still increase tensile strength due to a further homogenization via melt granulation process and the favoured immersion mechanism.

When using 15 % (w/w) binder in combination with A12, a shift in the compactibility curves (Fig. 3.6b and d) can be seen. At the same time, TS of these formulations could not be improved with increasing compaction pressure (Fig. 3.5b and d) and SF was not further increased (Fig. 3.7b and d). However, with 10 % (w/w) binder, the TS could still be improved for the formulations containing the small filler A12. This shift in the compactibility curve to higher SFs was associated with a percolation threshold of 30 % (V/V) (Tab. 3.3) and implies a more dominant effect of the polymer. This threshold is supposed to be related to a continuous network of the polymer with a pronounced effect in the case of the immersion mechanism and the small particle size of the filling material (Fig. 3.4c). Comparing PM and granules formulations having the same mass fraction of binder, granulation increased the distribution of the binder and therefore facilitated formation of an infinite binder network throughout the tablet matrix, i.e. getting closer to or exceeding the percolation threshold.

It is described in the literature that reducing particle size of one component reduces the percolation threshold of the fine component [71–74]. In this respect, melting and subsequent distribution by high shear energy during twin screw processing can be

regarded as infinite reduction of particle size enabling the material to form a close network and lower the percolation threshold of the binder. Therefore, granules of A12 and 15 % binder showed only a moderate increase of TS exceeding a compression pressure of 100 MPa with identical values of 3.8 N/mm² for 200 and 250 MPa (Fig. 3.5b and d), indicating the formation of a close binder network at low compaction pressure. This finding is again likely related to the percolation threshold reached at 15 % (w/w) of binder (Tab. 3.3), facilitating eased plastic flow. However, porosity, indicated by the lower SF of these tablets, and defined as 1-SF= porosity ε, of the granules produced using A12 and 10 % (w/w) binder could still be decreased at higher compaction pressure, resulting in a higher TS (Fig. 3.5b and d). Obviously, the A12 contributes to a higher extent to the formation of mechanical strength compared to the binder, although not in a linear manner as pure A12 resulted in far lower TS (Fig. 3.5b, d). We hence propose that the employed binder exhibiting easy plastic flow at a level of 5 % facilitated easy rearrangement at reduced inter-particle friction. At binder levels below 15 %, the interaction between calcium phosphate particles are still decisive to govern the overall tablet TS. At 15 % binder level however, the TS was more strongly governed by the P407 and lower TS values resulted at SF exceeding 0.96.

In the case of A60, higher porosity (lower SF: max. 0.96 at 250 MPa for granules independent of binder particle size) was seen in the compressibility curves (Fig. 3.7a and c), especially at the lower compaction pressures. Due to the proposed distribution mechanism for A60 granules, the inside exhibited pure calcium phosphate with inherently higher porosity upon compression ([61], Fig. 3.7a, c).

It is therefore postulated that the formulations containing A12 exhibit a larger binder network, reducing the porosity of these granules compared to the granules with A60 as filling material. In the case of A60, particles are surrounded by a thin polymer layer (Fig. 3.3a), and internal porosity might still be present to a greater extent in comparison to the tablets made from the A12 formulations.

Overall, the tensile strength of the tablets obtained from granules was independent of the primary particle size of the binder, as the high shear energy applied during the melt granulation could result in a homogenous distribution of the binder regardless of its particle size. However, the primary particle size of the filler significantly influenced the tabletability of the granules. Within this context, increasing particle size led to an increased dominance of the binding mechanism and the neat binding capacity of the filler. In the case of A60, the binder could not contribute to a decreased friction between the fractions of one A60 particle (distribution mechanism of the binder). In contrast, granules of A12 and P407 were formed based on an immersion mechanism, i.e. each small A12 particle could easily relocate during bond formation, leading to higher TS compared to A60. At the same time, this mechanism explains a resultant optimum of binder concentration. Exceeding a certain threshold (here 10 %), the interaction between the filler particles is less pronounced, leading thereby to TS values decreasing towards those of pure binder (percolation threshold). Hence, for fillers facilitating a predominant immersion mechanism during granule formation, the influence of the filler's compression behaviour was reduced and the tabletability of the respective granules was dramatically improved.

3.6.6 **SEM investigation and EDX image analysis**

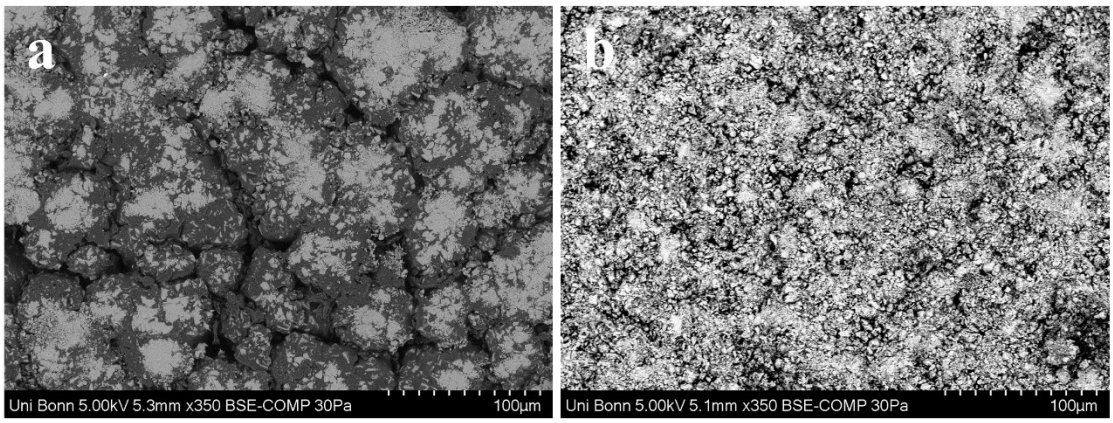

Fig. 3.8: Images of the tablet surface: (a): granules A60 P407 10 % (w/w); (b): granules A12 P407 10 % (w/w).

Prior EDX analysis, a SEM of the tablet surface was taken (Figs. 3.8 and 3.9). As shown by the example pictures of A60 and A12 with P407, tablets of granulated A60 (Fig. 3.8a) showed larger regions containing pure dicalcium phosphate, whereas tablets compressed from A12 showed homogenous surface structure (Fig. 3.8b). In the case of the distribution mechanism, primary dicalcium phosphate particles were embedded in the polymer (Fig. 3.8a), i.e. the internal structure consists mainly of neat dicalcium phosphate with absence of an intermeshing binder network. This led to a higher effect of the neat dicalcium phosphate behaviour, in terms of binding capacity and bond formation, in large regions and simultaneously explains the lower impact of granulation on increasing the TS (Fig. 3.5) compared to A12, as described above. This was also the case for the PM containing polymers with a large particle size, as shown by the example pictures at lower magnification using SE-detector of A60, A12 and P407 (Fig. 3.9c and d).

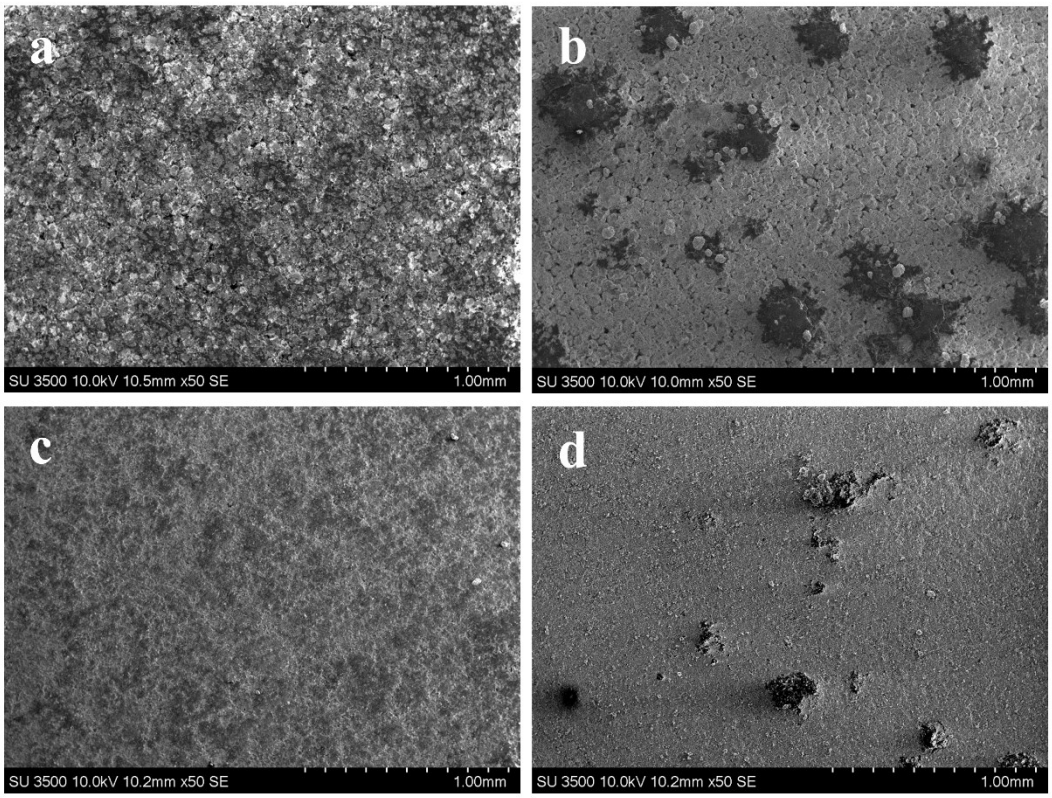

Fig. 3.9: Images of the tablet surface: (a): granules A60 P407 15 % (w/w); (b): PM A60 P407 15 % (w/w); (c): granules A12 P407 15 % (w/w); (d): PM A12 P407 15 % (w/w).

These larger volume units of neat calcium phosphate in the case of the formulations with A60 (d_{50} = 60 µm) strongly affected the tabletability, which resulted in a lower TS for PM and granules. Simultaneously, the larger areas of A60 explain the residual porosity (lower SF) of these compacts shown in the compressibility graphs (Fig. 3.7). However, when a filling material with small initial particle size was used for granulation (A12), the binder network was expected to be closer as in the case of a filling material with large particle size (A60). The mechanical strength of the tablet can be described as a function of the type of bonding force and the surface area over which these bonds are active [42]. Plastic deformation of the binding material promotes the formation of bonds during compaction and therefore enhances the TS. This behaviour has been shown for lactose polyvinylpyrrolidone granules produced with a two-step granulation technique to control the intragranular distribution of the binder [75].

Wikberg and Alderborn suggested that a homogenous intragranular binder distribution before compaction will result in binder interaction zones with a relatively narrow distribution in the resultant tablets. It should be noted that materials that do not undergo extensive fragmentation in the TSE or during the compaction process [61], as in our case, benefit from a small initial particle size prior to granulation. By virtue of the phenomenon described above, the small initial particle size will enhance the TS as a result of the formation of a narrow binder network in the absence of additional milling steps. Nevertheless, the importance of binder distribution is not limited to the mechanical properties of the tablets as discussed above. Van Melkebeke et al. (2006) showed that drug particles were finely dispersed in a molten matrix of PEG 400/ PEG 4000 and concluded that this microenvironment enhanced the dissolution profile of the formulation [3]. Additionally, Kowalski et al. (2009) showed that a thin coating of lipophilic binder could protect drug particles from moisture, while maintaining an immediate release profile [59]. A further study showed that only a polymer was needed to enhance the compactibility of metformin, and the tablets produced were not sensitive to a change in atmospheric moisture levels [2]. Moreover, Vasanthavada et al. (2011) used confocal Raman microscopic imaging to show that imatinib mesylate remained in an unmolten crystalline state and that the polymer was finely distributed on the surface and between the drug particles. They concluded that the observed distribution is responsible for a better compactibility, decreased friability and controlled release profile [4].

To confirm the findings of the tableting studies and to reinforce the hypothesis proposed to explain the results of the Kolliphor® micro-containing formulations, image analysis using an element specific mapping method was performed, where the binder distribution could be quantified using EDX-image analysis. Despite the potential to provide invaluable structural information, SEM/EDX has not been widely published for the characterization of pharmaceutical solid dosage forms. However, a few studies have benefited from the potential of EDX for the abovementioned purpose [76–79]. Vilhelmsen et al. (2005) used SEM/EDX to detect a poorly-water soluble drug in melt granules produced in a laboratory scale rotary processor. They were able to locate drug particles in cross-sections of the granules and to describe the predominant agglomeration mechanism by using different binder addition procedures [76].

Scoutaris et al. (2014) used this technique to characterize and compare tablets compressed from hot melt extrudates (premixed and non-premixed) with direct compressed tablet formulations. In case of the latter, X-Phase analysis showed the extensive mixing capabilities of the extrusion process and that the product is more homogenous if the formulation is premixed before extrusion [78]. In our study, carbon mapping was used to describe the binder distribution. In comparison to the filling material, the binder contained carbon as the representative element.

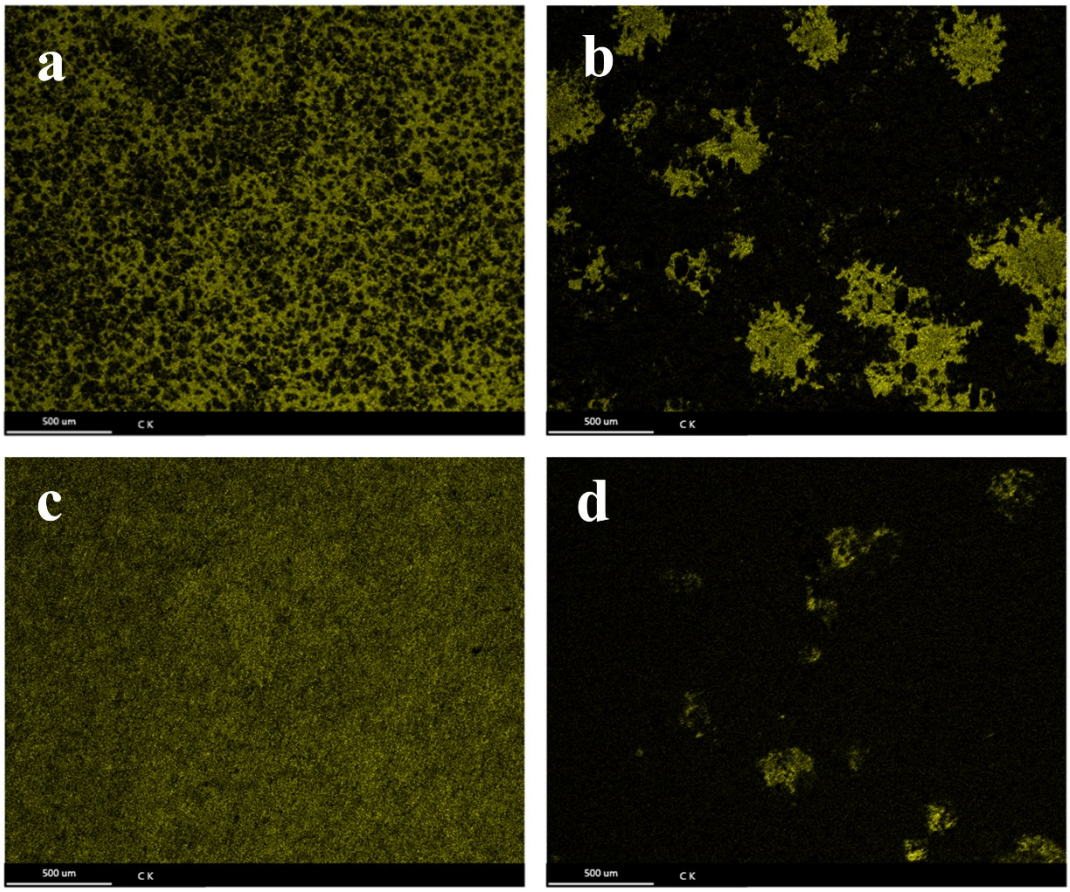

Fig. 3.10: Tablet surface SEM/EDX maps: (a): granules A60 P407 15 % (w/w); (b): PM A60 P407 15 % (w/w); (c): granules A12 P407 15 % (w/w); (d): PM A12 P407 15 % (w/w).

An example is given in Fig. 3.10 showing the tablet surface of Kolliphor® P407 15 % (w/w) in a combination with A60 and A12, showing the carbon signal of the binding material in yellow.

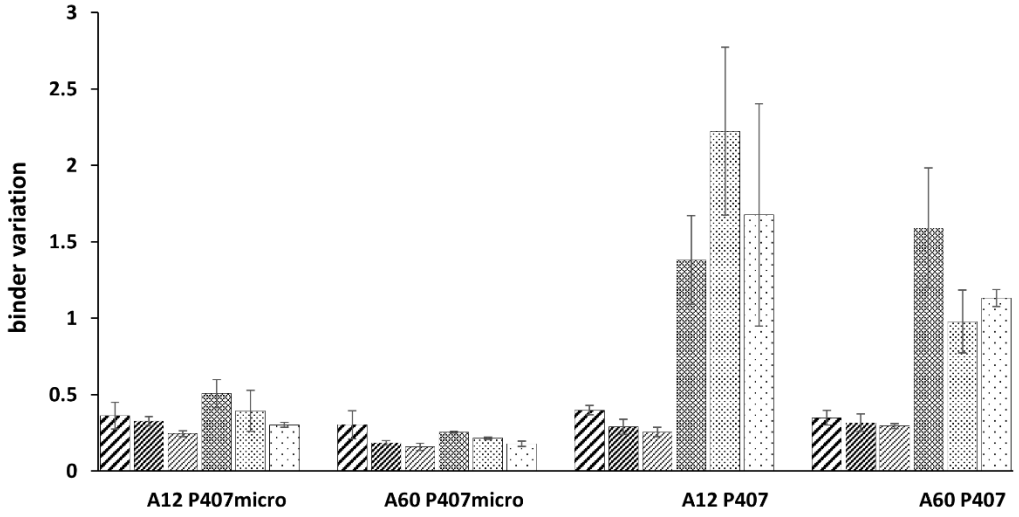

Fig. 3.11: EDX-Analysis showing the relative standard deviation as parameter for binder distribution: hatched charts: granules; dotted charts PM; bold: 5 % (w/w), middle: 10 % (w/w), fine: 15 % (w/w).

The diagram (Fig. 3.11) shows binder variation within and amongst the tablets of the different formulations under investigation. The lower the binder variation, derived from 3 tablet surfaces for each formulation divided in 35 sub-frames each, the better the distribution of binder in the tablet. Granulation increased homogeneous binder distribution, especially when using Kolliphor® P407, while the PM showed a high binder variation within one tablet (average value of binder variation, Fig. 3.11) and amongst the 3 tablets (high relative standard deviation, error bars in Fig. 3.11) compared to the granules. The high error bars in the case of the PMs show a high variation of the binder detected in the tablets, but also a high variation of the binder detected between the three tablet surfaces. A good distribution (low value of binder variation and small relative standard deviation) was observed for all granules, as was the case for the PM with Kolliphor® P407 micro.

This confirmed the hypothesis that the comparable tableting performance was due to the small particle size of Kolliphor® P407 micro, which enabled the material to be dispersed between the filler material particles. It should be noted that the compaction performance of both the granules and the PM was strongly dependent upon the quality of binder distribution. In other words, the primary role of the melt granulation within the context of improving the compaction performance was the optimal distribution of the binder based on the high mixing efficiency of the TSE, in combination with the initial particle size of the granulated material.

3.7 Conclusion

This study highlighted the potential of melt granulation to enhance the flowability, tabletability and compactibility of poorly compactable materials. While using fine grade filler resulted in granules formation via immersion mechanism showing superior tabletability, coarse filler particles were agglomerated through distribution mechanism, resulting in greater dominance of the neat filler material during compaction. A comparison of tabletability between the granules and the PMs, revealed the property to be mainly dependent on the binder distribution and the primary particle size of the filler rather than the process of granulation. Binder distribution was examined and quantified using image analysis of SEM/EDX carbon maps. These analyses showed the major role of binder distribution in determining the tabletability of the formulations under investigation. Even in a single case, where comparable tabletability and binder distributions were obtained in case of the PM and granules of A60 and P407 micro, the powder flow properties of the PM were inferior to the granules, unlikely to support potential commercial scale tablet production. Needless to say, while using this technique for granulation, attention should be payed to the initial particle size of the material to be agglomerated and the level of melt binder during the formulation development process, as these substantially impact the product performance. Nevertheless, the impact. of shear stress (screw speed and screw configuration), mean-residence time (e.g. throughput), viscosity of the melt binder, which also includes granulation temperature and material attributes of the filler (e.g. brittle or plastic deformation behaviour) needs to be further investigated, as they likely have additional impact on the granule attributes. Moreover, the impact of different particle-size distribution of the granules containing a comparable binder content, needs to be investigated, as it might affect tablet performance and potential lubricant sensitivity.

3.8 Acknowledgments:

The authors kindly thank Romaco/Kilian and Medelpharm for providing the single-punch compression simulator Styl'One Classic 105 ML. We would also like to thank Rachel C. Evans and Maryam Shetab Boushehri for reviewing the manuscript.

3.9 List of symbols and Abbreviations

APIs:	active pharmaceutical ingredients	
BSE:	backscattered electrons (detector)	
d:	diameter of the tablet	[mm]
D:	diameter of extruder	[mm]
EDX:	energy dispersive X-ray	
F:	crushing strength.[N]	
h:	thickness of the tablet	[mm]
L:	length of the extruder	[mm]
m:	tablet weight	[mg]
P_{app}:	apparent density	[mg/mm³]
P_{true}:	true density	[kg/cm³]
PEG:	polyethylene glycol	
PM:	physical mixture	
s_{rel} :	relative standard deviation	
SD:	standard deviation	
SEM:	scanning electron microscope	
SF:	solid fraction	
TS:	tensile strength	[N/mm²]
TSE:	twin-screw extruder	
V_p:	volume of the compact	[mm³]

4 Compression Behavior of Granules Produced via Twin-Screw Melt Granulation: Effect of Initial Particle Size on Granulation Efficiency

Kristina E. Steffens; Karl G. Wagner

This part was published as:

Steffens, Kristina E., and Karl G. Wagner. "Compression behaviour of granules produced via twin-screw melt granulation: Effect of initial particle size on granulation efficiency." Powder Technology 374 (2020): 430-442.

DOI: 10.1016/j.powtec.2020.07.037

4.1 Graphical abstract

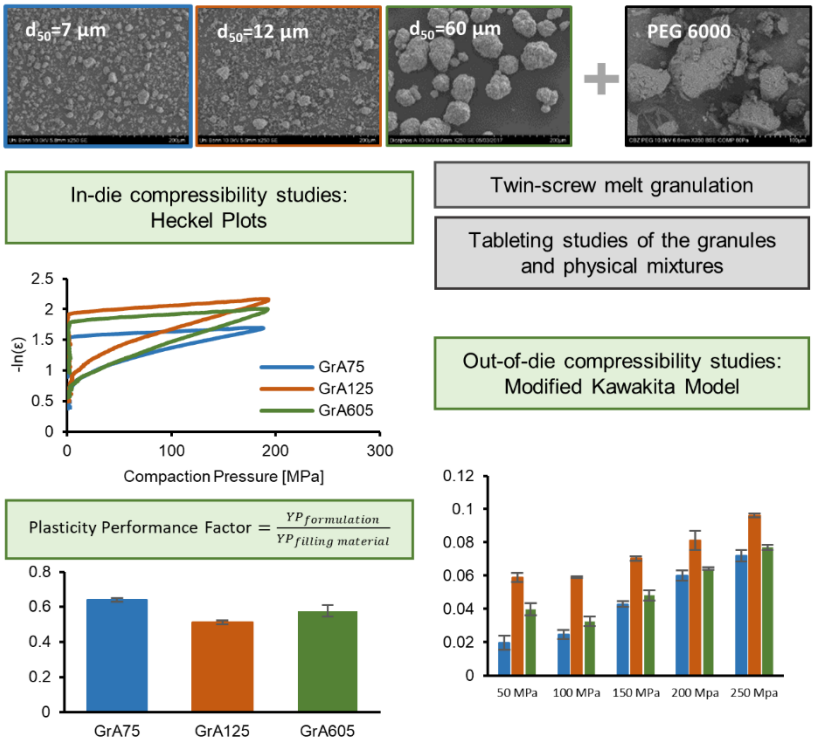

4.2 Abstract

This study focuses on the impact of initial particle size on the tabletability and the deformation behaviour (i.e. plasticity) of granules produced by twin-screw melt granulation (TSMG). As model substances, three different grades of anhydrous dicalcium phosphate (aDCP) were melt granulated with polyethylene glycol 6000 (PEG) using a twin-screw granulator. Compaction performance of the granules and the corresponding physical mixtures (PM) was evaluated by in-die and out-of-die compaction analysis. A major impact on granules deformation behaviour was found for the relation of the specific surface area of the filler material to the binder content. A relative yield pressure (YP) was introduced to describe the enhancement in plastic deformation behaviour, defined as the plasticity performance factor (PPF). Furthermore, a modified Kawakita model was used to describe the granulation efficiency, compared to a calculated physical mixture model. Granules under investigation showed an increased plastic deformation, enhanced tabletability and reduced elastic recovery (ER). The binder was shown to be finely distributed and to fill

the voids between the aDCP particles (image analysis of the carbon energy dispersive X-ray maps). A small initial particle size of filler material (DI-CAFOS®A7 and A12) was more efficient than a larger particle size (DI-CAFOS® A60). A very low particle size (DI-CAFOS® A7) required the addition of 1% (w/w) colloidal silicon dioxide to enable feeding of the material into the granulator. Moreover, due to the larger surface area of these particles, a higher amount of binder was necessary to achieve a low PPF and a high tensile strength (TS).

4.3 Keywords

Twin-screw melt granulation, tabletability, primary particle size, plasticity performance factor, kawakita model, heckel analysis

4.4 Introduction

Besides classic wet and dry granulation methods, melt granulation is an alternative technique to agglomerate powders or formulations to enhance critical quality attributes, e.g. flowability, compactibility and content uniformity. With growing interest in continuous processing methods, that are suitable for high drug loads or moisture sensitive active pharmaceutical ingredients (APIs), twin-screw-melt granulation (TSMG) was focused in the past years. Different groups reported several advantages of this alternative technique, including improved or modified dissolution, lower demand of excipients for further tablet production, high stability at high moisture level and increased tabletability [2,36,37,59,60,80,81]. In order to compare granules performance during further processing into tablets, most studies [36,37,81] determine tabletability, compactibility and compressibility. *Tabletability* is the ability of a powder to be transformed into tablets with a certain tensile strength (TS) under the applied compaction pressure. Tablet mechanical strength mainly depends on the number of contact points and on the attraction forces between the particles [42]. Therefore, the solid fraction (SF), which describes the apparent density of the compact in relation to the pycnometric density of the compressed material, is an important parameter when different formulations are compared. The *Compactibility* describes the resulting TS of the compact as a function of SF. It is therefore a descriptor for the number of bonding points or the binding force formed during the tableting process, whereas the

compressibility is defined as the ability of a powder to reduce volume under pressure (SF vs. applied compaction pressure).

During tableting three different states of the compression can be distinguished. First state is rearrangement, which results in a lower volume of the powder. Secondly, fragmentation of agglomerates of the primary particles may occur. At the same time, irreversible plastic deformation and reversible elastic deformation of the material can take place during the compression cycle, influencing both the resulting TS and SF of the compact. Brittle materials are known to undergo intensive fragmentation during compression. This fragmentation can improve TS, mainly due to the formation of a large new surface area, which is available for more binding forces. Furthermore, a rough surface structure increases the tablet hardness. For highly plastic materials, especially for those materials with this rough surface, e.g. microcrystalline cellulose, TS can be substantially high. On the other hand, elastic deformation during compaction can lower TS.

Compression analysis (either as in-die or out-of-die analysis) can provide a deeper understanding of the deformation behaviour of the investigated materials under pressure. The most commonly used compression models where developed by Heckel and Kawakita and Lüdde [43,48].

The Heckel-equation assumes that a volume reduction by plastic deformation follows a first order kinetic in the applied pressure range. However, for pharmaceutical powders the Heckel-plot often shows a curvature in the lower pressure range. This is caused by rearrangement of the particles in the die and/or brittle fragmentation in the case of non-plastic materials. Further deviations from a linear compression behaviour are caused by elastic deformation, which can be described by analysing the decompression phase [50,82].

Until now, few studies were dedicated to the comparison of simple physical mixtures (PM) and melt granules in dependence of their deformation behaviour during tableting. Furthermore, an analysis of the important respective influencing factors on their increased compactibility as well as the material dependent background (e.g. particle size of the filler and the binder content) is missing.

The deformation behaviour of granules from pharmaceutical powders was often described with the Heckel-equation [83–88]. The application of the Heckel-equation to granulated material is not trivial as their effective density might change during

compaction [89]. However, as a main focus in granulation is to improve the flowability and tabletability/compactibility of brittle materials, the Heckel model seems to be a suitable model to compare the change in yield pressure, i.e. the change in plasticity, by comparing the yield pressures of physical mixtures and melt granules based on the calculated pycnometric density of the composition from the densities of the single components.

The Kawakita-model assumes that the material under pressure is in an equilibrium at all stages of the compression cycle and that the product of volume and pressure is constant. In contrast to the Heckel-equation, it provides appropriate results over the entire pressure range. However, the initial powder volume, which is needed for the calculation, is highly sensitive to the applied pressure and difficult to determine accurately [90]. A modified Kawakita-model was validated by our group for predicting solid fractions of binary powder mixtures using various fractions of pre-agglomerated lactose and microcrystalline cellulose [91]. We chose a modified approach where the model was referenced on the lowest possible volume. Using the modified Kawakita-model, the initial volume can be determined simply by measuring the pycnometric density. Both methods can provide a deeper understanding of the compression behaviour during tableting and the mechanism of bond-formation. Prerequisites for any compression analysis are accurate determination of compaction pressure and tablet height. The tablet height is recorded either *in situ* during the compression (in-die) or after a specified period after ejection (out-of-die). For in-die analysis of the compact apparent volume under pressure, an instrumented tablet press is used. For evaluation, the deformation of the punch and the tablet press during compaction needs to be determined accurately to allow precise measurements of the tablet height during compaction. Using this method the minimal height of the tablet during compaction and reversible relaxation phenomena can be described *in situ*. Using the out-of-die method tablet dimensions are measured after a fixed period of time. This method includes reversible elastic relaxation phenomena, that occur during and immediately after the compression cycle [92]. However, it cannot distinguish between fast/immediate and slow elastic recovery.

The current study sought to compare PM and granules produced via TSMG, using raw materials of poor compactibility. Different initial particle sizes of the model excipient anhydrous dicalcium phosphate (aDCP) were investigated to highlight the important

role of the starting materials' particle size on the compression behaviour of the granules made thereof and to provide a deeper understanding of their deformation mechanism during tableting.

In the case of direct compression, aDCP causes comparatively low TS in the relevant pressure range for tableting without prior granulation. The investigated model substances were known to show less fragmentation and binding capacity than other dicalcium phosphate grades [61].

To define the enhancement in compactibility and compressibility gained via the TSMG process, theoretical SF of the tablets produced from a simple binary mixture was estimated using the modified Kawakita-model [91]. This theoretical SF was compared to the SF of the tablets produced from the granulated material and residuals were used to describe the granulation efficiency in terms of compressibility enhancement, using the out-of-die compression data. The existing model of Schmidtke et al (2017) was verified for all PMs investigated in our study. In-die compressibility data were used to describe the deformation characteristics by means of the Heckel equation [43]. The reduction yield pressure (*YP*) was used to describe change of the deformation characteristics to a more plastic deformation behaviour [93]. To provide a better comparability of the data obtained *YP,* was calculated as a relative value with regard to the *YP* of the filler material, defined as the plasticity performance factor (*PPF*). Additionally, the binder distribution was quantified by image analysis of carbon energy dispersive X-ray maps [81]. Elastic recovery (ER) was evaluated comparing in-die and out-of-die measurement data of the tablet height after 24 h of storage. With respect to the granulation process, granules deformation characteristics during tableting and the mechanical quality attributes of the tablets were compared with tablets made from a simple PM.

4.5 Material and methods

4.5.1 Material

As model substance with low compactibility and high degradation temperature, three different grades of anhydrous dicalcium phosphate (aDCP) with different particle sizes (DI-CAFOS® A7, A12 and A60) were investigated. All DI-CAFOS® types were kindly donated by Chemische Fabrik Budenheim KG (Budenheim, Germany). Polyethylene glycol (PEG) 6000 (melting point = 55-60 °C) was purchased from Carl Roth (Karlsruhe, Germany) and used as binder. Granulation of DI-CAFOS® A7 required the addition of 1% (w/w) colloidal silicium dioxide (AEROSIL® 200) which was a kind gift from Evonik (Evonik Industries AG, Hanau-Wolfgang, Germany).

4.5.2 Methods

4.5.2.1 Preparation of physical mixtures (PM)

All DI-CAFOS® types (A7; A12 and A60) were formulated with PEG 6000 in concentrations of 5, 10, and 15% (w/w). A7 required the addition of 1% (w/w) colloidal silicium dioxide to enable feeding of the material into the granulator. PMs in 100 g batch size were prepared using a Turbula blender (Willy A. Bachofen AG Maschinenfabrik, Switzerland), rotating at 50 rpm for 10 min. The obtained PMs were subsequently granulated in the twin-screw granulator. Short names used for the PMs in text and graphics of this study, are given in Tab. 4.1.

Tab. 4.1: Short names of the physical mixtures.

Mixture	Short name
PM 94% (w/w) A7 + 5% (w/w) PEG 6000 + 1% (w/w) Aerosil®	PMA75
PM 89% (w/w) A7 + 10% (w/w) PEG 6000 + 1% (w/w) Aerosil®	PMA710
PM 84% (w/w) A7 + 15% (w/w) PEG 6000 + 1% (w/w) Aerosil®	PMA715
PM 95% (w/w) A12 + 5% (w/w) PEG 6000	PMA125
PM 90% (w/w) A12 + 10% (w/w) PEG 6000	PMA1210
PM 85% (w/w) A12 + 15% (w/w) PEG 6000	PMA1215
PM 95% (w/w) A60 + 5% (w/w) PEG 6000	PMA605
PM 90% (w/w) A60 + 10% (w/w) PEG 6000	PMA6010
PM 85% (w/w) A60 + 15% (w/w) PEG 6000	PMA6015

4.5.2.2 Twin-screw melt granulation (TSMG)

TSMG was performed using a co-rotating twin-screw extruder/granulator (ZE12, Three-Tec GmbH, Seon, Switzerland) with a functional length of 25:1 L/D (length/diameter) and 12 mm screw diameter. The granulator barrel consisted of five individually adjusted heating zones to ensure sufficient melting and distribution of the binder. The screw and barrel temperatures used are given in Fig. 4.1. The process temperature was set up to 95 °C in the high shear region of the granulator screws (30°, 60°, 60° and 90° 4-disc-kneading elements).

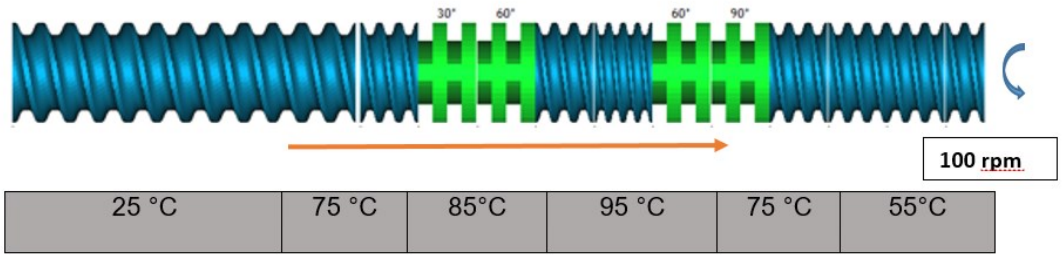

Fig. 4.1: Granulation conditions and screw configuration used (Ludovic® simulation software, Saint-Etienne, France).

At the terminal zone of the barrel, the temperature was reduced to 55 °C to allow solidification of the material. During melt granulation, the screw speed was set to 100 rpm and no die plate was mounted at the end of the extruder barrel. A volumetric feeder system ZD9 (Three-Tec GmbH, Seon, Switzerland) was used to enable a constant feed rate of 0.2 kg/h. Prior compaction, obtained granules were hand-sieved with a 2 mm laboratory sieve (Kressener-Sieb, Wepa Apothekenbedarf GmbH & Co KG,Hillscheid, Germany). In Tab. 4.2, short names of the obtained granules are listed. These declarations were further used in text and graphics.

Tab. 4.2: Short names of the granules.

Granules	Short name
Granules 94% (w/w) A7 + 5% (w/w) PEG 6000 + 1% (w/w) Aerosil	GrA75
Granules 89% (w/w) A7 + 10% (w/w) PEG 6000 + 1% (w/w) Aerosil	GrA710
Granules 84% (w/w) A7 + 15% (w/w) PEG 6000 + 1% (w/w) Aerosil	GrA715
Granules 95% (w/w) A12 + 5% (w/w) PEG 6000	GrA125
Granules 90% (w/w) A12 + 10% (w/w) PEG 6000	GrA1210
Granules 85% (w/w) A12 + 15% (w/w) PEG 6000	GrA1215
Granules 95% (w/w) A60 + 5% (w/w) PEG 6000	GrA605
Granules 90% (w/w) A60 + 10% (w/w) PEG 6000	GrA6010
Granules 85% (w/w) A60 + 15% (w/w) PEG 6000	GrA6015

4.5.2.3 Pycnometric Density

Pycnometric density was measured for the raw materials using the AccuPyc 1330 helium pycnometer (Micromeritics GmbH, Aachen, Germany). The raw materials were milled using a ball mill 400 MM (Retsch GmbH, Haan, Germany) for 10 min at 20 Hz. The chamber of the pycnometer was purged 20 cycles prior to analysis. A fill pressure of 136.86 kPa and an equilibration rate of 0.0345 kPa/min were set for measurements. Cycles were repeated up to 25 times or until a standard deviation of 0.01% was reached. The pycnometric density of the PMs and granules was calculated by their weight fraction. The pycnometric density was required for the calculation of the solid fraction (SF) and the Heckel-analysis.

4.5.2.4 Specific surface area analysis (BET)

The specific surface area was measured by a multipoint BET (Brunnauer, Emmert and Teller)-method using the equipment Nova 3000 (Quantachrome Instruments, USA). Before analysing the probe with nitrogen as adsorbate, it was degassed for 60 min.

4.5.2.5 Tableting/ In-die-analysis

Tablets (n = 5) were compressed on a single punch tablet press (StylOne Classic 105 ML, Medelpharm, Beynost, France/Romaco Kilian, Cologne, Germany) with a 8 mm flat-face tooling. Five equidistant levels of compaction pressures from 50 MPa to 250 MPa were applied at constant tableting speed (dwell-time: 6-7 ms; compression time on average: 110 ms). The die was filled manually and lubricated with magnesium stearate powder externally, if needed. For the displacement measurement, the tablet press was equipped with four external displacement transducers, which enabled an accuracy of ± 1 µm.

The compression behaviour of pure A7, A12 and A60 as well as the respective PM and granules made thereof were studied by means of the Heckel-Analyzer software (Mathias-Hucke-Software, Solingen, Germany). The displacement data, tablet weight and pycnometric density were used for the porosity calculation of the in-die powder bed as a function of compression pressure, as described by Heckel [43],

$$\ln\left(\frac{1}{1-SF}\right) = -\ln \varepsilon = kP + A \qquad \text{(Eq. 4.1)}$$

Where *SF* is the relative density at pressure *P*; *k* and *A* are material-dependent constants.

Variable *A* represents the intercept of the linear part of the Heckel-plot and can be interpreted as the porosity (ε), where first bonding occurs. SF_A is defined similar to its corresponding solid fraction (1-ε = SF).

The Heckel-analysis was performed for five tablets at a maximum pressure of 200 MPa. The tablets were subsequently weighed after ejection, using an analytical balance (AG 204, Mettler Toledo GmbH, Gießen, Germany). SF was calculated by dividing the apparent density, calculated from the displacement data, by the pycnometric density measured with the helium pycnometer. The displacement data were corrected by the elastic deformation of the tablet press (0.006 kN/µm) to enable an accurate measurement.

Data were fitted in a pressure range of 70 MPa out of the 200 MPa using linear regression method. The optimum position of these 70 MPa range, within the compression part of the Heckel-plot, was selected via the best correlation coefficient for the linear regression. Prior to linear regression of the $-ln\varepsilon$/compression data set, compression pressure values were selected equidistantly in order to ensure homoscedasticity. The procedure was performed automatically by the software Heckel-Analyzer (Mathias Hucke Software, Solingen, Germany). The first point of the linear slope is defined by the compaction pressure (P_{fit}) and the solid fraction (SF_{fit}).

The decrease in porosity ($\frac{1}{1-SF}$) during compression follows a first order kinetic. In a semi-logarithmic scale, the linear part of the Heckel-plot can be used to calculate the slope *k*. The reciprocal of *k* is a material related constant named yield pressure (*YP*). The *YP* is inversely correlated to the plastic deformation of the material [94].

Moreover, a relative *YP* was calculated, defined as the plasticity performance factor (*PPF*):

$$PFF = \frac{YP_{formulation}}{YP_{filling\ material}} \qquad \text{(Eq. 4.2)}$$

It describes the enhancement in plastic deformation in relation to the pure material without binder (e.g. A7; A12 or A60). The parameter was used to describe the influence of the binding material (PEG 6000) on reducing the initial *YP*. It is therefore a descriptor for the extent of influence of PEG 6000 on the deformation behaviour, either used in a simple PM or in a formulation that underwent the melt granulation process.

4.5.2.6 Out-of-die-analysis

After 24 h of storage, the tablets were analysed by means of their tablet weight (analytical balance, AG 204, Mettler Toledo GmbH, Gießen, Germany), height (Mitutoyo Absolute ID C125B, Mitutoyo Deutschland GmbH, Neuss, Germany), diameter and hardness (Erweka TBH 210, Erweka GmbH, Heusenstamm, Germany). TS and SF were calculated from the data obtained. TS is the tablet hardness normalized by the dimension of the tablet and is therefore independent of its geometry [64],

$$TS = \frac{2F}{\pi dh} \qquad \text{(Eq. 4.3)}$$

Where *F* is the breaking force, *d* the diameter and *h* the height of the tablet.
SF represents the apparent density (ρ_{app}) of the compact, calculated from tablet weight (*m*) and its volume, relative to the pycnometric density (ρ_{pyc}) of the powder.

$$SF = \frac{\rho_{app}}{\rho_{pyc}} \qquad \text{(Eq. 4.4)}$$

$$\rho_{app} = \frac{m}{Vp} \qquad \text{(Eq. 4.5)}$$

$$V_p = \pi * \left(\frac{d}{2}\right)^2 * h \qquad \text{(Eq. 4.6)}$$

V_p is the volume of the compact (round; biplanar), calculated from *d and h,* which describe the tablet diameter and height, respectively.

4.5.2.7 The modified Kawakita model

The original Kawakita-model [48] describes the volume reduction of a powder in a linearized form, were *P* is the applied pressure and *a* and *b* are constants.

$$\frac{P}{C} = \frac{P}{a} + \frac{1}{ab} \qquad \text{(Eq. 4.7)}$$

C is the relative volume decrease, calculated from the initial volume V_0 and the volume V_p under pressure *P*:

$$C = \frac{V_0 - V_p}{V_0} \qquad \text{(Eq. 4.8)}$$

Unfortunately, determination of the initial volume of the material (V_0) is often difficult [50]. According to Schmidtke et al., the degree of volume reduction (*C*) can be replaced by the SF. V_0 was changed to V_{min}, which can be simply determined via helium pycnometry, resulting in the following equation, where initial particle size is negligible, and the initial volume is only material-dependent [91]:

$$\frac{P}{SF} = \frac{P}{a} + \frac{1}{ab} \qquad \text{(Eq. 4.9)}$$

In the modified Kawakita-model, *a* represents the maximum SF that is achievable for the material. The reciprocal of *b* describes the pressure [MPa] to reach *a*/2 and can be interpreted as a deformation capacity [95]. *a* and *b* were determined for the pure materials (A7, A12, A60) using a linear regression method of the out-of-die SF data at the applied pressure *P* (Origin Pro 8G, OriginLab Corporation, USA). According to Schmidtke et al., the SF calculation of a mixture, based on *a* and *b*, can be estimated by a simple mass fraction (% w/w) of the pure components. They used the model to estimate SF of PMs from microcrystalline cellulose (MCC), pre-agglomerated lactose and carboxymethylcellulose sodium.

In this study the residuals of the predicted values using this simple mixture model, were used to describe the enhancement in compressibility obtained from the TSMG process. Moreover, the model was validated for mixtures with low content of one component (5; 10; 15%), exhibiting contrary compression behaviour (brittle vs. plastic), by comparing the data obtained for the PM.

4.5.2.8 Elastic Recovery (ER)

ER was calculated as percentage of the measured tablet height ($h_{out\text{-}of\text{-}die}$) after 24 h of storage at 25 °C for all tablets compressed with a compaction pressure of 200 MPa, in relation to the minimal corresponding in-die tablet height ($h_{in\text{-}die}$), corrected by the punch deformation (0.006 µm/kN).

$$ER = \frac{(h_{in-die} - h_{out-of-die})}{h_{in-die}} * 100\% \qquad \text{(Eq. 4.10)}$$

4.5.2.9 Binder variation

A scanning electron microscope (SEM) (SU 3500, Hitachi High Technologies, Krefeld, Germany), equipped with an energy dispersive X-ray detector (EDX) (EDAX Element-C2B, Ametek, Weiterstadt, Germany) was used to analyse the distribution of the binder. The samples were compressed with a pneumatic hydraulic tablet press (FlexiTab, Röltgen GmbH & Co. KG, Solingen, Germany) using 8 mm round flat-face tooling and a compaction pressure of 250 MPa to obtain a flat tablet surface. The tablets were further fixed on carbon paste and the analysis was performed without any coating. The surface of the tablets was mapped at high vacuum mode with an acceleration voltage of 10 kV and a magnification of 50x (total area: 5 mm²). Working distance was kept constant at 10 mm ± 0.5 mm. To parameterize the distribution of the binder, obtained micrographs from the EDX software containing the carbon signal only (512x400 pixels), were divided into 35 sub-frames (80x73 pixels). The percentage area of binder in each of the 35 sub-frames was calculated using image editing software ImageMagick 6.9 (ImageMagick Studio LLC). The relative standard deviation of the average area of the binder from all 35 sub-frames was calculated. This relative binder variation (calculated as relative standard deviation (s_{rel})) was taken as a value for describing the binder distribution. Low levels indicate homogeneous binder distribution, while high levels would represent high variation of binder distribution within the 35 sub-frames, i.e. inhomogeneous binder distribution. For every formulation, three tablets were analysed in total for mean value and standard deviation calculation of this distribution value, defined as the binder variation.

4.6 Results and Discussion

4.6.1 Density and BET measurement

Tab. 4.3: Pycnometric densities and the specific surface areas of the raw materials.

	A7+1% (w/w) Aerosil®	A12	A60
Pycnometric density [g/cm³]	2.9052 ±0.0035	2.8941 ±0.0008	2.8717 ±0.0022
Specific surface area [m²/g]	3.0171 (R^2=0.9998)	1.1965 (R^2=0.9999)	0.225 (R^2=1)

Tab. 4.3 shows the pycnometric densities and the specific surface areas of the excipients investigated. The specific surface area was increasing with smaller particle sizes, resulting in a ratio factor of 2.5 between A7 and A12 and 5.3 for A12 and A60.

4.6.2 Tabletability

The tabletability plots (compaction pressure vs. TS) of the PMs and granules from A7, A12, and A60 formulations are shown in Fig. 4.2. In general, tablets made of granules exhibited higher TS than those produced from the corresponding PMs. TS was found to increase as a function of increasing binder content. Furthermore, a small initial particle size of aDCP achieved the highest TS results, when a binder content of 15% (w/w) was used (Fig. 4.2a). For GrA715 at 250 MPa, a TS of 7.00 ± 0.37 N/mm² was achieved, whereas GrA1215 showed a TS of 6.10 ± 0.06 N/mm² and GrA6015 2.80 ± 0.07 N/mm² (Fig. 4.2b and c). However, by lowering the binder content to 5% (w/w) at GrA125, the TS was found to be higher (Fig. 4.2b) than for granules produced from A7 (Fig. 4.2a) (2.79 ± 0.08 vs. 1.19 ± 0.05 N/mm²). In the case of the formulation of A7 and A12 with 10% (w/w) binder content, TS at 250 MPa was comparable for both produced granules (5.85 ± 0.24 vs. 5.65 ± 0.15 N/mm²). Granules produced from A60 (Fig. 4.2c) achieved a TS less than a half, compared to the tablets made from granules with a smaller particle size of filler material.

In the case of the PMs, PEG 6000 could not increase the TS of the PMs in comparison to the neat aDCP A7 or A12 (Fig. 4.2a and b). However, in the case of A60, TS increased as a function of binder content even in the PM, but to a lower extent than for tablets made from granules with similar binder contents (Fig. 4.2c). When using 15% (w/w) PEG 6000 in the PMs, TS exceeded the TS of the granules, containing 5% of the binder (1.26 ± 0.11 vs.1.09 ± 0.03 N/mm²).

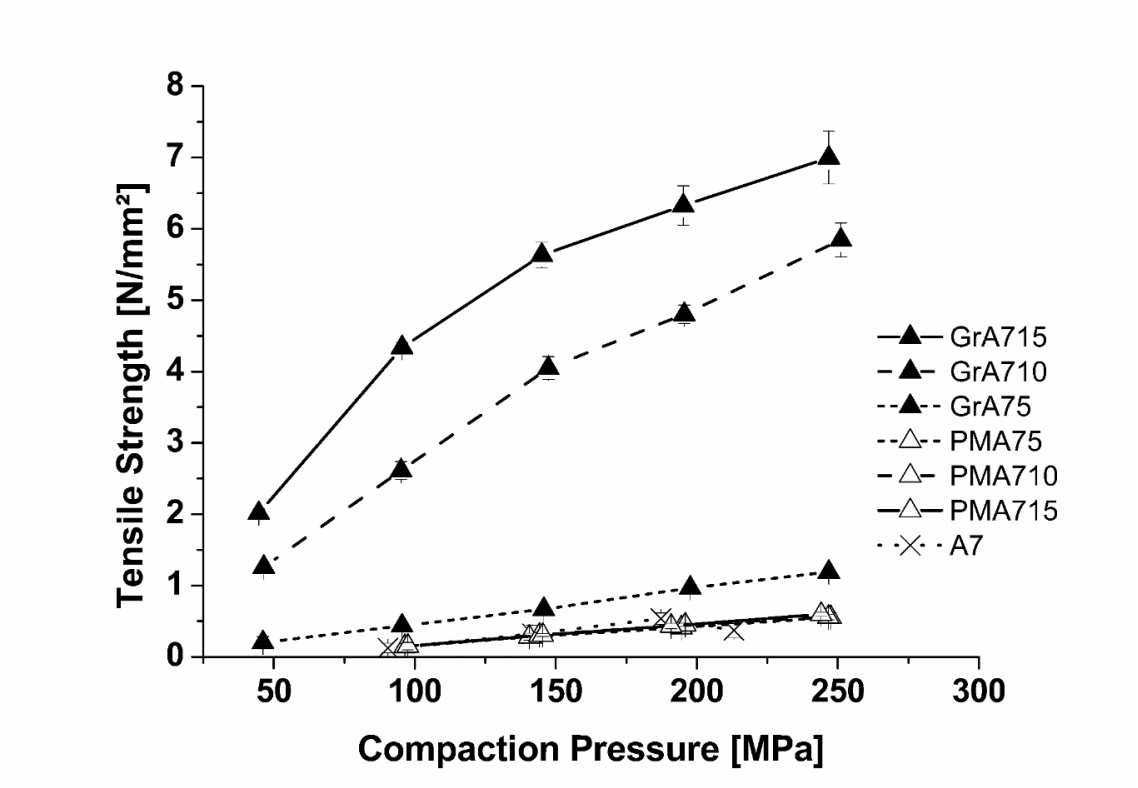

Fig. 4.2a: Tabletability plots for formulations with A7.

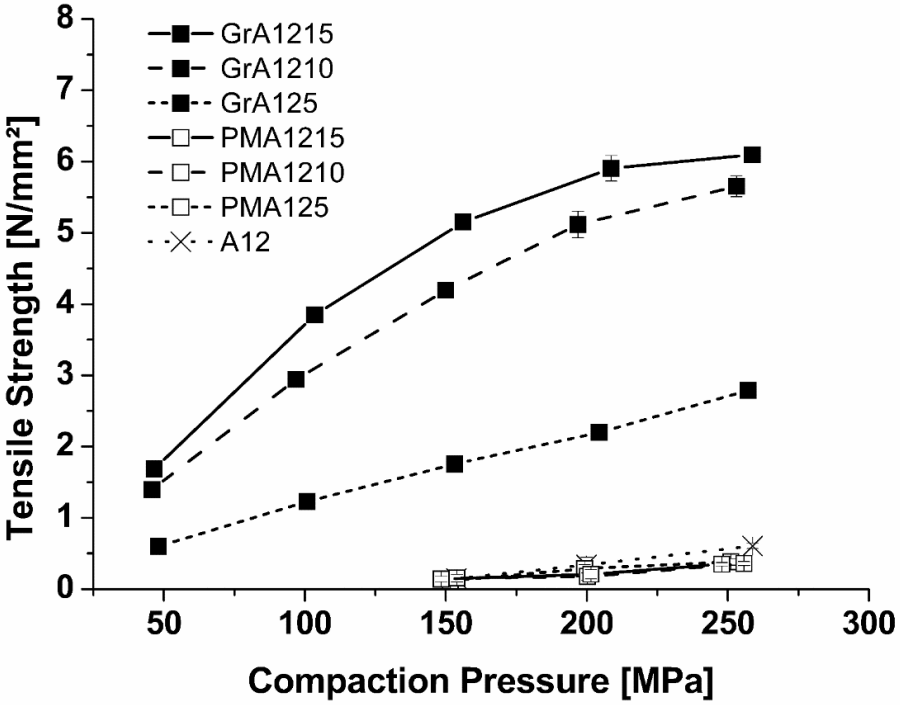

Fig. 4.2b: Tabletability plots for formulations with A12.

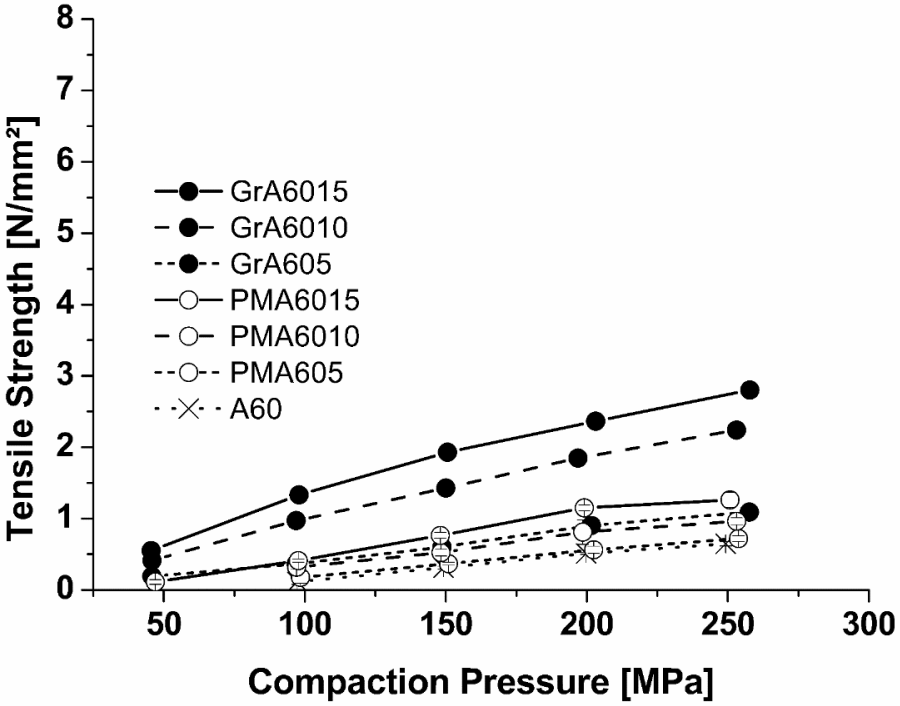

Fig. 4.2c: Tabletability plots for formulations with A60.

4.6.3 **Compactibility**

The compactibility plots (Fig. 4.3) indicated an increase of TS as a function of the SF, for the granules as well as for the respective PM. Granulation resulted in higher SF compared to the PM, which simultaneously increased TS. In the case of GrA715 (Fig. 4.3a) a maximum SF of 0.95 after granulation was achieved, when using a binder content of 15%. For GrA75, the TS were less affected by the granulation process, compared to GrA125. Similarly, only a low increase in TS was noticed for the PM of A7 and the PM containing A12 and PEG 6000 (Fig. 4.3b). However, when using A12, granulation with 5% (w/w) binder increased the SF and TS, compared to the respective PM. Moreover, a shift in SF was found for the A12 formulation with 15% binder, compared to the formulation with 10% binder. This resulted in the overall highest SF of 0.99 and no further increase in TS was feasible. Granules containing A60 as filler (Fig. 4.3c) showed a lower increase in TS and SF as a function of binder content, which was higher for the granules than for the corresponding PM, when a binder content of 10% (w/w) was exceeded. Overall, SF did not exceed a value of 0.94, which is equivalent to a porosity (ε) of 0.06 (ε = 1-SF) for the formulation with the largest initial particle size.

The effect of adding polyethylene glycol as dry binder on the mechanical strength of sodium chloride and sodium bicarbonate tablets was reported in literature. The authors showed that tablets tend to fracture around the filler materials, rather than through the particles [96]. However, synergistic effects were only seen in some cases, indicating that the dominance of one of the components should be avoided. Likewise, the results indicate the existence of an optimal binder content and optimal combinations, due to a various ways of interactions between the binder and the filler material.

The reduced porosity was shown relevant to increase the TS of sodium bicarbonate and calcium carbonate tablets, when PEG was added as a dry binder [96]. The ability of a binder to fill the pores of a tablet, thereby decreasing the porosity and its intrinsic properties, was further reported as important factor to enhance the TS [97]. Utilization of PEG as a dry binder was described to be very effective in improving the TS and to lower the porosity of a tablet [98]. This was linked to its low YP, high deformability and low ER. Moreover, a small particle size of the binder material was more effective than a larger particle size. Mattson and Nyström calculated a degree of binder saturation

(DBS), they evaluate the necessary amount of binder to theoretically fill the voids and they observed that with increasing binder content, the DBS increased and a lower porosity was achieved. They showed a close relationship between the decrease in porosity and the DBS for using high deformable binders like PEG 3000 [98]. Until now, these observations were only used to describe the effectiveness of PEG when used as dry binder as part of a simple mixture.

However, in our case the effect of PEG 6000 was increased by TSMG, compared to the simple PMs. Furthermore, the dependency of the effect on particle size of the filler material and the binder content was obvious.

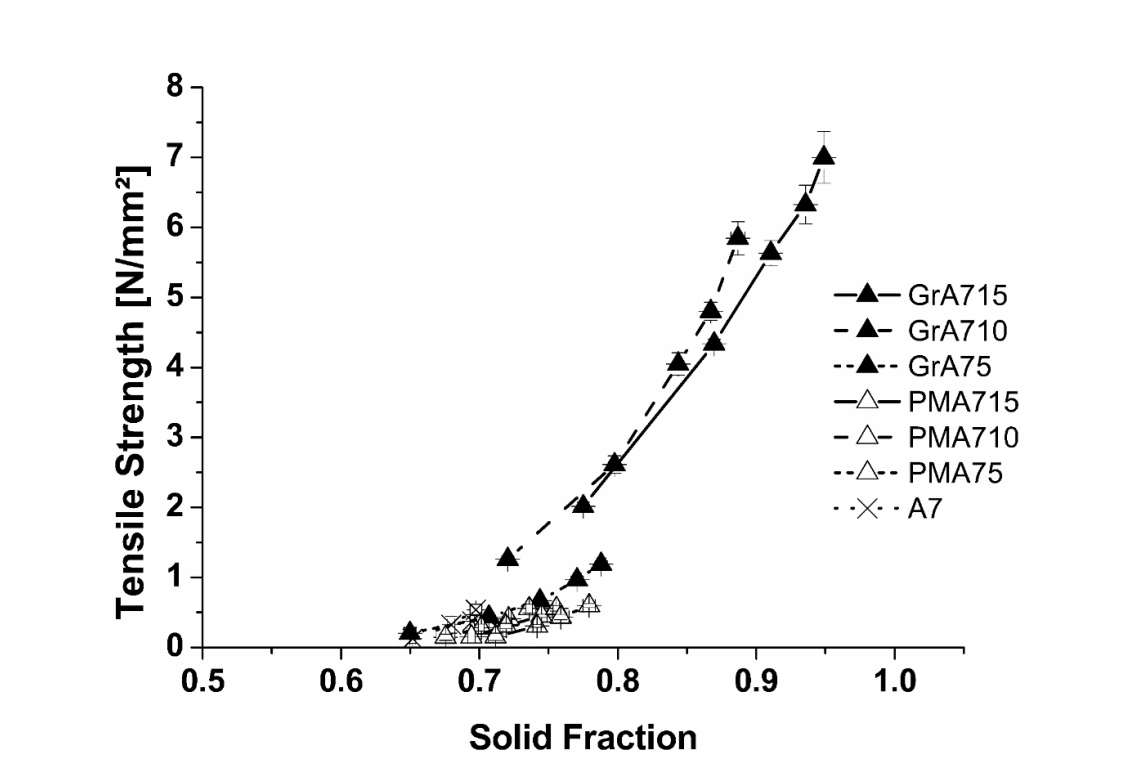

Fig. 4.3a: Compactibility plots for formulations with A7.

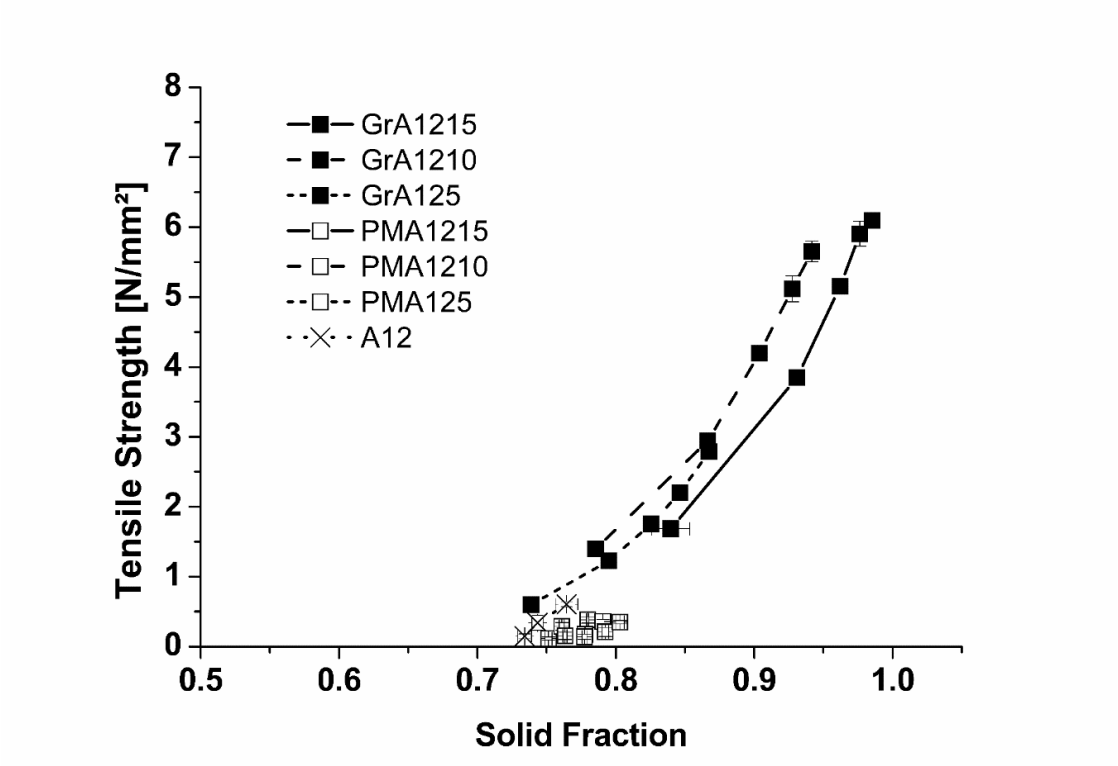

Fig. 4.3b: Compactibility plots for formulations with A12.

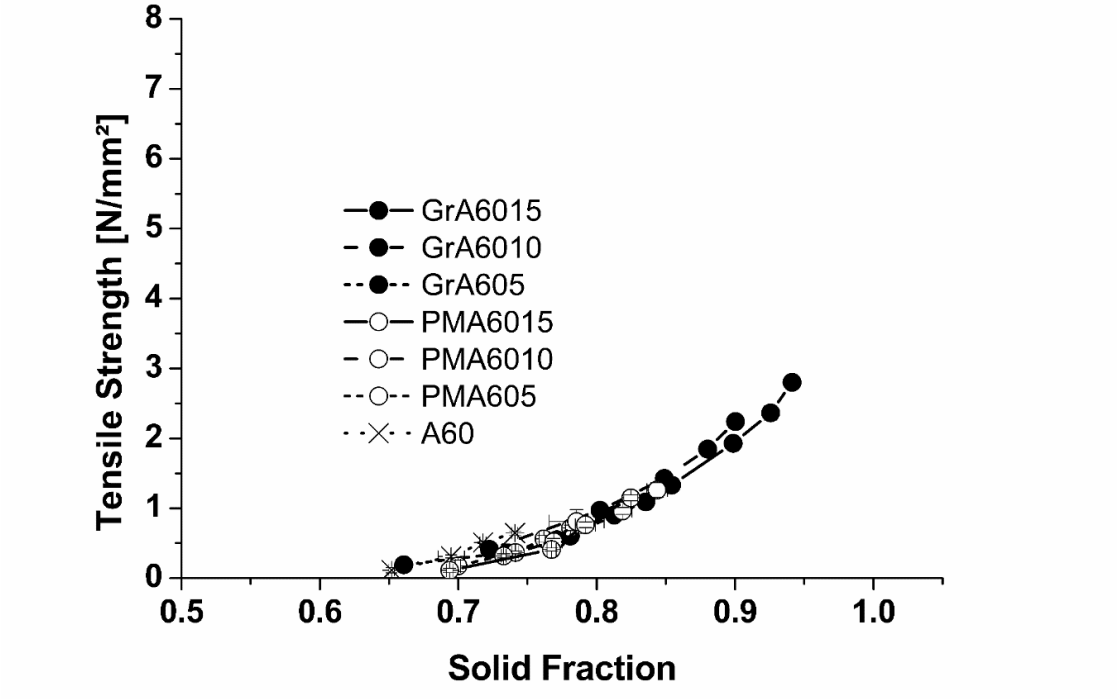

Fig. 4.3c: Compactibility plots for formulations with A60.

4.6.4 **Compressibility**

The compressibility plots for all formulations are shown in Fig. 4.4. The highest SF 0.99 has been found for GrA1215 (Fig. 4.4b). In sum, SF increased as a function of binder content and compaction pressure. SF of the granules made with A7 (Fig. 4.4a) and A60 (Fig. 4.4c) was lower in comparison to those of A12 (Fig. 4.4b), having equal binder contents. In the case of the PM, SF did not increase to the same extent as for the granulated material with the addition of PEG 6000.

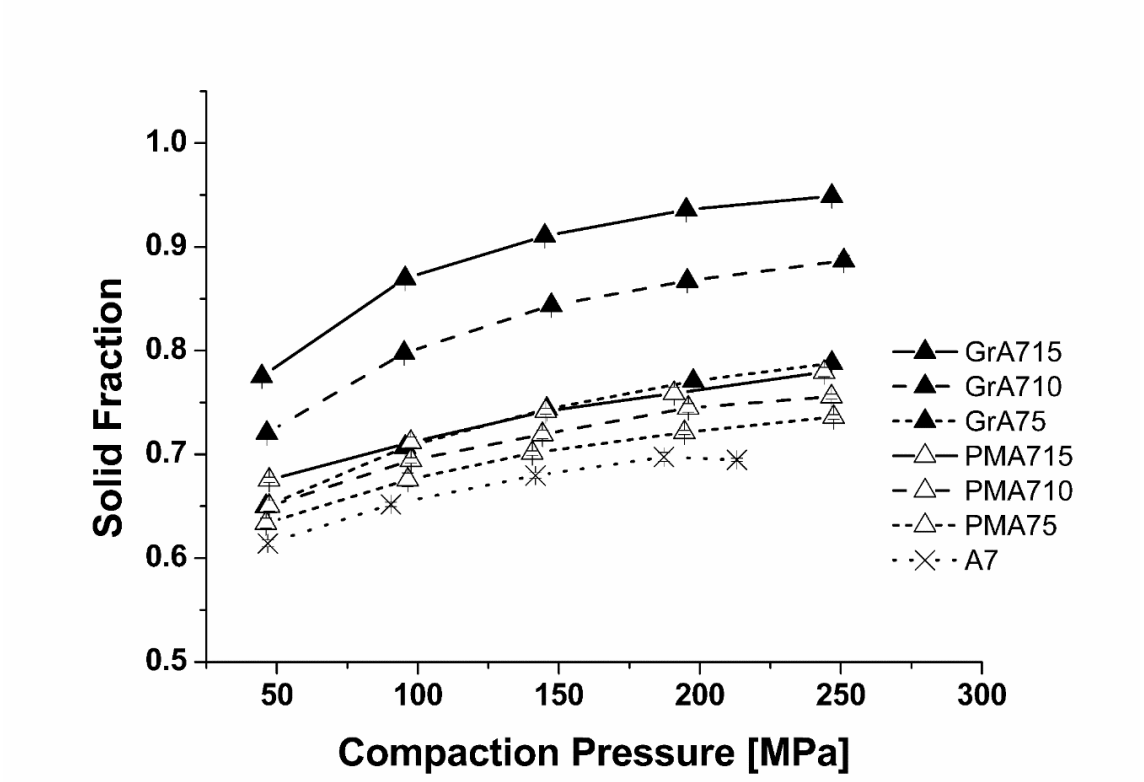

Fig. 4.4a: Compressibility plots for formulations with A7.

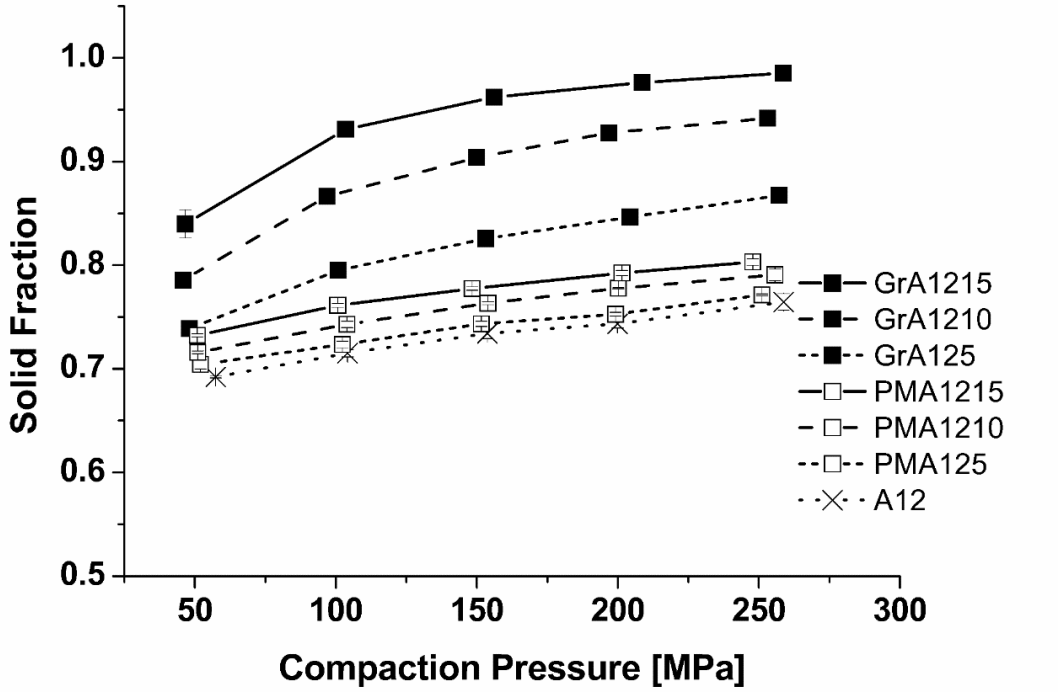

Fig. 4.4b: Compressibility plots for formulations with A12.

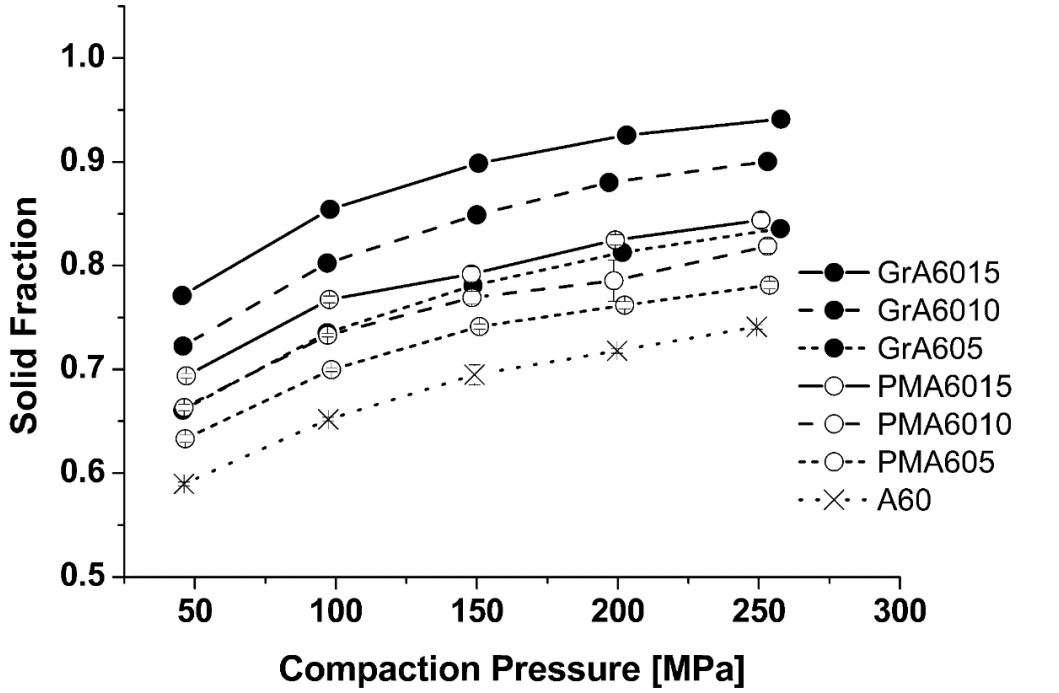

Fig. 4.4c: Compressibility plots for formulations with A60.

4.6.5 **Modified Kawakita model**

The out-of-die SF data of the pure materials was used to calculate the parameters ***a***, *b* and *1/b* of the Kawakita model (Tab. 4.4). For the PM and the granules, the SF was estimated by applying Eq. 4.8.

Tab. 4.4: Parameters *a, b* and *1/b* from the Kawakita model for the raw materials.

Substance	*a*	*b* [MPa^{-1}]	*(1/b)* [MPa]	R^2
PEG 6000	0.9572	0.5054	1.98	0.9998
A7 + 1% (w/w) Aerosil®	0.7276	0.1056	9.47	0.9997
A12	0.7872	0.1022	9.79	0.9990
A60	0.7881	0.0547	18.28	0.9988

As the actual compaction pressures differed slightly for the produced tablets of the PM and the granules, SF were estimated separately, even when they contained the identical binder content. The parameters *a* and *b* for the varied binder content (given in Tab. 4.5) were calculated using weight fraction and they were further used to estimate the SFs at different compaction pressures.

Tab. 4.5: Parameters *a, b* and *1/b* from the Kawakita model for the mixtures.

Formulation	**5% PEG**	**10% PEG**	**15% PEG**
	a	***a***	***a***
A7+1% (w/w) Aerosil®	0.7391	0.7506	0.7621
A12	0.7957	0.8042	0.8127
A60	0.7966	0.8051	0.8135

Formulation	**5% PEG**	**10% PEG**	**15% PEG**
	b **[MPa^{-1}]**	***b*** **[MPa^{-1}]**	***b*** **[MPa^{-1}]**
A7+1% (w/w) Aerosil®	0.1256	0.1456	0.1656
A12	0.1223	0.1425	0.1627
A60	0.0772	0.0998	0.1223

Formulation	**5% PEG**	**10% PEG**	**15% PEG**
	1/b **[MPa]**	***1/b*** **[MPa]**	***1/b*** **[MPa]**
A7+1% (w/w) Aerosil®	7.96	6.87	6.04
A12	8.17	7.02	6.15
A60	12.95	10.02	8.18

In Fig. 4.5, the measured compressibility plots and the estimated SF for the different mixtures of A7 (Fig. 4.5a), A12 (Fig. 4.5b) and A60 (Fig. 4.5c) were shown.

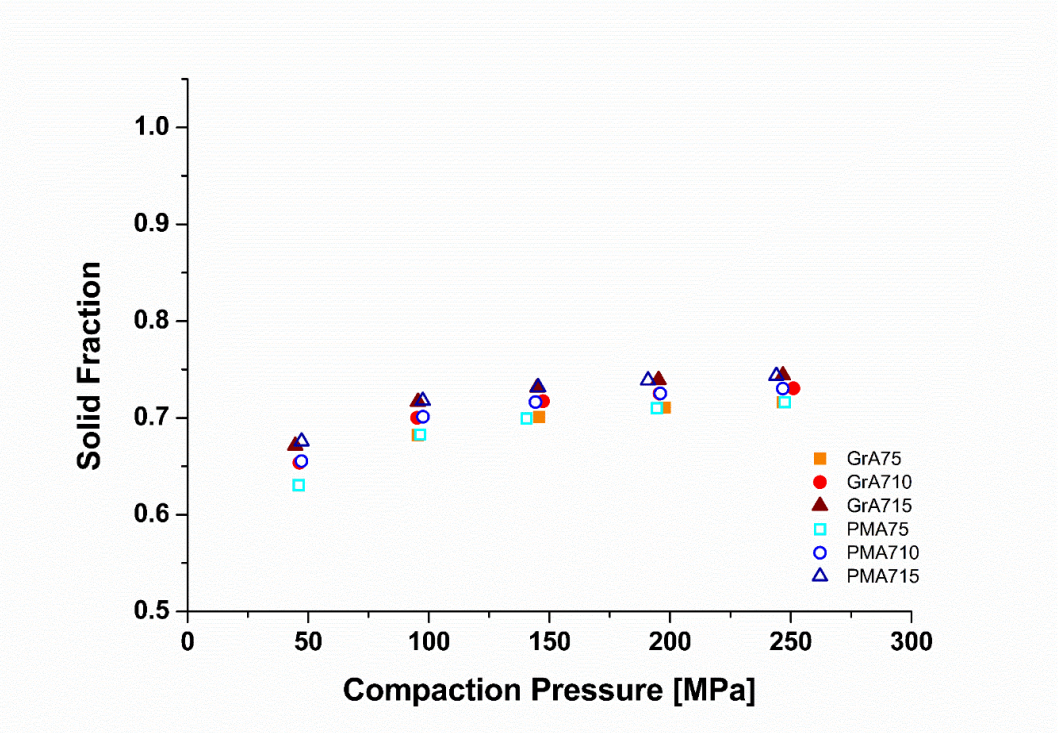

Fig. 4.5a: Estimated solid fractions for formulations with A7.

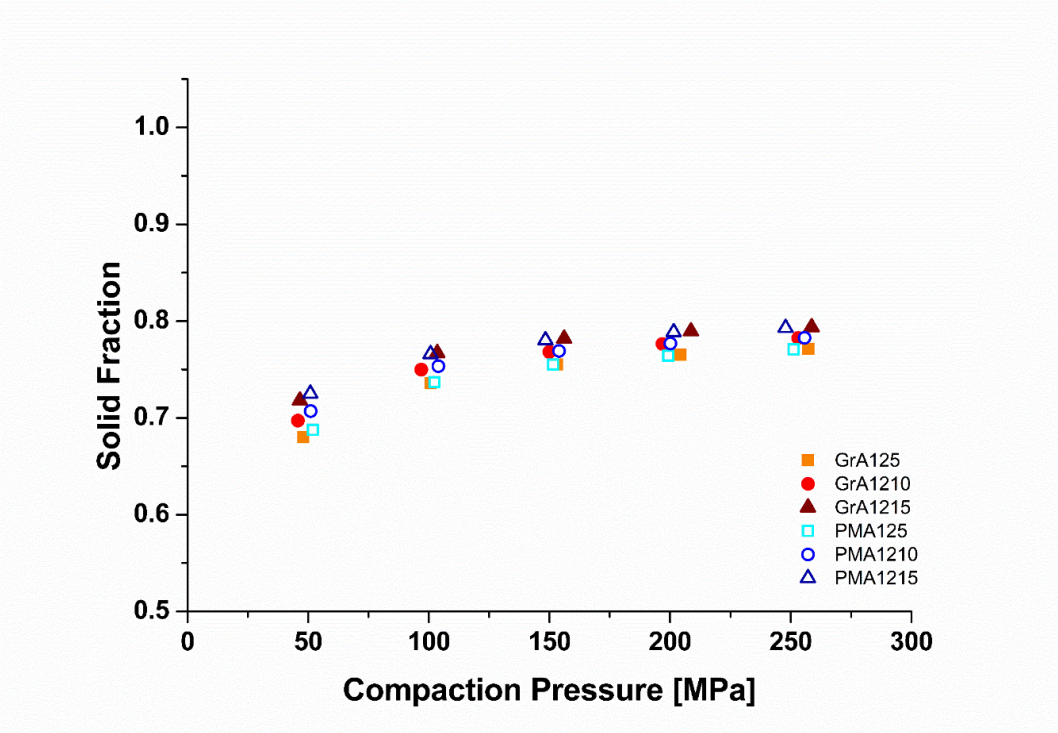

Fig. 4.5b: Estimated solid fractions for formulations with A12.

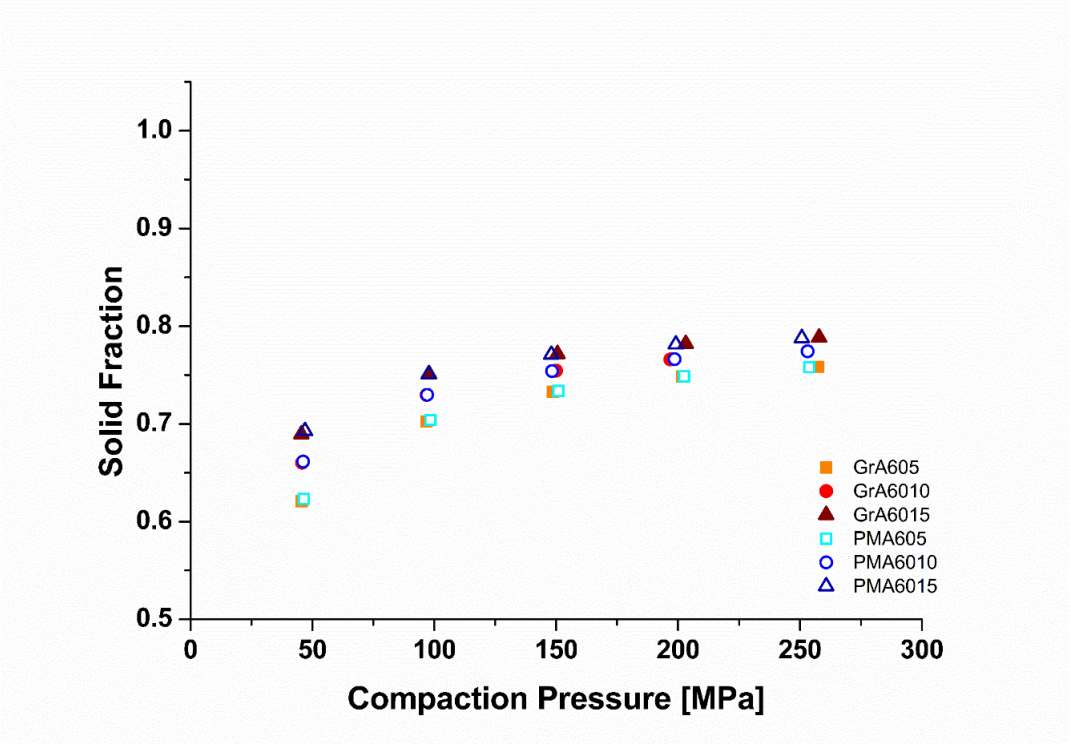

Fig. 4.5c: Estimated solid fractions for formulations with A60.

Residuals (Fig. 4.6a, b and c) form the measured out-of-die SF data (Fig. 4.4) to the estimated SF data from the modified Kawakita-model (Fig. 4.5) were calculated to describe the difference in compressibility for the formulations at similar compaction pressure. The obtained values were used to verify the model for the mixtures. Moreover the residuals were used describe the granulation efficiency using TSMG. Additionally, the obtained residuals were compared to describe difference in compression behaviour as a function of binder content and initial filler particle size.

Due to low residual data for the PMs, the prediction of the respective SF by applying the modified Kawakita-model was valid. At low compaction pressures, the SF was overestimated (negative values), but it was underestimated (positive values) for higher compaction pressures. However, residual deviations amongst the investigated particle sizes were minor, indicating that the modified Kawakita-model was independent from the initial filler particle size.

Moreover, the model exhibited a good prediction power for PMs of two materials with major differences in pycnometric density, particle size and an opposite deformation behaviour (plastic vs. brittle), even at low binder contents (5% (w/w)).

In the case of the granules, where the granulation process increased the compressibility compared to their PM, SF deviation increased. Thus, the deviations between measured SF and estimated SF can be used to describe the degree of improved compressibility by applying melt granulation.

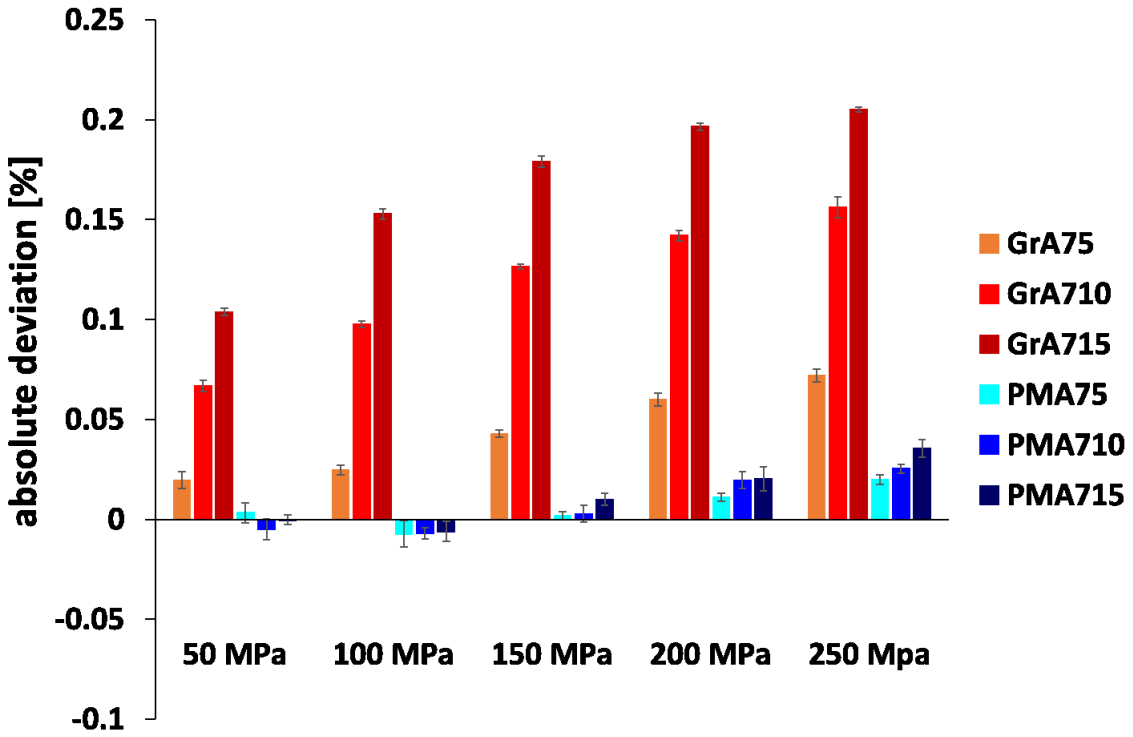

Fig. 4.6a: Absolute deviation in solid fraction from the estimated values for formulations with A7 at different compaction pressures.

Relative deviations from the estimated SFs to the calculated SFs are given in Tab. 4.6a, b and c. In the case of the PMs, only minimal deviation from the calculated SF was observed. The highest deviation of 7.10 ± 0.94% was identified for the PMs containing 15% (w/w) PEG 6000 and A60 as filler material, compressed at 250 MPa. At lower compaction pressures, the estimation with the help of the modified Kawakita-model was close to the measured values of the PMs. Quality of the prediction decreased with increasing compaction pressures, but no dependency of the prediction on the initial particle size of the filler was seen.

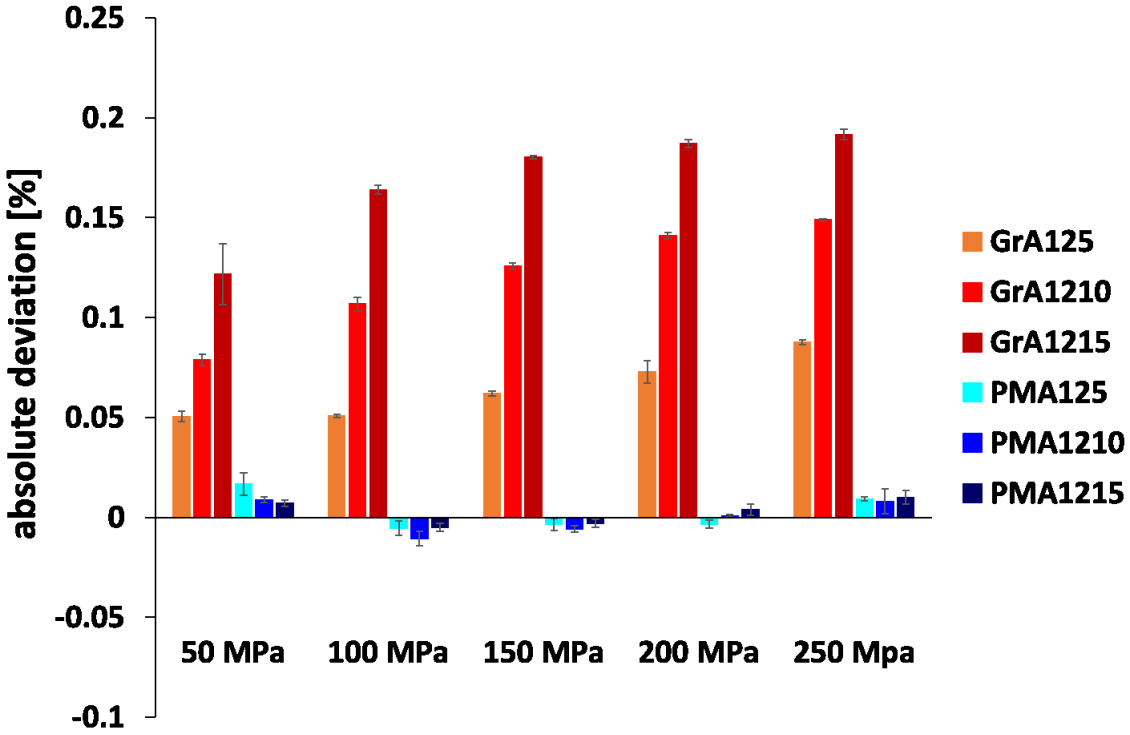

Fig. 4.6b: Absolute deviation in solid fraction from the estimated values for formulations with A12 at different compaction pressures.

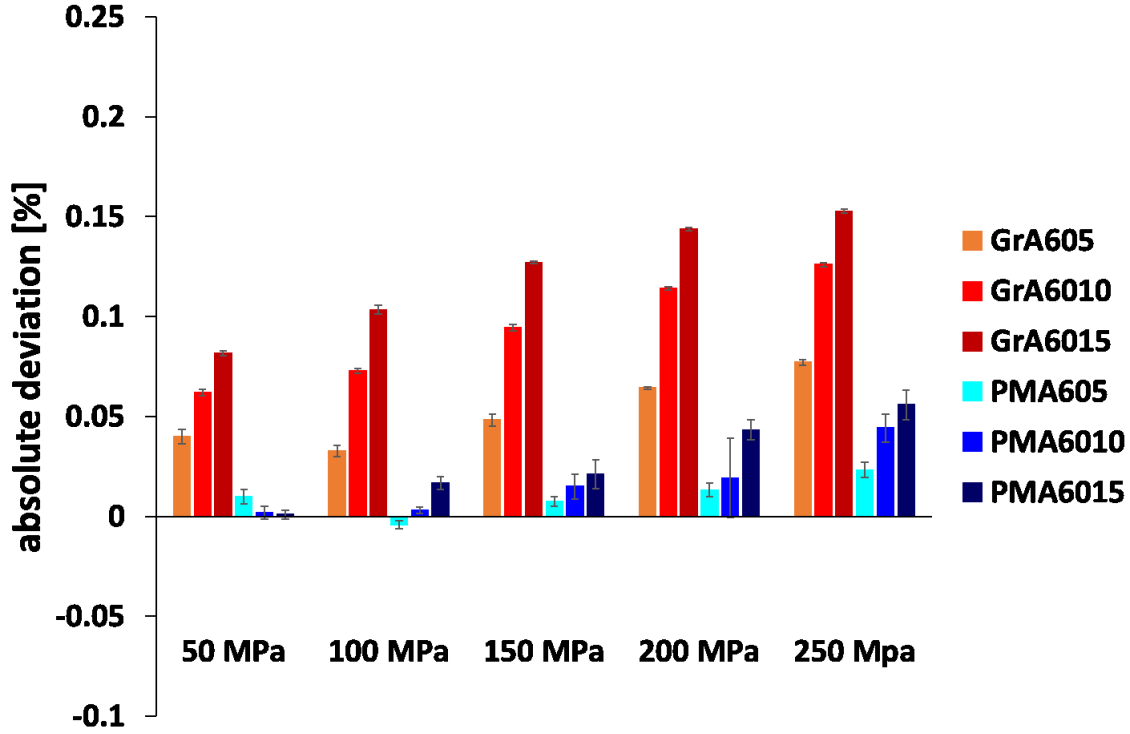

Fig. 4.6c: Absolute deviation in solid fraction from the estimated values for formulations with A60 at different compaction pressures.

In the case of the granules, deviations were increased with increasing binder content at similar compaction pressures. Analysing granules, the highest deviation and therefore the highest increase in compressibility was shown for the 15% (w/w) mixtures of PEG 6000 and A7 or A12 (27.57 ± 0.18% and 24.13 ± 0.32% at 250 MPa). The extent of enhancement was comparable for granules with A7 or A12 and 10 or 15% (w/w) binder (Fig. 4.6a and b). At lower concentrations, PEG 6000 acted more efficient on A12 than on A7, indicating that less binder was needed to lower effectively the porosity during compaction. Overall, the compressibility of the larger particle size of filler (A60) was lower than for smaller particle size qualities, especially when using high binder concentrations (Fig. 4.6c).

Tab. 4.6a: Relative deviation [%] in solid fractions from estimated values for formulations with A7 at different compaction pressures.

	Granules A7 [%] ± SD			**PM A7 [%] ± SD**		
	5% PEG	10% PEG	15% PEG	5% PEG	10% PEG	15% PEG
50 MPa	3.10 ± 0.68	10.21 ± 0.44	15.47 ± 0.25	0.52 ± 0.77	-0.78 ± 0.80	-0.03 ± 0.36
100 MPa	3.62 ± 0.38	13.94 ± 0.24	21.33 ± 0.35	-1.06 ± 0.98	-1.00 ± 0.39	-0.83 ± 0.73
150 MPa	6.11 ± 0.26	17.65 ± 0.16	24.46 ± 0.38	0.25 ± 0.31	0.38 ± 0.60	1.36 ± 0.40
200 MPa	8.45 ± 0.43	19.58 ± 0.35	26.58 ± 0.26	1.56 ± 0.28	2.71 ± 0.57	2.18 ± 0.80
250 MPa	10.05 ± 0.47	21.37 ± 0.70	27.57 ± 0.18	2.77 ± 0.32	3.47 ± 0.32	4.78 ± 0.60

Compressibility models might be helpful to describe the DBS and effectiveness of the melt granulation process in enhancing compressibility, compared to a simple binary mixture. The residuals of the modified Kawakita-model increased as a function of decreased porosity and consequently DBS was increased in relation to the respective PMs.

Tab. 4.6b: Relative deviation [%] in solid fractions from estimated values for formulations with A12 at different compaction pressures.

	Granules A12 [%] ±SD			**PM A12 [%] ±SD**		
	5% PEG	10% PEG	15% PEG	5% PEG	10% PEG	15% PEG
50 MPa	8.65 ± 0.38	12.65 ± 0.43	16.96 ± 2.14	2.42 ± 0.82	1.24 ± 0.20	0.99 ± 0.23
100 MPa	8.02 ± 0.09	15.55 ± 0.46	21.36 ± 0.28	-0.74 ± 0.47	-1.40 ± 0.47	-0.62 ± 0.26
150 MPa	9.30 ± 0.18	17.65 ± 0.21	23.04 ± 0.12	-0.47 ± 0.38	-0.76 ± 0.21	-0.38 ± 0.25
200 MPa	10.61 ± 0.75	19.46 ± 0.19	23.67 ± 0.25	-0.45 ± 0.26	-0.10 ± 0.08	0.48 ± 0.35
250 MPa	12.46 ± 0.16	20.35 ± 0.07	24.13 ± 0.32	1.18 ± 0.13	1.02 ± 0.81	1.26 ± 0.44

Tab. 4.6c: Relative deviation [%] in solid fractions from estimated values for formulations with A60 at different compaction pressures.

	Granules A60 [%] ±SD			**PM A60 [%] ±SD**		
	5% PEG	10% PEG	15% PEG	5% PEG	10% PEG	15% PEG
50 MPa	6.42 ± 0.57	9.40 ± 0.25	11.85 ± 0.18	-1.61 ± 0.58	0.26 ± 0.48	0.14 ± 0.32
100 MPa	4.65 ± 0.42	9.98 ± 0.18	13.78 ± 0.28	-0.60 ± 0.27	0.43 ± 0.23	2.23 ± 0.44
150 MPa	6.57 ± 0.41	12.50 ± 0.21	16.47 ± 0.09	1.04 ± 0.33	1.99 ± 0.82	2.72 ± 0.94
200 MPa	8.58 ± 0.09	14.90 ± 0.11	18.38 ± 0.09	1.77 ± 0.47	2.50 ± 2.58	5.54 ± 0.64
250 MPa	10.16 ± 0.21	16.26 ± 0.14	19.37 ± 0.11	3.07 ± 0.49	5.72 ± 0.90	7.10 ± 0.94

4.6.6 **Heckel analysis/ plasticity performance factor**

Results of the Heckel-analysis are listed in Tab. 4.7 and 4.8. Regarding the *YP*, pure A7 (including 1% (w/w) colloidal silicium dioxide), A12 and A60 exhibited the highest *YP* of 448.9 ± 5.5 MPa; 403.4 ± 39.0 MPa and 315.1 ± 37.0 MPa, respectively. In general, the *YP* decreased with the addition of PEG 6000, which was more pronounced in the case of the granulated material than for the PM. In the case of GrA1210, granulation decreased the *YP* from 352.6 ± 3.6 MPa to 95.0 ± 3.4 MPa. The lowest *YP* was found for GrA1215 (55.6 ± 1.2 MPa). Granules produced from A7 and A60 at the equal binder content of 15% (w/w) showed comparable values of 85.1 ± 1.4 MPa and 86.0 ± 1.0 MPa. Using a low binder content (5% (w/w)) for granulation, it resulted in a high *YP* of 287.2 ± 4.6 MPa for A7; 206.9 MPa ± 4.7 for A12 and a comparatively low *YP* of only 181.8 ± 10.0 MPa for A60. Similarly, for the PM, the highest *YP* was found for formulations with A7 and A12, whereas the lowest *YP* was determined for formulations containing A60 as filler material.

Tab. 4.7: Calculated parameters from the Heckel analysis for A7, A12 and A60.

Substance:	YP [MPa] ±SD	SF_A ±SD	P_{fit} [MPa] ±SD	SF_{fit} ±SD
A7+1% (w/w) Aerosil®:	448.9 ± 5.5	0.6081 ± 0.0039	97.3 ± 4.6	0.6845 ± 0.0053
A12	403.4 ± 39.0	0.6686 ± 0.0106	91.8 ± 30.6	0.7343 ± 0.0239
A60:	315.1 ± 37.0	0.5706 ± 0.0211	92.1 ± 27.5	0.6768 ± 0.0320

In addition, a relative *YP* (Tab. 4.8), a ratio of the measured *YP* and the corresponding *YP* of the neat aDCPs (Tab. 4.7), was calculated and defined as the plasticity performance factor (*PPF*). The lower the *PPF*, the higher the impact of the plastic deformable binding material. Overall, the *PPF* was lower for the granules compared to the respective PMs. GrA125 had a *PPF* of 0.513 ± 0.012 whereas the corresponding PM showed a *PPF* of 0.879 ± 0.049. In comparison, granulation of A60 decreased its *PPF* from 0.878 ± 0.082 to 0.577 ± 0.032, when using 5% (w/w) binder. Comparing the different initial particle sizes of filler material, the lowest *PPF* was achieved when using A12 and a high binder content of 15% (w/w) (0.138 ± 0.003), whereas respective granules from A7 had a *PPF* of 0.190 ± 0.003 and A60 had a *PPF* of 0.273 ± 0.003. As a comparative value, the *PPF* represents better the influence of the granulation in enhancing plastic deformation, than the measured *YP*. This is explained and given by the fact that *YP* value of the initial A7 is higher (448.9 ± 5.5) than that for A12 (403.4 ± 39.0 MPa), which is once more higher than that of A60 (315.1 ± 37.0 MPa). This normalization of the measured *YP* showed a higher plastic deformation in the case of A7 and A12, compared to A60.

Interestingly, the *PPF* for the PM resulted in similar values for all three filler materials, using the same binder content, indicating a similar relative influence on the plastic deformation behaviour in a simple PM. Only PMA6015 showed a lower value compared to PMA715 and PMA1215, which might be explained by a deviation from the calculated pycnometric density and/or segregation of the PM under investigation. In-die Heckel-analysis and *PPF* were useful tools to describe this decrease in porosity and increase in plastic deformation behaviour.

Tab. 4.8: Calculated parameters from the Heckel analysis for Granules and physical mixtures.

Formulation	Granules				
	YP [MPa] ±SD	PPF ±SD	SFA ±SD	Pfit [MPa] ±SD	SFfit ±SD
A75	287.2 ± 4.6	0.640 ± 0.010	0.6434 ± 0.0025	115.9 ± 1.7	0.7622 ± 0.0022
A710	151.9 ± 1.8	0.338 ± 0.004	0.6527 ± 0.0037	101.1 ± 14.6	0.8208 ± 0.0197
A715	85.1 ± 1.4	0.190 ± 0.003	0.6297 ± 0.0059	50.0 ± 7.1	0.7934 ± 0.0195
A125	206.9 ± 4.7	0.513 ± 0.012	0.6949 ± 0.0052	103.2 ± 22.1	0.8079 ± 0.0206
A1210	95.0 ± 3.4	0.236 ± 0.008	0.6725 ± 0.0105	56.2 ± 20.5	0.8140 ± 0.0428
A1215	55.6 ± 1.2	0.138 ± 0.003	0.6658 ± 0.0053	32.5 ± 4.2	0.8130 ± 0.0146
A605	181.8 ± 10.0	0.577 ± 0.032	0.6006 ± 0.0142	84.3 ± 25.6	0.7452 ± 0.0397
A6010	117.4 ± 4.4	0.373 ± 0.014	0.6199 ± 0.0094	62.7 ± 25.5	0.7716 ± 0.0521
A6015	86.0 ± 1.0	0.273 ± 0.003	0.6449 ± 0.0079	49.0 ± 5.1	0.7999 ± 0.0104
	Physical mixtures				
	YP [MPa] ±SD	PPF ±SD	SFA ±SD	Pfit [MPa] ±SD	SFfit ±SD
A75	410.0 ± 8.9	0.913 ± 0.020	0.6438 ± 0.0017	113.1 ± 5.2	0.7296 ± 0.0036
A710	362.8 ± 16.2	0.808 ± 0.036	0.6659 ± 0.0064	108.1 ± 16.3	0.7514 ± 0.0133
A715	327.5 ± 7.7	0.730 ± 0.017	0.6868 ± 0.0016	115.3 ± 3.1	0.7797 ± 0.0035
A125	354.5 ± 19.7	0.879 ± 0.049	0.6863 ± 0.0060	93.3 ± 24.9	0.7578 ± 0.0186
A1210	333.9 ± 3.5	0.828 ± 0.009	0.7127 ± 0.0026	116.8 ± 5.2	0.7975 ± 0.0043
A1215	292.9 ± 4.5	0.726 ± 0.011	0.7253 ± 0.0022	106.4 ± 9.8	0.8088 ± 0.0077
A605	276.8 ± 25.7	0.878 ± 0.082	0.6135 ± 0.0144	107.9 ± 19.3	0.7372 ± 0.0208
A6010	253.1 ± 55.7	0.803 ± 0.177	0.6373 ± 0.0203	105.0 ± 27.3	0.7592 ± 0.0320
A6015	196.0 ± 7.3	0.622 ± 0.023	0.6661 ± 0.0036	115.2 ± 3.8	0.8145 ± 0.0027

The decreased *YP* indicated an enhanced plastic deformation after TSMG in comparison to the respective PM. In literature, linear relation of the *YP* was reported for binary mixtures, as a function of volume percent for sodium chloride and pre-gelatinized starch (PGS) [99]. Similar trends were observed for materials with similar compression behaviour. However, dominating effects on the *YP* for the plastic material (MCC or PGS) were described, when it was mixed with a brittle component (dicalcium phosphate dehydrate and α-lactose monohydrate) [100].

Our intention was to describe the effect of PEG 6000 using a relative value, the plasticity performance factor, while applying this factor to describe the effectiveness in increasing the plastic deformation of the starting material using the material granulation process. In the case of the PMs, similar *PPFs* were found for the identical binder content, whereas *YP* was increased as a function of a decreased initial particle size. In literature, the increase in *YP* for brittle materials, when the particle size was decreased, was confirmed for several materials [45]. Our results using the *PPF* indicated that this relative value is able to describe the influence of PEG 6000, independent of the particle size of the brittle filler used, as PM resulted in similar *PPFs*. Contrary, granulation caused a higher extent of deviation for *PPF* in dependence of filler particle sizes. As the *YP* of the smaller pure aDCP particles is higher, the PPF better reflects the influence of PEG 6000 on plastic deformation in comparison to the starting material and therefore the effect of granulation. Similar to the results obtained from the out-of-die analysis, results from in-die analysis indicated that the internal effect of the filler material can be reduced, using a smaller initial particles size (A7 and A12 in comparison to A60). In the case of 5% (w/w) binder, A12 outperformed A7.

This result is in good agreement to the data obtained using the modified Kawakita-model. In the case of using the *PPF*, A12 performed superior, even when using 15% (w/w) binding material, which was not the case, when using the Kawakita-model. This might be attributed to the sensitivity of the Heckel-plot in the low porosity range (here only 1%), were small difference at very low porosities, result in high deviations, due to its logarithmic nature. However, the smaller the particles, the more binder is necessary to effectively fill the voids between the particles, explaining the low increase in *PPF* observed when comparing A7 to A12 at the equal binder content, especially when using lower binder contents of only 5 or 10% (w/w).

The SF related to the parameter A (SF_A) and to the first point of the linear slope (SF_{fit}) and the corresponding pressure (P_{fit}), are shown in Tab. 4.7 and 4.8. The parameter SF_A was higher in the case of A12 (0.6686 ± 0.0106), than for A7 (0.6081 ± 0.0039), and A60 (0.5706 ± 0.0211). This indicates the stronger rearrangement of the A12 particles, compared to A7 +1% (w/w) Aerosil® and A60 (Tab. 4.7).
The SF_{fit}, values indicated that the plastic deformation started at a similar porosity range for A7 (0.6845 ± 0.0053), A12 (0.7343 ± 0.0239) and A60 (0.6768 ± 0.0320) at similar compaction pressures of 97.3 ± 4.6, 91.8 ± 30.6 and 92.1 ± 27.5 MPa. The respective results for the granules and PM are shown in Tab. 4.8. SF_A and SF_{fit} were also higher for A12 formulations, compared to A7 and A60 formulations. In the case of the PMs, SF_A and SF_{fit} increased with increasing binder content, the highest SF_A were again found for the A12 formulations. For the granules, no trend can be observed for the parameters SF_A and SF_{fit}. In the case of A60 using 5% (w/w) of binder similar values were obtained for P_{fit} of the granules (84.3 ± 25.6 MPa) and the PMA6010 (105.0 ± 27.3 MPa). Similar data were also obtained for GrA710 and PMA710 (101.1 ± 14.6 vs. 108.1 ± 16.3 MPa), whereas for A12, both parameters differed (56.2 ± 20.5 MPa vs 116.8 ± 5.2 MPa). However, in the case of 15% (w/w) binder, the difference between PM and granules were also pronounced for A7 and A60, indicating a strong impact of the binder.

Nevertheless, granules were not milled and were therefore of different particle sizes, which can cause high deviations in in-die porosity determination and therefore have influence on the SF_A and SF_{fit} values of the granulated material. However, a strong reduction of the value P_{fit} was observed for granules in comparison to the PM, indicating that the critical SF for the formation of strong bonds and plastic deformation of the material was at low compaction pressures.

To summarize, both compressibility models (in-die Heckel-analysis and out-of-die modified Kawakita-model) showed comparable results for the investigated formulations. A7 and A12 showed tablets with higher compressibility and enhanced plastic deformation compared to A60. Moreover, A12 needed less binding material compared to A7 to show enhanced compressibility (residuals of the modified Kawakita-model) and plastic deformation (*PPF*), which can be explained by its lower specific surface area. Nyström et al. (1982) reported, that in the case of using small particles of dry binder (methyl cellulose), a sufficient surface coating with binder particles can promote TS of the tablet, whereas fragmentation of the coated particles (in the case of lactose) can reduce effective bonding [70]. TSMG might be tested with other materials, which undergo intensive fragmentation, show high ER, or deform plastically during compaction into tablets and show inadequate TS. The potential of other binding materials might be tested with regard to their effectiveness in de- and increasing porosity and TS of the resulting tablets, respectively, using in-die and out-of-die compression analysis. The *PPF* and the residuals of the estimated porosity using the modified Kawakita-model might be beneficial descriptors, as they are independent of the starting materials compression behaviour.

4.6.7 **Elastic Recovery**

Fig. 4.7a, b and c show the ER of the tablets compressed at 200 MPa, comparing the out-of-die tablet height after 24 h of storage in relation to the minimal in-die tablet height during the compaction process. Overall, ER was in the range of 5% for pure A7 and A12 and also for the PMs. For the PMs, ER did not decrease as a function of binder content. In the case of the granules, the ER was reduced up to half of the initial value. Moreover, ER decreased with increasing binder content. Using A60, ER was not decreased in the case of the PMs and equivalent in the case of the granulated material, indicating less reduction in ER compared to smaller particle size of filler material.
Reduced ER indicated stronger bonding in the tablet. The higher ER for A60 tablets might be due to a higher degree of interactions between the aDCP crystals itself and a lower influence of PEG 6000 on this formulation. Due to the large particle size, aDCP interactions are active over a larger range of different inner surface areas inside the tablet. In the case of using smaller filler particles, the interaction can be reduced, due to the larger specific surface areas of A7 and A12, which are in contact with PEG.

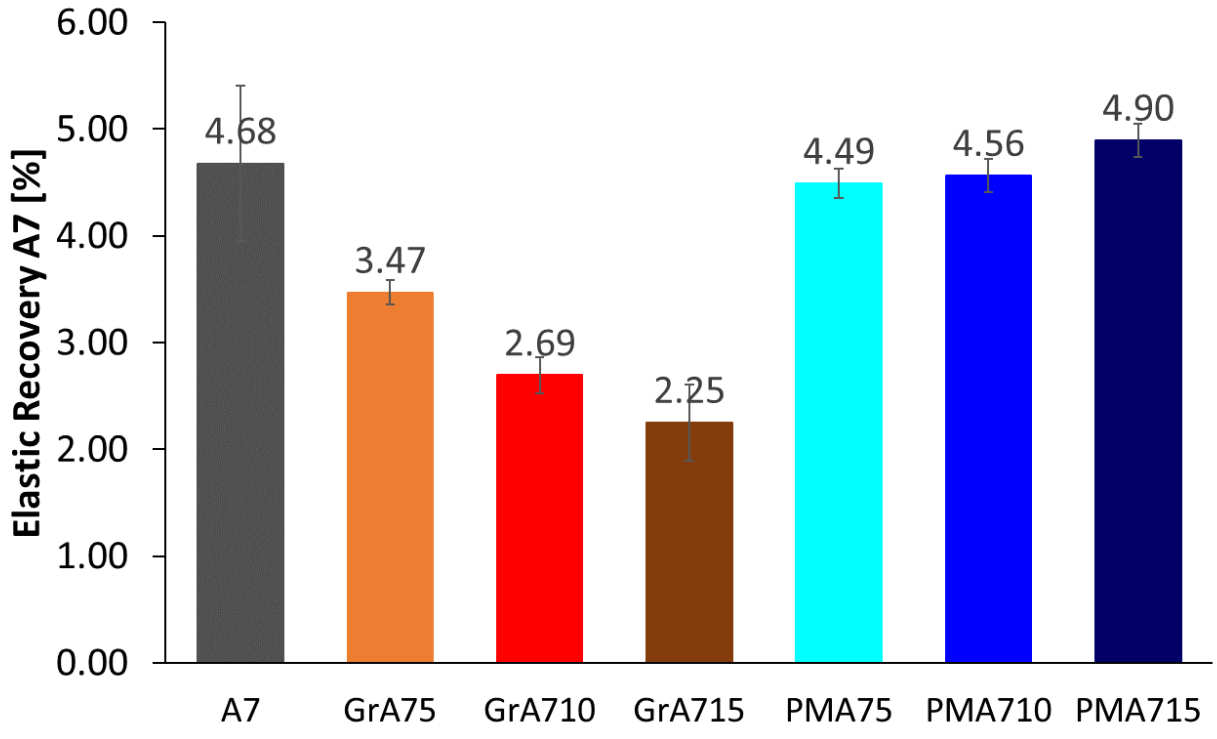

Fig. 4.7a: Elastic recovery of formulations with A7.

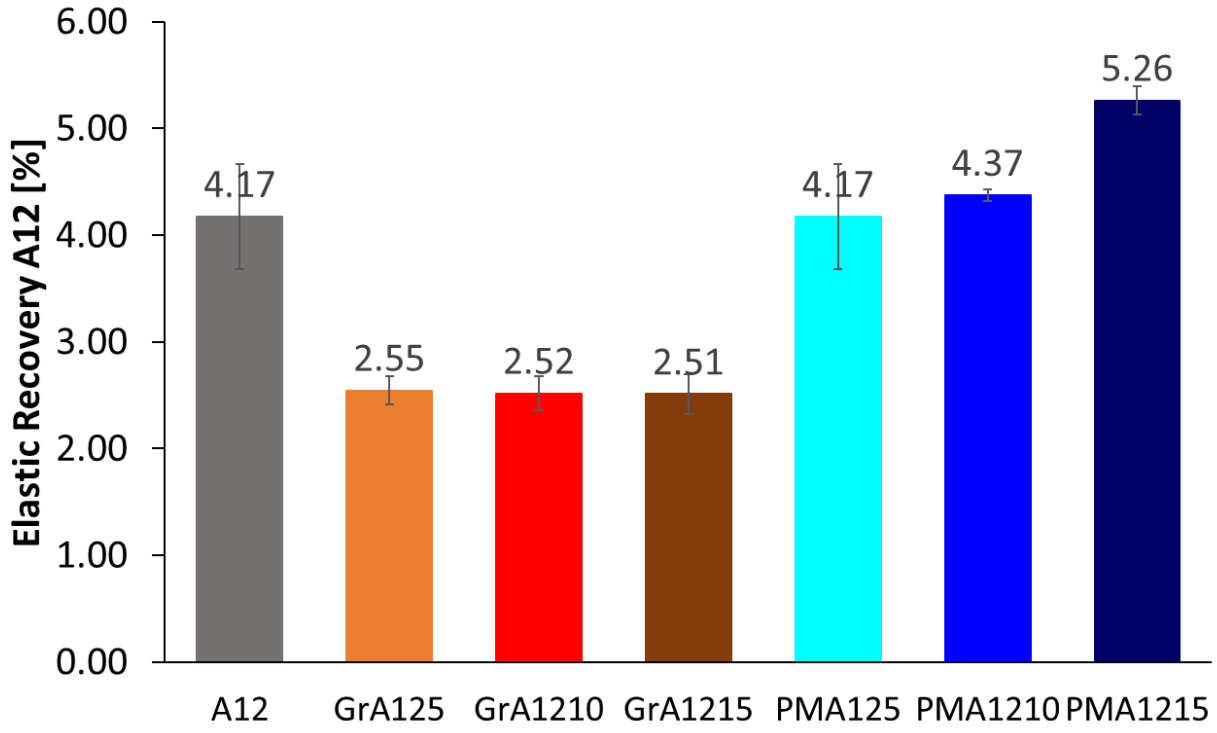

Fig. 4.7b: Elastic recovery of formulations with A12.

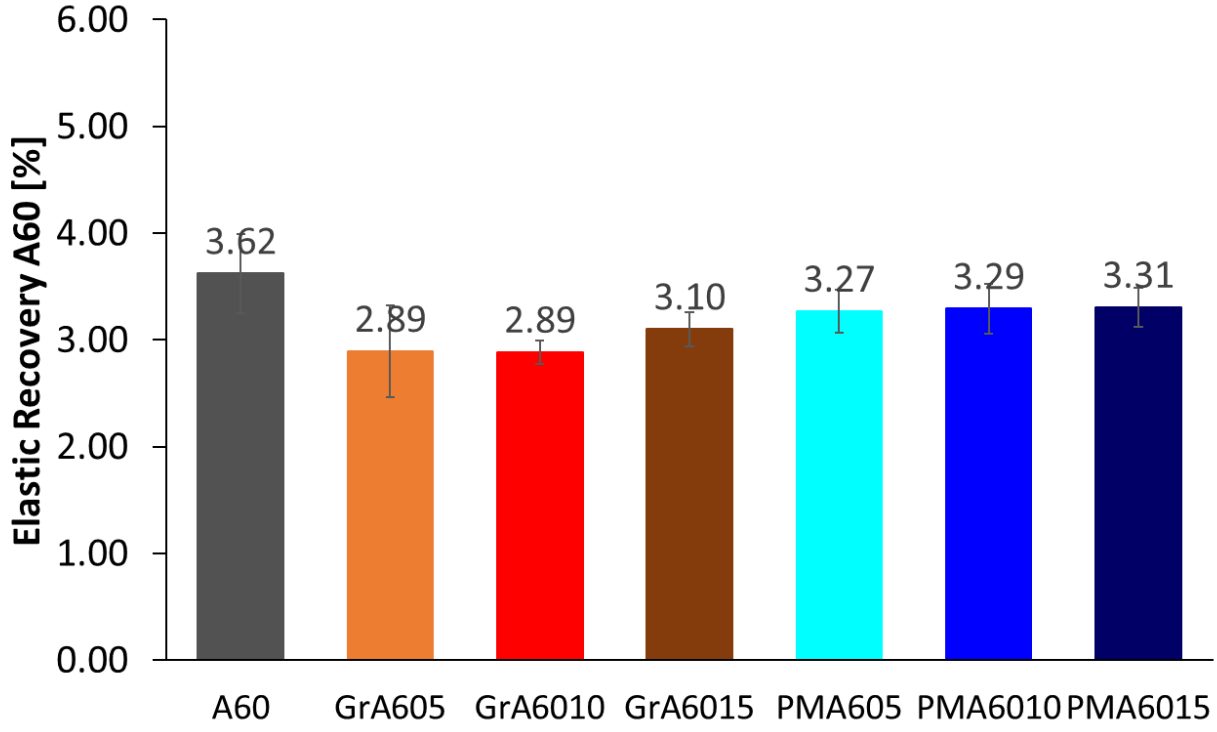

Fig. 4.7c: Elastic recovery of formulations with A60.

4.6.1 **Binder variation**

The diagram (Fig. 4.8) shows binder variation within and amongst the tablets of the different formulations. The lower the binder variation derived from three tablet surfaces for each formulation, the better the distribution of binder in the tablet. Granulation increased distribution of the binder PEG 6000, while the PM showed a high binder variation within one tablet (average value of binder variation, Fig. 4.8) and amongst the three tablets (high relative standard deviation, error bars in Fig. 4.8) compared to the granules. The high error bars in the case of the PMs, show a high variation of the binder detected in the tablets, but also a high variation of the binder detected between the tablet surfaces. A good distribution (low value of binder variation and small relative standard deviation) was observed for all granules except for the GrA75 formulation that was more comparable to the PM. While GrA715 resulted in a low binder variation, which was more comparable to the formulations containing A12 and A60.

Results of the compressibility analysis were confirmed by binder variation analysis using image-analysis of the carbon EDX-maps. Smaller initial particle sizes and the related higher specific surface area of A7 explain the deviation in TS, when the granules of A7 and A12 were compared. In the case of A12, an increase from 10 to 15% (w/w) binder was less effective in enhancing TS and SF than in the case of A7 as starting material. In the case of A12, already 5% (w/w) were sufficient to achieve a high impact on SF and TS.

In the case of A60, large areas in the tablet are unaffected by the binding material, due to its larger particle size, which resulted in the lowest increase in SF, compared to the estimated values. The measured binder variation shows, that binder was finely distributed after the granulation process.

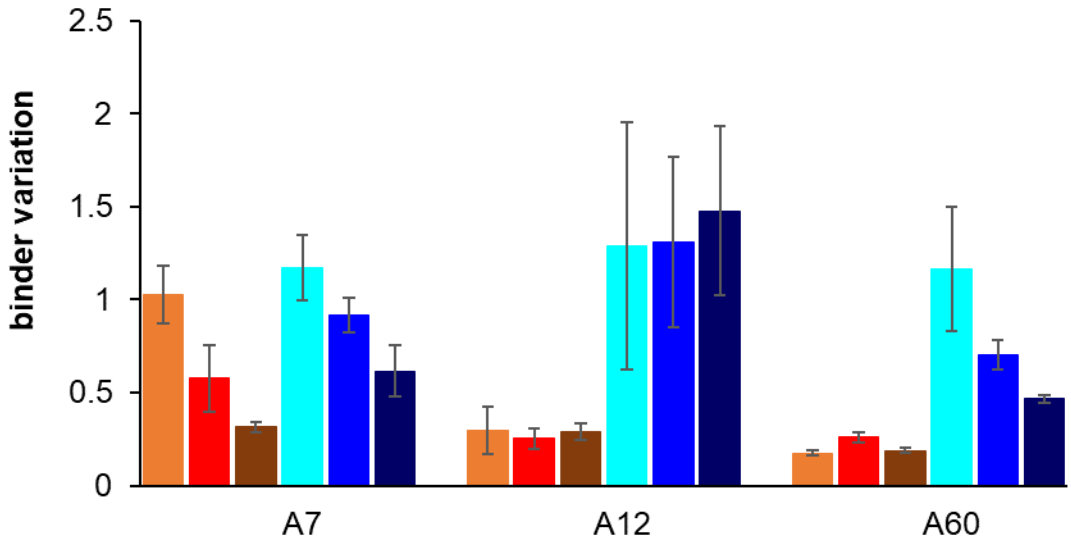

Fig. 4.8: EDX-analysis showing the relative standard deviation as parameter for binder distribution: red bars: granules; blue bars: PM; light: 5 % (w/w), middle: 10 % (w/w), dark: 15 % (w/w).

In the case of GrA75 binder variation was higher compared to the value obtained for GrA125 and GrA605. This might be on the one hand attributed to the larger specific surface area of A7 when compared to A12, where more binder was necessary to achieve a comparable effect on the binder variation and on the SF. Comparable trends in porosity decrease and even higher TS can be achieved if this “critical” binder concentration is exceeded.

On the other hand, neat material compression behaviour might be prominent in the case of a small specific surface area and a larger internal structure of the filler material, as e.g. seen in the case of using A60. This explains its lower performance in enhancing TS and SF, even if a homogenous distribution of the binder was achieved (low binder variation). Tablets made of the PMs showed an inferior distribution of the binder. This was very pronounced in the case of the PMs containing A12. The better distribution of the PEG in tablets containing PMs of A7 might be explained by the effect of added Aerosil (1%). This was necessary in order to obtain suitable feeding into the twin-screw granulator.

4.7 Conclusion

Overall, the current study showed that TSMG could drastically improve TS by achieving higher SF in the pharmaceutical relevant pressure range of materials that show low TS and/or volume reduction upon compression. Due to the melt granulation process, the binder is finely distributed between the starting material particles and can effectively enhance the TS and lower the porosity of the resulted tablets. Granules show enhanced plastic deformation behavior, especially when small particles of filler are used. This might be important when formulating high drug loads or other materials, as initial particle size of solid material can dramatically influence the product performance. Moreover, the need of a binder is influenced by this initial particle size as well, as surface area of the particles increases with decreasing particle size, increasing the amount of binder necessary to cover the surface and fill the pores between those particles in the later produced tablet.

The potential of melt granulation to enhance the tabletability and compressibility of poorly compactable materials was highlighted. Therefore, a modified Kawakita-model and the plasticity performance factor were used to describe the enhancement in compressibility, which simultaneously resulted in higher tensile strength. The results of the modified Kawakita-model and the PPF were used to describe the effectiveness of PEG 6000 as binder in the melt granulation process. They provide suitable tools to explain the high TS of tablets compressed from granules that underwent the granulation process, as the binder was shown to be finely distributed and to fill the voids between the aDCP particles (image analysis of the carbon EDX-maps).

The primary particle size of the filler played a major role in the efficiency of the melt granulation process on enhancing the compressibility and plastic deformation during tableting. Particle size of the filler influences the need of binder to sufficiently cover the surface of the filler and fill the voids in the tablet, resulting in strong bonds. However, large particle size of filler can result in a high influence of the neat fillers compression behavior on the resulted tablet properties. In the case of filler material with a larger particle size, larger areas in the tablet exhibit the tableting properties of the filler resulting in a lower plasticity performance factor and a lower efficiency of the melt granulation process in enhancing solid fraction and tensile strength. Likewise, the results indicate the existence of minimal binder content that should be exceeded to

effectively increase compressibility, which depends on the filler particle size and its corresponding specific surface area.

4.8 Acknowledgement

We thank Romaco Kilian GmbH and Medelpharm S.A.S for providing the Styl'One classic single-punch compression simulator. Furthermore, we would like to thank Chemische Fabrik Budenheim KG for the generous donation of material.

4.9 List of Symbols and Abbreviations

a:	parameter of the Kawakita-model	
A:	the intercept of the linear part of the Heckel-plot	
aDCP:	anhydrous dicalcium phospahte	
APIs:	active pharmaceutical ingredients	
b:	parameter of the Kawakita-model	
BET:	Brunnauer, Emmert and Teller	
C:	parameter of the Kawakita-model (relative volume decrease)	
d:	diameter of the tablet	[mm]
DBS:	degree of binder saturation	
EDX:	energy dispersive X-ray	
ER:	elastic recovery	[%]
ε =	porosity	
F:	breaking force	[N]
h:	height of the tablet	[mm]
k:	linear slope of the Heckel-plot	
L/D:	length/diameter [mm]	
m:	tablet weight [mg]	
MCC:	microcrystalline cellulose	
P:	applied pressure	[MPa]
ρ_{app}:	apparent density	[g/cm³]
ρ_{pyc}:	pycnometric density	[g/cm³]
P_{fit}:	first compaction pressure of the linear fit of the Heckel-plot	[MPa]
PEG:	polyethylene glycol	

PGS:	pre-gelatinized starch	
PM:	physical mixture	
PPF:	plasticity performance factor	[%]
s_{rel}:	relative standard deviation	
SEM:	scanning electron microscope	
SF:	solid fraction	
SFA:	solid fraction corresponding to the parameter A of the Heckel-equation	
SF_{fit}:	solid fraction corresponding to the first point of the linear fit of the Heckel-plot	
TSMG:	Twin-screw melt granulation	
TS:	tensile strength	[N/mm²]
V0:	initial volume	[mm³]
V_{min}:	minimal volume of the compact	[mm³]
V_p:	volume of the compact	[mm³]
YP:	yield pressure	[MPa]

4.10 Authors contributions:

Conceptualization: K.G.W and K.E.S.; Data curation: K.E.S; Methodology: K.E.S and K.G.W.; Investigation: K.E.S; Resources: K.G.W.; Writing-Original Draft Preparation: K.E.S; Writing-Review & Editing: K.G.W.; Supervision: K.G.W.; Project Administration: K.G.W.

5 Melt Granulation: a Comparison of Granules produced via High-Shear Mixing and Twin-Screw Granulation

Kristina E. Steffens; Marvin B. Brenner; Michael U. Hartig;

Marius Monschke; Karl G. Wagner

This part was published as:

Steffens, Kristina E., et al. "Melt granulation: A comparison of granules produced via high-shear mixing and twin-screw granulation." International Journal of Pharmaceutics 591 (2020): 119941.

DOI: 10.1016/j.ijpharm.2020.119941

5.1 Graphical Abstract

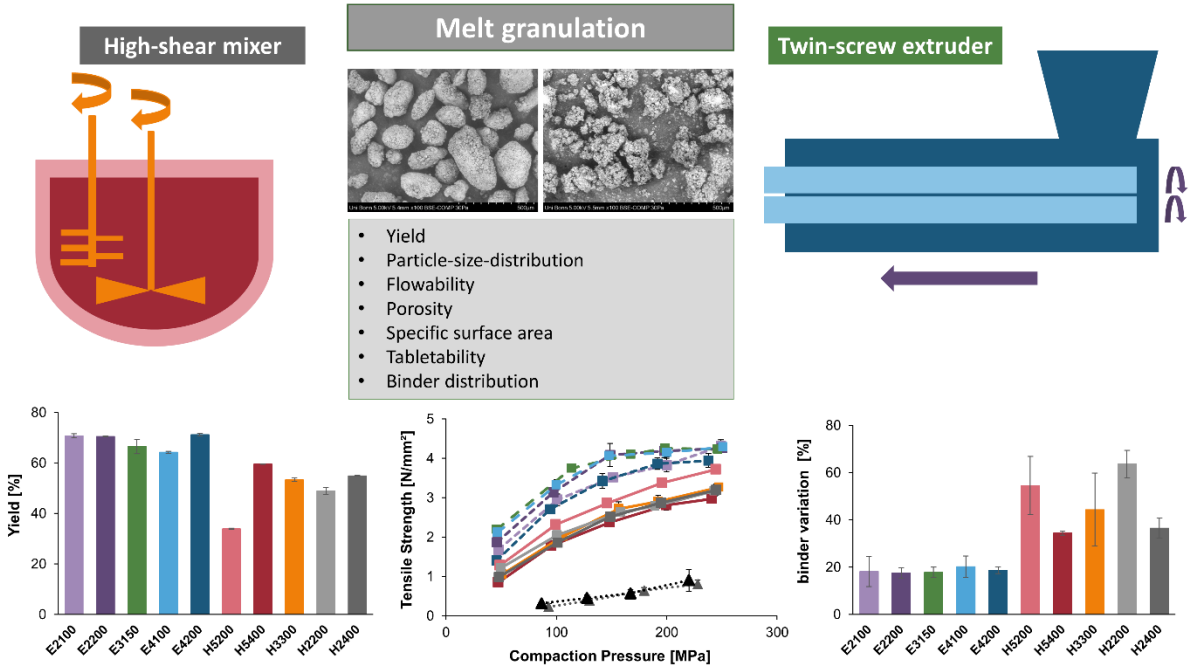

5.2 Abstract

Melt granules of DI-CAFOS® A12 and 15% (w/w) Kolliphor® P407 were manufactured in a twin-screw granulator (TSG) at five different conditions (screw speed and throughput varied) and compared to granules manufactured in a high-shear granulator (HSG) (rotation speed of chopper/impeller and granulation time varied). Evaluated granules characteristics were process yield, particle-size distribution (PSD), particle morphology, flowability, porosity, specific surface area (SSA), tabletability, compressibility and binder distribution. Compared to TSG, granules produced from HSG were more spherical in shape with lower porosity, smaller mean particle size and a superior flowability. Granules made by TSG showed a more elongated structure, higher porosity and larger mean particle size with smaller SSA instead. Concerning the compression process of granules, tablets made of TSG granules exhibited a higher tabletability compared to HSG granules, whereas the compressibility remained similar. In the case of the TSG granules, energy-dispersive-X-ray (EDX) measurements of the tablet surface indicated an enhanced homogenous binder distribution. Additionally, the

EDX-analyses determined that more binder was available between the individual particles, resulting in a stronger bonding.

5.3 Keywords

Melt granulation, twin-screw granulator, high-shear mixer, binder distribution, tabletability, porosity, flowability

5.4 Introduction

Being a continuous process, twin-screw granulation (TSG) has gained more and more attention over the recent years. As a continuous process, it can reduce processing time and costs in pharmaceutical manufacturing. Further advantages of this technique are the simplified scale-up, which is accessible by increasing the processing time, which provides more flexibility and less technology transfer during process development [28]. Moreover, the process offers the possibility of real-time monitoring and in-line analysis to enable a real-time release of the final product. However, several drawbacks of continuous granulation processes can be listed, like a difficult batch definition, and a high amount of material, that needs to be discarded at start until the process equilibrium is reached. Additionally, to ensure product uniformity when low-dose APIs are processed, an accurate dosing of the single components in continuous production is mandatory because the premixing-step, which can be performed in an HSG prior the granulation process, is missing. Therefore, when an offline blending in TSG should be avoided, an optimal mixing efficiency and accurate dosing of the feeding systems is required [28].

In the pharmaceutical field, the choice of the granulation process depends on the requirements of the active pharmaceutical ingredient to be formulated (e.g. dose, water-sensitivity, heat-sensitivity or compaction properties) and the desired granule properties (e.g. particle-size distribution, dissolution behaviour, porosity and flowability). Attention should be paid, when changing batch processes to continuous processing. This can have a major impact on the product performance and might require a complex adaptation of the manufacturing process.

Melt granulation as such is a process, where a particle size increase is achieved by using a meltable binder, e.g. polyethylene glycols or waxes. The binder is heated

above its melting point to lower its viscosity. Due to the introduction of shear-energy, the binder is softened and distributed between or on the filling material. While subsequent cooling, the binder solidifies again and it forms solid bridges between the particles. Melt granulation has several advantages over wet granulation. It avoids the need to add water, thus omitting the drying phase and is therefore less energy and time consuming [3]. Moreover, it makes the process suitable for water-sensitive materials and it can be used to protect the API from moisture in the final product [59]. Melt granulation can also handle high-dose API formulations, since it needs a binder only to achieve a processable formulation [4]. By choice of the right binder material, the dissolution profile of the final product is effectively controlled. When using hydrophilic binders, e.g. polyethylene glycols or poloxamers, a formulation with immediate release is obtained [3,6,9,23]. Lipophilic binders instead, like waxes, fatty acids or fatty alcohols, are used for the manufacturing of controlled-release formulations [3,10,39,101–103]. Melt granulation might also improve the solubility and the dissolution rate of poorly soluble drugs [6,7,9,80,104]. Furthermore, several working groups examined the potential of melt granulation to enhance the compactibility of poorly compactible APIs, which facilitates the production of tablets containing high API contents [2,36,59,60,81].

Classically, melt granulation is performed in high-shear mixers. The binder is added as dry powder or as molten liquid, and melting is induced by heating of the jacket, or by utilizing the heat of friction, generated by the mixing process. Particle-size distribution (PSD) of the granules is effectively influenced by the proper choice of the binder concentration and process time [16]. Twin-screw extruders, which can operate in a continuous mode, could also be used for melt granulation. Another benefit of melt granulation made by TSG is the high processing temperature that can be achieved. It widens the range of binding materials that can be processed [36]. However, one must keep in mind that higher temperatures and shear forces might induce thermal degradation of the active ingredient [105], but it can be compensated by controlling the shear rate of the process [106].

Due to the TSG setup and its first-in-first-out principle, the granules undergo reproducible mixing/shear conditions, which result in a more homogenous product than for products from traditional batch process [105]. In the case of TSG, the mean

residence time is reduced to seconds, which might lower the thermal stress of the product, compared to classical batch processes with its longer processing times [21]. Having regard to literature, several studies comparing the performance of granules produced by wet granulation using TSG and HSG are available [107–110]. However, the product performances of granules produced either by TSMG or HSMG, where not yet compared. This is especially interesting when changing from batch to continuous processes, but also for the implementation of TSMG as alternative granulation strategy. Therefore, this study was designed to characterize process-induced differences in the granules' critical quality attributes (CQAs), made either by TSMG or HSMG. It includes process yield, PSD, particle morphology, flowability, porosity, specific surface area (SSA), tabletability, compressibility and binder distribution. At the end, advantages and disadvantages of the product attributes of both melt granulation techniques should be clearly pointed out.

5.5 Material and methods

5.5.1 Material

Dicalcium phosphate anhydrous (DI-CAFOS® A12) was used as an inert filling material with a high degradation temperature and low tabletability. It was kindly donated by Chemische Fabrik Budenheim KG, (Budenheim, Germany). Kolliphor® P407 was investigated as binding material. It was a kind gift of BASF SE (Ludwigshafen, Germany). Kolliphor® P407 is a poloxamer with a low melting point of 56°C [63] and low viscosity, making it suitable as melt binder for both granulation methods under investigation. Filler and Binder were further selected because of their difference in atomic composition and atomic weight to allow analysis of the granules structure via scanning electron microscope (SEM) using a backscattered electron (BSE) detector and element-specific mapping of the binding material in the tablets using EDX-analysis.

5.5.2 **Methods**

5.5.2.1 Preparation of physical mixtures (PMs)

Prior to TSMG, DI-CAFOS® A12 was premixed with Kolliphor® P407 in a Turbula blender (Willy A. Bachofen AG Maschinenfabrik, Switzerland) at a rotating speed of 50 rpm for 10 min. Each batch had a size of 500 g. The obtained PMs were used for melt granulation with the TSG and additionally characterized as reference material for the produced melt granules.

5.5.2.2 Twin-screw melt granulation (TSMG)

TSMG was performed on a co-rotating twin-screw extruder (ZE12, Three-Tec GmbH, Seon, Switzerland) with a functional length of 25:1 L/D (length/diameter) and a screw diameter of 12 mm. The extruder barrel consisted of five individually adjustable heating zones (zone 1: 50 °C; zone 2: 60 °C; zone 3: 70 °C; zone 4: 60 °C; zone 5: 50 °C), which ensured a sufficient melting and distribution of the binder. The process temperature was set to 70 °C in the high-shear region of the extruder screws (30°, 60°, 60° and 90° 4-disc-kneading elements). The maximum temperature was adjusted to the maximum achievable temperature in the HSG. To allow a sufficient solidification of the material, the temperature at the terminal zone of the barrel was reduced to 50 °C. The screw-configuration was not varied in this study. During melt granulation, no die plate was mounted at the end of the extruder barrel. A volumetric feeder system ZD9 (Three-Tec GmbH, Seon, Switzerland) was used to enable a constant feed rate. In Tab. 5.1, throughputs and screw speeds of the different batches were listed. The screw speed was selected based on the maximum screw speed of the equipment (33% and 66% of the maximum screw speed). The throughput was chosen based on a mean-residence time of 2.5 and 5 min in the extruder (measured with the pigment iron oxide (Sicovit® Red 30 E 172, BASF SE, Ludwigshafen, Germany) and calculated by using ExtruVis3 (ExtruVis, Riedstadt, Germany). The mean-residence time of the granules was independent of the selected screw speed. Obtained granules were milled in a Bohle turbo-sieve (BTS) (L.B. Bohle Maschinen+Verfahren GmbH, Ennigerloh, Germany) at 500 rpm and with a 2 mm friction sieve.

The milled granules were separated into subsamples using a sample divider (Retsch PT/DR 1000, Retsch GmbH, Haan, Germany).

Tab. 5.1: Throughput and screw speed used to produce the different TSG formulations.

Short name	Throughput [g/min]	Screw-speed [rpm]
E2100	2	100
E2200	2	200
E3150	3	150
E4100	4	100
E4200	4	200

5.5.2.3 High-shear melt granulation

High-shear melt granulation (HSMG) was performed on a VMA10 high-shear granulator (L.B. Bohle Maschinen+Verfahren GmbH, Ennigerloh, Germany) with a heatable double jacket. The conducted melt granulation process can be divided into three parts, after the non-premixed powder (batch size: 3000 g) was filled in manually:

1. **Pre-mixing:** The powder was mixed for 5 min at an impeller speed of 150 rpm and a chopper speed of 300 rpm (Mixing-Phase).
2. **Melt granulation**: The impeller and chopper speed were increased and the jacket was heated up to 75 °C. The beginning of the granulation process is defined as the time point, when the product temperature exceeded 60°C.
3. **Cooling:** After the main granulation time, the jacket was cooled with the integrated water-cooling system. Chopper and Impeller were run in an interval mode of 5 sec and a pause of 25 sec. The granules were removed when the product temperature fell below 50°C.

Chopper and impeller speed were varied in the main granulation phase (Tab. 5.2). The parameters were set 33% and 66% of the maximum operable speed of the equipment. The main granulation time was adjusted to the mean-residence time of the granules in the extruder. The obtained granules were milled by in a Bohle turbo-sieve (BTS) (L.B. Bohle Maschinen+Verfahren GmbH, Ennigerloh, Germany) at 500 rpm and it was equipped with a 2 mm friction sieve. The milled granules were separated into subsamples by using a sample divider (Retsch PT/DR 1000, Retsch GmbH, Haan, Germany).

Tab. 5.2: Mean granulation time and chopper/impeller speed used to produce the different HSG formulations.

Short name	Mean granulation time [min]	Speed chopper; impeller [rpm]
H5200	5	1000;200
H5400	5	2000;400
H3300	3.75	1500;300
H2200	2.5	1000;200
H2400	2.5	2000;400

5.5.2.4 Particle size distribution

After milling ,the obtained granules were sieved using a sieve stack (bottom pan, 63, 100, 180, 250 355, 500, 710, 1000 and 2000 µm size) and the analytical sieving was performed on a sieve shaker (AS 200 digital, Retsch GmbH, Haan, Germany) for 10 min at an amplitude of 2 mm. The retained amount on each sieve was determined by weighing. The yield was defined as the fraction of granules in the class between 100 and 710 µm. Granules of this sieve fraction were further investigated and analysed. Therefore, granules smaller than 100 µm and larger than 710 µm were removed using the analytical sieves and residual fractions were homogenized in a Turbula blender (Willy A. Bachofen AG Maschinenfabrik, Switzerland) at a rotating speed of 50 rpm for 5 min.

5.5.2.5 Granules shape factor

The sieve fraction (100-710 µm) was analysed using a dynamic image analysis (Camsizer X2, Retsch GmbH, Haan, Germany) with the gravimetric module X-Fall. Approximately 10 g of granules were used for one measurement (n=3). The measured particle size range was between 10 µm and 2000 µm.

Different shape factors of the granules were evaluated, including a ratio calculated from the width (*b*) and the length (*l*) (Eq. 5.1). Moreover, the SPHT3 (Eq. 5.2) was evaluated, which gives information on the roundness of the particles and is calculated from the area (*A*) and the circumference (*p*). Additionally, *Symm* (Eq. 5.3) was calculated, which considers particles that are aspherical, which were formed due to immersion or coalescence of two particles. Here, r1 and r2 represent the distances from the centre of the particle pictured area to the margin in the set measuring direction. *Symm* is the minimum value of symmetry values in all measured directions.

$$\frac{b}{l} = \frac{Xcmin}{Xfemax} \qquad \text{(Eq. 5.1)}$$

$$SPHT = \frac{4\pi A}{P^2} \qquad \text{(Eq. 5.2)}$$

$$Symm = \left(\frac{1}{2}\right) * \left(1 + \min\left(\frac{r1}{r2}\right)\right) \qquad \text{(Eq. 5.3)}$$

The x_{cmin} particle diameter is the shortest chord of the measured set of maximum chords of a particle projection (result close to sieving) and the x_{femax} particle diameter is the longest Feret diameter of the measured set of Feret diameter of a particle (result close to microscopy).

The SPAN represents the width of the PSD and is calculated using Eq. 5.4:

$$SPAN = \frac{d90 - d10}{d50} \qquad \text{(Eq. 5.4)}$$

5.5.2.6 Bulk density, tapped density, and compressibility index

The bulk volume (V_0) was determined by filling approx. 100 g of each sample (100-710 µm) into a 250 ml volumetric cylinder. Tapped volume (V_{tapped}) was determined after 1250 taps using an Erweka SVM 22 (Erweka GmbH, Heusenstamm, Germany). The bulk (ρ_0) and tapped density (ρ_{tapped}) were calculated, respectively. All measurements were conducted three times. The compressibility index (C) was calculated by employing the following equation (Eq. 5.5):

$$C\ [\%] = \left(\frac{\rho tapped - \rho 0}{\rho tapped}\right) * 100\% \qquad \text{(Eq. 5.5)}$$

5.5.2.7 Flowability (angle of repose and mass flow)

Approximately 30 g of each sample was used to measure the flowability of the granules in an automatic test system (Erweka GT, Erweka GmbH, Heusenstamm, Germany). The powder was filled into a metal hopper with an orifice of a defined size (8 mm). The time needed to flow out of the hopper was measured with an electronic balance and it was characterized in s/100 g. Measurements were repeated three times.

5.5.2.8 Porosity

The pore-size distribution was determined by a mercury porosimeter (Pascal 140-240/440, POROTEC GmbH, Hofheim am Taunus, Germany). Approximately 0.5 g of granules (100-710 µm) were placed into a 488 mm³ dilatometer. The maximum pressure was 400 MPa and the pore size distribution was determined from 0.001 to 100 µm.

5.5.2.9 Specific surface area

The specific surface area was determined using dynamic image analysis (Camsizer X2, Retsch GmbH, Haan, Germany) with the gravimetric module X-Fall. Approximately 10 g of granules were used for one measurement (n=3). The measured particle size range was between 10 µm and 2000 µm. The specific surface area was calculated as unit of mass [m²/g] having regard to the pycnometric density.

5.5.2.10 Pycnometric Density

The pycnometric density of PM and granules was measured by an AccuPyc 1330 helium pycnometer (Micromeritics GmbH, Aachen, Germany). Prior to any measurement (n=1), the chamber was purged with 20 cycles. For analysis, a filling pressure of 136.86 kPa and an equilibration rate of 0.0345 kPa/min were used. Each measurement cycle was repeated up to 25 times or until a standard deviation of 0.01% was reached. The density was used for the calculation of the porosity, specific surface area and solid fraction (SF).

5.5.2.11 Scanning electron microscopy (SEM)

A scanning electron microscope (SU 3500, Hitachi High Technologies, Krefeld, Germany), equipped with a backscattered electron detector (BSE) and an energy dispersive X-ray detector (EDX) (EDAX Element- C2B, Ametek, Weiterstadt, Germany), was used to investigate the granules' morphology and the distribution of the binder. BSE images were collected at an acceleration voltage of 5 kV at a variable pressure mode of 30 Pa. To ensure the visualization of the material contrast, the samples were mounted with a conductive carbon paste (Leit-C-Plast, Plano GmbH, Wetzlar, Germany) and they were not coated beforehand. The intensity of the backscattered electrons correlated with the atomic weight of the molecules in the sample. The micrographs were then evaluated to describe the granules' PSD, porosity and morphology.

For EDX-analysis, the samples were compressed with a pneumatic hydraulic tablet press (FlexiTab, Röltgen GmbH & Co. KG, Solingen, Germany), using an 8 mm round flat-face tooling and a compaction pressure of 250 MPa to obtain a flat tablet surface. The tablets were further fixed on carbon paste and the analysis was performed without any coating. The surface of the tablets was mapped at the high vacuum mode with an acceleration voltage of 5 kV and a magnification of 300x. Working distance was kept constant at 10 mm ±1 mm. The percentage of detected carbon was evaluated by the TEAM software (Version 4.4.1, Ametek, Weiterstadt, Germany).

5.5.2.12 Image analysis of SEM/EDX-maps

To parameterize the distribution of the binder, the obtained micrographs from the EDX software with the carbon signal only (512x400 pixels), were divided into 35 sub-frames (80x73 pixels). The percentage of the area with binder in each of the 35 sub-frames was calculated using image editing software ImageMagick 6.9 (ImageMagick Studio LLC). The relative standard deviation of the average binder area (carbon signal in yellow) from all 35 sub-frames was calculated. This relative binder area variation (calculated as relative standard deviation (s_{rel})) was taken as a descriptor for the binder distribution. Low levels in s_{rel} indicate a homogeneous binder distribution, whereas high levels would represent a high variation of binder distribution among the 35 sub-frames, i.e. an inhomogeneous binder distribution. For every formulation, three tablets were analysed in total for mean value and standard deviation calculation of this distribution value, defined as the binder variation.

5.5.2.13 Tableting

Tablets (n = 5) were compressed on a Styl'One 105 ML (StylOne Classic 105 ML, Medelpharm, Beynost, France/Romaco Kilian, Cologne, Germany) using a 8 mm flat-face tooling. Five compaction pressures from 50 MPa to 250 MPa were applied at a constant tableting speed (dwell-time: 6-7 ms; average compression time: 110 ms). The die was filled manually and lubricated externally, if needed. After 24 h of storage, the tablets were analysed in terms of tablet weight (analytical balance, AG 204, Mettler Toledo GmbH, Gießen, Germany), thickness (Mitutoyo Absolute ID C125B, Mitutoyo Deutschland GmbH, Neuss, Germany), diameter and crushing strength (Erweka TBH 210, Erweka GmbH, Heusenstamm, Germany). The tensile strength (TS) (Eq. 5.6) and the solid fraction (SF); (Eq. 5.7, 5.8 and 5.9) were calculated from the obtained data. TS is the tablet crushing strength normalized by the dimension of the tablet and is therefore independent of its geometry [64],

$$TS = \frac{2F}{\pi dh} \qquad \text{(Eq. 5.6)}$$

where *F* is the crushing strength, *d* the diameter and *h* the thickness of the tablet.
SF represents the apparent density (P_{app}) of the compact, calculated from the tablet weight (m) and its volume (V_p) relative to the true density (P_{true}) of the powder.

$$SF = \frac{P_{app}}{P_{true}} \qquad \text{(Eq. 5.7)}$$

$$P_{app} = \frac{m}{V_p} \qquad \text{(Eq. 5.8)}$$

$$V_p = \pi * \left(\frac{d}{2}\right)^2 * h \qquad \text{(Eq. 5.9)}$$

Where V_p is the volume of the compact calculated based on *d* and *h*, which describe the tablet diameter and thickness.

The parameters were used to determine the tabletability, which is known as the ability of a powder to be transformed into a tablet with a certain TS under the applied compaction pressure. Moreover, the parameters were used to plot the compressibility, which defines the ability of a powder to reduce its volume under pressure (SF vs. applied compaction pressure).
Additionally, the compactibility, which describes the resulting TS as a function of SF, was evaluated. Therefore, it is a descriptor for the number of bonding points between particles or the binding force generated by the tableting process.

5.5.2.14 Statistical evaluation

The statistical evaluation of the process settings (2^2 full factorial design including one centerpoint was evaluated using the software Modde (Modde for Windows, V. 12.1, Umetrics, Satorius AG, Sweden). The number of experiments was low (N=5). Therefore, only a screening of the process settings (throughput [g/min] / screw speed [rpm] and mean granulation time [min] / chopper/impeller speed [rpm]) and their influence on the response factors (yield [%], d_{50} [µm], shape factor b/l3, compressibility index C [%], mass flow [s/100g], porosity [%], tensile strength TS at 150 MPa [N/mm²] and binder variation) was performed. Results of the TSG and HSG were analysed using a multiple linear regression model. R^2 is the percent of the variation of the response explained by the model. R^2 is a measure of fit, i.e. how well the model fits the data. Process settings and response factors were screened for correlation.

5.6 Results

5.6.1 Particle size distribution (PSD) and yield

In Fig. 5.1, the process yield (quantity of granules between 100 and 710 µm) of the different granulation trails are shown. Overall, TSG exhibited a higher yield (approx. 70%) than HSG (max. 60%). Furthermore, TSG is a very robust process in terms of the obtained yields, even when changing throughput and screw speed (min: 64.2 ±0.4; max: 70.76 ±0.79%). In HSG, higher operation speeds resulted in a higher yield (33.91 ±0.24 vs. 59.58 ±0.13 and 48.93 ±1.37 vs. 54.90 ±0.09%). The lowest yield was found for the formulation H5200 (33.91 ±0.24%).

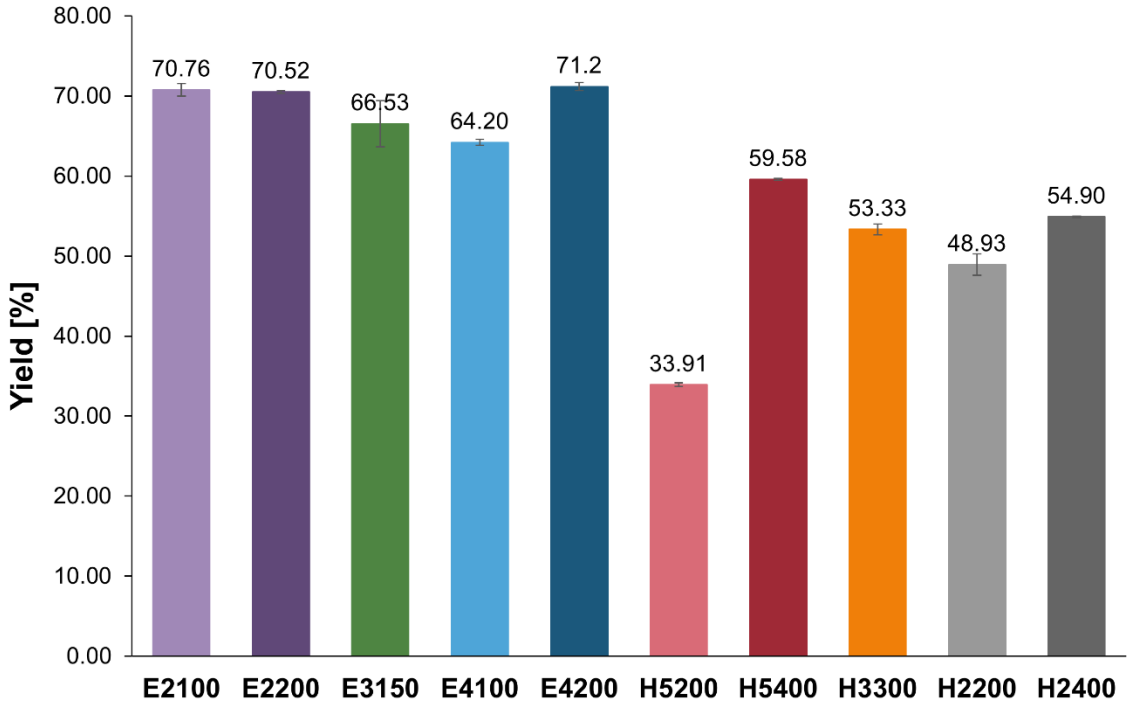

Fig. 5.1: Yield (100-710 µm) of the manufacturing processes: E2100=TSG, 2g/min, 100rpm; E2200=TSG, 2g/min, 200rpm; E3150=TSG, 3g/min, 150rpm; E4100= TSG, 4g/min, 100rpm; E4200=TSG, 4g/min, 200rpm; H5200=HSG, 5min, 200rpm impeller speed, 1000rpm chopper speed; H5400=HSG, 5min, 400rpm impeller speed, 2000rpm chopper speed; H3300=HSG, 3.75min, 300rpm impeller speed, 1500rpm chopper speed; H2200=HSG, 2.5min, 200rpm impeller speed, 1000rpm chopper speed; H2400=HSG, 2.5min, 400rpm impeller speed, 2000rpm chopper speed.

In Tab. 5.3, the particle sizes and shape factors within the target size fraction (100-710 µm), which were determined via dynamic image analysis, are listed. In general, granules produced via HSG showed a smaller particles size, than granules produced via TSG within the analysed fraction (100-710 µm), indicated by the d_{50} [µm]. A higher quantity of large particles was found for granules deriving from TSG, compared to HSG granules (demonstrated by the d_{90} [µm]). However, the TSG granules achieved a narrower PSD within this fraction, indicated by the SPAN. Overall, TSG resulted in a less quantity of fines (d_{10} [µm]).

The granules produced by HSG were more spherical in shape than the TSG granules, indicated by the respective shape factors. Regarding the TSG and HSG, no clear trend in the shape factors was observed, when comparing the five different granulation settings of process variables.

5.6.2 **Bulk and tapped density, compressibility index and flowability**

In Tab. 5.4, the data out of flowability tests are listed. In terms of bulk density (ρ_0 [g/cm³]), granules produced via TSG showed a lower bulk density (ρ_0 [g/cm³]) than pure A12, PM and granules produced via HSG. In general, the flowability of granules were good, whereas A12 and the PM showed poor and very poor flowability, respectively. The granules produced via HSG showed a slightly lower compressibility index (C [%]) than granules produced with TSG. The flowability of the granules can be described as good, according to the classification of the Ph. Eur. 2.9.36.

Regarding the mass flow (MF [s/100g]), A12 and the PM were not freely flowing and were not measurable, even when using the largest available orifice (25 mm) and agitation of a stirrer. Therefore, flowability is classified as very, very poor. The granules obtained via HSG flow faster (s/100g) compared to granules obtained from TSG. Different process operation conditions did not change the flow properties to a major extent.

Tab. 5.3: Particle size and shape factors of the sieve fraction (100-710 µm): E2100=TSG, 2g/min, 100rpm; E2200=TSG, 2g/min, 200rpm; E3150=TSG, 3g/min, 150rpm; E4100=TSG, 4g/min, 100rpm; E4200=TSG, 4g/min, 200rpm; H5200=HSG, 5min, 200rpm impeller speed, 1000 rpm chopper speed; H5400=HSG, 5min, 400rpm impeller speed, 2000 rpm chopper speed; H3300=HSG, 3.75min, 300rpm impeller speed, 1500 rpm chopper speed; H2200=HSG, 2.5min, 200rpm impeller speed, 1000 rpm chopper speed; H2400=HSG, 2.5min, 400rpm impeller speed, 2000 rpm chopper speed.

Sample	d_{10} [µm] ±SD	d_{50} [µm] ±SD	d_{90} [µm] ±SD	SPAN ±SD	SPHT3 ±SD	Symm3 ±SD	b/l3 ±SD
E2100	234.0 ±5.4	481.5 ±2.1	698.3 ±0.1	0.964 ±0.010	0.686 ±0.001	0.838 ±0.001	0.619 ±0.001
E2200	239.7 ±16.0	501.2 ±1.8	728.9 ±1.3	0.976 ±0.037	0.678 ±0.003	0.835 ±0.001	0.608 ±0.001
E3150	153.8 ±26.6	476.8 ±6.4	711.6 ±5.9	1.048 ±0.072	0.679 ±0.004	0.835 ±0.001	0.631 ±0.002
E4100	253.8 ±10.2	487.0 ±17.4	712.5 ±12.7	0.942 ±0.040	0.692 ±0.004	0.839 ±0.001	0.639 ±0.002
E4200	254.3 ±30.4	544.3 ±9.3	753.6 ±1.6	0.918 ±0.068	0.669 ±0.003	0.830 ±0.001	0.625 ±0.002
H5200	163.7 ±26.2	442.5 ±46.0	677.3 ±14.1	1.171 ±0.157	0.870 ±0.006	0.918 ±0.003	0.716 ±0.007
H5400	136.7 ±6.8	384.9 ±15.0	644.2 ±12.0	1.320 ±0.042	0.858 ±0.002	0.921 ±0.002	0.712 ±0.001
H3300	113.3 ±0.7	333.9 ±5.4	623.6 ±4.1	1.528 ±0.038	0.841 ±0.002	0.909 ±0.002	0.710 ±0.001
H2200	85.5 ±29.0	358.7 ±53.7	627.4 ±18.8	1.538 ±0.272	0.839 ±0.017	0.906 ±0.009	0.714 ±0.007
H2400	156.3 ±12.8	395.9 ±8.3	657.2 ±6.8	1.266 ±0.055	0.860 ±0.002	0.922 ±0.001	0.701 ±0.001

Tab. 5.4: Bulk and tapped density [g/cm³], compressibility index [%] and mass flow [s/100g] of the granules (100-710 µm): E2100=TSG, 2g/min, 100rpm; E2200=TSG, 2g/min, 200rpm; E3150=TSG, 3g/min, 150rpm; E4100=TSG, 4g/min, 100rpm; E4200=TSG, 4g/min, 200rpm; H5200=HSG, 5min, 200rpm impeller speed, 1000 rpm chopper speed; H5400=HSG, 5min, 400rpm impeller speed, 2000 rpm chopper speed; H3300=HSG, 3.75min, 300rpm impeller speed, 1500 rpm chopper speed; H2200=HSG, 2.5min, 200rpm impeller speed, 1000 rpm chopper speed; H2400=HSG, 2.5min, 400rpm impeller speed, 2000 rpm chopper speed; PM = physical mixture; A12: DI-CAFOS A12.

Material	ρ_0 [g/cm³]	ρ_{tapped} [g/cm³]	C [%]	MF [s/100g]
A12	0.94 ±0.04	1.26 ±0.04	25.1 ±3.2	N/A
PM	0.84 ±0.01	1.22 ±0.01	31.5 ±0.8	N/A
E2100	0.66 ±0.01	0.77 ±0.01	14.3 ±0.5	15.0 ±0.7
E2200	0.72 ±0.01	0.82 ±0.01	12.7 ±1.7	14.9 ±0.0
E3150	0.68 ±0.00	0.78 ±0.01	12.5 ±0.4	16.1 ±0.1
E4100	0.68 ±0.01	0.78 ±0.01	12.5 ±0.2	16.1 ±0.3
E4200	0.71 ±0.02	0.82 ±0.02	14.0 ±0.5	13.1 ±0.9
H5200	1.03 ±0.01	1.17 ±0.01	11.9 ±0.7	8.6 ±0.1
H5400	1.10 ±0.01	1.24 ±0.02	11.1 ±2.4	7.9 ±0.0
H3300	1.13 ±0.01	1.26 ±0.01	10.5 ±1.2	7.8 ±0.2
H2200	1.06 ±0.01	1.19 ±0.01	10.8 ±0.7	8.3 ±0.1
H2400	1.12 ±0.02	1.26 ±0.03	10.9 ±1.0	7.9 ±0.0

5.6.3 **Porosity**

In Tab. 5.5, the total porosity of the different formulations, measured by mercury porosimetry (combined high- and low-pressure measurements), are shown. Overall, all granules showed a bimodal distribution and few pores in the larger pore diameter region (> 10 µm, graph not shown). In comparison to granules of HSG, the granules produced from TSG had an overall higher porosity. The granules from TSG contained a high volume of pores (up to 40 mm^3/g) with a radius larger than 1 µm. The total porosity increased with increasing throughput (E4100 and E4200), the effect of the screw speed was minor. The lowest porosities were found for the formulations E2100 and E2200. In the case of HSG, a larger set of pores was found (up to 20 mm^3/g), when low-shear granulation was applied (H5200 and H2200). The porosity decreased with increasing chopper and impeller speed (H5400, H3300 and H2400). No substantial effect of the granulation time was found for the HSG formulations.

5.6.4 **Specific surface area and pycnometric density**

The results for the SSA and the pycnometric density measurements are shown in Tab. 5.5. A lower SSA [m^2/g] was observed for granules made by TSG than for HSG granules. Results were determined using image analysis and were therefore in concordance to the results obtained from the particle size analysis, where TSG granules showed a larger mean particle size, than granules produced using HSG. Additionally, the HSG granules showed slightly lower pycnometric density [g/cm^3] than granules from TSG

Tab. 5.5: Total porosity [%] determined via mercury porosimetry, SSA [m²/g] and pycnometric density of the granules (100-710 µm): E2100=TSG, 2g/min, 100rpm; E2200=TSG, 2g/min, 200rpm; E3150=TSG, 3g/min, 150rpm; E4100=TSG, 4g/min, 100rpm; E4200=TSG, 4g/min, 200rpm; H5200=HSG, 5min, 200rpm impeller speed, 1000 rpm chopper speed; H5400=HSG, 5min, 400rpm impeller speed, 2000 rpm chopper speed; H3300=HSG, 3.75min, 300rpm impeller speed, 1500 rpm chopper speed; H2200=HSG, 2.5min, 200rpm impeller speed, 1000 rpm chopper speed; H2400=HSG, 2.5min, 400rpm impeller speed, 2000 rpm chopper speed.

Sample	Total porosity [%]	SSA [m^2/g] ± SD	Pycnometric density [g/cm^3] ± SD
E2100	42.280	0.0065 ±0.0000	2.3769 ±0.0008
E2200	41.821	0.0061 ±0.0002	2.3707 ±0.0004
E3150	43.126	0.0075 ±0.0008	2.3476 ±0.0051
E4100	45.086	0.0061 ±0.0002	2.3524 ±0.0060
E4200	46.922	0.0057 ±0.0003	2.3711 ±0.0006
H5200	29.459	0.0080 ±0.0011	2.2673 ±0.0003
H5400	23.519	0.0097 ±0.0004	2.2857 ±0.0003
H3300	23.075	0.0118 ±0.0001	2.2233 ±0.0105
H2200	26.860	0.0144 ±0.0025	2.2322 ±0.0004
H2400	23.245	0.0087 ±0.0003	2.2604 ±0.0004

5.6.5 **Scanning Electron Microscopy of the granules**

In Fig. 5.2 and 5.3, SEM pictures (100x and 500x magnification) of the granules are shown. Granules produced by HSG achieved a more spherical shape and smoother surface than the granules obtained from TSG. The TSG granules were more irregularly shaped and higher in the internal porosity. Moreover, the granules produced from HSG had a lighter appearance compared to granules from TSG. Using the BSE detector, dicalcium phosphate appears brighter than the binder Kolliphor® P407, due to their high difference in their atomic weight (the higher the atomic weight the lighter the appearance using BSE mode). This indicates that in the case of HSG less binder is located on the surface of the granules. No difference in appearance was detected among the granules produced by TSG or HSG.

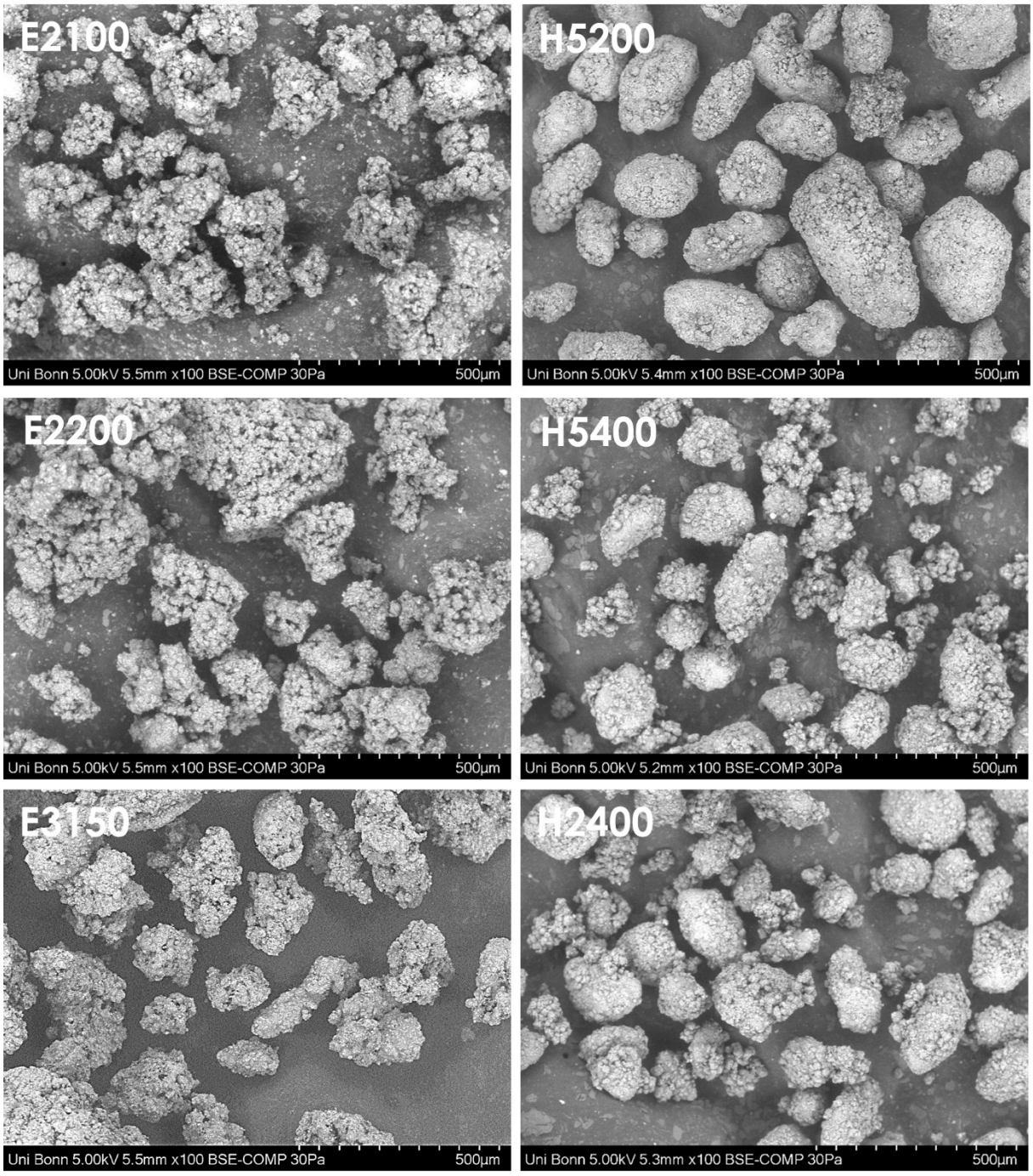

Fig. 5.2: SEM images of the granules (100-710 µm) 100x: E2100=TSG, 2g/min, 100rpm; E2200=TSG, 2g/min, 200rpm; E31500=TSG, 3g/min, 150rpm; H5200=HSG, 5min, 200rpm impeller speed, 1000 rpm chopper speed; H5400=HSG, 5min, 400rpm impeller speed, 2000 rpm chopper speed; H2400=HSG, 2.5min, 400rpm impeller speed, 2000 rpm chopper speed.

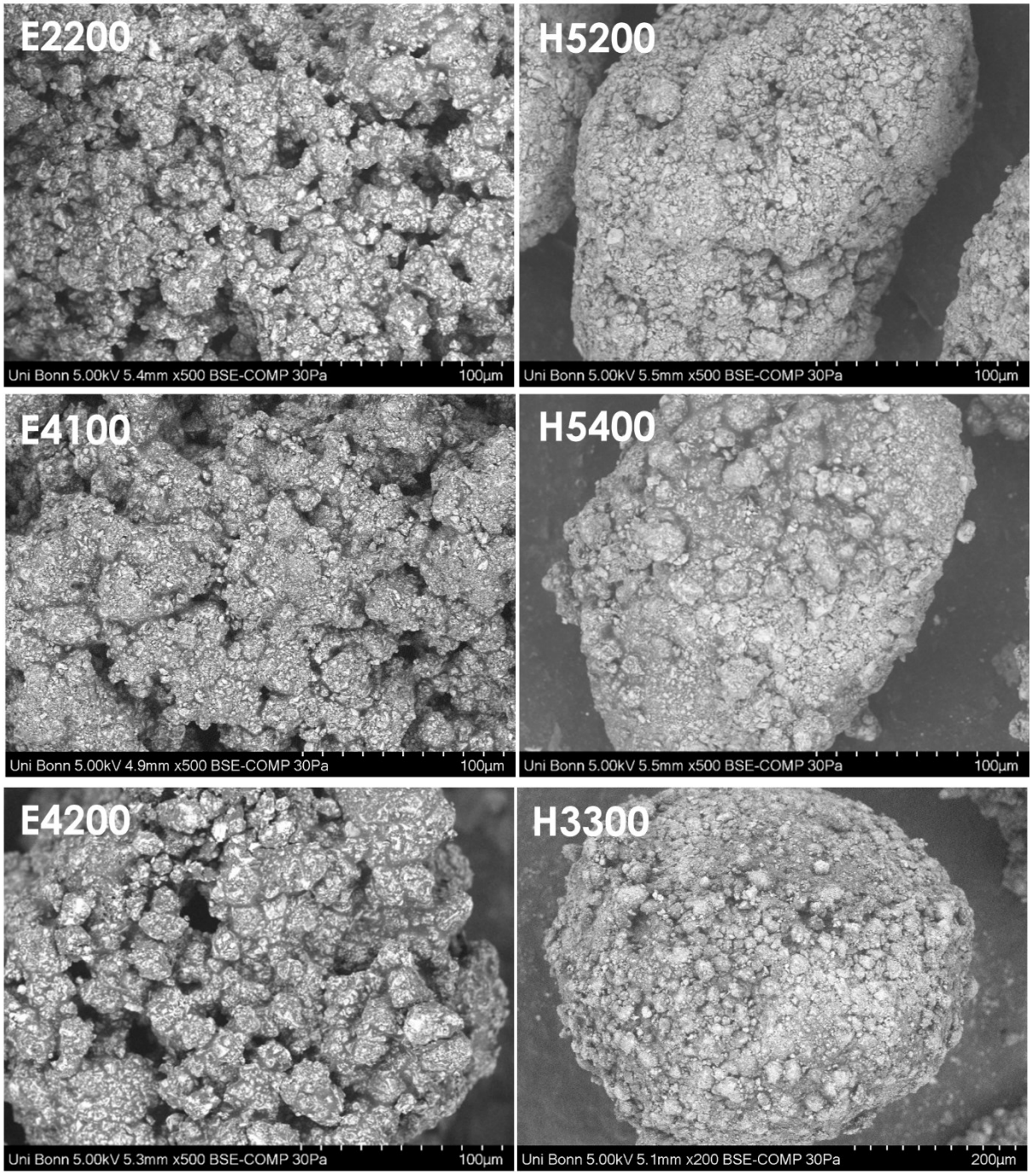

Fig. 5.3: SEM images of the granules (100-710 µm) 500x: E2200=TSG, 2g/min, 200rpm; E4100=TSG, 4g/min, 100rpm; E4200=TSG, 4g/min, 200rpm; H5200=HSG, 5min, 200rpm impeller speed, 1000 rpm chopper speed; H5400=HSG, 5min, 400rpm impeller speed, 2000 rpm chopper speed; H3300=HSG, 3.75min, 300rpm impeller speed, 1500 rpm chopper speed.

5.6.6 **Results of the tableting process**

The tabletability plots are shown in Fig. 5.4. In general, neat A12 achieved only low TS. Also, in the case of the PM, TS could not be increased. Melt granulation as a process as such, was found to increase TS. Comparing both granulation processes, TSG granules reached a higher TS at similar compaction pressure than granules manufactured by HSG. The highest tabletability was found for E2200, E3150 and E4100. E2100 and E4200 showed a lower tabletability especially when using lower compaction pressures (< 150 MPa). It should be noted, that the difference in tabletability between the different granulation trails using the extruder, became smaller with increasing compaction pressure. Using 200 or 250 MPa for compaction all granules produced with via TSG achieved comparable TS. Among the HSG granules, H5200 showed the highest tabletability. All other granules produced using HSG achieved a similar tabletability, independent of the speed of the chopper and impeller and the mean granulation time.

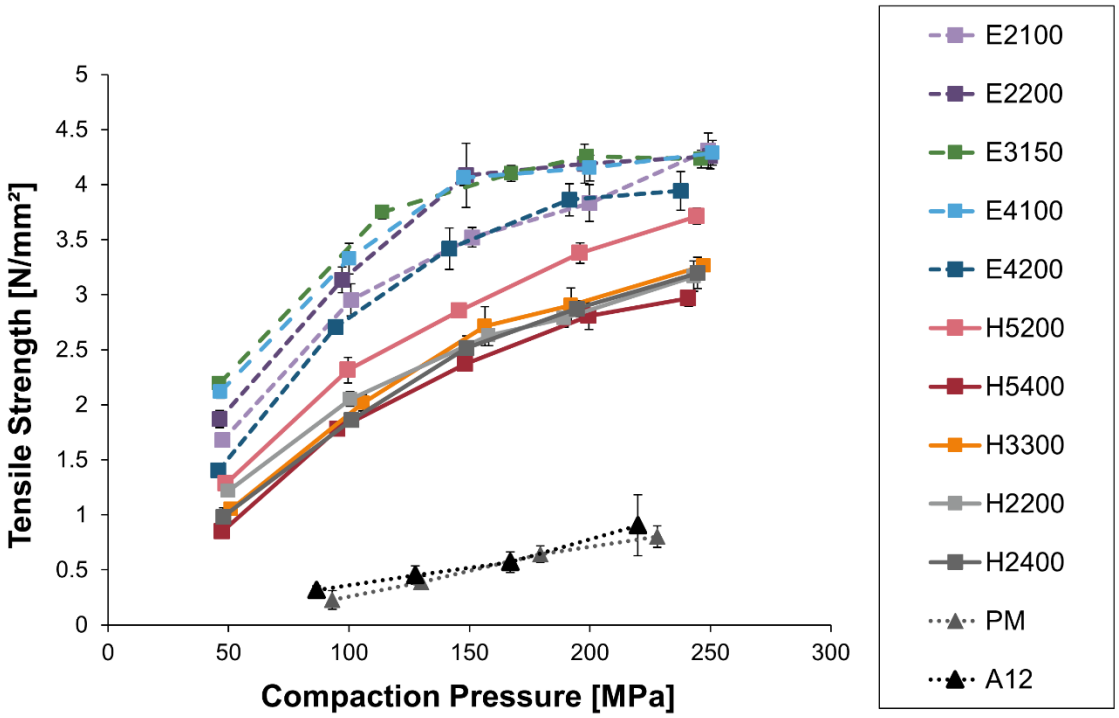

Fig. 5.4: Tabletability plot: E2100=TSG, 2g/min, 100rpm; E2200=TSG, 2g/min, 200rpm; E3150=TSG, 3g/min, 150rpm; E4100= TSG, 4g/min, 100rpm; E4200=TSG, 4g/min, 200rpm; H5200=HSG, 5min, 200rpm impeller speed, 1000rpm chopper speed; H5400=HSG, 5min, 400rpm impeller speed, 2000rpm chopper speed; H3300=HSG, 3.75min, 300rpm impeller speed, 1500rpm chopper speed; H2200=HSG, 2.5min, 200rpm impeller speed, 1000rpm chopper speed; H2400=HSG, 2.5min, 400rpm impeller speed, 2000rpm chopper speed; PM = physical mixture; A12: DI-CAFOS A12.

In Fig. 5.5, the compactibility plots are shown. The addition of Kolliphor® as part of a PM, increased SF of A12, which was more pronounced in the case of melt granulation. Compared to the PM, a similar increase in SFs were found for the granules, independent of the granulation process (TSG or HSG) (Fig. 5.5 and Fig. 5.6). However, using the extruder, the TS was increased more pronouncedly. Therefore, the compactibility was higher for the TSG granules, than for HSG granules, indicating that TSG resulted in a higher bonding capacity of the granules compared to the granules produced via HSG.

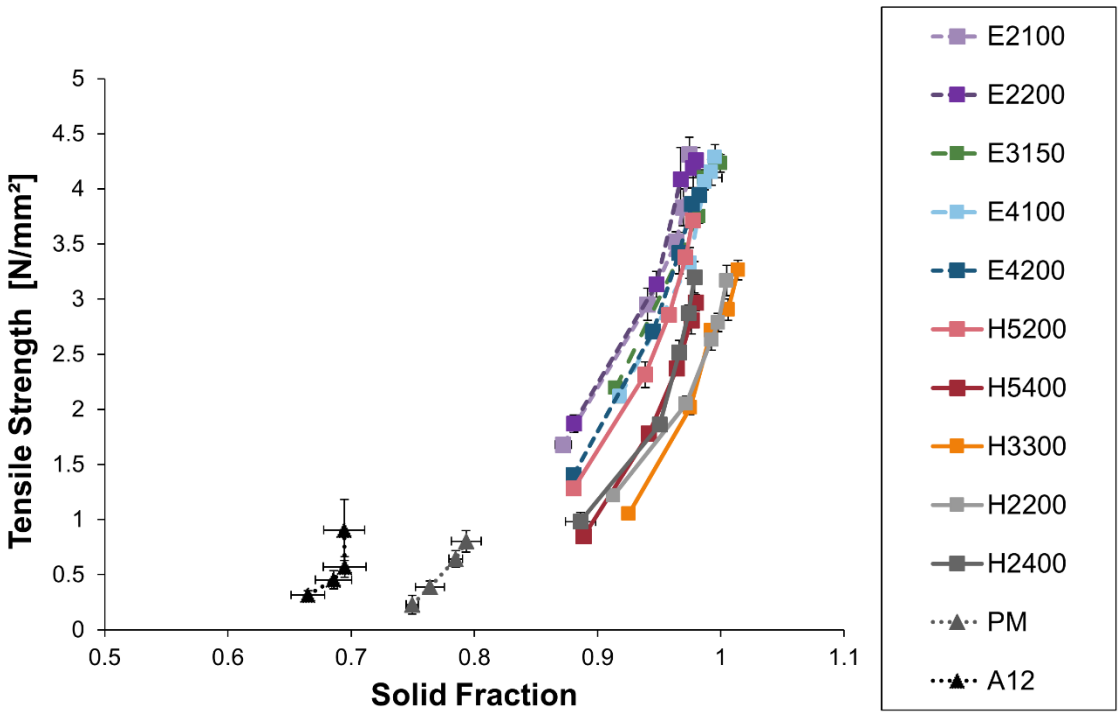

Fig. 5.5: Compactibility plot: E2100=TSG, 2g/min, 100rpm; E2200=TSG, 2g/min, 200rpm; E3150=TSG, 3g/min, 150rpm; E4100= TSG, 4g/min, 100rpm; E4200=TSG, 4g/min, 200rpm; H5200=HSG, 5min, 200rpm impeller speed, 1000rpm chopper speed; H5400=HSG, 5min, 400rpm impeller speed, 2000rpm chopper speed; H3300=HSG, 3.75min, 300rpm impeller speed, 1500rpm chopper speed; H2200=HSG, 2.5min, 200rpm impeller speed, 1000rpm chopper speed; H2400=HSG, 2.5min, 400rpm impeller speed, 2000rpm chopper speed; PM = physical mixture; A12: DI-CAFOS A12.

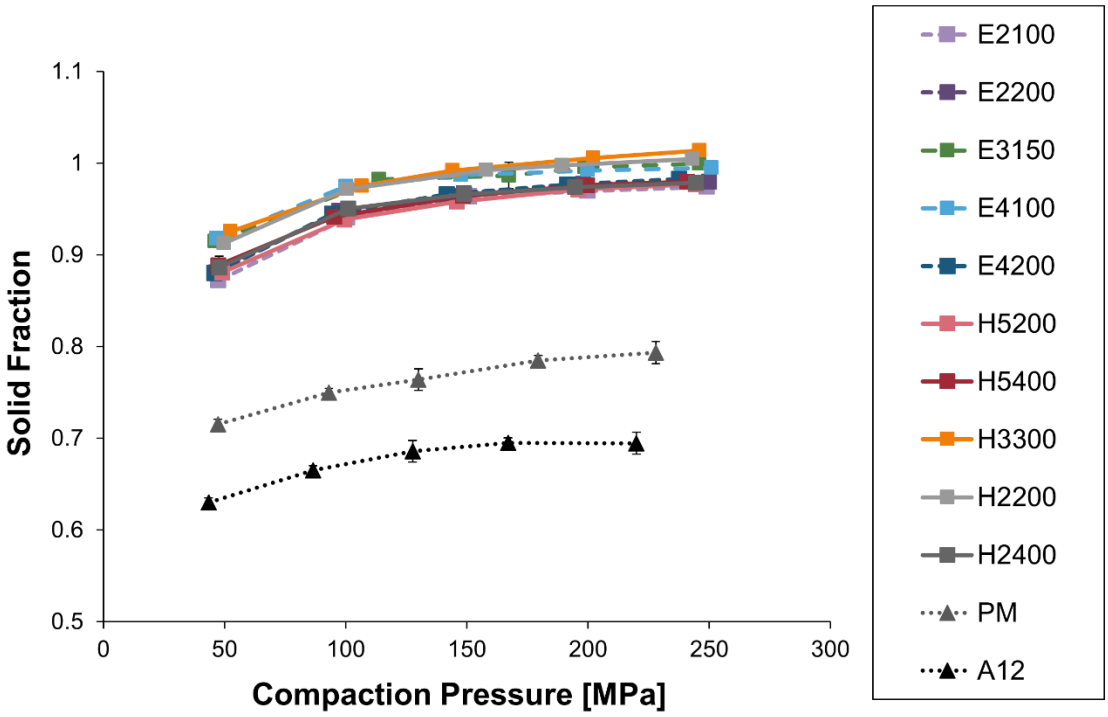

Fig. 5.6: Compressibility plot: E2100=TSG, 2g/min, 100rpm; E2200=TSG, 2g/min, 200rpm; E3150=TSG, 3g/min, 150rpm; E4100= TSG, 4g/min, 100rpm; E4200=TSG, 4g/min, 200rpm; H5200=HSG, 5min, 200rpm impeller speed, 1000rpm chopper speed; H5400=HSG, 5min, 400rpm impeller speed, 2000rpm chopper speed; H3300=HSG, 3.75min, 300rpm impeller speed, 1500rpm chopper speed; H2200=HSG, 2.5min, 200rpm impeller speed, 1000rpm chopper speed; H2400=HSG, 2.5min, 400rpm impeller speed, 2000rpm chopper speed; PM = physical mixture; A12: DI-CAFOS A12.

5.6.7 **Scanning Electron Microscopy and EDX of the tablets**

In Fig. 5.7 carbon EDX maps of the tablet surfaces from tablets made of TSG or HSG granules are shown. The yellow colour is the carbon signal, which belongs to the binder Kolliphor® P407. At similar scanning time, the tablets comprising of TSG granules achieved a more intense signal, compared to those made of HSG granules. Moreover, the distribution of the carbon signal is more homogenous in the case of the tablets made of TSG granules. To describe the binder distribution, a relative standard deviation of the tablet surface map subpictures were calculated, given as the binder variation (Fig. 5.9). In here, a low value indicates a homogenous distribution of the binder in the tablet. The higher the deviation in binder between the subpictures, e.g. an inhomogeneous binder distribution, the higher the relative standard deviation value becomes.

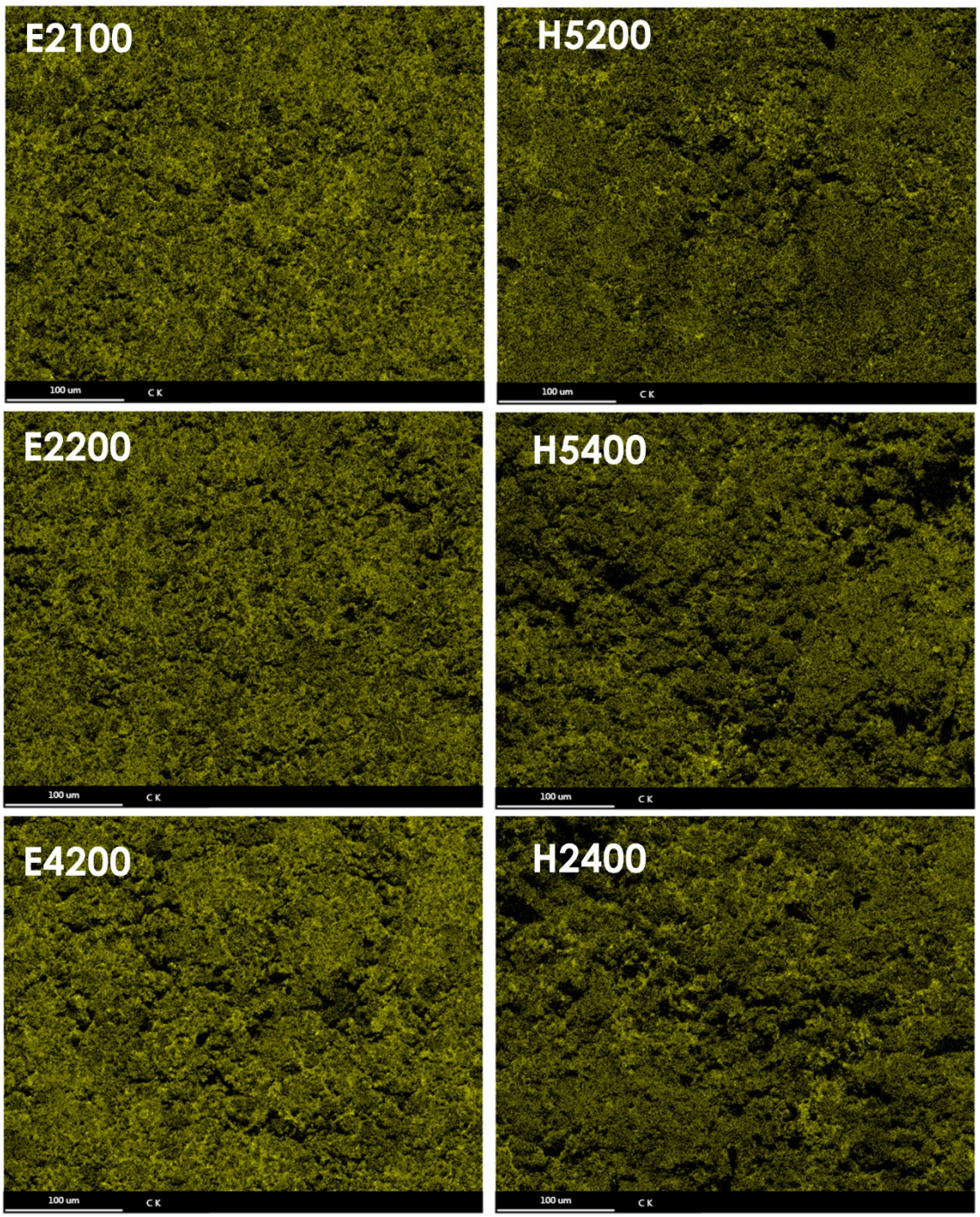

Fig. 5.7: EDX maps of the tablet surfaces produced from the granules (carbon-signal): E2100=TSG, 2g/min, 100rpm; E2200=TSG, 2g/min, 200rpm; E4200=TSG, 4g/min, 200rpm; H5200=HSG, 5min, 200rpm impeller speed, 1000rpm chopper speed; H5400=HSG, 5min, 400rpm impeller speed, 2000rpm chopper speed; H2400=HSG, 2.5min, 400rpm impeller speed, 2000rpm chopper speed.

Additionally, Fig. 5.8 shows the mean content [%] of carbon from three tablets. The value was determined by the EDX software (TEAM, Ametek, Weiterstadt, Germany). The carbon signal intensity was correlated to the amount of binder, which was available in the tablet for bonding. For the tablets comprising of TSG granules, more binder was detected than in the case of the tablets produced from HSG granules. Moreover, the binder in the TSG granule tablets was more homogenously distributed than in the HSG granule tablets (Fig. 5.9). No difference in carbon content was observed among the tablets produced from HSG or TSG, respectively (Fig. 5.8). However, when using higher process operational speeds, the binder distribution was increased for TSG as well as for HSG tablets (Fig. 5.9), indicated also by the decreased standard deviation (Bin σ) of the binder variation among the investigated tablets.

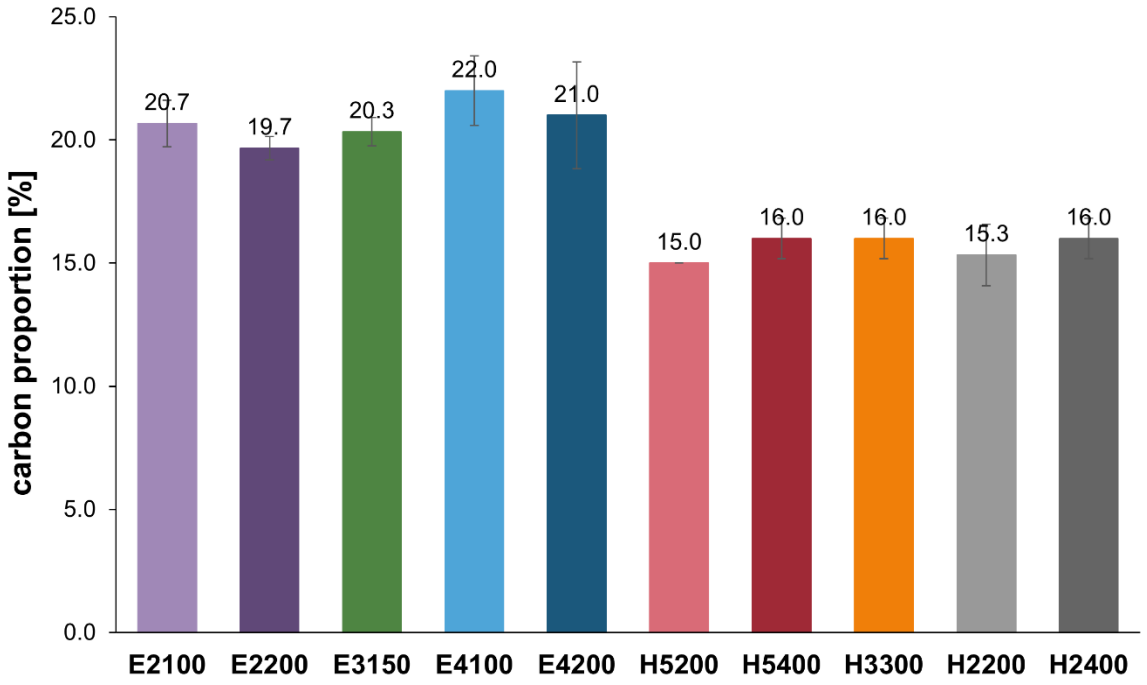

Fig. 5.8: Carbon proportion in the tablets produced from the granules: E2100=TSG, 2g/min, 100rpm; E2200=TSG, 2g/min, 200rpm; E3150=TSG, 3g/min, 150rpm; E4100= TSG, 4g/min, 100rpm; E4200=TSG, 4g/min, 200rpm; H5200=HSG, 5min, 200rpm impeller speed, 1000rpm chopper speed; H5400=HSG, 5min, 400rpm impeller speed, 2000rpm chopper speed; H3300=HSG, 3.75min, 300rpm impeller speed, 1500rpm chopper speed; H2200=HSG, 2.5min, 200rpm impeller speed, 1000rpm chopper speed; H2400=HSG, 2.5min, 400rpm impeller speed, 2000rpm chopper speed.

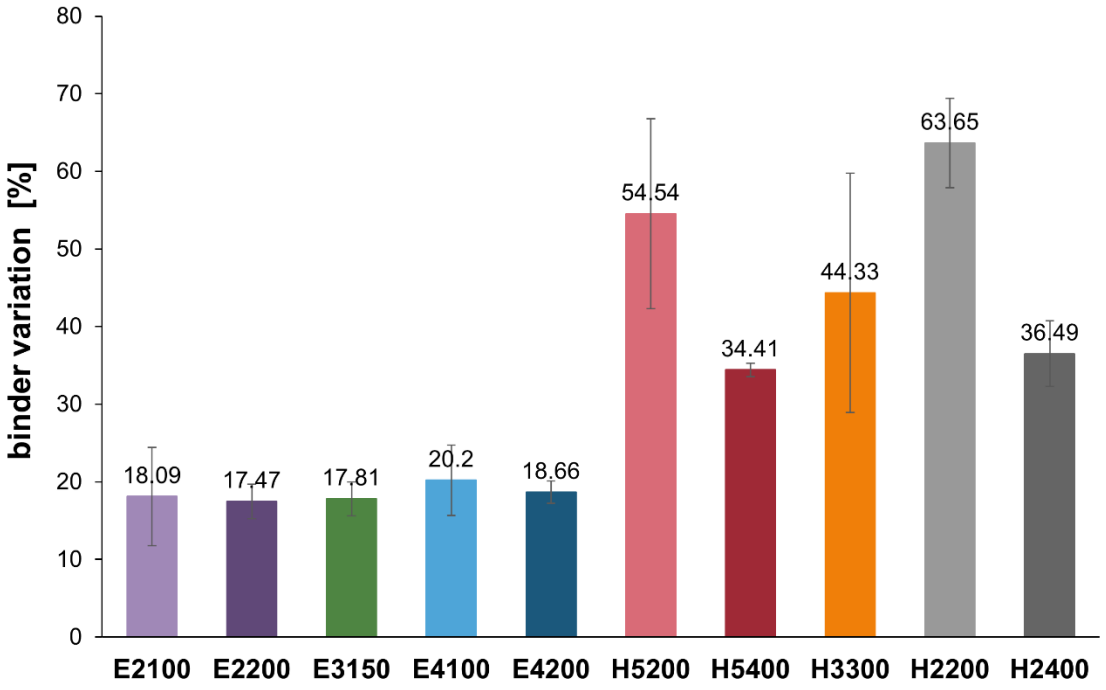

Fig. 5.9: Binder variation in the tablets produced from the granules: E2100=TSG, 2g/min, 100rpm; E2200=TSG, 2g/min, 200rpm; E3150=TSG, 3g/min, 150rpm; E4100= TSG, 4g/min, 100rpm; E4200=TSG, 4g/min, 200rpm; H5200=HSG, 5min, 200rpm impeller speed, 1000rpm chopper speed; H5400=HSG, 5min, 400rpm impeller speed, 2000rpm chopper speed; H3300=HSG, 3.75min, 300rpm impeller speed, 1500rpm chopper speed; H2200=HSG, 2.5min, 200rpm impeller speed, 1000rpm chopper speed; H2400=HSG, 2.5min, 400rpm impeller speed, 2000rpm chopper speed.

5.6.8 **Statistical evaluation / correlation plots**

Tab. 5.6 shows the R^2 of the multiple linear regression model. R^2 is the percent of the variation of the response explained by the model. R^2 is a measure of fit, i.e. how well the model fits the data. In the case of TSG a linear correlation was found for the shape factor b/l3 (R^2=0.99), the binder variation (R^2=0.99) and the porosity (R^2=0.96). For the HSG a strong correlation was found for the shape factor b/l3 (R^2=1), the binder variation (R^2=0.99) and the yield (R^2=0.97). Fig. 5.10 and Fig. 5.11 show the correlation plots for the TSG and HSG results. For TSG the highest correlation was found for the compressibility index C [%] and the TS (R^2=-0.9692). The higher the C, the lower the TS. Moreover, the porosity correlated with the throughput (R^2=0.93) and the mass flow MF [s/100g] was linked to the d_{50} [µm] (R^2=-0.9204). Further correlations were found for the product of screw speed and throughput [rpm·g/min] and the TS [N/mm²] (R^2=-0.8921), as well as for the compressibility index C [%] (R^2=0.8832).

A correlation was found for the screw speed and the standard deviation of the binder variation Bin σ (R^2=-0.8861). For the HSG process, correlations were found for the MF [s/100g] and the porosity [%] (R^2=0.9965). Additionally, correlations were identified for the chopper/impeller speed [rpm] and the binder variation, the porosity [%], the TS [N/mm²] and the yield [%]. The higher the chopper/impeller speed the lower the binder variation (R^2=-0.9576), the lower the porosity (R^2=-0.8439), the lower the TS (R^2=-0.8067) and the higher the process yield (R^2=0.8044).

Tab. 5.6: R^2 (percent of the variation of the response) obtained from the MLR model for the critical quality attributes of the granules produced via HSG and TSG.

Response factor	R^2 TSG	R^2 HSG
Yield [%]	0.85	0.97
d_{50} [µm]	0.81	0.55
b/l3	0.99	1
C [%]	0.8	0.67
MF [s/100g]	0.77	0.76
Porosity [%]	0.96	0.82
TS at 150 MPa [N/mm²]	0.81	0.92
Binder Distribution	0.99	0.99

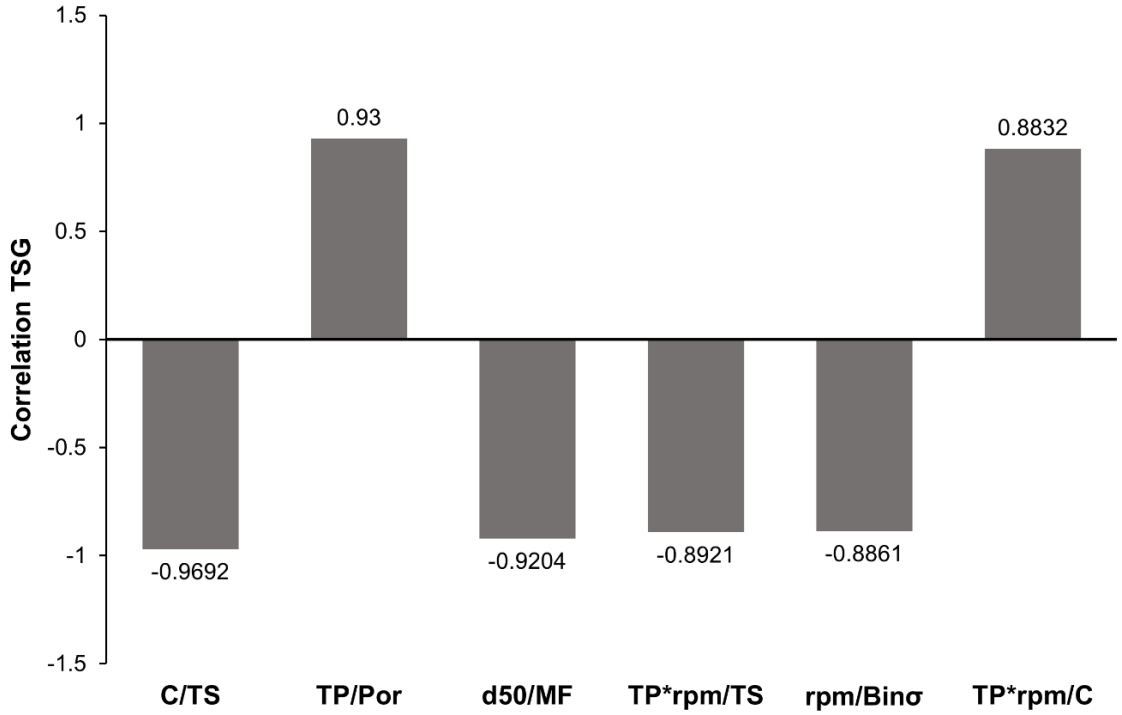

Fig. 5.10: Correlation plot for the TSG results: Bin= Binder variation, C= compressibility index [%], d50= mean particle size [µm], MF= mass flow [s/100g], Por= porosity [%], rpm= screw speed [rpm], TS= tensile strength at 150 MPa [N/mm²], TP= throughput [g/min].

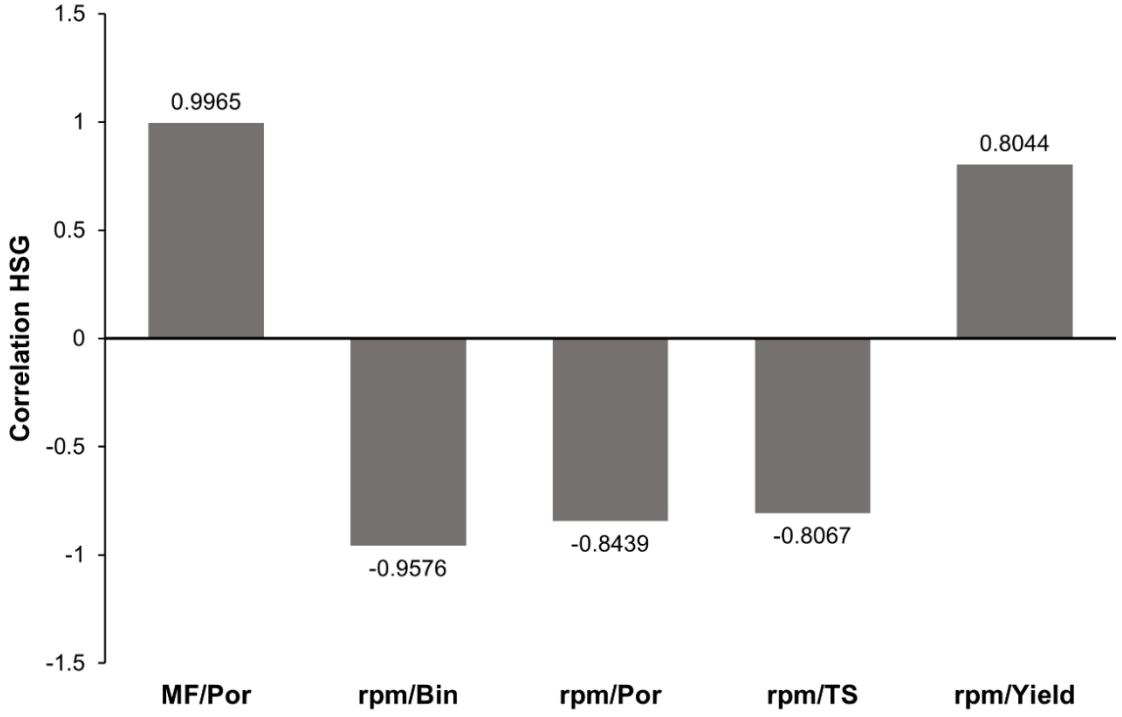

Fig.5.11: Correlation plot for the HSG results: Bin= Binder variation, MF= mass flow [s/100g], Por= porosity [%], rpm= chopper and impeller speed [rpm], TS= tensile strength at 150 MPa [N/mm²], Yield [%].

5.7 Discussion

A summary of the critical quality attributes (CQAs) under investigation is given in Tab. 5.7. In general, melt granulation increased particle size, flowability and tabletability compared to the physical mixture (PM). However, granules product performance including the yield, PSD, shape, flowability, porosity, density, SSA, compactibility and binder distribution was different for the formulations either produced via HSG or TSG.

Tab. 5.7: Summary of the results obtained for critical quality attributes of the granules produced via HSG and TSG.

Critical quality attribute	HSG	TSG
Particle size distribution	Broader	Narrow
Yield (100-710 µm)	Lower	Higher
Shape	Spherical	Elongated
Flowability	Good*	Good*
Porosity	Lower	Higher
Density	Higher	Lower
SSA	Higher	Lower
Compactibility	Lower	Higher
Binder Distribution	Less homogenous	More homogenous
Available binder content for bonding	Lower	Higher

*Compressibility Index C [%] scaled according to Ph.Eur. 9.8, 2.9.36

In terms of PSD granules produced by HSG showed a broader PSD with a larger content of fines, compared to the granules from TSG (Tab. 5.3). Their more spherical shape (Tab. 5.3) can explain the improved flowability (lower C, faster MF) and higher ρ_{tapped} of the HSG granules (Tab. 5.4). Moreover, the HSG granules showed less porosity (Tab. 5.5) and a smoother surface (Fig. 5.3) than the TSG granules.

The mercury porosity (Tab. 5.5) showed an overall higher porosity for the TSG granules. Additionally, very large internal pores can be seen in the SEM-micrographs (Fig. 5.3) of the TSG granules.

However, it is challenging to distinguish inter- and intragranular porosity by using mercury porosimetry. Therefore, the results might reflect the overall lower bulk density (Tab. 5.4) of the granules from TSG, including intergranular pores as well as the higher intragranular pores, observed by SEM. Overall, the TSG granules showed a more irregular structure and higher internal porosity, compared to the more spherical and poreless HSG granules (Fig. 5.2 and 5.3). Similar observations were made when comparing TSG and HSG for wet granulation, where X-ray tomography determined a higher porosity and less spherical shape of the granules produced via TSG [109].

TSMG can be described as a very robust process and variation of the granulation parameters (throughput and screw speed) had only a minor impact on PSD and yield (Fig. 5.1 and Tab. 5.3). The higher yield in TSG in producing the desired particle size indicated that TSG is the more efficient process, compared to HSG. Similar results were already obtained for wet granulation of lactose, paracetamol and cimetidine, where extrusion granulation resulted in a higher yield than for granules produced by HSG [108].

The tablets of TSG granules achieved higher TS at similar compaction pressure, which made the TSG tablets superior over tablets produced of HSG granules (Fig. 5.4). Similar results were found for wet granulation [107–109]. This was often explained with the higher density of the HSG granules, resulting in a poorer compactibility [107,109]. A high correlation of the compressibility index C [%] and the TS [N/mm²] was found for the TSG granules in this study. However, additional properties of the granules might have impact on the resulting TS, when being compressed into tablets.

When being analysed by SEM using BSE detector, the HSG granules achieved a lighter surface than TSG granules, indicating that less binder is present on the surface of HSG granules (Fig. 5.3). This observation supported the results from the tableting

studies and EDX-analysis of these tablets. The EDX analysis measured an overall higher carbon content on the tablet surface of TSG granules, compared to the tablets made of HSG granules (Fig. 5.8). The enhanced tabletability and the higher TS of the TSG granules (Fig. 5.4) was probably based on the higher availability of binder at the granules surface (Fig. 5.8), which resulted in a stronger intergranular binding capability (Fig. 5.5).

Moreover, in TSG, the binder is more homogenously distributed (Fig. 5.9), likely linked to a higher tabletability [81] and the more narrow PSD, compared to HSG granules (Tab. 5.3). The standard deviation of the binder variation could be decreased using higher screw speed for TSG. In HSG, the binder variation could be decreased using higher chopper/impeller speeds.

In our comparison, TSG mostly resulted in superior CQAs, compared to HSG. However, HSG is known to be strongly influenced from process parameters, excipient and/or active ingredient properties [111–114].I.e. there might be process settings for HSG facilitating similar CQAs compared to the TSG. A higher chopper/impeller speed resulted in a higher yield. For the given formulation, a higher granulation time of HSG resulted in pelletization, rather than agglomeration. This was indicated by the formation of large spherical granules with a diameter ≥ 1mm. TSG instead, proved to be the more robust process, which is in line with observations of other authors for wet or melt granulation [4,34,109]. In our study no process optimization was done beforehand. The aim of our study was a comparison of the critical quality attributes using different process settings, rather than process optimization. The speed was adjusted to the maximum speed of the equipment and the throughput used for TSG was chosen based on the mean granulation time in the HSG. We cannot exclude that the yield, the TS or the binder distribution in the tablets of the HSG can be improved using other process settings. However, our study showed that TSG resulted in a higher yield, a narrower PSD and higher TS more easily, independently of the process parameters chosen. However, further studies on the process settings in TSMG are needed to describe the effects of throughput and screw speed in detail. I.e., the wider process window of TSG compared to HSG might ease new development tasks.

5.8 Conclusion

Granules produced by twin-screw granulation (TSG) achieved a narrower particle-size distribution (PSD) and a higher yield than the high-shear (HSG) granules. Overall, TSG was found to be very robust and variation of the granulation parameters (throughput and screw speed) had only a minor impact on the PSD and yield. The HSG granules were less porous and more spherical in shape, which explained the slightly better flowability and higher ρ_{tapped} of these granules. Tablets made of the TSG granules achieved higher compactibility, which was traced back to a more homogenous binder distribution and higher available binder content in the tablet surface structure (detected by energy dispersive X-ray analysis). When changing from batch (HSG) to a continuous process (TSG), a slightly different product quality will likely result, which is mainly attributed to a different shape, PSD, porosity and binder distribution.

5.9 Authors contributions:

Conceptualization: K.G.W and K.E.S.; Data curation: K.E.S, M.B:B., M.U.H. and M.M.; Methodology: K.E.S and K.G.W.; Investigation: K.E.S, M.B:B., M.U.H. and M.M.; Resources: K.G.W.; Writing-Original Draft Preparation: K.E.S; Writing-Review & Editing: K.G.W.; Supervision: K.G.W.; Project Administration: K.G.W.

5.10 Acknowledgement

We kindly thank Romaco/Kilian and Medelpharm for providing the single-punch compression simulator Styl'One Classic 105 ML. Furthermore, we like to kindly thank Boehringer Ingelheim and L.B. Bohle Maschinen + Verfahren GmbH for providing the high-shear mixer VMA 10. We greatly thank Kai Berkenfeld and Esther S. Bochmann for reviewing the manuscript.

5.11 List of Symbols and Abbraviations

BSE	backscattering electrons	
C	compressibility index	[%]
EDX	energy-distributive X-ray	
HSG	high-shear granulation/granulator	
HSMG	high-shear melt granulation/granulator	
L/D	length/diameter	
MF	mass flow	[s/100g]
PM	physical mixture	
PSD	particle-size-distribution	
ρ_0	bulk density	[g/cm³]
ρ_{tapped}	tapped density	[g/cm³]
SE	scanning electron	
SEM	scanning electron microscope	
SF	solid fraction	
P	throughput	[g/min]
TS	tensile strength	[N/mm²]
TSG	twin-screw granulation/ granulator	
TSMG	twin-screw melt granulation	
V_0	bulk volume	[cm³]
V_p	volume of the compact	[mm³]
V_{tapped}	tapped volume	[cm³]

6 Dissolution Enhancement of Carbamazepine using Twin-screw Melt Granulation

Kristina E. Steffens, Karl G. Wagner

This part was published as:

Steffens, Kristina E., and Karl G. Wagner. "Dissolution enhancement of carbamazepine using twin-screw melt granulation." European Journal of Pharmaceutics and Biopharmaceutics 148 (2020): 77-87.

DOI: 10.1016/j.ejpb.2020.01.006

6.1 Graphical abstract

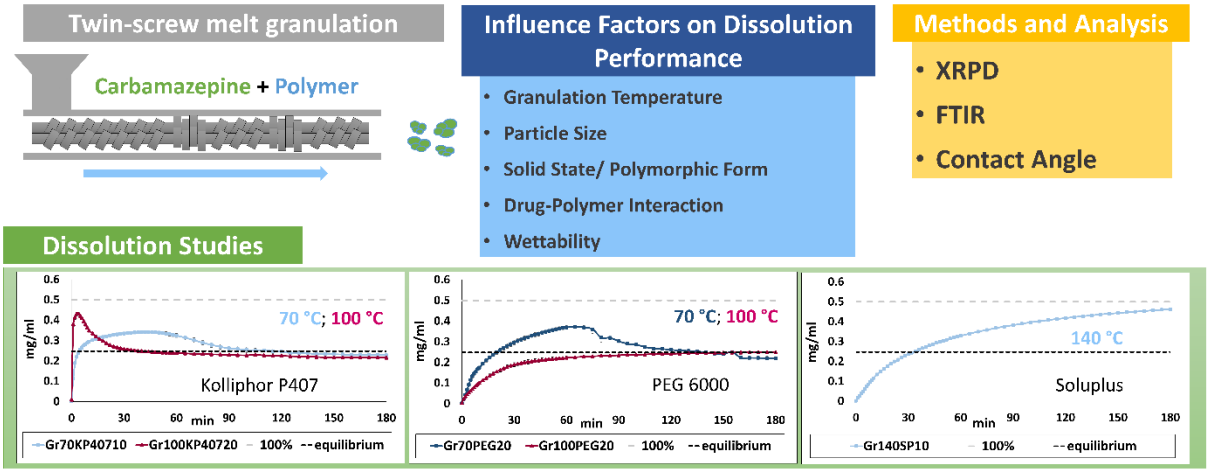

6.2 Abstract

The current study explored the twin-screw melt granulation (TSMG) as a potential technology for the water solubility enhancement of biopharmaceutical classification system (BCS) class II drugs. As a model drug, carbamazepine (CBZ) was formulated with three different polymers as melt granules produced in a co-rotating twin-screw granulator. Polyethylene glycol 6000 (PEG 6000) and Kolliphor® (poloxamer) P407 were used as binding materials at two different granulation temperatures (T_{max}: 70 °C; 100 °C). Additionally, Soluplus® (polyvinyl caprolactam-polyvinyl acetate-polyethylene glycol graft copolymer) was chosen as binder of higher melting/ granulation temperature (T_{max}: 140 °C). Temperature dependent polymorphic transition of CBZ during melt granulation was observed and identified using XRPD- (X-ray powder diffraction) and FTIR- (Fourier transform infrared spectroscopy) analysis. The effects of polymer type, polymer content (10, 15, 20% (w/w)) and granulation temperature on polymorphic transition, their impact on wettability (contact angle via drop shape-analysis), and the resulting dissolution performance at non-sink conditions in phosphate buffer (pH 6.8), were studied. This study showed that TSMG led to a crystalline system facilitating supersaturation when brought in solution, even when high drug loads (up to 90% (w/w)) were used.

In general, for all granules produced, the supersaturation level and its duration varied with the extent of polymorphic transition and binder concentration. The results of this

study indicated the importance of temperature control and polymer selection for tailoring desired dissolution profiles.

6.3 Keywords

Melt granulation, twin-screw granulator, extruder, dissolution enhancement, crystalline state, carbamazepine, polymer content, polymorphic transition

6.4 Introduction

Most new active pharmaceutical ingredients (APIs) belong to the biopharmaceutical classification system (BCS) - class II, which means that their oral bioavailability is limited by their poor solubility in aqueous media [115]. Amorphous solid dispersions (ASDs), either produced via hot-melt extrusion or spray drying, are often used to overcome poor dissolution behaviour of such APIs. Nevertheless, due to the instable nature of the amorphous state, ASDs tend to recrystallize during storage, which causes a change in dissolution profile. Moreover, the API solubility in the polymer limits the drug load of ASDs often to values lower than 30% (*w*/*w*), although drug loads up to 50% (*w*/*w*) in some cases are feasible [116]. Compared to high-shear mixers, where water-assisted heating limits the process temperature, twin screw extruders offer the possibility to use functional polymers with higher melting points/ glass transition temperatures [36]. Using twin-screw melt granulation (TSMG) high drug loads of up to 90% (w/w) can be achieved, as not much more than the binder is necessary as an additive [4]. Furthermore, due to the high drug load, the system remains in a crystalline state and therefore might not be affected by recrystallization during storage. The potential of the melt granulation process to produce immediate release dosage forms has been shown, especially when using hydrophilic binders like polyethylene glycol (PEG) [7,9,23,117]. Moreover, the possibility to run twin-screw melt granulation processes at adiabatic conditions on continuous processing lines renders them very attractive in terms of process and product control, scale-up, and additionally provides benefits from an economic and ecological point of view.

In this study, Carbamazepine (CBZ) was chosen as model API, with the goal of exploring the potentials of the twin-screw melt granulation process for enhancing the dissolution of BCS II APIs, while maintaining their crystalline state. What makes CBZ an interesting candidate is, that recent work has demonstrated the crystalline CBZ to act superior in terms of achieving a supersaturated (540 µg/ml) state in solution compared to the amorphous CBZ. Within this context, no supersaturation was achieved in the case of the latter, as the drug converted too quickly into the dihydrate (DH) form [118], which is one of the pseudo-polymorphic forms of CBZ. Polymorphic forms of a drug may vary in their physicochemical properties such as solubility and dissolution performance, hence affecting the overall bioavailability of the formulation [119]. Furthermore, it has been shown, that the presence of functional polymers in solution can limit CBZ transformation into the DH form, mainly stabilized by hydrophobic drug polymer interactions [120]. Similar effects were found for the combination of CBZ and hydroxypropyl methylcellulose or methylcellulose, which inhibited nucleation and crystal growth in solution [121]. Tian et al. identified hydrophobicity, as well as the ability of hydrogen bonding of the polymer, as key factors for stabilization of CBZ [122]. Adsorption of the polymer to the hydrate crystal surface was identified as main mechanism of transformation inhibition [123]. Melt granulation might be an interesting formulation strategy, as the functional polymer can simultaneously act as binding material, thereby increasing particle-size, tabletability and flowability of the formulation, but also to achieve superior dissolution properties of the drug compared to a simple physical mixture (PM). Dissolution can be enhanced by a more homogenous distribution of the binding material in the granulated material compared to PMs [81] bringing polymer and drug in closer contact, when brought in solution. For CBZ, identification and the control of polymorphic transitions are of fundamental importance when assessing the performance of a given formulation. Four polymorphic forms (triclinic; trigonal; P-monoclinic and C-monoclinic) as well as additional pseudo-polymorphic forms, including a dihydrate (DH) form (P-monoclinic), have been hitherto reported in the literature [124–126]. CBZ forms its DH is upon contact with water [127,128] and is therefore created during dissolution experiments [118,119,129]. Form III (P-monoclinic) is the commercial form. Form I is formed upon exposure to higher temperatures, e.g. 150 °C for 3 h [130] or 170 °C for 1 h [131] and is therefore accessible via twin-screw melt granulation. In this technique, the increase

of temperature is not only generated by heat transfer from external sources (barrel heating) into the product, but also from the dissipation of mechanical energy introduced via the twin-screw rotation.

The aim of the present study was to evaluate the dissolution performance of CBZ melt granules, which were produced using three different types of polymers in a co-rotating twin-screw granulator. Polyethylene glycol (PEG) 6000 and Kolliphor® (poloxamer) P407 were used as binding materials at two different granulation temperatures (T_{max}: 70 °C; 100 °C). Additionally, Soluplus® (polyvinyl caprolactam-polyvinyl acetate-polyethylene glycol graft copolymer) was chosen as melt binder at a higher granulation temperature (T_{max}: 140 °C). Granulation temperatures were selected based on the polymer melting points (Kolliphor® P407: 56 °C [132]; PEG 6000 55-60 °C [133]) or glass transition temperatures (Soluplus®: 70 °C [132]). The effect of polymer type, polymer content (10, 15, 20 % (w/w)), and granulation temperature on the solid-state of the formulation, drug-polymer interaction, wettability and dissolution performance using two-fold non-sink conditions in a phosphate buffer (pH 6.8) compared to the related PM was studied.

6.5 Material and methods

6.5.1 Material

Carbamazepine (CBZ) (form III), Kolliphor® (poloxamer) P407 and Soluplus® (polyvinyl caprolactam-polyvinyl acetate-polyethylene glycol graft copolymer) were a kind gift of BASF SE (Ludwigshafen, Germany). Polyethylene glycol (PEG) 6000 was purchased from Carl Roth. Trichloromethane (analytical grade) was obtained from VWR (VWR International GmbH, Langenfeld, Germany). Citric acid was obtained from Fagron (Fagron GmbH & Co. KG, Barsbüttel, Germany) and di-sodium-hydrogen-phosphate-anhydrous was purchased from Alfa Aesar (Thermo Fisher (Kandel) GmbH, Karlsruhe, Germany).

6.5.2 **Methods**

6.5.2.1 Preparation of physical mixtures (PM)

CBZ was premixed with one of the three polymers (Kolliphor® P407, PEG 6000 and Soluplus®) at a polymer content of 10, 15, 20% (w/w). PMs were blended in a Turbula mixer (Willy A. Bachofen AG Maschinenfabrik, Switzerland), rotating at 50 rpm for 10 min. The obtained PMs were used for granulation and in addition characterised as reference for the melt granules. An overview of the formulations under investigation is given in Tab. 6.1.

6.5.2.2 Twin-screw-melt granulation (TSMG)

TSMG was performed using a co-rotating twin-screw extruder/granulator ZE12 (Three-Tec GmbH, Seon, Swiss) with a functional length to diameter ratio of 25:1 and a screw diameter of 12 mm. The barrel of the granulator consisted of five individually adjustable heating zones, enabling complete melting and an even distribution of the API. Process temperature was at maximum in the high-shear zone of the screws (30° and 60° 4-disc-kneading elements (zone 1), 60° and 90° 4-disc-kneading elements (zone 2)). The temperature was reduced at the terminal zone of the barrel in order to initiate the solidification of the material. Tab. 6.2 shows the set barrel temperatures of each zone with respect to the different melting points/ glass transition of the polymers used. The granulator was operated in an open configuration (without a die plate), and the screw speed was set to 100 rpm. A volumetric feeder system ZD9 (Three-Tec GmbH, Seon, Switzerland) was used and feed rate was set to 0.2 kg/h.

After TSMG, granules were milled using an Erweka wet granulator FGS with AR 402 drive unit (Erweka, GmbH, Heusenstamm, Germany) equipped with a 630 µm sieve at a rotation speed of 50 rpm

Tab. 6.1: Overview of the formulations under investigation.

Shortname	Binder	Binder content [%]	CBZ content [%]	Shortname	Binder	Binder content [%]	CBZ content [%]	Tmax during extrusion [°C]	Shortname	Binder	Binder content [%]	CBZ content [%]	Tmax during extrusion [°C]
PMKP40710	Kolliphor® P407	10	90	**Gr70KP40710**	Kolliphor® P407	10	90	70	**Gr100KP40710**	Kolliphor® P407	10	90	100
PMKP40715	Kolliphor® P407	15	85	**Gr70KP40715**	Kolliphor® P407	15	85	70	**Gr100KP40715**	Kolliphor® P407	15	85	100
PMKP40720	Kolliphor® P407	20	80	**Gr70KP40720**	Kolliphor® P407	20	80	70	**Gr100KP40720**	Kolliphor® P407	20	80	100
PMPEG10	PEG 6000	10	90	**Gr70PEG10**	PEG 6000	10	90	70	**Gr100PEG10**	PEG 6000	10	90	100
PMPEG15	PEG 6000	15	85	**Gr70PEG15**	PEG 6000	15	85	70	**Gr100PEG15**	PEG 6000	15	85	100
PMPEG20	PEG 6000	20	80	**Gr70PEG20**	PEG 6000	20	80	70	**Gr100PEG20**	PEG 6000	20	80	100
PMSP10	Soluplus®	10	90						**Gr140SP10**	Soluplus®	10	90	140
PMSP15	Soluplus®	15	85						**Gr140SP15**	Soluplus®	15	85	140
PMSP20	Soluplus®	20	80						**Gr140SP20**	Soluplus®	20	80	140

Tab. 6.2: Barrel temperatures set for melt granulation.

Binder	Zone 1 [° C]	Zone 2 [° C]	Zone 3 [° C]	Zone 4 [° C]	Zone 5 [° C]
Kolliphor® P407	50	60	70	60	50
Kolliphor® P407	80	90	100	90	80
PEG 6000	50	60	70	60	50
PEG 6000	80	90	100	90	80
Soluplus®	120	130	140	130	120

6.5.2.3 Classification of the granules

Analytical sieving was performed with a sieve shaker (AS 200 digital, Retsch GmbH, Haan, Germany) for a duration of 10 min and an amplitude of 2 mm. The amount retained in the class between 200 and 355 µm was used for further analysis of the granules to exclude the effect of different particle-size distribution of the granules obtained.

6.5.2.4 Preparation of CBZ polymorphs

Form I was produced by exposing the commercial CBZ to a temperature of 170 °C for 4 h. Form II was obtained by slowly evaporating (200 mbar, 30 °C) a solution of CBZ in chloroform. The dihydrate was produced by suspending the commercial CBZ in purified water at 37 °C for 72 h in a water bath (GFL 1083, Gesellschaft für Labortechnik GmbH, Burgwedel, Germany). The resulting suspension was filtrated using filter paper (Grade 1, Whatman, Merck KGaA, Darmstadt, Germany) and dried for 24 h.

6.5.2.5 Scanning electron microscope (SEM)

An SEM (SU 3500, Hitachi High Technologies, Krefeld, Germany) equipped with a backscattered electron detector (BSE) was used to visualize the structure of the polymorphs. BSE images were collected at an acceleration voltage of 10 kV at variable pressure mode (70 Pa). Samples were attached to SEM stubs using conductive carbon paste and left uncoated for analysis.

6.5.2.6 X-ray powder diffraction (XRPD)

XRPD measurements were performed in reflection mode (X'Pert MRD Pro, PANalytical, Almelo, Netherlands) with an X'Celerator detector and nickel filtered CuKα1 radiation (λ = 1.5406 Å) at 45 kV and 40 mA. Scans were performed in the range from 4° to 38° 2□ with a scanning rate of 0.04°/s and a resolution of 0.001°.

6.5.2.7 Fourier transform infrared spectroscopy (FTIR)

FTIR analysis were carried out using a Bruker alpha P with an ATR (attenuated total reflectance) diamond module. Transmission scans were recorded from 400 to 4000 cm-1 with a resolution of 2 cm-1. For analysis, all samples were compressed into thin tablets with a pneumatic hydraulic press (FlexiTab, Röltgen GmbH & Co. KG, Solingen, Germany) using a 10 mm flat-face tooling and a compaction pressure of 200 MPa. All tablets were subsequently analysed by FTIR. 25 scans were conducted for each spectrum.

6.5.2.8 Contact angle

Contact angles were measured using a sessile drop method (Drop shape analysis system DSA 25, Krüss GmbH, Hamburg, Germany). Raw materials, physical mixtures (PMs) and granules were compressed into flat compacts using a pneumatic hydraulic press (FlexiTab, Röltgen GmbH & Co. KG, Solingen, Germany). The tablet press was equipped with a 10 mm flat-face tooling and a compaction pressure of 200 MPa was applied, to ensure the formation of a flat surface.

8 µl of demineralised water (T= 25 °C) were placed on the top of the compact using a 1 mm needle. The contact angle was measured after 10 sec of contact using linear baseline fitting. For each material, six measurements were performed.

6.5.2.9 Equilibrium solubility

The equilibrium solubility (C_{eq}, [mg/ml]) of the CBZ DH was determined by adding 2.0 g of CBZ to 50 ml of a 0.05 molar phosphate buffer pH 6.8. The obtained suspension was subsequently shaked for 72 h in a horizontal shaker (GFL 1083, Gesellschaft für Labortechnik GmbH, Burgwedel, Germany). The suspension was filtered using a 0.22 µm membrane filter. The dissolved amount of CBZ was quantified with an Agilent 8453 UV-VIS spectrophotometer (Agilent Technologies, Waldbronn, Germany) at 285 nm.

6.5.2.10 Intrinsic dissolution

Intrinsic dissolution tests (n=3) were performed using a rotating disc method. For this purpose, small metal dies with a circle opening of 0.50 cm² were used. 100 mg of powder was compressed into this die using a pneumatic hydraulic press (FlexiTab, Röltgen GmbH & Co. KG, Solingen, Germany). The press was equipped with an 8 mm flat-face tooling. A compaction pressure of 200 MPa and a dwell time of 4000 ms were used for compaction of the powder into the die. These metal dies were mounted to a basket holder and sealed from the backside to ensure that only one side of the compact is in contact with the dissolution medium (450 ml of phosphate buffer, pH= 6.8; 37 °C ±0.5 °C). The baskets rotated with a speed of 150 rpm. For quantitative analysis, an Agilent 8453 in-line UV-VIS spectrophotometer (Agilent Technologies, Waldbronn, Germany) was used. Absorption was detected at 285 nm and the dissolution tests were performed for 2 h with a minimal measuring interval of 2 min. Sink conditions were maintained during the entire measurement. The intrinsic dissolution rate (*IDR*) was calculated by the following equation (Eq. 6.1),

$$IDR = (dc/dt) * V/A \text{ [µg/min/cm²]} \qquad \text{(Eq. 6.1)}$$

where (*dc*/*dt*) is the concentration over time, *V* is the volume used and *A* is the compact surface area in contact with the dissolution medium.

6.5.2.11 Dissolution Test

Dissolution tests were performed using a USP Dissolution Apparatus 2 (paddle method) (Sotax AT7, Sotax GmbH, Lörrach, Germany) with a rotation speed of 100 rpm. Analyses were performed at two-fold non-sink conditions using 450 ml of 0.05 molar phosphate buffer at a pH of 6.8 ±0.1. The temperature was set to 37.0 °C ±0.5 °C. The amount of granules used was based on a target CBZ content of 225 mg for each experiment (C_{eq}= 0.25 mg/ml). For the quantitative analysis, an Agilent 8453 in-line UV-VIS spectrophotometer (Agilent Technologies, Waldbronn, Germany) was used. Absorption was determined at a fixed wavelength of 285 nm. The dissolution test duration was 3 h with a minimum interval of 5 min between the instants of measurement. Light scattering correction was carried out with a fixed wavelength correction (365 nm). All experiments were carried out in triplicate.

The obtained dissolution profiles were evaluated by comparing the maximum concentration ($C_{max)}$ [mg/ml] and the corresponding timepoint ($t_{max)}$ [min], as well as the degree of supersaturation, given by the supersaturation ratio S (Eq. 6.2):

$$S = \frac{C}{C_{eq.}} \qquad \text{(Eq. 6.2)}$$

Additionally, the time, where C_{eq} was exceeded, was defined as t_{eq1} [min]. For the case that C dropped again, due to precipitation below C_{eq}, this point was defined as t_{eq2} [min]. The parameter t_{eq2}-t_{eq1} (Δt_{eq}) gives the time interval [min] of supersaturation.

6.6 Results and Discussion

6.6.1 Comparison of the polymorphic forms as reference material

For reference, the CBZ polymorphic forms, that could be generated during granulation and dissolution, were produced and analysed.

6.6.1.1 XRPD

The identity and purity of the polymorphic forms of CBZ (form I, form II, form III and the form DH) were analysed by means of XRPD analysis and compared to the spectra reported in literature [119,125,130,134].

In XRPD, the CBZ polymorph form I generated major peaks at 8.0, 9.4, 12.3 and 20.0° 2Θ (Fig. 6.1). The CBZ form II showed characteristic peaks at 5.0, 8.7, and 24.4° 2Θ instead, whereas signal characteristics for form III were found at 13.1, 15.3 and 27.5° 2Θ. The form DH exhibited two pronounced peaks at 9.0° and 12.4° 2Θ and a strong signal at 19.5° 2Θ (Fig. 6.1). All diffractograms obtained were in line with those reported in literature [119,125,130,134].

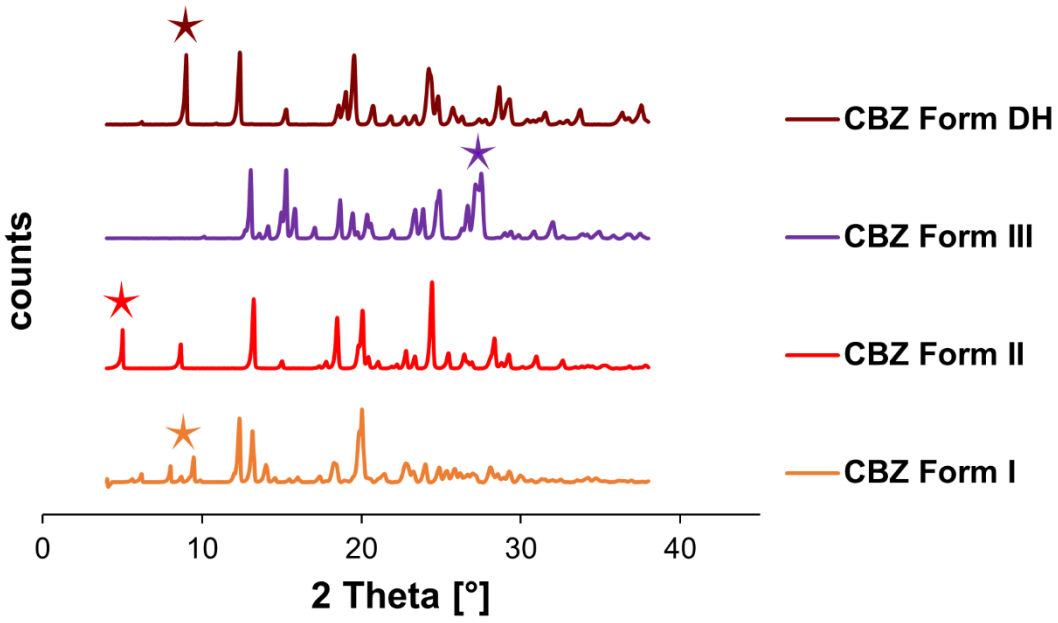

Fig. 6.1: XRP diffractograms of the polymorphic forms of CBZ.

6.6.1.2 FTIR

FTIR is an accepted method to identify drug-polymer interaction e.g. H-bonding and was therefore chosen as an additional analytical characterisation method. Fig. 6.2 depicts the results of FTIR-analysis for the four polymorphic CBZ forms. The CBZ form I exhibited a sharp peak at 3483 cm^{-1} (-NH valence vibration) and pronounced absorption at 1682 cm^{-1} (–CO–R vibration) and 1389 cm^{-1}. Form II showed a similar absorption profile with a sharp peak at 3484 cm^{-1} and nearly identical peak positions at 1686 and 1389 cm^{-1}. Due to similarity of the spectra of form I and form II, a differentiation of the latter is not possible. In contrast to the FTIR spectroscopy, XRPD analysis are able to distinguish between both polymorphs. The absorption spectrum of the monoclinic form III was shifted to lower wavenumbers, and thus differed from the profile of the trigonal CBZ form II, as well as from the spectrum obtained from the triclinic form I. Form III generated peaks at 3464, 1674 and 1380 cm^{-1}. In the case of the DH, the N-H stretching vibration was shifted to 3432 cm^{-1}. Additional peaks were observed at 3179, 1676 and 1402 cm^{-1}. Results were found in good agreement with the FTIR spectra reported in literature [125,130,135].

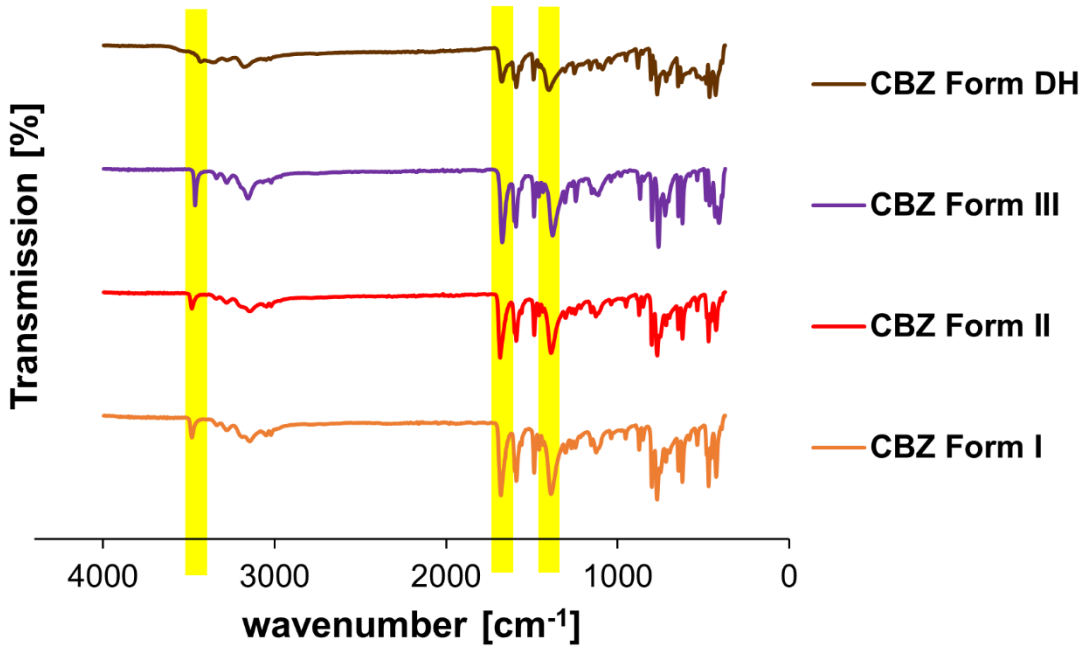

Fig. 6.2: FTIR spectra of the polymorphic forms of CBZ.

6.6.1.3 SEM

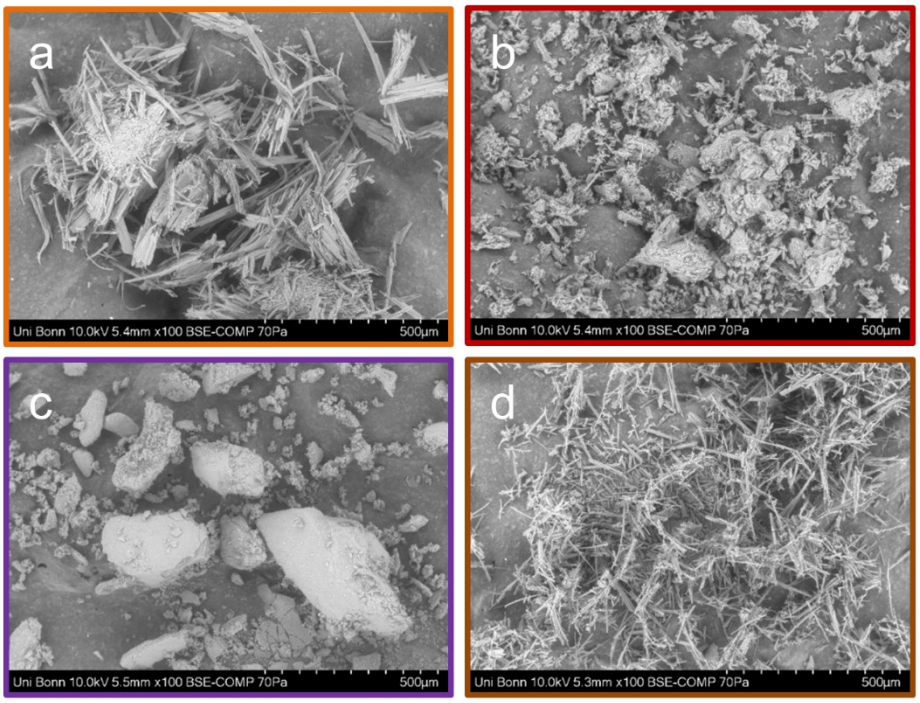

Fig. 6.3: SEM micrographs of the polymorphic forms of CBZ a: CBZ Form I; b: CBZ Form II; c: CBZ Form III; d: CBZ Form DH.

Scanning electron micrographs (Fig. 6.3) were taken to identify the structural difference of the polymorphic forms. CBZ form I (Fig. 6.3a) showed a characteristic needle form [124,125,131], whereas form II (Fig. 6.3b) had a more rod-like shape. The commercially available form III (Fig. 6.3c) exhibited a broad particle size distribution and a more angular structure. In Fig. 6.3d, the very thin needle-like structure of the form DH is depicted, as often reported in literature [128,129,135,136].

6.6.1.4 Contact angle

In Fig. 6.4, the measured contact angles of the different CBZ polymorphs are depicted. The contact angle of the anhydrous polymorphic forms (form I, II and III) did not deviate from each other (47.7° ±5.5, 45.7° ±8.2 and 45.1° ±5.3), indicating that polymorphic transition had no major impact on the wettability. Only the form DH showed a slightly higher contact angle of 55.4° ±5.4.

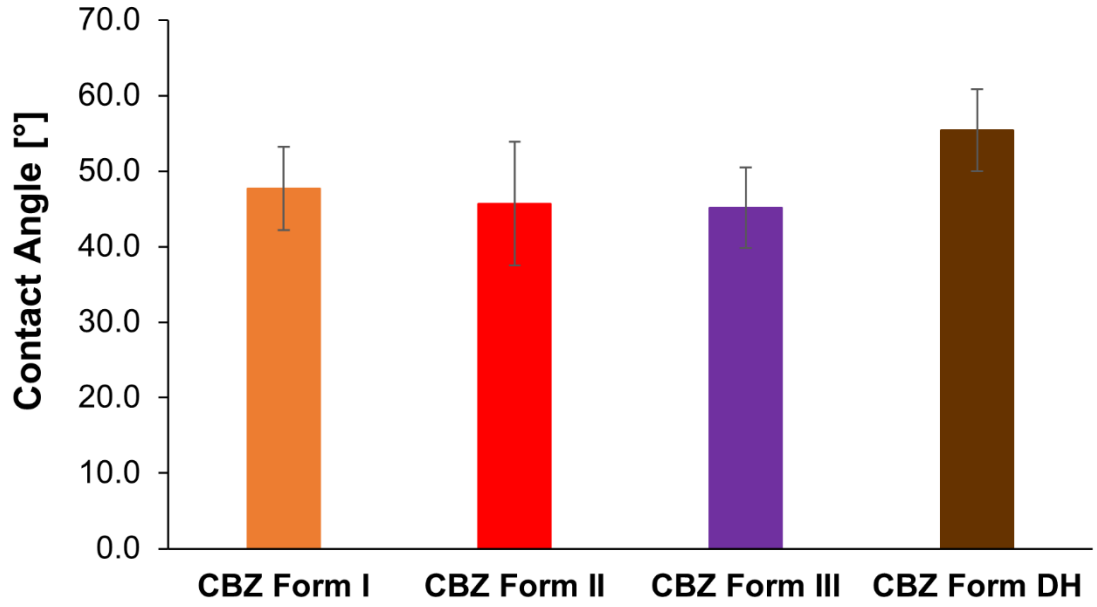

Fig. 6.4: Contact angles of the polymorphic forms of CBZ.

6.6.1.5 Intrinsic dissolution

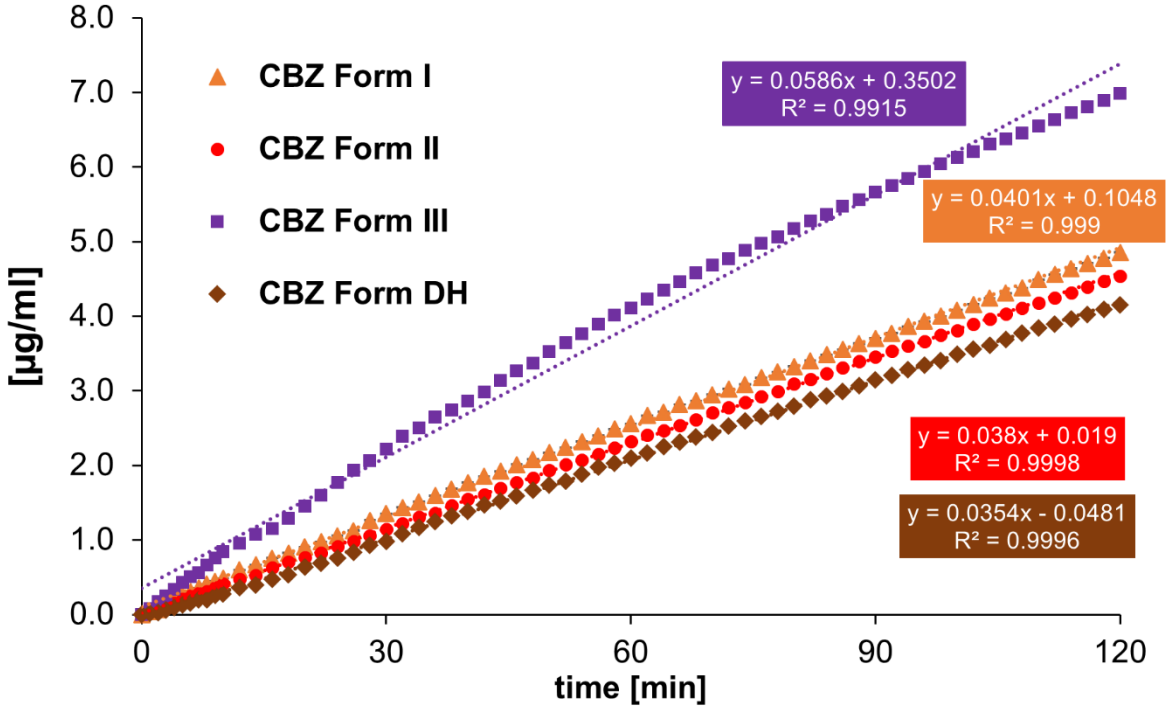

Fig. 6.5: Intrinsic dissolution profiles of the polymorphic forms of CBZ using rotating disc method (0.5 cm²; 150 rpm) in 450 ml phosphate buffer (pH= 6.8; 37 °C ±0.5 °C).

Based on the findings of the SEM analysis, intrinsic dissolution experiments were performed to exclude any potential effects of the different particle size and morphology of various polymorphic forms on the dissolution rate. Within this context, the concentration profile as a function of time should yield a linear curve progression (Fig. 6.5). The slope of this linear regression characterizes the intrinsic dissolution rate. The obtained dissolution rate was normalized to the surface of the compact used for experiment using Eq. 6.1. The obtained value is characteristic for a polymorph under fixed experimental conditions (e.g. dissolution medium, temperature). The order of the intrinsic dissolution rates (*IDR*) of the polymorphic forms of CBZ was form III > form I > form II > DH. The dissolution rate of form III (50.07 ±1.16 µg/min/cm²) was almost twice as high as the dissolution rate of the other polymorphs. The lowest dissolution rate was found for the form DH (30.20 ±0.30 µg/min/cm²). However, dissolution rates of the form I (34.21 ±0.54 µg/min/cm²) and II (32.42 ±0.82 µg/min/cm²) were comparable and only slightly higher than the dissolution rate of the DH. This can be attributed to a slower dissolution rate of the polymorph itself, or else their very rapid transformation into the form DH, manifesting thereby a dissolution profile related to the latter. In the case of form III, the dissolution rate was decreasing as a function of time, which resulted in the lowest correlation coefficient of 0.9915, compared to 0.999 for form I, 0.9998 for form II and 0.9996 for the form DH.

It should be noted that the transformation of the polymorphic forms in contact with water could occur, affecting thereby both the dissolution rate and the quality of the linear regression model. The low regression coefficient being observed in the case of form III, was attributed to a slow transformation into the form DH resulting in a decrease of the dissolution rate over time. Intrinsic dissolution rates might be therefore indicative of the different hydration kinetics of the polymorphic forms [125]. The calculated IDR values were in good agreement with values reported in literature [137,138], a high variability was shown for CBZ from III obtained from different manufacturers [139,140] explaining a slight difference compared to literature data.

6.6.2 **Characteristics of the granulated material**

6.6.2.1 XRPD

Fig. 6.6a shows the XRPD patterns of the PMs and granules produced with Kolliphor® P407. Kolliphor® P407 is a semi-crystalline polymer with two prominent peaks at 19.1° and 23.3° 2Θ. As previously mentioned, CBZ form I showed characteristic peaks at 6.2°, 8.0°, 9.4°, 12.3° and 20.0° 2Θ, whereas CBZ form III exhibits less peaks in the low 2Θ region, pronounced peaks at 13.1°, 15.3° and a broad peak with a maximum at 27.5° 2Θ. Diffractograms of the PMs indicated the presence of the commercial CBZ form III and Kolliphor® P407. Peaks of CBZ decreased with increasing polymer content, whereas the characteristic peak of Kolliphor® P407 at 19.1° 2Θ increased and was visible as a shoulder owing to concentration effects. The peak of Kolliphor® P407 at 23.3° 2Θ was overlapping with the CBZ peak. Nevertheless, due to the amorphous parts of the polymer, the overall intensity of the peak decreased with increasing polymer content. TSMG at 70 °C did not change the solid state of the API. Granules were found to show prominent peaks at 13.1°, 15.3° and a broad peak 27.5° 2Θ. In contrast, diffractograms of the granules produced at higher granulation temperatures indicated the formation of CBZ form I, with the most intense peaks found in samples containing 15% (w/w) binder (Gr100KP40715). In the case of 20% (w/w) of Kolliphor® P407, the peaks in the diffractogram decreased again.

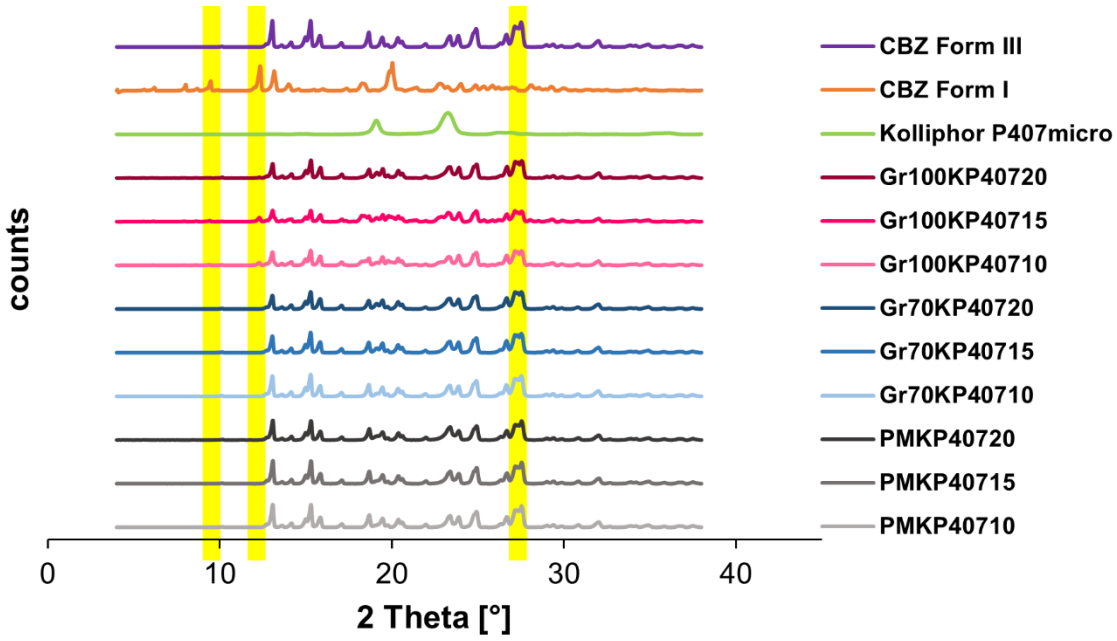

Fig. 6.6a: XRPD of the physical mixtures and granules produced with Kolliphor® P407.

In the case of PEG 6000, the XRPD patterns of the granules indicated a polymer content- and temperature-dependent transformation of CBZ from III into form II (Fig. 6.6b). Generally, the formation of CBZ form I is generated by exposure to high temperatures. In our case, the addition of PEG 6000 favoured the formation of from II than of form I during melt granulation. The form II showed characteristic peaks at 5.0, 8.7 and 24.4° 2Θ and PEG 6000 at 19.1° and 23.3° 2Θ, similar to Kolliphor® P407 but it had additional smaller peaks at 13.5° and 15.1° 2Θ. Compared to Kolliphor® P407, the PEG 6000 containing PMs had a peak at 19.9° 2Θ, rather than a shoulder. The CBZ peak overlaid the peak of PEG 6000 at 23.3° 2Θ as well. CBZ peaks indicated the presence of the commercial form III in the PMs. The transformation into form II occurred already in minor extent at lower granulation temperatures of 70 °C for Gr70PEG15 and Gr70PEG20. The formation rate of form II increased as a function of PEG 6000 content, which becomes apparent by an increase in peak intensities at 5.0 and 8.7° 2Θ. However, a high amount of the API remained in form III, since peaks at 15.3 and 27.5° 2Θ were still present. Using higher granulation temperatures resulted in an increase of transformation into form II. The amount of form II increased with

increasing polymer content, which resulted in the highest conversion into form II in the case of Gr100PEG20.

The relative amount of form II demonstrated that the transformation was promoted and stabilized by PEG 6000. The increased formation of form II when combined with PEG 6000 has been already reported [141].

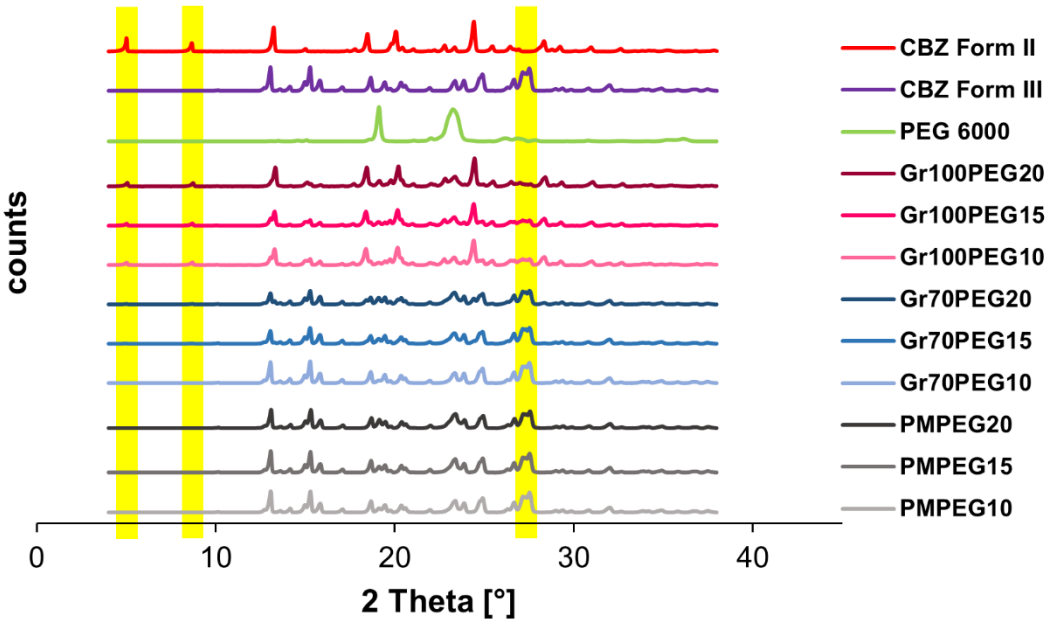

Fig. 6.6b: XRPD of the physical mixtures and granules produced with PEG 6000.

Being an amorphous polymer, Soluplus® showed no characteristic peaks in the XRPD pattern (Fig. 6.6c). In the case of the PMs, prominent peaks of CBZ form III at 13.1° 15.3° and 27.5° 2Θ were present. In the case of the granules, a complete transformation into CBZ form I was observed, indicated by the peaks at 6.2°, 8.0°, 9.4°, 12.3° and 19.9° 2Θ and the absence of a peak at 15.3° 2Θ. The overall intensity of CBZ peaks were decreasing with increasing polymer content, as expected, due to the amorphous nature of the polymer.

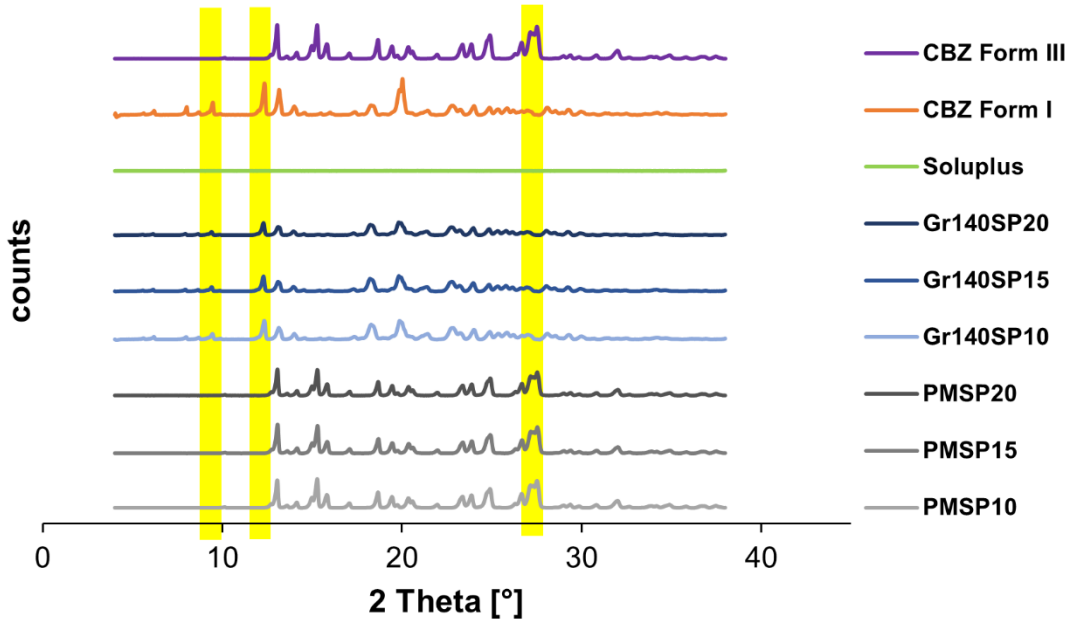

Fig. 6.6c: XRPD of the physical mixtures and granules produced with Soluplus®.

6.6.2.2 FTIR analysis

FTIR analysis was used to investigate and describe interactions between CBZ and the binder. Within this context, H-bond interactions were expected between the API and the polymers. Due to the enhanced distribution of the binder after TSMG, these interactions might occur more likely after granulation.

H-bonding could be possible between the hydroxyl groups of PEG 6000; Kolliphor® P407 and the Soluplus® PEG-backbone and the carbonyl-group of the API.

Kolliphor® and PEG 6000 (Fig. 6.7a and 6.7b) showed similar spectra due to their chemical similarity (C-H-stretching at 2879/2877 cm^{-1} and C-O-stretching at 1095/1098 cm^{-1}). Soluplus®, on the other hand (Fig. 6.7c), showed a double peak at 2925 cm^{-1} (C-H-stretching), 1731 cm^{-1} and 1626 cm^{-1} (C-O-stretching). The obtained FTIR spectra of the neat materials were in accordance with the spectra previously reported [142–144].

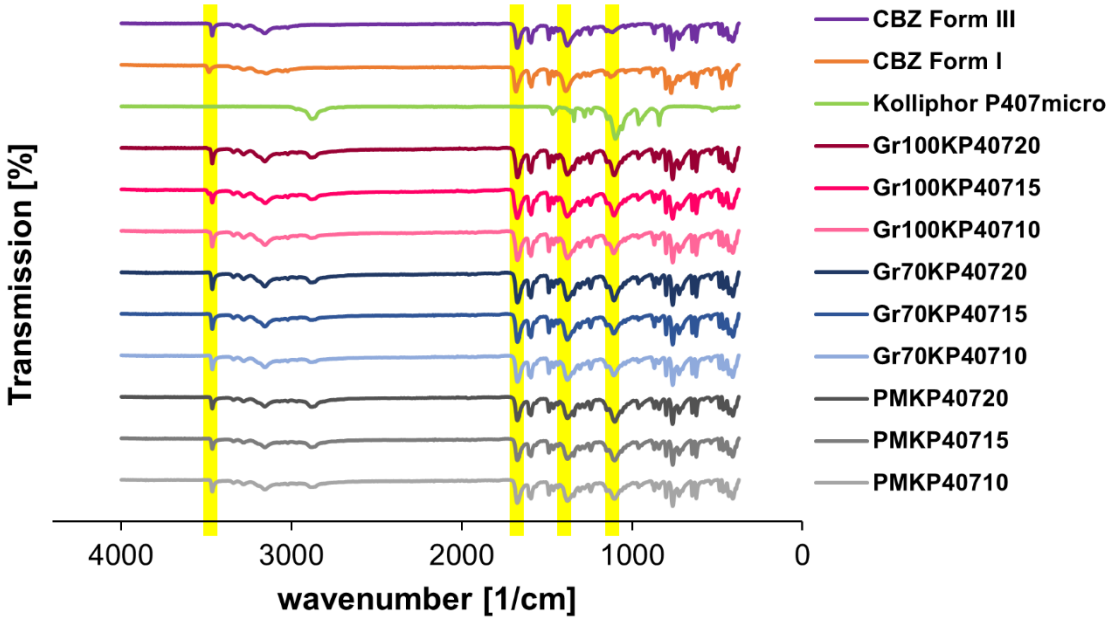

Fig. 6.7a. FTIR spectra of the physical mixtures and granules produced with Kolliphor® P407.

The PMs produced with Kolliphor® P407 showed characteristic peaks of the respective substances at 2879, 1103 cm^{-1} (Kolliphor® P407) and 3464, 1674, 1380 cm^{-1} (CBZ form III). Kolliphor® P407 peak intensity increased as a function of polymer content. When manufactured at 70 °C, peaks occurred at 3464, 2885, 1673, 1380 and 1109 cm^{-1}, indicating a slight shift in the bands of the binding material. However, no shift was seen in the carbonyl-stretching band of the API. Therefore, only weak interaction between the API and the polymer in the solid state were expected. When the granules were produced at higher granulation temperatures and a 15% (w/w) binder content, additional characteristic peaks of form I occurred at 3483 cm^{-1}. Here again, similar to the obtained data from the XRPD, a decrease of form I was noticed when using 20% (w/w) binder, and only a small peak was seen for the 10% (w/w) blend. Additional peaks for this formulations were found at 2880, 1675, 1381 and 1106 cm^{-1}, showing only a slight shift to higher wavenumbers. Thus, H-bonding seemed unlikely to exist in the solid-state and hence was not promoted by TSMG. The absence of drug-polymer interactions, when processing a combination of CBZ and poloxamer, was in good agreement with literature [145].

The PMs with PEG 6000 (Fig. 6.7b) showed peaks at 3464, 2881, 1674, 1380 and 1100 cm^{-1}, indicating no pronounced shift, when compared to the reference material. Similar spectra were obtained for granulation at 70 °C. However, granules produced at higher granulation temperatures (T_{max}: 100 °C) showed a double peak at 3484 and 3465 cm^{-1}, caused by the temperature-induced formation of CBZ form II, as already observed by XRPD. The PEG C-H stretching shifted to a lower wavenumber of 2871 cm^{-1}. Moreover, the peak was broader compared to the PMs and the granules produced at 70 °C, indicating a weak drug-polymer interaction, which was very pronounced at higher process temperature conditions. This shift might explain the preferred formation and stabilization of CBZ form II when formulated with PEG 6000 compared to formulations using other binding materials. A shift in the CBZ bands was not noticed, which might be explained by overlapping bands due to the coexistence of different polymorphic forms.

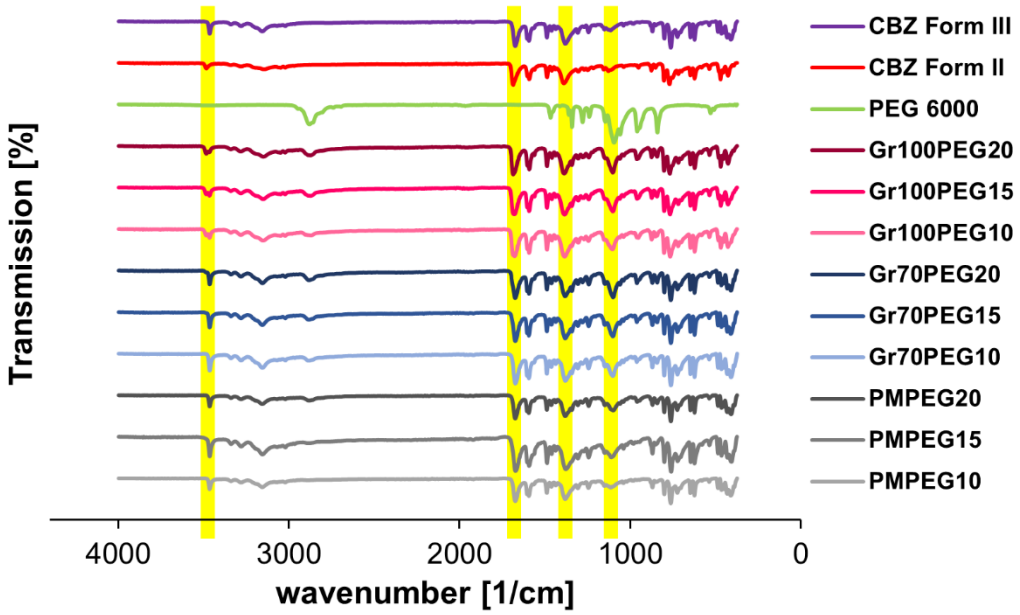

Fig. 6.7b: FTIR spectra of the physical mixtures and granules produced with PEG 6000.

FTIR-spectra of Soluplus® formulations (Fig. 6.7c) indicated the presence of the polymorphic form III in the PMs, since peaks at 3464, 1674 and 1380 cm^{-1} were observed. The characteristic peaks of Soluplus® at 2925, 1731 and 1626 cm^{-1} were low in intensity and barely traceable, both in the PMs and in the granules. In the case of the granules, only a small peak at 1735 cm^{-1} was found. This weak shift to higher wavenumbers indicated only a weak interaction between CBZ and Soluplus® in the solid state, which was in agreement with literature [142]. Furthermore, the granules showed the characteristic peaks of CBZ form I at 3483, 1682 and 1389 cm^{-1} without additional peaks at the characteristic bands of form III. On the other hand, lower extent of transmission was found for the granules when compared to the PMs. This might be due to the incorporation of small CBZ particles in the polymeric matrix.

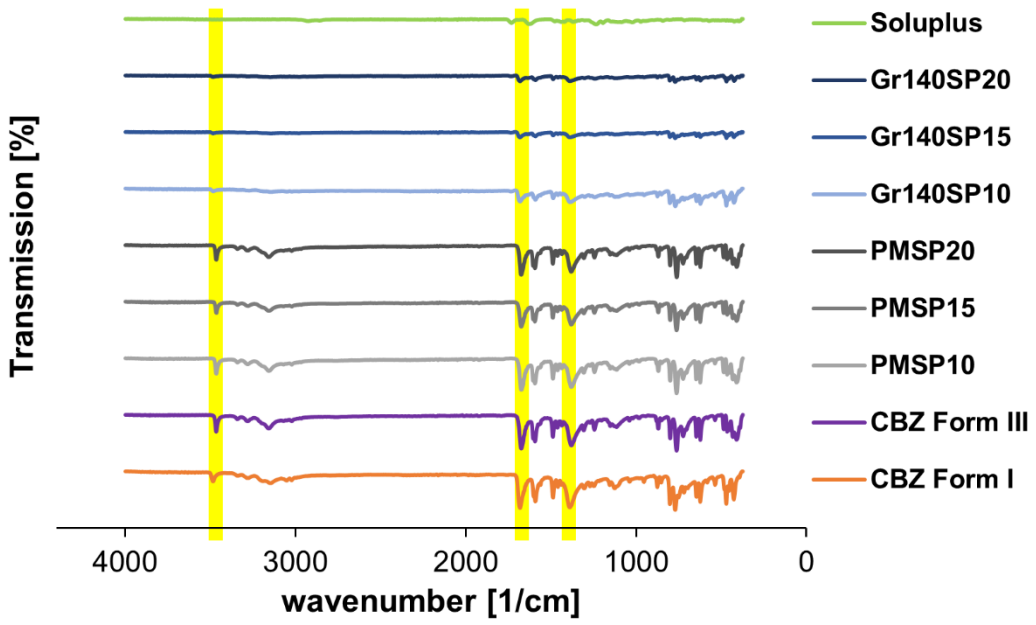

Fig. 6.7c: FTIR spectra of the physical mixtures and granules produced with Soluplus®.

6.6.2.3 Contact angle

The contact angle of pure Kolliphor® P407 was higher (60.8° ±0.7) than the contact angle of pure CBZ form I (47.7° ±5.5) and CBZ form III (45.1° ±5.3) (Fig. 6.8a). However, contact angles of the PMs were in the range of the pure CBZ. Surprisingly, granules using low binder contents, produced at either 70 °C or 100 °C, exhibited smaller contact angles than the pure materials.

This synergistic effect might be attributed to a preferred orientation of the polymer. Due to its amphiphilic character, the lipophilic polypropylene oxide units might be orientated towards the CBZ particles. Consequently, the ethylene units would preferably orientate towards the gas phase, resulting in a more hydrophilic surface and enhanced wettability. Conversely, contact angles were found to increase at increasing binder content, which might be attributed to the saturation of the lipophilic surface of the API with binding material, which would in turn result in a reduction of this preferred orientation. Contact angle of the granules produced at higher temperature was higher demonstrating a poorer wetting of the granules containing CBZ form I (Gr70KP40710: 23.6°±2.6 vs. Gr100KP40710: 35.5° ±2.2).

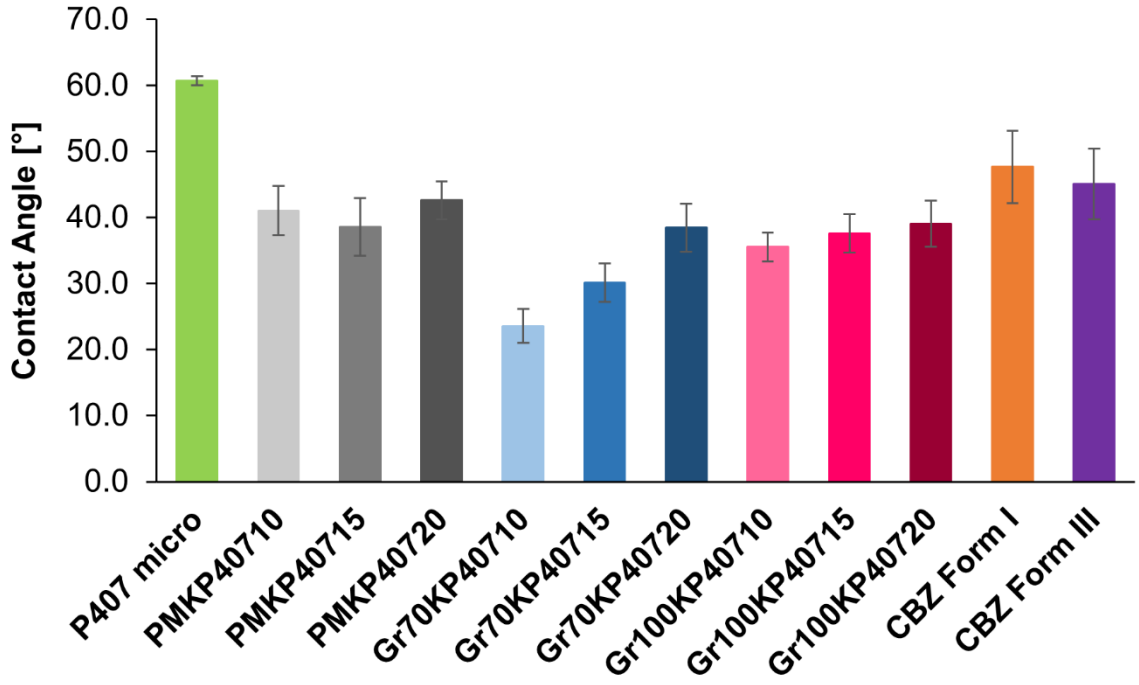

Fig. 6.8a: Contact angles of the physical mixtures and granules produced with Kolliphor® P407.

The contact angles of the PEG 6000 formulations were independent of the polymorph composition within the granules, as it was already shown for pure polymorphic forms (Fig. 6.8b). In the case of pure PEG 6000, the contact angle was lower than for the pure API (PEG 6000: 15.6° ±3.0 vs. CBZ form II: 45.7° ±8.2 and CBZ form III: 45.1° ±5.3). As expected, contact angles were decreasing with increasing PEG 6000 content. However, contact angles of the granules were generally lower than for the PMs. For the granules produced at 70 °C and 100 °C, no difference was found. In the case of 15% binder, the contact angle of PMPEG15 was 43.7° ±5.0, whereas Gr70PEG15 showed a contact angle of 29.2° ±1.8 and Gr100PEG15 a comparable value of 30.0° ±1.5. The increased effect of PEG 6000 on lowering the contact angle in the case of the granules compared to PM might be attributed to a more homogenous distribution of the binder in the formulation after granulation.

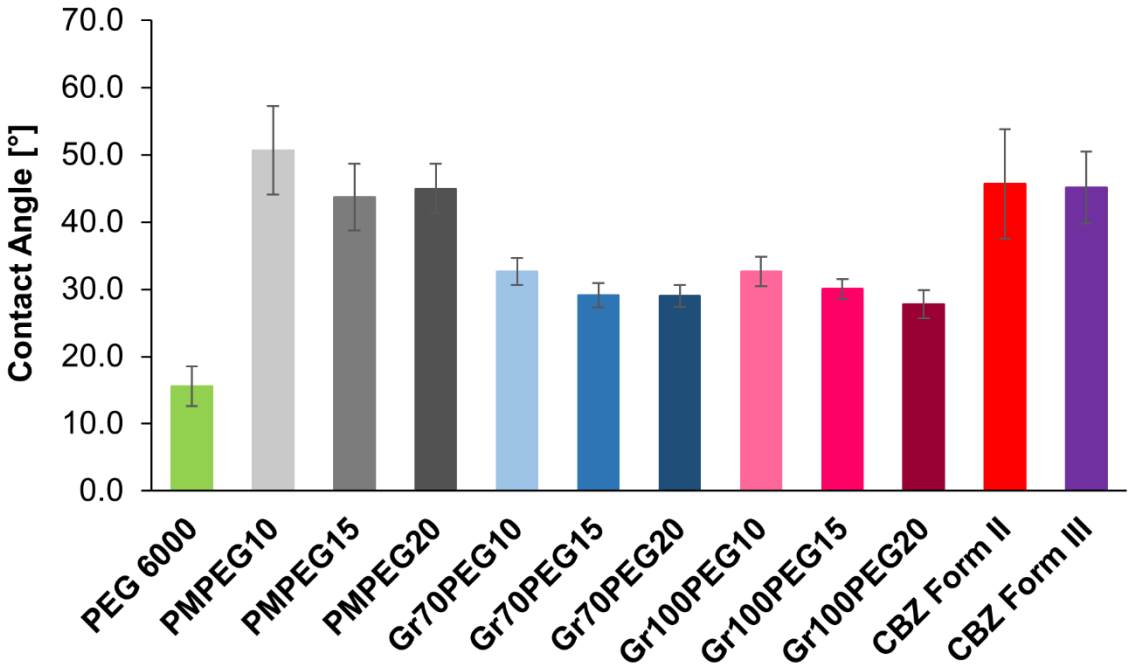

Fig. 6.8b: Contact angles of the physical mixtures and granules produced with PEG 6000.

The contact angle of pure Soluplus® (50.0° ±3.1) (Fig. 6.8c) was in the same range as that of pure CBZ. The contact angle of the PMs was as high as for pure CBZ and Soluplus®. In the case of the Soluplus® granules, the contact angle decreased, signifying a synergistic effect and a resultant improved wettability for the granulated material compared to their pure state or the respective PM. The contact angle of PMSP10 was 58.5° ±5.7, whereas Gr140SP10 showed a contact angle of 34.3° ±2.0, indicating a better wettability of the granules compared to the PMs. These results support the hypothesis that the lipophilic part (polyvinyl-caprolactam) of the amphiphilic polymer might interact with the lipophilic API, while the hydrophilic entities (polyethylene glycol-backbone) being orientated towards the surface, resulting in the decreased contact angle. However, in this case, contact angles did not undergo a further increase with increasing polymer content, as it was observed for the Kolliphor® P407 formulations (Fig. 6.8a).

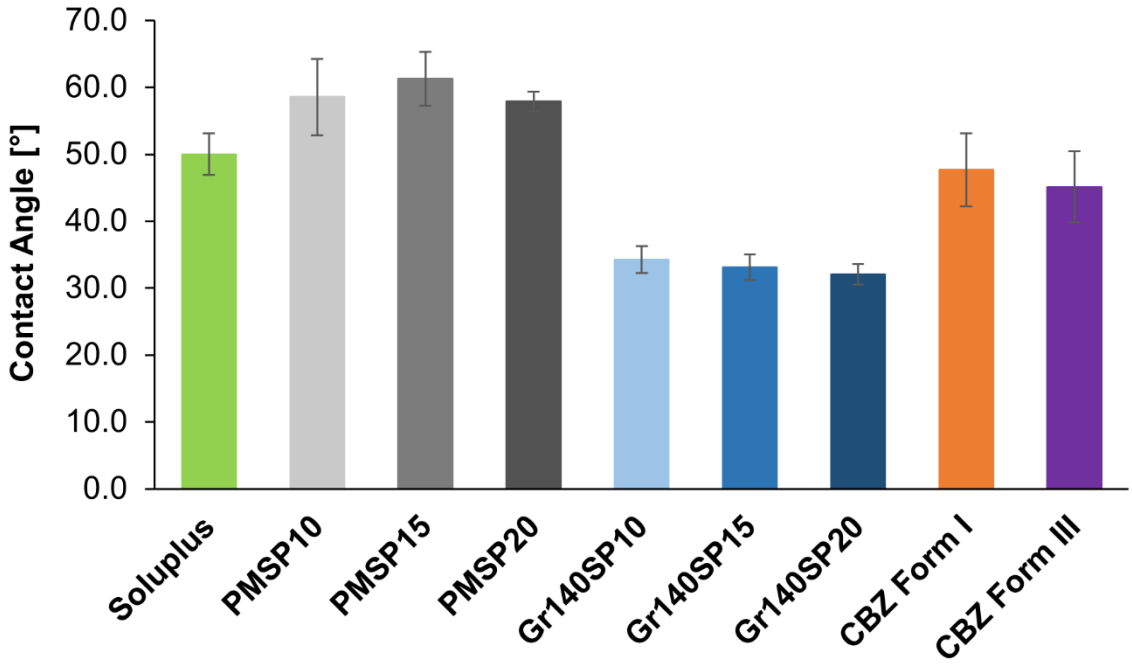

Fig. 6.8c: Contact angles of the physical mixtures and granules produced with Soluplus®.

6.6.2.4 Dissolution Results

Fig. 6.9a depicts the dissolution profile of the granules prepared with Kolliphor® P407 and the respective PMs. As observed, all granules showed faster dissolution and higher C_{max}-values within in the first minutes of dissolution run than the simple PMs (Fig. 6.9a). Furthermore, the formation of a supersaturated solution within the first 30 min was observed only for the granules. The final solubility after 180 min was slightly lower for the precipitating formulations (granulated material) than for the PMs.

Parameters used to describe the dissolution profile are given in Tab. 6.3. The highest degree of supersaturation was found for Gr70KP40720 (S=1.71 ±0.02) and Gr100KP40720 (S=1.74 ±0.03), as well as for Gr100KP40715 (S=1.76 ±0.02).

In comparison to these formulations, the maximum concentrations in solution for Gr100KP40710 and Gr70KP40715 were reached a few minutes later (10 ±1 min vs. 5 ±0 min) and they achieved smaller supersaturation ratios (S= 1.65 ±0.02 and S = 1.62 ±0.01). A higher supersaturated state was associated with a faster precipitation (indicated by the parameter Δt_{eq}, which defines the time [min] of the supersaturated solution). This indicated that P407 was not able to stabilize the high supersaturated state of CBZ (40 ±4 min vs. 73 ±9 min for Gr100KP40720 and Gr100KP40710, and 110 ±20 min vs. 58 ±9 for Gr70KP40710 and Gr70KP40720). Gr70KP40710 showed a slower initial dissolution and a much lower C_{max} value (0.34 ±0.01 mg/ml), but a more pronounced parachute effect over a duration of 110 ±20min, demonstrating a lower tendency of DH formation of this formulation in solution. This is comparable to literature results of ASDs, where the rate of generation of supersaturation was inversely proportional to precipitation kinetic in solution [146].

This observation indicated that the lower initial dissolution rate enables the polymer to stabilize the supersaturated solution for a longer period of time, but at a lower level. Notwithstanding, it should be kept in mind that in vivo performance might differ from in-vitro dissolution tests. It has been for instance shown that when male beagle dogs received high doses of 200 mg CBZ, the C_{max} and AUC (area under the curve) were half in the case of the form DH when compared to form III, and they were also lower in the case of form I compared to form III. This was explained by the higher tendency of CBZ form I to recrystallize as form DH, which exhibits a lower bioavailability [119].

This phenomenon seen in vivo, might also explain the difference in dissolution behaviour using the same polymer content but different granulation temperatures, e.g. the 10% and 15% (w/w) granules prepared at higher and lower granulation temperatures. This is because form I, which was present in the granules produced at high temperatures, has a higher initial dissolution rate, but the high potential of recrystallization as form DH limited the further solubility.

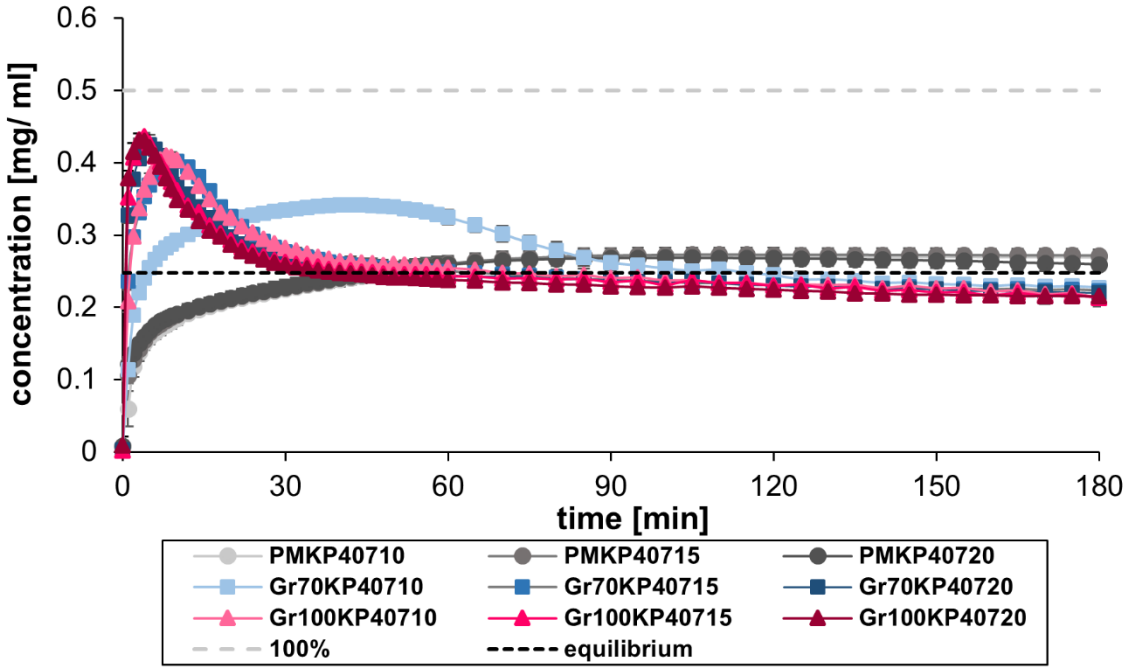

Fig. 6.9a: Dissolution profiles of the physical mixtures and granules produced with Kolliphor® P407 using paddle method (100 rpm; two-fold non-sink conditions, ceq= 0.25 mg/ml) in 450 ml phosphate buffer (pH= 6.8; 37 °C ±0.5 °C).

Tab. 6.3: Dissolution parameters of the physical mixtures and granules produced with Kolliphor® P407.

	C_{max} [mg/ml] ±SD	t_{max} [min] ±SD	S ±SD	t_{eq1} [min] ±SD	t_{eq2} [min] ±SD	Δt_{eq} [min]
PMKP40710	0.27 ±0.01	117 ±16	1.09 ±0.03	49 ±6	∞	∞
PMKP40715	0.27 ±0.01	113 ±10	1.10 ±0.04	48 ±10	∞	∞
PMKP40720	0.27 ±0.01	100 ±13	1.08 ±0.04	50 ±13	∞	∞
Gr70KP40710	0.34 ±0.01	41 ±3	1.38 ±0.02	5 ±0	115 ±20	110 ±20
Gr70KP40715	0.40 ±0.00	10 ±1	1.62 ±0.01	2 ±0	68 ±8	66 ±8
Gr70KP40720	0.43 ±0.00	5 ±0	1.71 ±0.02	1 ±0	59 ±21	58 ±21
Gr100KP40710	0.41 ±0.01	9 ±1	1.65 ±0.02	2 ±0	75 ±9	73 ±9
Gr100KP40715	0.44 ±0.01	4 ±0	1.76 ±0.02	2 ±0	44 ±5	42 ±5
Gr100KP40720	0.43 ±0.01	3 ±1	1.74 ±0.03	1 ±0	41 ±4	40 ±4

Contrary to the granules prepared with Kolliphor® P407, those produced with a high PEG 6000 content showed an opposite dissolution behaviour, dependent on the granulation temperature (Fig. 6.9b and Tab. 6.4). Dissolution graphs showed, an increased initial dissolution rate as a function of PEG 6000 content in the granules, produced at lower granulation temperature. Gr70PEG15 and Gr70PEG20 showed slight supersaturation within the first two hours (Δt_{eq} = 126 ±8 min and 114 ±17 min) and a comparable C_{max} (S= 1.53 ±0.02 and S= 1.52 ±0.03), which was reached after one hour (66 ±9 min and 67 ±8 min). The extent of supersaturation, was much lower compared to that the Kolliphor® P407 formulations (Fig. 6.9a). Gr70PEG10 showed only a slight increase in solubility (S= 1.36 ±0.05 at 112 ±15 min), which was nevertheless more stable, since only a slight precipitation occurred at a later time point. A similar profile (S=1.30 ±0.07 at 95 ±15 min) was found for Gr100PEG10. However, the initial dissolution rate was slightly slower and the degree of supersaturation began to decrease after 90 min. This might be attributed to the non-amphiphilic binder, which did not stabilize the supersaturated state of CBZ.

Previous records examined that PEG can slow down the conversion rate of commercial CBZ to the corresponding DH form in aqueous suspension by hydrogen bonding [147], which might explain the higher dissolution rates and supersaturation ratio of the granules produced at 70°C and Gr100PEG10. In contrast the formulations produced at 100 °C, Gr100PEG15 and Gr100PEG20 hardly showed any supersaturation, and the solubility was found to decrease as a function of PEG content (*S*= 1.09 ±0.03, 1.01 ±0.02 at 162 ±24 min and 178 ±3 min). This might be attributed to the formation of a higher ratio of polymorphic form II within the granules produced at 100 °C. Form II showed a much slower dissolution rate and rapid transformation into the DH.

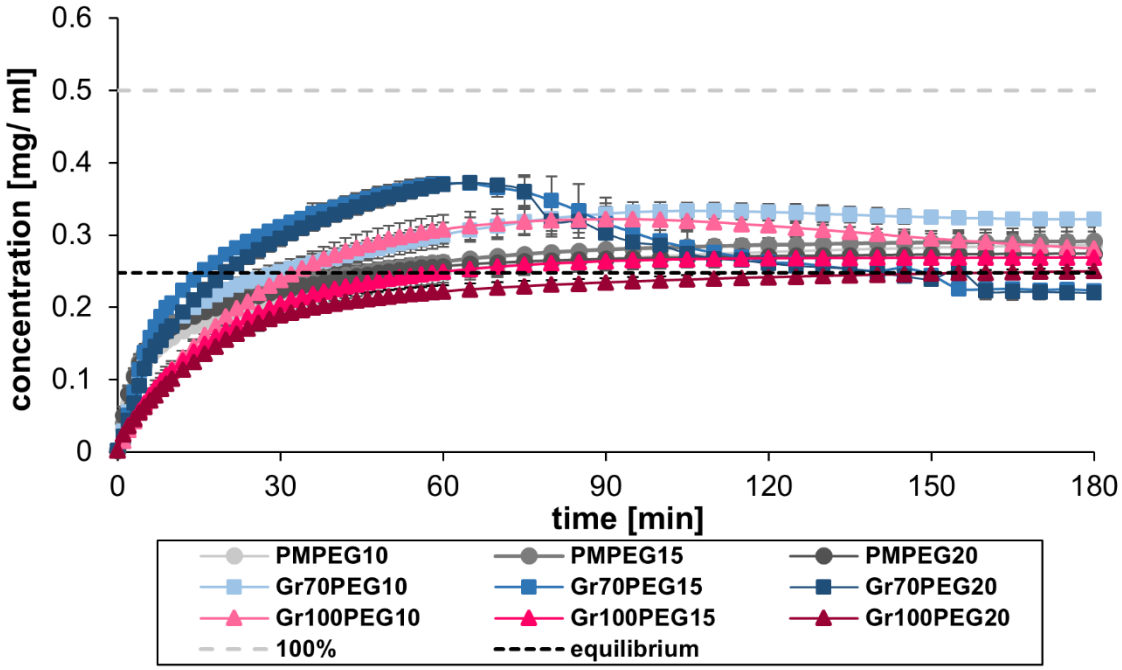

Fig. 6.9b: Dissolution profiles of the physical mixtures and granules produced with PEG 6000 using paddle method (100 rpm; two-fold non-sink conditions, ceq= 0.25 mg/ml) in 450 ml phosphate buffer (pH= 6.8; 37 °C ±0.5 °C).

Tab. 6.4: Dissolution parameters of the physical mixtures and granules produced with PEG 6000.

	C_{max} [mg/ml] ±SD	t_{max} [min] ±SD	S ±SD	t_{eq1} [min] ±SD	t_{eq2} [min] ±SD	Δt_{eq} [min]
PMPEG10	0.29 ±0.03	178 ±3	1.16 ±0.10	63 ±15	∞	∞
PMPEG15	0.29 ±0.01	168 ±20	1.18 ±0.05	45 ±5	∞	∞
PMPEG20	0.28 ±0.01	150 ±28	1.11 ±0.03	51 ±16	∞	∞
Gr70PEG10	0.34 ±0.01	112 ±15	1.36 ±0.05	31 ±6	∞	∞
Gr70PEG15	0.38 ±0.01	66 ±9	1.53 ±0.02	16 ±0	142 ±8	126 ±8
Gr70PEG20	0.38±0.01	67 ±8	1.52 ±0.03	21 ±1	135 ±17	114 ±17
Gr100PEG10	0.32 ±0.02	95 ±15	1.30 ±0.07	34 ±4	∞	∞
Gr100PEG15	0.27 ±0.01	162 ±24	1.09 ±0.03	63 ±23	∞	∞
Gr100PEG20	0.25 ±0.01	178 ±3	1.01 ±0.02	158 ±29	∞	∞

The Soluplus® granules showed an increased solubility, compared to the PMs (Fig. 6.9c). For all samples including the PMs, a supersaturation was obtained after 34 ±2 min or later (Tab. 6.5). The degree of supersaturation was found to increase over time and no precipitation was observed over a duration of 3h, indicating a stable supersaturated solution, even if the granules contained polymorphic form I. After 180 min, the overall highest supersaturation ratio was observed for Gr140SP10 (*S*= 1.87 ±0.02). Gr140SP15 and Gr140SP20 achieved a lower supersaturation at the end of the dissolution test (S= 1.72 ±0.03 and 1.69 ±0.04).

In the case of the PMs containing Soluplus® (PMSP10, PMSP15 and PMSP20) supersaturated solutions were obtained (*S*= 1.32 ±0.01; 1.31 ±0.03 and 1.27 ±0.06). The initial dissolution rate of the PMs was higher compared to the granules, but the following decrease over time resulted in a lower overall C_{max} compared to the granules at the end of the dissolution test.

Initial dissolution rates of the granules containing Soluplus® were limited and slower compared to the other binding materials under investigation. This effect increased with increasing polymer content. Due to its amphiphilic nature, Soluplus® is able to form micelles in solution. Even so, the dissolution rate of Soluplus® itself is limited, as it is known to form a viscous gel [148], which might decrease the dissolution rate compared to the other investigated binders (PEG 6000 and Kolliphor® P407). The slow dissolution rate of Soluplus® itself also explains the slower dissolution observed for the formulations containing higher amounts of this binder. Moreover, gel formation is a time dependent process, explaining the higher initial dissolution of the PMs compared to the granules, where the binding material was distributed more homogenously, simplifying a rapid continuous gel formation in and around the dissolving granules.

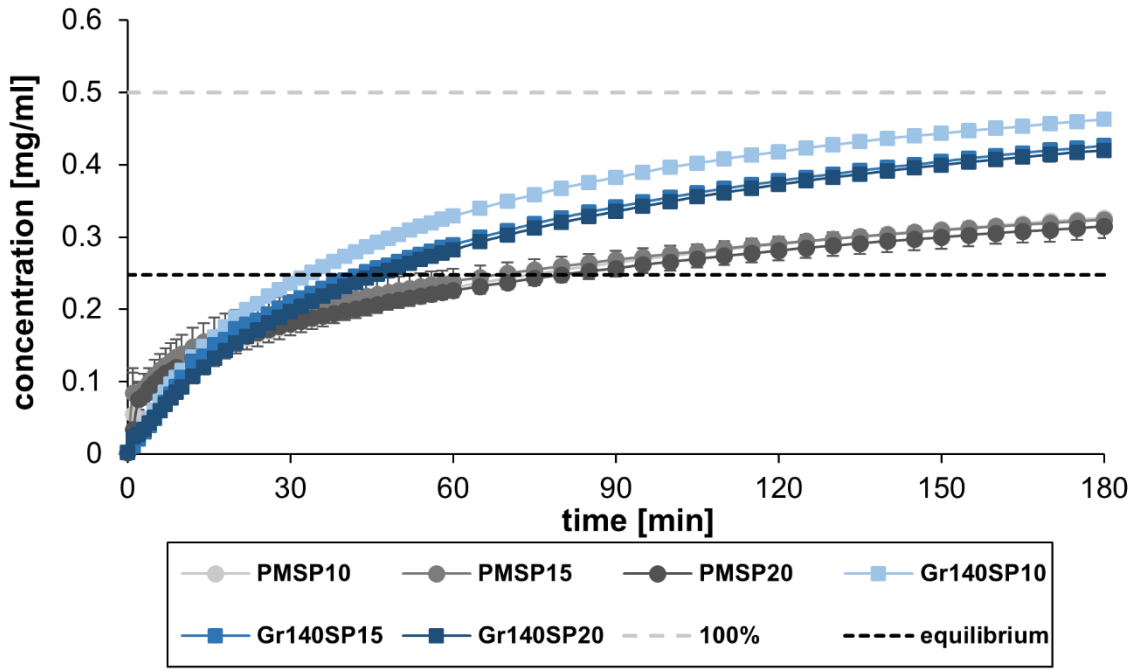

Fig. 6.9c: Dissolution profiles of the physical mixtures and granules produced with Soluplus® using paddle method (100 rpm; two-fold non-sink conditions, ceq= 0.25 mg/ml) in 450 ml phosphate buffer (pH= 6.8; 37 °C ±0.5 °C).

Tab. 6.5: Dissolution parameters of the physical mixtures and granules produced with Soluplus®.

	C_{max} [mg/ml] ±SD	t_{max} [min] ±SD	S ±SD	t_{eq1} [min] ±SD	t_{eq2} [min] ±SD	Δt_{eq} [min]
PMSP10	0.33 ±0.00	180 ±0	1.32 ±0.01	78 ±3	∞	∞
PMSP15	0.32 ±0.01	180 ±0	1.31 ±0.03	69 ±14	∞	∞
PMSP20	0.32 ±0.02	180 ±0	1.27 ±0.06	83 ±10	∞	∞
Gr140SP10	0.46 ±0.01	180 ±0	1.87 ±0.02	34 ±2	∞	∞
Gr140SP15	0.43 ±0.01	180 ±0	1.72 ±0.03	44 ±2	∞	∞
Gr140SP20	0.42 ±0.01	180 ±0	1.69 ±0.04	47 ±1	∞	∞

6.7 Conclusion

The present study highlights the potential of twin-screw melt granulation (TSMG) to enhance the dissolution of a poorly water-soluble model API (Carbamazepine (CBZ)). Using a single polymer serving as both, a binder and dissolution enhancer, this technique could yield significant drug loads up to 90% (w/w). In contrast to the often-desired ASD (amorphous solid dispersions), the high API content in this case leads to the fact that the drug particles remained in a crystalline state. The study also indicated the importance of temperature control during TSMG regarding polymorphic transition of CBZ. Furthermore, different polymers were found to result in a change of the dissolution profile, with the physicochemical characteristic of the polymer and its content playing a determining role in this scenario. Soluplus® overall achieved the highest supersaturation ratio without subsequent precipitation. However, the dissolution rate was slow due to the slow dissolution of Soluplus®. Therefore, the maximum API concentration in the dissolution medium was obtained at the end of the dissolution test (3h). Kolliphor® 407 showed a polymer content-dependent fast initial dissolution and high supersaturation ratios within the first minutes of dissolution testing. In contrast to Soluplus® formulations, Kolliphor® P407 precipitated fast, which was associated with the formation of the less soluble dihydrate form. The rate of precipitation correlated with the increasing supersaturation ratio (*S*), indicating that the polymer was not able to stabilize CBZ in solution, as it was seen for Soluplus®. PEG 6000 as binding material did not achieve high supersaturation ratios. Moreover, the formation of CBZ form II, especially at higher granulation temperatures, decreased dissolution of the formulations. Overall, this study showed that the choice of the binder and its concentration controlled the dissolution performance of the granules. Therefore, binder and its concentration should be selected appropriately to achieve the desired dissolution profile.

6.8 Acknowledgements

The authors kindly thank Kai Berkenfeld, Esther S. Bochmann and Maryam Shetab Boushehri for reviewing the manuscript.

6.9 List of Symbols and Abbraviations

API	active pharmaceutical ingredient	
ASD	amorphous solid dispersion	
AUC	area under the curve	
BCS	biopharmaceutical classification system	
BSE	backscattering electrons	
CBZ	Carbamazepine	
C_{eq}	equilibrium solubility	[mg/ml]
C_{max}	maximum concentration	[mg/ml
DH	Dihydrate	
FTIR	Fourier transform infrared spectroscopy	
IDR	intrinsic dissolution rate	[µg/min/cm²]
L/D	length/diameter	
PEG	polyethylene glycol	
PM	physical mixture	
S	supersaturation ratio	
SEM	scanning electron microscope	
Δt_{eq}	time interval of supersaturation	[min]
t_{max}	timepint C_{max}	[min]
T_{max}	maximum granulation temperature	[°C]
TSMG	twin-screw melt granulation	
XRPD	X-ray powder diffraction	

6.10 Authors contributions:

Conceptualization: K.G.W and K.E.S.; Data curation: K.E.S; Methodology: K.E.S and K.G.W.; Investigation: K.E.S; Resources: K.G.W.; Writing-Original Draft Preparation: K.E.S; Writing-Review & Editing: K.G.W.; Supervision: K.G.W.; Project Administration: K.G.W.

.

7 Immediate-Release Formulations produced via Twin-screw Melt Granulation: Systematic Evaluation of the Addition of Disintegrants

Kristina E. Steffens; Karl G. Wagner

This part was submitted as:

Steffens, Kristina E., and Karl G. Wagner. “Immediate-Release Formulations Produced via Twin-Screw Melt Granulation: Systematic Evaluation of the Addition of Disintegrants.” AAPS PharmSciTech.

7.1 Graphical abstract

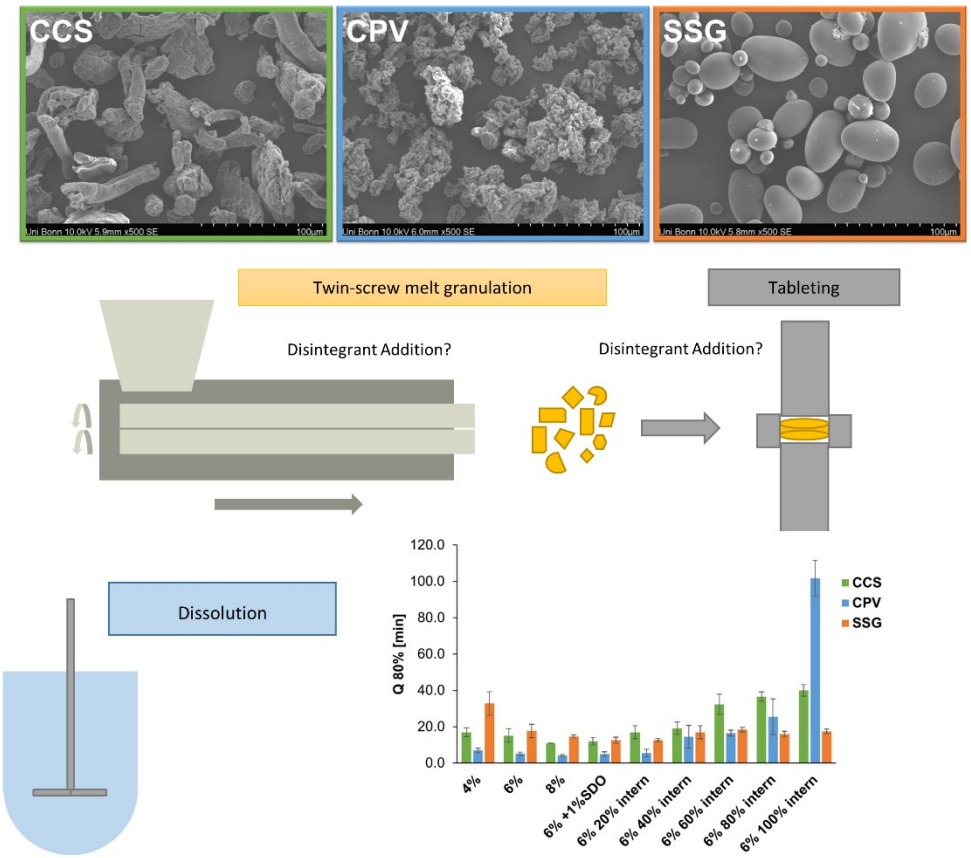

7.2 Abstract

Introduction: The current study evaluated the effect of location and amount of various superdisintegrants on the properties of tablets made by twin-screw melt granulation (TSMG).

Material and Methods: Sodium-croscarmellose (CCS), crospovidone (CPV) and sodium-starch glycolate (SSG) were used in various proportions intra- and extra-granular. Tabletability, compactibility, compressibility as well as friability, disintegration and dissolution performance were assessed.

Results and Discussion: The extra-granular addition resulted in the fasted disintegration and dissolution. CPV performed superior to CCS and SSG. Even if the solid fraction (SF) of the granules was lower for CPV, only a minor decrease in tabletability was observed, due to the high plastic deformation of the melt granules. The intra-granular addition of CPV resulted in a more prolonged dissolution profile, which could be correlated to a loss in porosity during tableting. The 100% internal addition of the CPV resulted in a distinct decrease of the disintegration efficiency, whereas the performance of SSG was unaffected by the granulation process. CCS was not suitable to be used for the production of an immediate release formulation, when added in total proportion into the granulation phase, but its efficiency was less impaired compared to CPV.

Conclusion: Shortest disintegration (78 s) and dissolution (Q_{80}: 4.2 min) was achieved with CPV in the extra granular phase. Introducing CPV and CCS into the granular phase disintegration time and Q_{80} increased. Only SSG showed a process and location independent disintegration and dissolution performance however, at a higher level at appx. 500 s and appx. 15 min, respectively.

7.3 Keywords

Twin-screw melt granulation, immediate release, tablets, disintegration, dissolution

7.4 Introduction

Melt granulation is an alternative granulation method to formulate powders that are not suitable for direct tableting because of their poor flowability or compactibility. Since melt granulation does not require the addition of solvents, the process is also interesting for water-sensitive compounds [59]. The granules are formed by using a meltable binder (like waxes or polymers) in a heatable process equipment. Different techniques are approved, which include fluid-bed granulators, high shear mixers and twin-screw extruders [2,4–6,11,23,24,104,149,150].

With growing interest in continuous processing methods, twin-screw melt granulation (TSMG) became an attractive technique to granulate active pharmaceutical ingredients (APIs) especially, as a process time limiting drying step is avoided [6] . Furthermore, in TSMG, only a very low excipient content is needed, resulting in high drug-load final products [2]. However, compared to wet granules no pore formation by the removal of water can be observed. Therefore, melt granules show low porosities, especially when obtained from high-shear granulation processes, like TSMG. The potential of this method to achieve an improved tabletability was often reported in literature [2,4,36,37]. This improved tabletability is mainly deriving from the obtained closer binder network in the tablets, which simultaneously causes a low porosity of the produced compacts [81]. Due to the strong relationship between the relative density and disintegration, the disintegration of these compacts might be limited. Moreover, the binding material, which are often soluble polymers, tend to form viscous gels upon dissolution, which further reduces the tablet disintegration and finally the API release [80].

Immediate-release formulations are often desired to obtain a fast onset of the therapeutic effect of the API. Disintegration of these tablets is the first step before the drug dissolves and therefore of fundamental importance to achieve bioavailability and a rapid onset of the therapeutic effect of the drug.

In general, disintegrants cause the tablet to break-up, when it comes in contact with water and helps to overcome the cohesive forces in the compact. The resulting particle size and the available surface generated after disintegration, enhances the dissolution rate of the API. Early disintegrants included starch- and cellulose-based excipients, such as natural starch, pregelatinized starch, microcrystalline cellulose and low-substituted hydroxypropylcellulose. Due to chemical modifications, which decreased solubility and increased hydrophilicity at increased swelling, more effective disintegrants were developed; so called superdisintegrants. They can be classified in chemically modified cellulose (croscarmellose-sodium (CCS)), chemically modified starches (sodium starch glycolate (SSG)) and in pure synthesized copolymers, like crospovidone (CPV). Disintegrants act via different mechanism (e.g. swelling or shape recovery). In the case of swelling, the disintegrant uptakes water from the surrounding medium. This swelling results in multidirectional disruption of the tablets or granules structure during the disintegration process.

The effectiveness of the disintegrant is dependent on the swelling extent and the swelling force generated during the water uptake. In the case of shape recovery, particles that are deformed, e.g. by the tableting process, regain their original shape, if water penetrates into the tablets, resulting on a unidirectional deformation of the tablet matrix.

The disintegration effect is often content-dependent, resulting in an optimal concentration to achieve the best disintegration effect [151,152]. At the same time, the effect of disintegrants is often particle size- and particle shape-dependent [153–155]. In wet granulation, the inclusion of the disintegrant in both intra-granular and extra-granular phase is often recommend, since the generated dispersion was reported to be finer, thereby increasing the available surface area [156,157].

This is especially important, when high drug concentrations with a poor solubility are in focus [158]. However, depending on the formulation used, the disintegration was reported to be faster when the disintegrant was added extra-granular only [159].

When disintegrants are added intra-granular prior to the melt granulation step, temperature and shear during the granulation process might influence the disintegrant performance. Until now, no systematic evaluation of different superdisintegrants exists concerning their suitability to be added to the melt granulation process.

The current study sought to examine the need of disintegrants to obtain immediate release tablets prepared from twin-screw melt granules.

In this study, the three different superdisintegrants (CCS; CPV; SSG), with a comparable mean particle size of 40 µm were tested in three weight fractions (4, 6 and 8% (w/w)). Moreover, in the case of the 6% (w/w) formulation, varying portions of this amount were added intra-granular. The effect on tabletability, friability, disintegration and drug dissolution were tested on a model formulation of paracetamol (PCM) and polyethylene glycol 6000 (PEG) as a melt binder.

As model excipient, the good soluble drug paracetamol, (PCM) was chosen to show process related influences on the disintegration and drug dissolution, rather than effects that are related to poor wettability or poor solubility of the drug itself. PCM has no lack in solubility (23.7 mg/ml at 37°C), its solubility is not pH-dependent below pH 9 and it belongs to the biopharmaceutical classification system (BCS) class III [160].

7.5 Material and methods

7.5.1 Material

PCM was obtained from Mallinckrodt Pharmaceuticals (Staines-Upon-Thames, United Kingdom). Due to its low melting point (55-60°C), the binder PEG 6000 was used and purchased from Carl Roth (Karlsruhe, Germany). Granulation of PCM required the addition of 1% (w/w) colloidal silicium dioxide (AEROSIL® 200) which was a gift from Evonik (Evonik Ressource Efficiency GmbH, Hanau-Wolfgang, Germany). Sodium starch glycolate (Vivastar® P) and croscarmellose sodium (Vivasol® GF) were donated by JRS (J. RETTENMAIER & SÖHNE GmbH + Co KG, Rosenberg, Germany). Additionally, crospovidone (Kollidon® CL-F) was tested as a disintegrant, which was a gift from BASF (BASF SE, Ludwigshafen, Germany). Magnesium stearate (Ligamed® MF-2-V) was donated by Peter Greven (Peter Greven GmbH & Co. KG, Bad Münstereifel, Germany).

7.5.2 Methods

7.5.2.1 Physical mixtures (PM)

PCM was formulated with 10% (w/w) PEG as binding material. PCM required the addition of 1% (w/w) colloidal silicium dioxide (SDO) to enable feeding of the material into the extruder. PMs were prepared by using a Turbula blender (Willy A. Bachofen AG Maschinenfabrik, Switzerland), rotating at 50 rpm for 10 min. The obtained PMs were further used for twin-screw melt granulation (TSMG). Depended on the formulation, disintegrants were added proportional in the mixture. Short names used in text and graphics of this study, are given in Tab. 7.1 (CCS), Tab. 7.2 (CPV) and Tab. 7.3 (SSG). The external phase (disintegrant and magnesium stearate (MGST)) was added after granulation. Disintegrants were added externally and mixed for another 5 min using a Turbula blender (Willy A. Bachofen AG Maschinenfabrik, Switzerland), rotating at 50 rpm. MGST was added in a second step and mixed for further 30 sec.

Tab. 7.1: Short names of the croscarmellose sodium (CCS) formulations under investigation (% w/w).

Short name	internal Phase	external Phase
Gr. PCM 10% PEG	Granules PCM 88.11% +9.9% PEG +0.99% SDO	1% Mgst
CCS 4%	Granules PCM 84.55% +9.5% PEG +0.95% SDO	1% Mgst +4% CCS
CCS 6%	Granules PCM 82.77% +9.3% PEG +0.93% SDO	1% Mgst +6% CCS
CCS 6% SDO 1%	Granules PCM 81.88% +9.2% PEG +0.92% SDO	1% Mgst + 6% CCS +1% SDO
CCS 8%	Granules PCM 80.99% +9.1% PEG +0.91% SDO	1% Mgst +8% CCS
CCS 6% 20% intern	Granules PCM 82.77% +9.3% PEG +0.93% SDO+1.2% CCS	1% Mgst +4.8% CCS
CCS 6% 40% intern	Granules PCM 82.77% +9.3% PEG +0.93% SDO+2.4% CCS	1% Mgst +3.6% CCS
CCS 6% 60% intern	Granules PCM 82.77% +9.3% PEG +0.93% SDO+3.6% CCS	1% Mgst +2.4% CCS
CCS 6% 80% intern	Granules PCM 82.77% +9.3% PEG +0.93% SDO+4.8% CCS	1% Mgst +1.2% CCS
CCS 6% 100% intern	Granules PCM 82.77% +9.3% PEG +0.93% SDO+6% CCS	1% Mgst

CCS: croscarmellose sodium, Mgst: magnesium stearate, PCM: paracetamol, PEG: polyethylene glycole, SDO: colloidal silicium dioxide

Tab. 7.2: Short names of the crospovidone (CPV) formulations under investigation (% w/w).

Short name	internal Phase	external Phase
Gr. PCM 10% PEG	Granules PCM 88.11% +9.9% PEG +0.99% SDO	1% Mgst
CPV 4%	Granules PCM 84.55% +9.5% PEG +0.95% SDO	1% Mgst +4% CPV
CPV 6%	Granules PCM 82.77% +9.3% PEG +0.93% SDO	1% Mgst +6% CPV
CPV 6% SDO 1%	Granules PCM 81.88% +9.2% PEG +0.92% SDO	1% Mgst +6% CPV +1% SDO
CPV 8%	Granules PCM 80.99% +9.1% PEG +0.91% SDO	1% Mgst +8% CPV
CPV 6% 20% intern	Granules PCM 82.77% +9.3% PEG +0.93% SDO+1.2% CPV	1% Mgst +4.8% CPV
CPV 6% 40% intern	Granules PCM 82.77% +9.3% PEG +0.93% SDO+2.4% CPV	1% Mgst +3.6% CPV
CPV 6% 60% intern	Granules PCM 82.77% +9.3% PEG +0.93% SDO+3.6% CPV	1% Mgst +2.4% CPV
CPV 6% 80% intern	Granules PCM 82.77% +9.3% PEG +0.93% SDO+4.8% CPV	1% Mgst +1.2% CPV
CPV 6% 100% intern	Granules PCM 82.77% +9.3% PEG +0.93% SDO+6% CPV	1% Mgst

CPV: crospovidone, Mgst: magnesium stearate, PCM: paracetamol, PEG: polyethylene glycole, SDO: colloidal silicium dioxide

Tab. 7.3: Short names of the sodium starch glycolate (SSG) formulations under investigation (% w/w).

Short name	internal Phase	external Phase
Gr. PCM 10% PEG	Granules PCM 88.11% +9.9% PEG +0.99% SDO	1% Mgst
SSG 4%	Granules PCM 84.55% +9.5% PEG +0.95% SDO	1% Mgst +4% SSG
SSG 6%	Granules PCM 82.77% +9.3% PEG +0.93% SDO	1% Mgst +6% SSG
SSG 6% SDO 1%	Granules PCM 81.88% +9.2% PEG +0.92% SDO	1% Mgst +6% SSG +1% SDO
SSG 8%	Granules PCM 80.99% +9.1% PEG +0.91% SDO	1% Mgst +8% SSG
SSG 6% 20% intern	Granules PCM 82.77% +9.3% PEG +0.93% SDO+1.2% SSG	1% Mgst +4.8% SSG
SSG 6% 40% intern	Granules PCM 82.77% +9.3% PEG +0.93% SDO+2.4% SSG	1% Mgst +3.6% SSG
SSG 6% 60% intern	Granules PCM 82.77% +9.3% PEG +0.93% SDO+3.6% SSG	1% Mgst +2.4% SSG
SSG 6% 80% intern	Granules PCM 82.77% +9.3% PEG +0.93% SDO+4.8% SSG	1% Mgst +1.2% SSG
SSG 6% 100% intern	Granules PCM 82.77% +9.3% PEG +0.93% SDO+6% SSG	1% Mgst

Mgst: magnesium stearate, PCM: paracetamol, PEG: polyethylene glycole, SDO: colloidal silicium dioxide, SSG: sodium starch glycolate

7.5.2.2 Twin-screw melt granulation (TSMG)

TSMG was performed using a co-rotating twin-screw extruder (ZE12, Three-Tec GmbH, Seon, Switzerland) with a functional length of 25:1 L/D (length/diameter) and a 12 mm screw diameter. The extruder barrel consisted of five individually adjustable heating zones to ensure sufficient melting and distribution of the binder. The process temperature was set up to 95°C in the high-shear region of the extruder screws (30°, 60°, 60° and 90° 4-disc-kneading elements).

At the terminal zone of the barrel, the temperature was reduced to 75 °C to allow solidification of the material. During melt granulation, the screw speed was set to 100 rpm and no die plate was mounted at the end of the extruder barrel. A volumetric feeder system ZD9 (Three-Tec GmbH, Seon, Switzerland) was used to enable a constant feed rate of 0.1 kg/h. Granules obtained were further dry sieved using a 1 mm sieve in an Erweka wet granulator FGS with an AR 402 drive unit (Erweka, GmbH, Heusenstamm, Germany) prior to compaction.

7.5.2.3 Investigation of the disintegrants

7.5.2.3.1 Particle-size distribution

The particle size distribution of the disintegrants were measured with a laser-diffraction (λ= 655 nm) particle size analyser (Horiba LA-920, Horiba Ltd, Japan). A dry dispersion method was used with a pressure of 3 bar. The SPAN represents the width of the PSD and is calculated using Eq. 7.1:

$$SPAN = \frac{d90 - d10}{d50} \qquad \text{(Eq. 7.1)}$$

7.5.2.3.2 Scanning electron microscopy

Images of the disintegrants were taken using a scanning electron microscope (SU 3500, Hitachi High Technologies, Krefeld, Germany). The samples were mounted with a double adhesive photo sticker and coated with a thin layer of gold using a sputter coater for 2 min at 1.7 kV (Polaron SC7640, Quorum Technologies Ltd, Lewes, United Kingdom). Images were captured at an acceleration voltage of 10 kV in high vacuum mode and a secondary electron detector.

7.5.2.4 Density

Pycnometric density was measured using the AccuPyc 1330 helium pycnometer (Micromeritics GmbH, Aachen, Germany). The chamber was purged 20 cycles prior to analysis. A fill pressure of 136.86 kPa and an equilibration rate of 0.0345 kPa/min were used for measurements. The cycle was repeated up to 25 times or until a standard deviation of 0.01% was reached. The density was employed for the calculation of the SF.

7.5.2.5 Compaction studies

The tablets (n = 5) were compressed on a single punch tablet press (StylOne Classic 105 ML, Medelpharm, Beynost, France/Romaco Kilian, Cologne, Germany) with a 8 mm flat-face tooling. Five levels of compaction pressures from 50 MPa to 250 MPa were applied at constant tableting speed (dwell-time: 6-7 ms; compression time on average: 110 ms). The die was filled manually.

7.5.2.6 Out-of-die-analysis

After 24 h of storage, the tablets were analysed by means of their tablet weight (analytical balance, AG 204, Mettler Toledo GmbH, Gießen, Germany), height (Mitutoyo Absolute ID C125B, Mitutoyo Deutschland GmbH, Neuss, Germany), diameter and crushing strength (Erweka TBH 210, Erweka GmbH, Heusenstamm, Germany). The tensile strength (TS; Eq. 7.2) and the solid fraction (SF; Eq. 7.3; 7.4 and 7.5) were calculated from the obtained data. TS (Eq. 7.2) is the tablet crushing strength normalized by the dimension of the tablet and it is therefore independent of its geometry [64],

$$TS = \frac{2F}{\pi dh} \qquad \text{(Eq. 7.2)}$$

where *F* is the crushing strength, *d* the diameter and *h* the thickness of the tablet.
SF (Eq. 7.3-5) represents the apparent density (P_{app}) of the compact calculated from the tablet weight (*m*) and its volume relative to the true density (P_{true}) of the powder.

$$SF = \frac{Papp}{Ptrue} \qquad \text{(Eq. 7.3)}$$

$$Papp = \frac{m}{Vp} \qquad \text{(Eq. 7.4)}$$

$$Vp = \pi * \left(\frac{d}{2}\right)^2 * h \qquad \text{(Eq. 7.5)}$$

In Eq. 7.5, *Vp* is the volume of the compact calculated based on *d and h*, which describe the tablet diameter and thickness.

7.5.2.7 Production of Tablets for further testing

The tablets for friability, disintegration and dissolution studies were produced with a clinical relevant concentration of 500 mg PCM. Tablets were compressed with a compaction simulator (StylOne Classic 105 ML, Medelpharm, Beynost, France/Romaco Kilian, Cologne, Germany) and a 13 mm round tooling. A compaction pressure of 150 MPa was applied at constant tableting speed (dwell-time: 6-7 ms; compression time on average: 110 ms).

7.5.2.8 Friability test

The friability of the tablets was tested according to Ph. Eur. 2.9.7 [161]: Friability of uncoated tablets. Approx.: 6.5 g of tablets (removed from dust and accurately weighed) were placed into a friability tester (Erweka TA3R, Erweka GmbH, Heusenstamm, Germany), which operated at 25 ±1 rpm. After 100 rotations, the dust was removed and the tablets were weighed using an analytical balance (AG 204, Mettler Toledo GmbH, Gießen, Germany). According to Ph. Eur. 2.9.7, a maximum loss of mass not greater than 1.0% is acceptable [161].

7.5.2.9 Disintegration test

The disintegration test was performed according to Ph. Eur. 2.9.1. and the monography of uncoated tablets [162]. The disintegration time of the tablets (n=6) was determined in 800 ml demineralized water (37 ±1 °C) using an automatic disintegration tester, according to Test A of the Ph. Eur. (Erweka ZT72, Erweka GmbH, Heusenstamm, Germany). To meet the requirements, the uncoated tablets should disintegrate within 15 min (= 900 s) [162].

7.5.2.10 Dissolution test

Dissolution tests were performed using a USP Dissolution Apparatus 2 (paddle method) (Sotax AT7, Sotax GmbH, Lörrach, Germany) with a rotation speed of 50 rpm. Analysis was performed according to the USP monography for acetaminophen tablets with 900 ml of phosphate buffer at a pH of 5.8 ±0.1 and a set temperature of 37.0 °C ±0.5 °C. Tablets (n=6) containing 500 mg PCM were used for each experiment. For quantitative analysis, an Agilent 8453 in-line UV-VIS spectrophotometer (Agilent Technologies, Waldbronn, Germany) was used. Absorption was determined at a fixed wavelength of 260 nm. Dissolution tests were performed over a maximum period of 6 h with a maximum interval of 10 min between the measurements. Dissolution results were compared using $Q_{80\%}$, giving the time point at which 80% of the formulation is released. The USP 41 requires are minimum of 30 min for the 80% dissolution of the “Acetaminophen Tablets” in phosphate buffer (pH= 5.8) [163], whereas in the Ph. Eur. 5.17.1, 45 min or less for the release of 80% API is reported (for conventional release dosage forms) [161].

7.6 Results

7.6.1 Investigation of the disintegrants

Tab. 7.4: Particle-size distribution of the disintegrants (laser diffraction, dry dispersion, 3bar).

Disintegrant	d_{10} [µm]	d_{50} [µm]	d_{90} [µm]	SPAN
CCS	23.1 ±0.1	39.7 ±0.1	69.0 ±0.4	1.16
CPV	17.0 ±0.5	40.4 ±0.4	109.7 ±1.3	2.30
SSG	23.2 ±0.3	39.9 ±0.3	66.3 ±0.2	1.08

All disintegrants had a comparable mean particle size of 40 µm (Tab. 7.4). The particle size of CPV was broader compared the particle size of CCS and SSG. This is indicated by the higher SPAN of 2.30 for CPV.

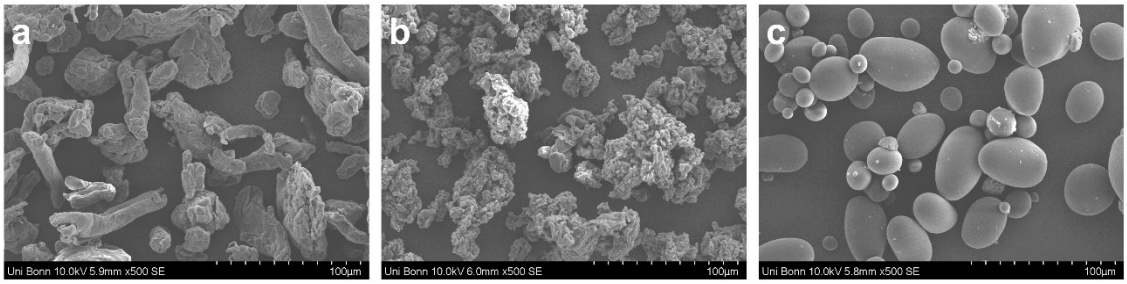

Fig. 7.1: Scanning electron images of the disintegrants under investigation: a: croscarmellose sodium (CCS); b: crospovidone (CPV); c: sodium starch glycolate (SSG).

SEM images determined similar particle size-distribution of the disintegrants, but a different morphology and shape. CCS (Fig. 7.1a) had a more elongated and fibre-like structure, whereas CPV showed a “popcorn” structure with a high porosity (Fig. 7.1b). SSG consisted of round particles with a very smooth surface structure (Fig. 7.1c).

7.6.2 **Density**

Densities of the formulations under investigation are given in Tab. 7.5. The values were used for the calculation of the SF of the tablets.

Tab. 7.5: Pycnometric densities of the formulations.

Formulation	Pycnometric density [g/cm³]	Formulation	Pycnometric density [g/cm³]	Formulation	Pycnometric density [g/cm³]
Gr. PCM 10% PEG			1.3050 ±0.0034		
CCS 4%	1.3094 ±0.0012	**CPV 4%**	1.3136 ±0.0022	**SSG 4%**	1.3158 ±0.0005
CCS 6%	1.3158 ±0.0011	**CPV 6%**	1.3452 ±0.0049	**SSG 6%**	1.3275 ±0.0006
CCS 6% SDO 1%	1.3203 ±0.0003	**CPV 6% SDO 1%**	1.3443 ±0.0004	**SSG 6% SDO 1%**	1.3378 ±0.0004
CCS 8%	1.3194 ±0.0003	**CPV 8%**	1.3684 ±0.0005	**SSG 8%**	1.3331 ±0.0004
CCS 6% 20% intern	1.3222 ±0.0021	**CPV 6% 20% intern**	1.3245 ±0.0004	**SSG 6% 20% intern**	1.3284 ±0.0005
CCS 6% 40% intern	1.3262 ±0.0000	**CPV 6% 40% intern**	1.3295 ±0.0006	**SSG 6% 40% intern**	1.3247 ±0.0032
CCS 6% 60% intern	1.3205 ±0.0010	**CPV 6% 60% intern**	1.3183 ±0.0019	**SSG 6% 60% intern**	1.3323 ±0.0006
CCS 6% 80% intern	1.3262 ±0.0004	**CPV 6% 80% intern**	1.3273 ±0.0034	**SSG 6% 80% intern**	1.3245 ±0.0005
CCS 6% 100% intern	1.3217 ±0.0019	**CPV 6% 100% intern**	1.3443 ±0.0031	**SSG 6% 100% intern**	1.3270 ±0.0004

CCS: croscarmellose sodium, CPV: crospovidone, Mgst: magnesium stearate, PCM: paracetamol, PEG: polyethylene glycole, SDO: colloidal silicium dioxide, SSG: sodium starch glycolate

7.6.3 **Compaction studies**

7.6.3.1 Tabletability

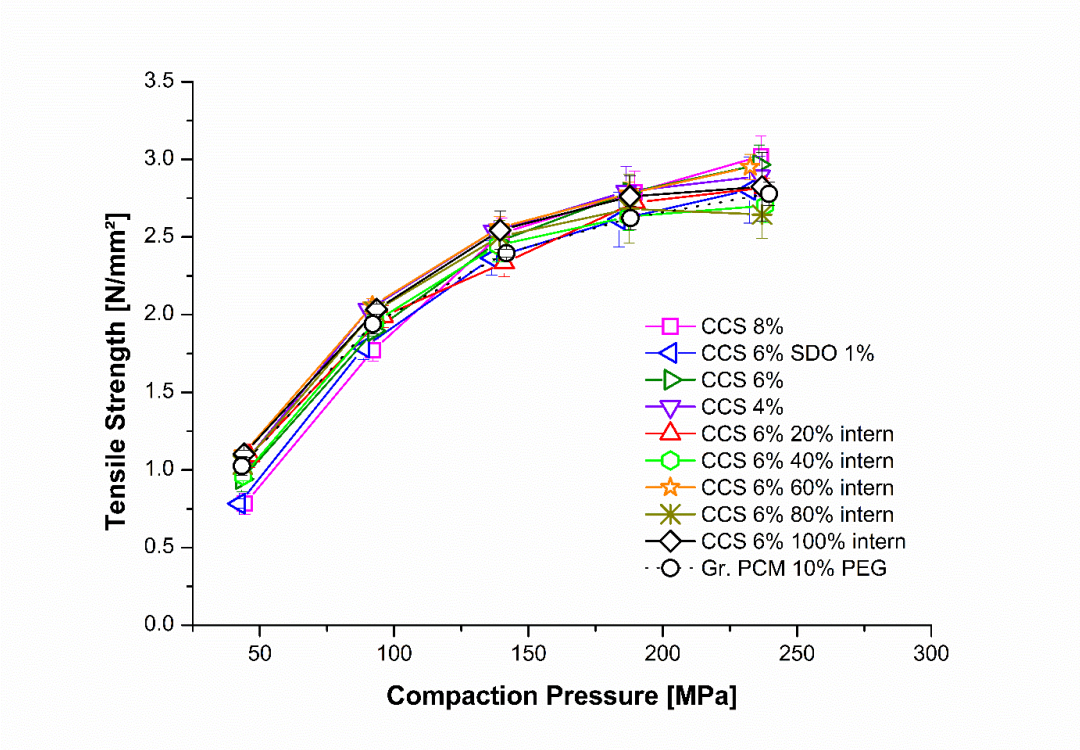

Fig. 7.2a: Tabletability plot of the croscarmellose sodium (CCS) formulations.

Fig. 7.2a shows the tabletability studies of the croscarmellose sodium (CCS) formulations. In general, the addition of CCS in the formulation had no impact on the tabletability (e.g. Gr. PCM 10% PEG: 2.40 ±0.03 N/mm² at 150 MPa vs. CCS 8%: 2.53 ±0.10 N/mm² at 150 MPa). In the case of using crospovidone (CPV), the addition of the disintegrant can slightly lower tensile strength (TS). This was pronounced, when high weight fractions of CPV were added extra-granular: CPV 8% (2.08 ±0.05 N/mm² at 150 MPa); 6% (2.26 ±0.07 N/mm² at 150 MPa) and 6% 20% intern (2.03 ±0.16 N/mm² at 150 MPa) (Fig. 7.2b).

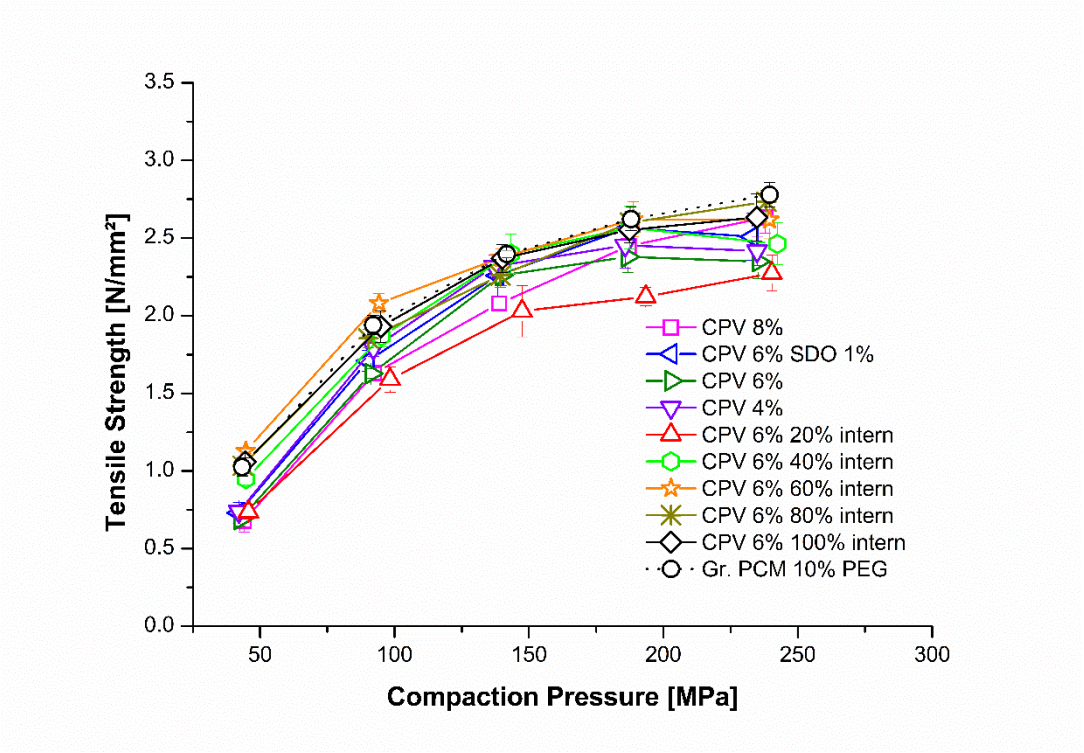

Fig. 7.2b: Tabletability plot of the crospovidone (CPV) formulations.

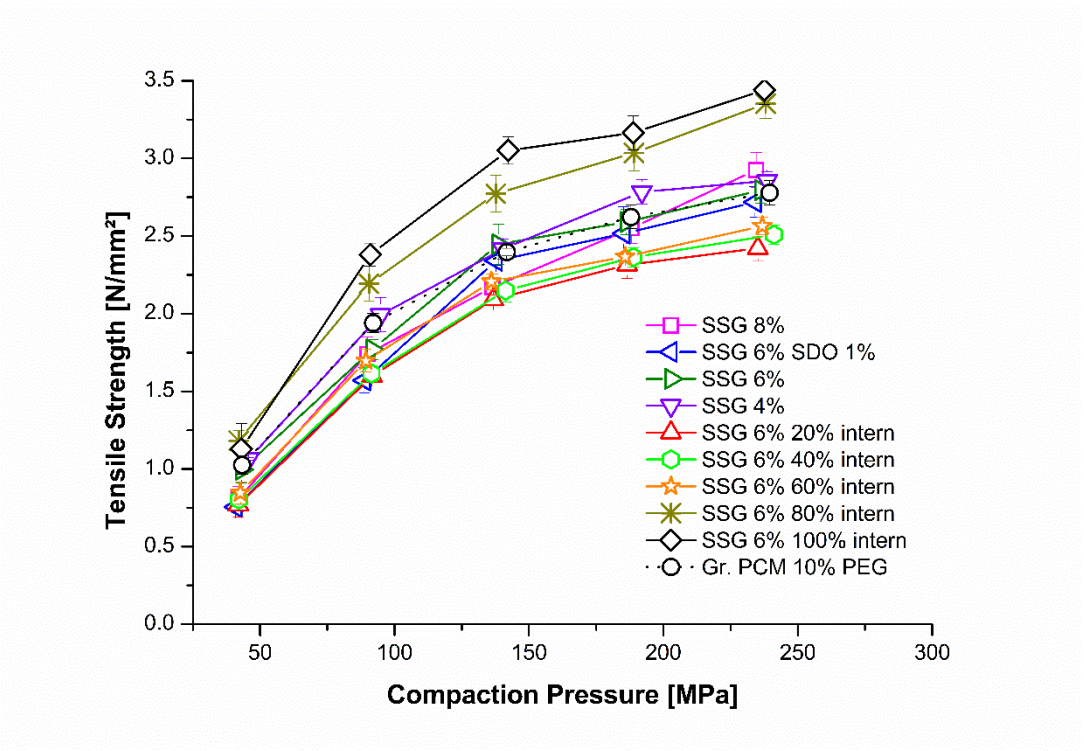

Fig. 7.2c: Tabletability plot of the sodium starch glycolate (SSG) formulations.

Fig. 7.2c shows the tabletability of the sodium starch glycolate (SSG) formulations in which a high weight fraction of the disintegrant intra-granular had a positive effect on the TS (SSG 6% 80% (2.77 ±0.12 N/mm² at 150 MPa) and 100% intern (3.05 ±0.09 N/mm² at 150 MPa)). When high weight fractions of SSG were added extra-granular, (SSG 6% 20% intern (2.09 ±0.03 N/mm² at 150 MPa), SSG 6% 40% intern (2.15 ±0.08 N/mm² at 150 MPa) and SSG 6% 60% intern (2.21 ±0.05 N/mm² at 150 MPa)) TS was slightly lowered. However, the effect was not pronounced for the SSG 6% (2.45 ±0.13 N/mm² at 150 MPa) extra-granular, indicating that the effect was not concentration dependent.

7.6.3.2 Compactibility

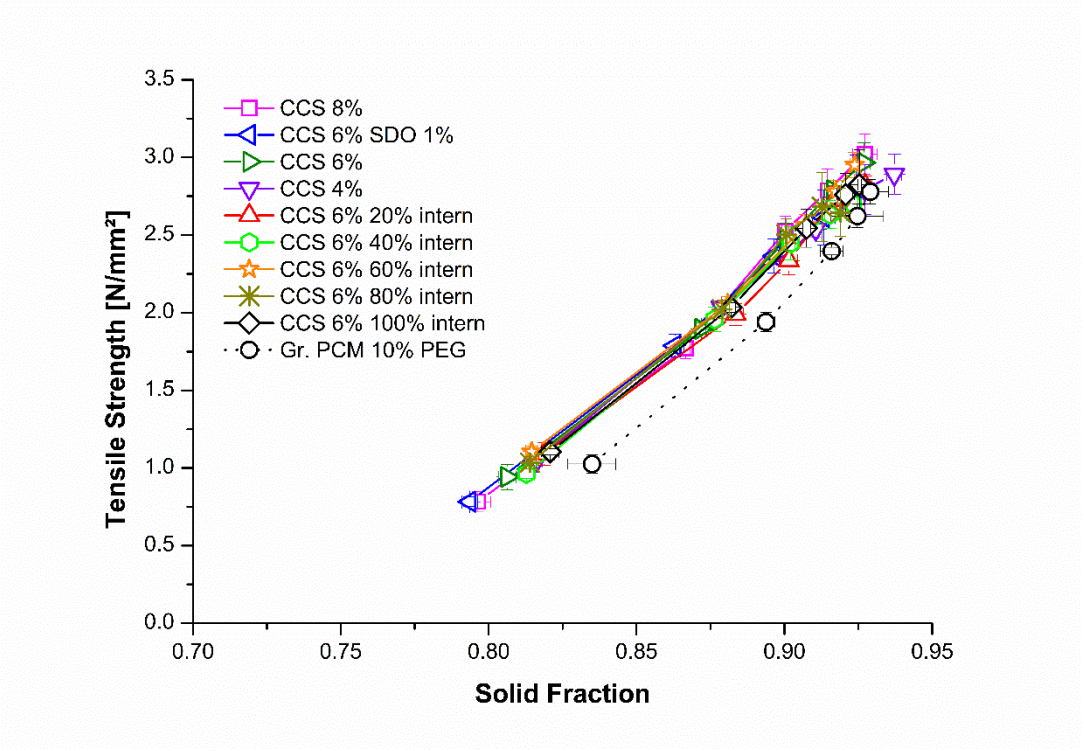

Fig. 7.3a: Compactibility plot of the croscarmellose sodium (CCS) formulations.

In Fig. 7.3a, the compactibility plot of the CCS formulations are shown. It can be seen that the formulations containing CCS showed lower SF at comparable TS than the formulation without disintegrant (Gr. PCM 10% PEG). The shift to lower SFs was independent of the CCS concentration and the way of addition (extra- or intra-granular).

Using CPV (Fig. 7.3b) as disintegrant, the effect on lowering the SFs of the tablets was higher compared to the CCS formulations (Fig. 7.3a). Being added extra-granular, CPV lowered TS and the SF of the formulation as a function of increased CPV weight fraction (4; 6; and 8%). The intra-granular addition of CPV compensated this effect concentration dependent. Regarding the 6% (w/w) formulations, the higher the intra-granular amount of CPV the higher the SFs of the tablets. These formulations showed higher SFs and TS, but still lower than the Gr. PCM 10% PEG, which contained no disintegrant. The effect of SSG addition on the SF was minor (Fig. 7.3c).
However, using SSG intra-granular (SSG 6% 80% intern and 100% intern) showed a higher bonding capacity than the formulation without disintegrant (Gr. PCM 10% PEG) and the formulations with high amounts of SSG extra-granular.

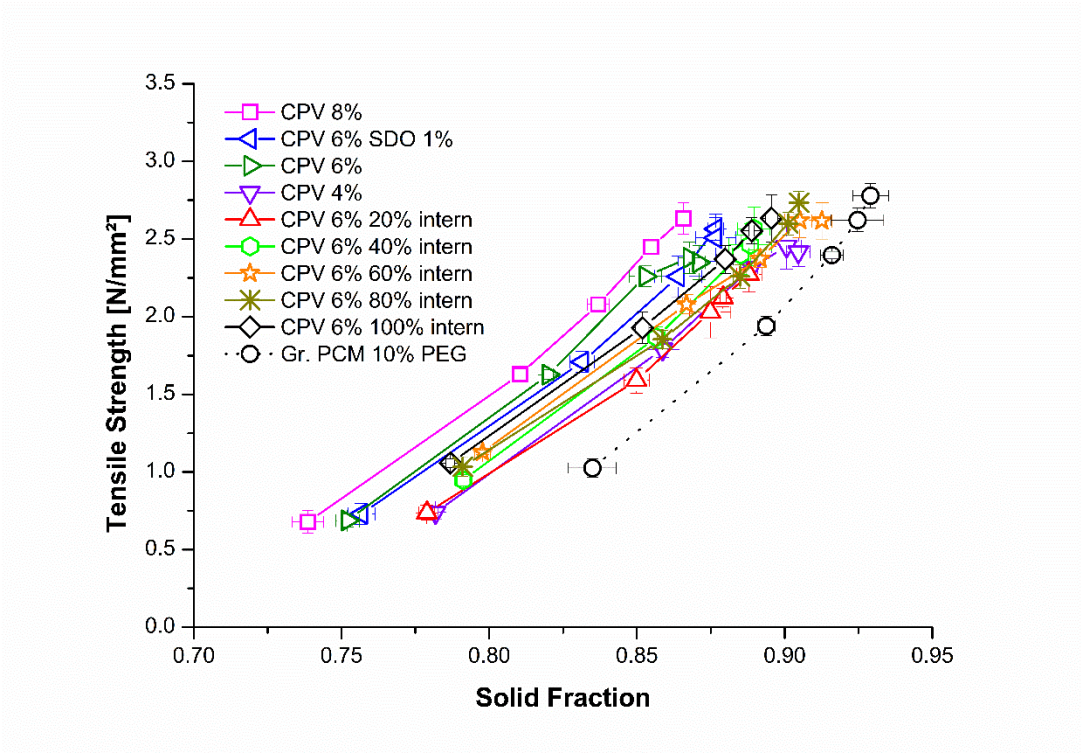

Fig. 7.3b: Compactibility plot of the crospovidone (CPV) formulations.

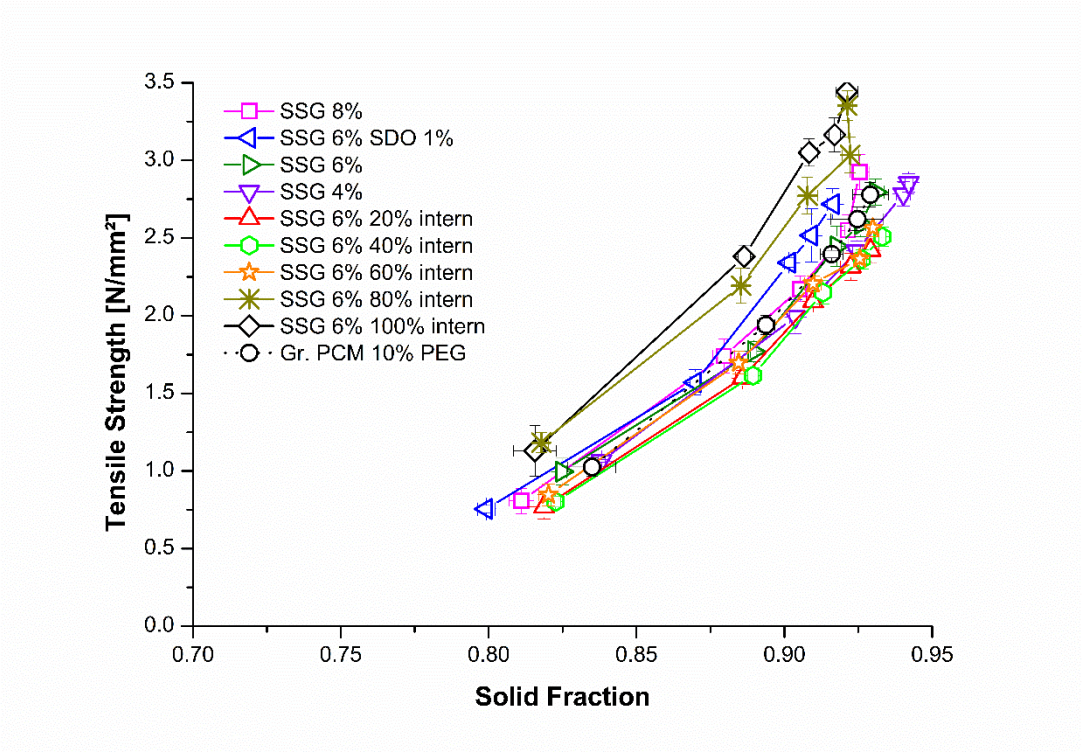

Fig. 7.3c: Compactibility plot of the sodium starch glycolate SSG formulations.

7.6.3.3 Compressibility

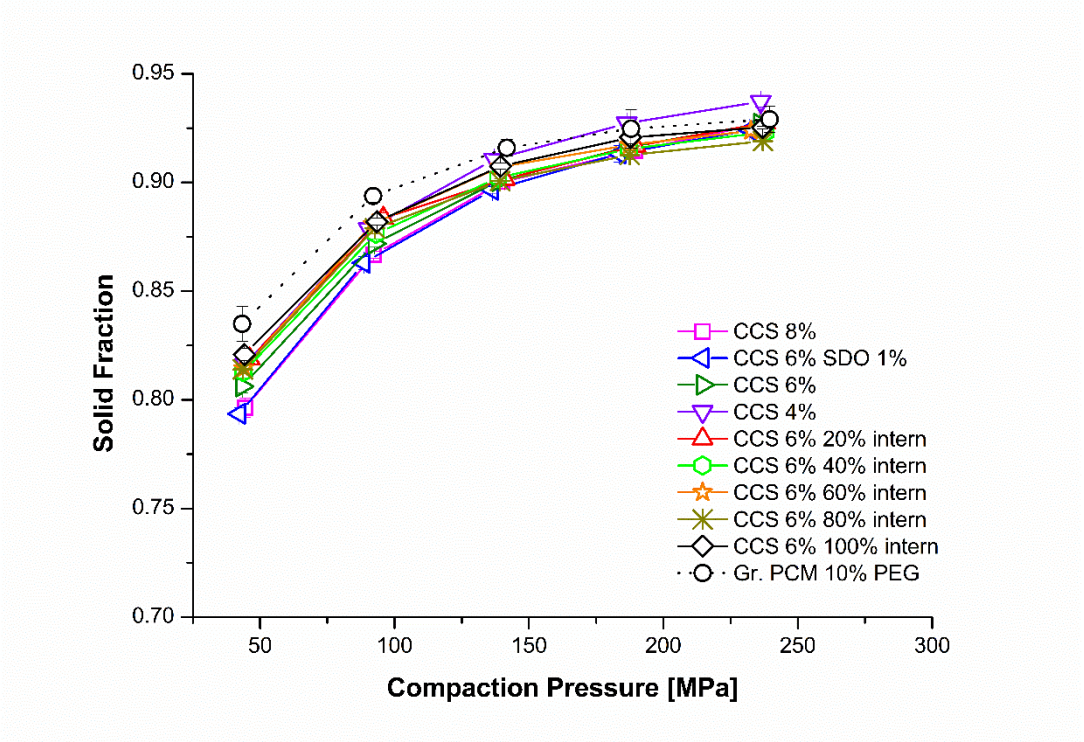

Fig. 7.4a: Compressibility plot of the croscarmellose sodium (CCS) formulations.

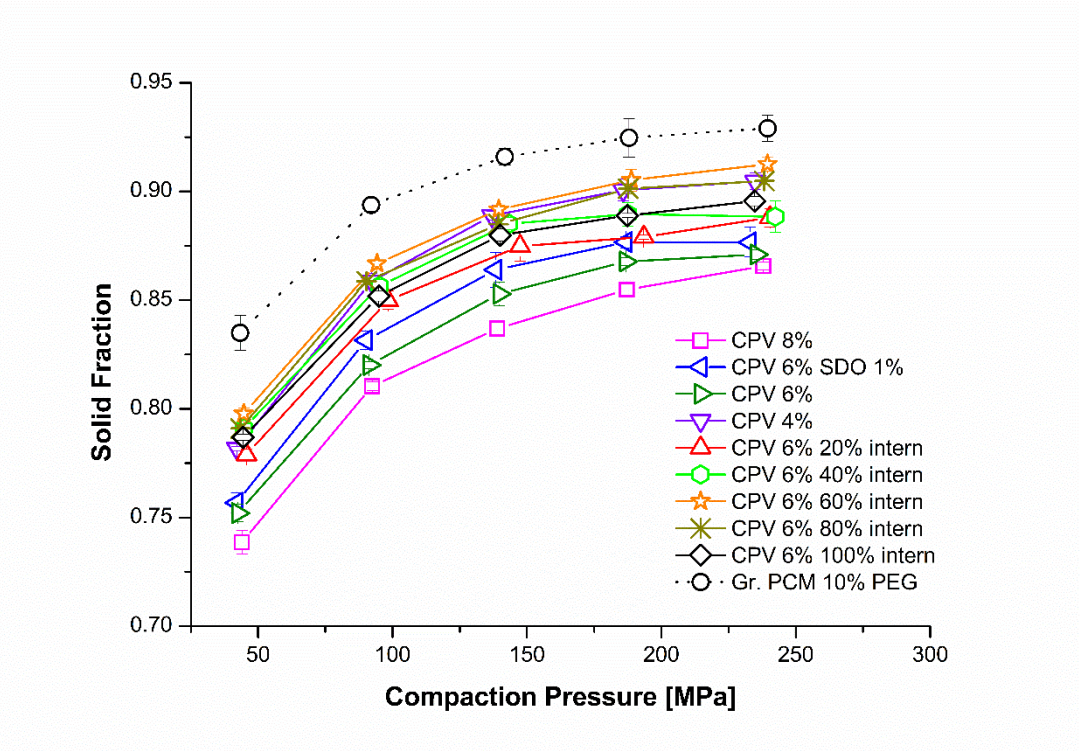

Fig. 7.4b: Compressibility plot of the crospovidone (CPV) formulations.

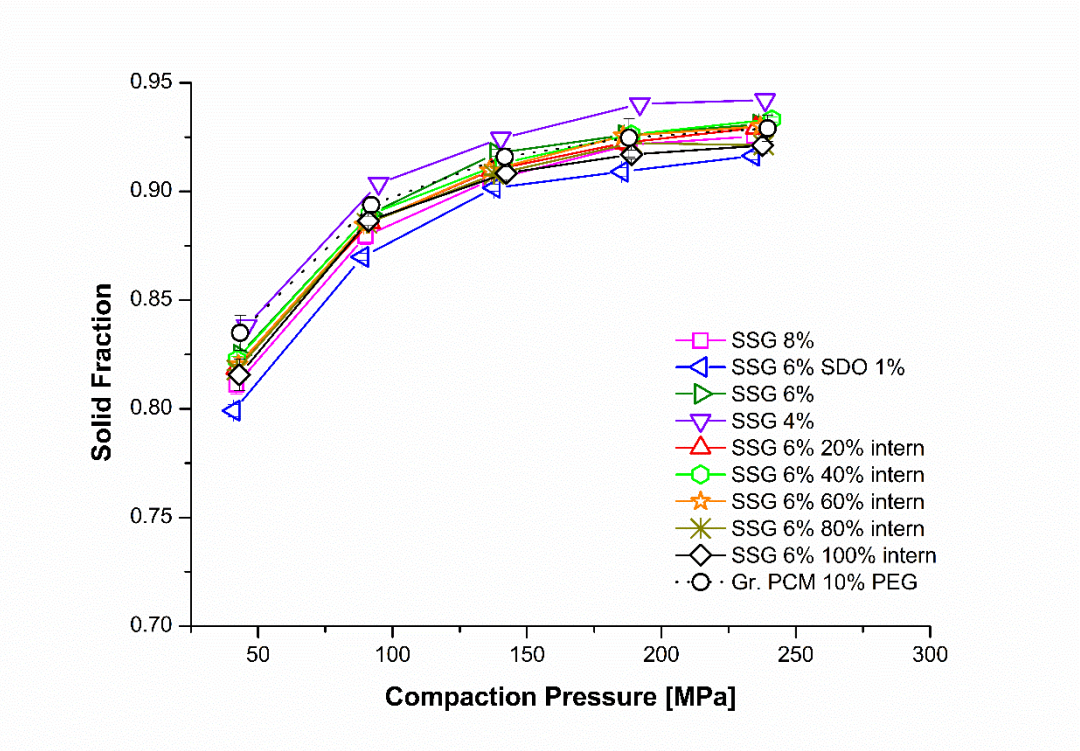

Fig. 7.4c: Compressibility plot of the sodium starch glycolate (SSG) formulations.

All CCS formulations showed a weight fraction-independent slightly lower SF than the Gr. PCM 10% PEG formulation (e.g. Gr. PCM 10% PEG: 0.92 ±0.01 at 150 MPa vs. CCS 8%: 0.90 ±0.01 at 150 MPa) (Fig. 7.4a). Fig. 7.4b depicts the compressibility plots of the CPV formulations. In comparison to CCS, a higher effect on the SF can be seen. Moreover, the effect of CPV was weight fraction-dependent (CPV 4% (0.89 ±0.01), CPV 6% (0.85 ±0.01), CPV 8% (0.84 ±0.01)). When adding CPV in high concentrations intra-granular, the effect was minor (CPV 6% 60% intern (0.91 ±0.01), CPV 6% 80% intern (0.90 ±0.01) and CPV 6% 100% intern (0.91 ±0.01)). In the case of the SSG formulations (Fig. 7.4c), the SFs were less affected by the disintegrant addition.

7.6.4 **Friability**

In general, friability studies confirmed the results obtained from the tabletability studies (Tab. 7.6). All tablets produced with CCS showed acceptable friability (<1%) without any trend. The highest friability was obtained at a weight fraction of CCS 4% (0.47%), whereas the lowest friability occurred at CCS 6% and 6% 20% intern (0.22%), indicating that CCS has no positive or negative effect on the abrasiveness of the tablets.

Concerning their friability, all tablets produced with CPV met the requirements of the Ph. Eur. No clear trend among the different weight fractions of CPV was observed, which verified the results obtained from the compression studies. The lowest friability was measured for the tablets containing 6% CPV and 1% SDO (0.13%) extra-granular, followed by the tablets with 6% intra-granular (0.16%), indicating no influence on tablets friability.

Overall, the friability of the tablets produced with SSG was slightly higher than the friability of the tablets produced from the granules without any disintegrant (Gr. PCM 10% PEG: 0.22%). In addition, an increasing friability as a function of SSG weight fraction was obvious (SSG 4%: 0.28% vs. SSG 8%: 0.43%). The SSG intra-granular addition decreased the effect again, towards that of the tablets without disintegrant (SSG 6% 100% intern: 0.26 % vs. Gr. PCM 10% PEG: 0.22%). However, the effect might be not relevant for commercial tablet production, since all tablets meet the requirements of the Ph. Eur., as they showed a friability less than 1% (w/w).

Tab. 7.6: Friability [%] of the formulations under investigation.

Formulation	Gr. PCM 10% PEG [%]		
	0.22		
	CCS [%]	**CPV [%]**	**SSG [%]**
4 %	0.47	0.27	0.28
6 %	0.22	0.26	0.35
8 %	0.31	0.29	0.43
6% +1% SDO	0.35	0.13	0.45
20 % intern	0.27	0.38	0.32
40 % intern	0.33	0.26	0.32
60 % intern	0.22	0.29	0.30
80 % intern	0.25	0.27	0.28
100 % intern	0.23	0.16	0.26

CCS: croscarmellose sodium, CPV: crospovidone, Mgst: magnesium stearate, PCM: paracetamol, PEG: polyethylene glycole, SDO: colloidal silicium dioxide, SSG: sodium starch glycolate

7.6.5 **Disintegration**

According to Ph. Eur. 2.9.1., uncoated tablets must disintegrate within 15 min, which is equal to a time of 900 s. Tablets produced without disintegrants disintegrated within 30 min (1775 ±327 s), indicating that these tablets did not meet the requirements for an immediate-release formulation. Using CCS as disintegrant, all formulations under investigation showed an acceptable disintegration time (Tab. 7.7). No clear trend can be seen between the different formulations using CCS. A clear trend can be seen for the CPV formulations. CPV reduced the disintegration time more effectively than CCS, especially when incorporated extra-granular prior tableting (CPV 8%: 78 ±7 s vs. CCS 8%: 390 ±93 s). The disintegration time decreased with increasing CPV content. However, the addition of CPV to the granulation phase resulted in increasing disintegration time.

The higher the integrated amount, the slower the disintegration process. Tablets using 100% CPV intra-granular (957 ±97 s) did not disintegrate within 15 min and did not meet the requirements of the Ph. Eur. 2.9.1.

Overall, formulations using SSG showed the longest disintegration times (SSG 8%: 513 ±38 s). SSG 6% 20% intern (319 ±50 s) exhibited lower disintegration time, than the other formulations. No clear trend could be observed concerning the disintegration efficiency, as it was seen for CPV (Tab. 7.7).

Tab. 7.7: Disintegration times [s] of the formulations under investigation.

Formulation	**Gr. PCM 10% PEG [s ±SD]**		
	1775 ±327		
	CCS [s ±SD]	**CPV [s ±SD]**	**SSG [s ±SD]**
4 %	435 ±69	211 ±27	598 ±37
6 %	360 ±88	129 ±29	492 ±67
8 %	390 ±93	78 ±7	513 ±38
6% +1% SDO	307 ±109	109 ±15	471 ±27
20 % intern	237 ±63	127 ±11	319 ±50
40 % intern	249 ±46	257 ±71	513 ±44
60 % intern	325 ±67	299 ±40	559 ±56
80 % intern	287 ±45	407 ±36	532 ±33
100 % intern	434 ±70	957 ±97	553 ±68

CCS: croscarmellose sodium, CPV: crospovidone, Mgst: magnesium stearate, PCM: paracetamol, PEG: polyethylene glycole, SDO: colloidal silicium dioxide, SSG: sodium starch glycolate

7.6.6 **Dissolution**

To meet the USP, a Q=80% release within 30 min for PCM tablets is needed [163], whereas the Ph. Eur. 5.17.1 requires a dissolution of 45 min for “conventional release” dosage forms [161].

Tablets without any disintegrant exhibited a slow dissolution, which followed a zero-order kinetic in the first hours (Fig. 7.5). A release of 80% was obtained after approx. 220 min, which does not meet the requirements of the USP and Ph. Eur. for a conventional release formulation or for PCM tablets.

Fig. 7.5a, 7.5b and 7.5c present the obtained dissolution curves of the formulations under investigation. Fig. 7.6 and Tab. 7.8 show the $Q_{80\%}$ interval [min]. Regarding the CCS formulations, dissolution increased only slightly as a function of disintegrant content (Fig. 7.5a).

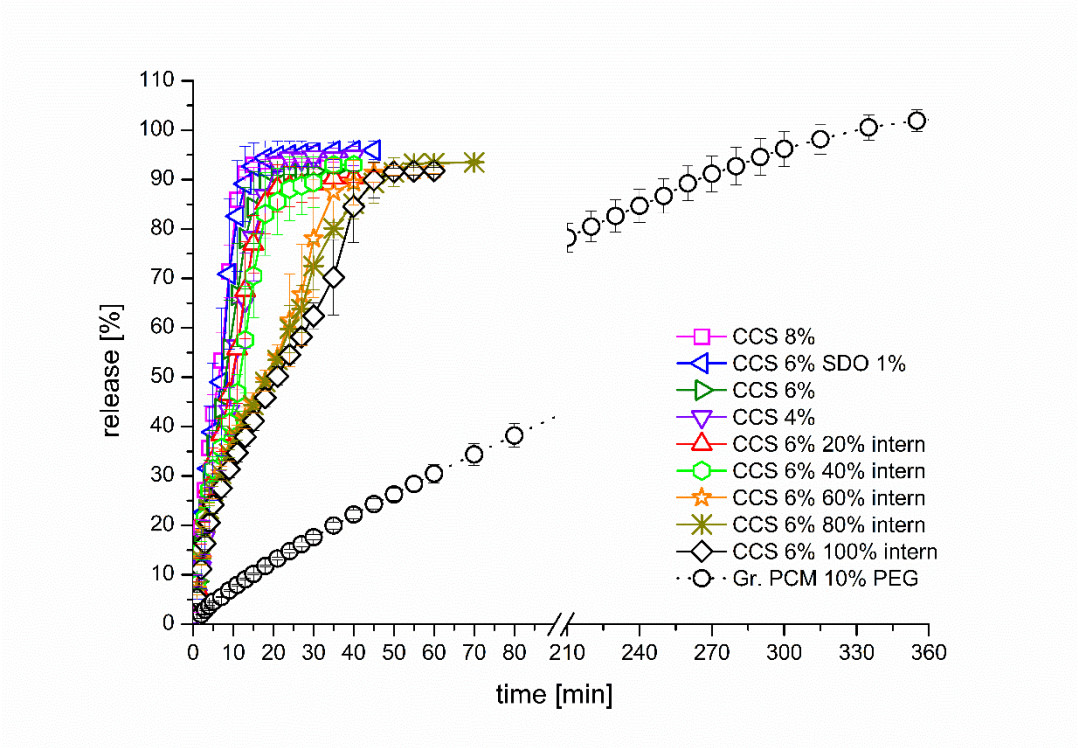

Fig. 7.5a: Dissolution of the croscarmellose sodium (CCS) formulations.

In the case of the incorporation of CCS intra-granular, a significant delay was observed when more than the half of the content of disintegrant was integrated. The $Q_{80\%}$ occurred later than 30 min, which is the required value for the USP. However, no significant difference can be seen between CCS 6% 60% intern ($Q_{80\%=}$ 32.3 ±5.5 min), CCS 6% 80% intern ($Q_{80\%=}$ 36.7 ±2.6 min) and CCS 6% 100% intern ($Q_{80\%=}$ 40.0 ±3.2 min).

In the case of CPV, the fastest release was obtained, when 8% CPV ($Q_{80\%=}$ 4.2 ±0.4 min) was integrated extra-granular (Fig. 7.5b). Also 4% CPV ($Q_{80\%=}$ 7.0 ±1.3 min) and 6% CPV ($Q_{80\%=}$ 5.2 ±1.0 min) extra-granular resulted in a very fast release, indicating the high potential of the disintegrant to enhance dissolution of the tablets. Using CPV intra-granular, delayed release, especially when more than 20% where integrated. However, tablets with 20% ($Q_{80\%=}$ 5.5 ±2.1 min), 40% ($Q_{80\%=}$ 14.5 ±6.3 min) and 60% ($Q_{80\%=}$ 16.5 ±1.6 min) of the 6% CPV intra-granular still met the requirements of the USP and tablets achieved more than 80% drug release within the first 30 min.

When 100% of CPV were granulated, CPV lost a remarkable proportion of its disintegration efficiency. Tablets of CPV 6% 100% intern achieved 80% release within more than 90 min ($Q_{80\%=}$ 101 ±9.8 min).

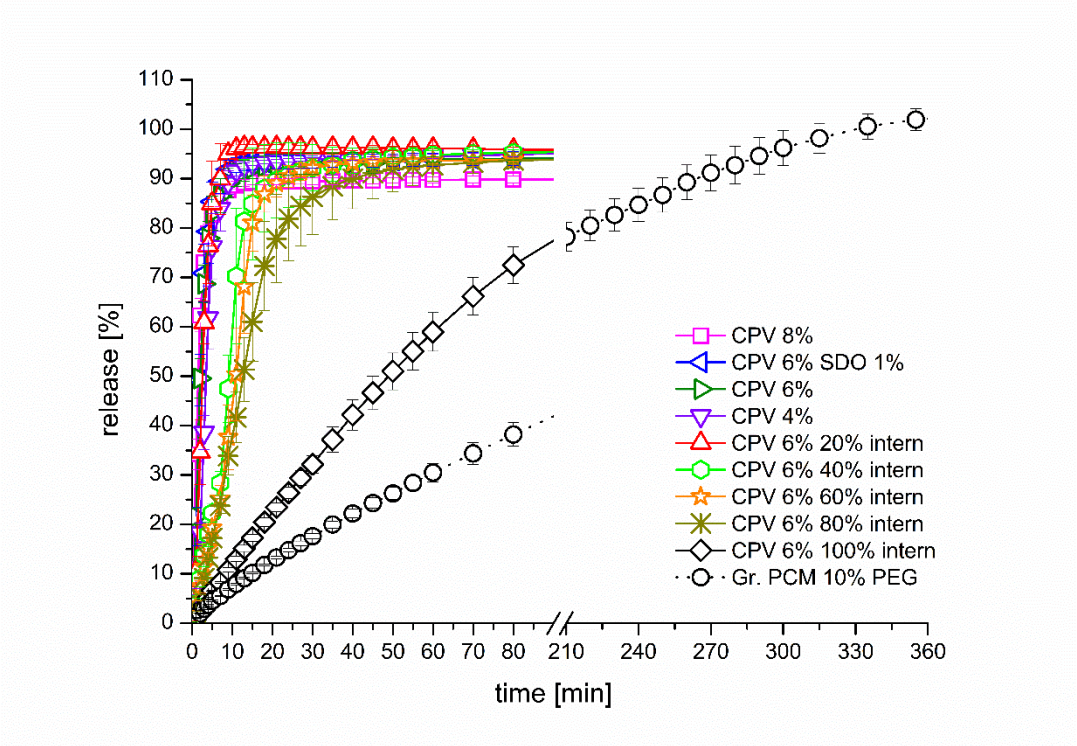

Fig. 7.5b: Dissolution of the crospovidone (CPV) formulations.

Using SSG resulted in the slowest dissolution profile when the 4% extern formulations of the three disintegrants are considered (Fig. 7.5c). The formulation SSG 4% extern ($Q_{80\%=}$ 32.8 ±6.5 min) did not meet the requirements of the USP. However, in the case of 6% ($Q_{80\%=}$ 17.7 ±3.7 min) results were comparable to those of CCS, but not as effective as CPV. Interestingly, the incorporation intra-granular of SSG does not result in any loss of the disintegrant efficiency, as it was seen for CCS and CPV.

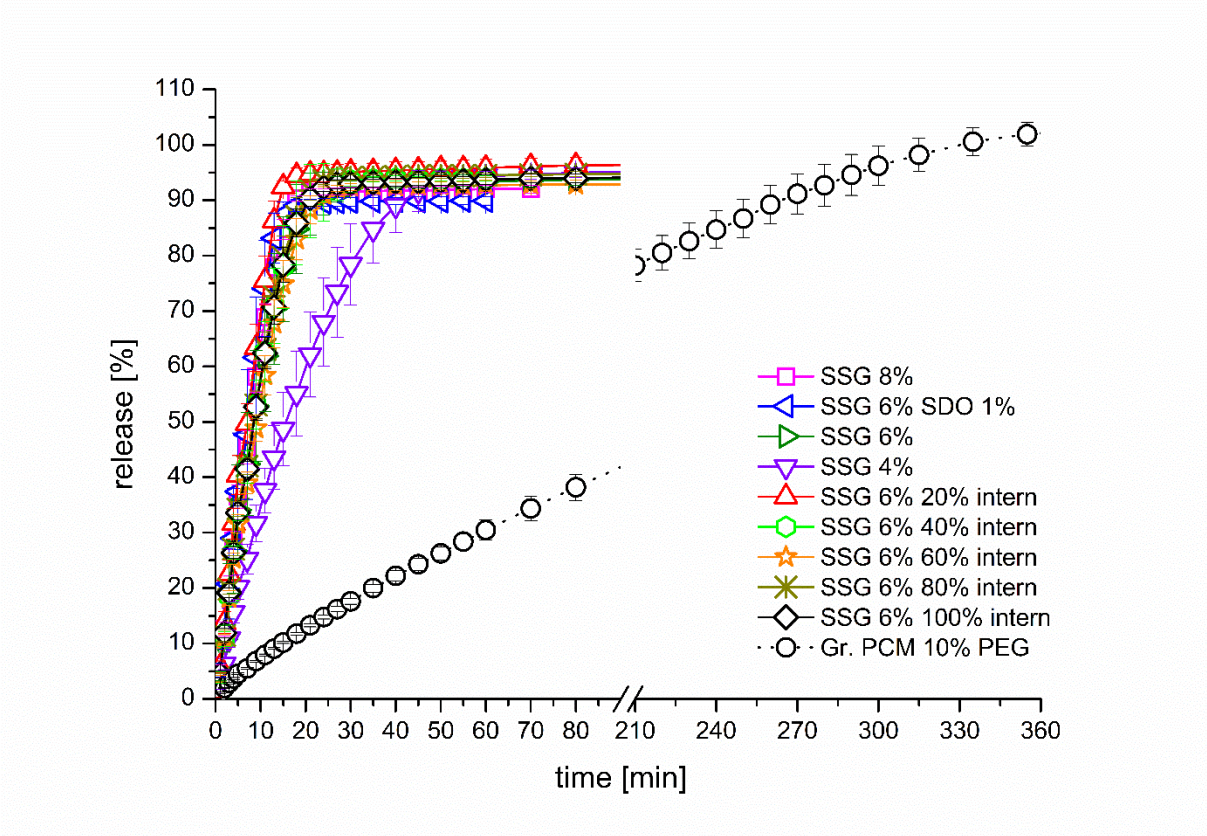

Fig. 7.5c: Dissolution of the sodium starch glycolate (SSG) formulations.

Using 4% extra-granular, CPV ($Q_{80\%=}$ 7.0 ±1.3 min) performed more effective than CCS ($Q_{80\%=}$ 17.0 ±2.4 min) and CCS was more effective than SSG ($Q_{80\%=}$ 32.8 ±6.5 min). Using 6% extra-granular, CCS and SSG performed similar ($Q_{80\%=}$ 15.2 ±3.7 min and 17.7 ±3.7 min), whereas the 8% extra-granular CCS ($Q_{80\%=}$ 11.0 ±0.0 min) was more efficient than the respective SSG formulation ($Q_{80\%=}$ 14.7 ±0.8 min). In both cases (6% and 8% extra-granular) CPV was superior, showing very short time to achieve 80% release of only 5.2 ±1.0 min and 4.2 ± 0.4 min. Using 1% SDO as additional wicking agent had only a minor effect on the release rate and did not significantly impact the dissolution, when compared to the 6% disintegrant extra-granular.

In the case of adding 20% of the 6% disintegrant intra-granular, $Q_{80\%}$ did not change compared to the 100% extra-granular formulation using CCS and CPV. For SSG, the 6% 20% intern formulation performed marginally faster than the SSG 6% formulation ($Q_{80\%=}$ 12.7 ±0.8 vs. 17.7 ±3.7). Similar relations were already seen in the disintegration results (Tab. 7.7). In the case of 40% intern formulations, the $Q_{80\%}$ increased for CPV ($Q_{80\%=}$ 14.5 ± 6.3 min), but for CCS and SSG, the data were similar to those of the 6% formulation containing the disintegrant extra-granular. Using CCS, $Q_{80\%}$ increased above the critical value of 30 min, using more than 60% intra-granular. In the case of CPV, using more than 80% intra-granular resulted in tablets that did not meet this requirement of the USP. Using 100% intra-granular resulted in tablets that achieved 80% release within more than 90 min, indicating noteworthy loss of the disintegration efficiency. SSG showed no remarkable loss of its disintegration efficiency when integrated into the granulation process.

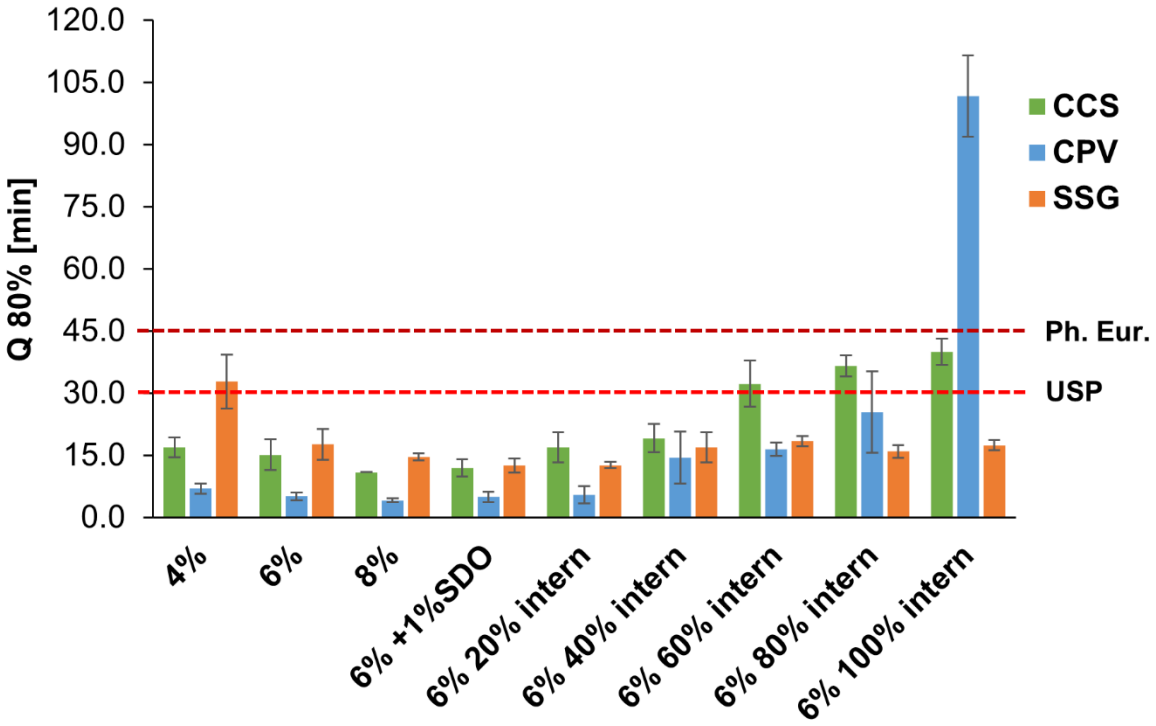

Fig. 7.6: $Q_{80\%}$ of the formulations under investigation.

Tab. 7.7: $Q_{80\%}$ for the formulations under investigation.

Formulation	$Q_{80\%}$ Gr. PCM 10% PEG [min ±SD]		
	223.3 ±12.1		
	$Q_{80\%}$ CCS [min ±SD]	$Q_{80\%}$ CPV [min ±SD]	$Q_{80\%}$ SSG [min ±SD]
4 %	17.0 ±2.4	7.0 ±1.3	32.8 ±6.5
6 %	15.2 ±3.7	5.2 ±1.0	17.7 ±3.7
8 %	11.0 ±0.0	4.2 ±0.4	14.7 ±0.8
6% +1% SDO	12.0 ±2.1	5.0 ±1.2	12.6 ±1.7
20 % intern	17.0 ±3.6	5.5 ±2.1	12.7 ±0.8
40 % intern	19.2 ±3.4	14.5 ±6.3	17.0 ±3.6
60 % intern	32.3 ±5.5	16.5 ±1.6	18.5 ±1.2
80 % intern	36.7 ±2.6	25.5 ±9.8	16.0 ±1.5
100 % intern	40.0 ±3.2	101.7 ±9.8	17.5 ±1.2

7.7 Discussion:

Results show that the disintegration and the dissolution of the tablets was less dependent on the disintegrants concentration but, rather on the location of the disintegrant (extra- or intra-granular).

In general, the extra-granular disintegrant addition resulted in the fastest dissolution of the model compound PCM. Looking at the formulations with disintegrant extra-granular, the rank order of performance was: CPV faster than CCS faster than SSG. Furthermore, the concentration needed of SSG was higher than that of CCS and CPV to meet the requirements of the USP.

Except for the SSG formulation, no difference between the 4% and 6% extra-granular formulations was seen. However, 8% CPV and CCS extern was more effective than using 4% CPV and CCS, but the effect might be irrelevant for the patient's therapy.

In literature, the three superdisintegrants are often compared [164–169] and variations between different test methods (e.g. pH of the test medium) or different vendors (e.g. extent of crosslinking or the degree of substitution) might explain the unclear order of their effectiveness at similar weight fractions [155,170,171]. Also the influence of particle-size of different disintegrants has been shown by several working groups [166,172–174]. In this study disintegrants with comparable particle-size were used.

The results obtained in this study might be explained by the different mechanisms of action of the disintegrants. Proposed mechanisms of disintegration are wicking, swelling, shape recovery and particle repulsion, which lead to a disruption of the physicochemical bonds in the tablets [53,175,176]. Synergistic combination of the proposed mechanisms are possible [152]. After contact with water, wettability and the penetration of water into the tablet are the first steps that need to be fulfilled, before the tablet disintegrates into smaller particles. Wicking is the proposed mechanism for microcrystalline cellulose (MCC), which describes the capillary action of the material and its potential to pull water into the tablet. Presumably wicking supports swelling and shape recovery by absorbing more water into the tablet, but does not active generate pressure to destroy particle bonds [177], similar effects might be achieved using low proportions of SDO. However, using even 1% of SDO did not show any significant effects on the formulations in this study.

CCS and SSG are known to act via swelling, which leads to a multidirectional volume expansion of the compact. However, the water uptake and swelling capacity of SSG is higher compared to CCS, whereas CPV shows only a low swelling capacity [170,178]. The authors described an enormous volume expansion of SSG. Recently it was proposed that CPV mainly acts via shape-recovery, which is a reversible viscoelastic process of deformation, which is activated after contact with water [179]. The proposed mechanism was confirmed by high resolution real-time magnetic resonance imaging [180] and simple image analysis using a digital camera [181]. In contrast to swelling, shape recovery results in a more unidirectional volume expansion of the tablet, in the opposite direction of compression, while releasing the energy, which is stored in the compact. The disintegrant particles are regaining their original shape, when they come into contact with water. This mechanism also explains that its dissolution efficiency increased with compaction force [182].

The predominant mechanism described for CCS is wicking and swelling [169,183]. Disintegrants that act primary via wicking and swelling (CCS and SSG), show high capillary action and swelling. Moreover their disintegration time decreased, with increasing compaction pressure [179]. Recently a change from predominant swelling mechanism to shape recovery was proposed for CCS depending on its concentration [181]. This behaviour was explained with the formation of a hydrated gel matrix, maintaining tablets integrity at high concentrations. Concentration dependent decrease of disintegration time was also described from other authors [152,184,185]. However, for the melt granulation process, we did not see any decrease in disintegration using higher disintegrant concentrations.

This might be attributed to the very low porosity of the tablets made from the TSMG in contrast to the study of Berardi et al. 2018 and Ferrero et al. 1997 and where tablets were made by direct compression. With the low porosity achieved via TSMG any volume expansion went into bond weakening and subsequent disintegration rather than gel formation, which would also explain the reached plateau in terms of disintegration and dissolution rather than an optimum.

In this study CCS and CPV showed a concentration dependent decrease, when integrated intra-granular. The effect was more pronounced for CPV. Tablets using 100% CPV intra-granular did not disintegrate within 15 min, whereas tablets using 100% CCS still meet the requirements of the Ph.Eur. However, looking at the dissolution profiles, tablets with more than 40% of CCS intra-granular did not meet the requirements of the USP. This concentration dependent behaviour was not seen for the formulation produced with SSG.

The effect of extra- and intra-granular addition of disintegrant is diversely discussed in literature, mainly depending on the formulation characteristics, rather than on the disintegrant itself. Some authors found improved efficiency of the disintegrant when added into the intra-granular phase, whereas others found contrary results [156–159,186,187]. Johnson et al. studied the effect of tablet formulation solubility and hygroscopicity on dissolution efficiency. The decrease in disintegration efficiency occurred in wet-granulated formulations containing highly soluble and or hygroscopic excipients [188]. Similar results were shown by Gordon et al., who showed that hygroscopic ingredients can decrease the effectiveness of superdisintegrants [189]. Both authors explained the decrease with a competitive inhibition of the disintegrant

by the other tablet components competing for the locally available water. The different behaviour of the disintegrant when in-cooperated in the granulation step might be again explainable with their different disintegration mechanism.

If the disintegrant is coated with a film of hydrophobic or slowly dissolving substance, disintegration might be negatively affected. This effect is well described for MGST, which can slow down disintegration or the dissolution rate, due to a hydrophobic surface coating. This effect was shown to be less pronounced for disintegrants that undergo intensive swelling like SSG [190,191].

The omnipresent PEG in the tablet after the granulation process results in a viscous gel when coming into contact with water. This effect might explain a loss in dissolution efficiency of CPV and CCS.

The loss of disintegration efficiency, e.g. during wet-granulation process, was already described [164,192], including the effect of recompression on disintegrant efficiency in tablets prepared by wet granulation [164]. Very similar results were obtained for the disintegrants under investigation. Gould et al. 1985 showed that, all disintegrants placed intra-granular showed a loss of disintegration efficiency. Explotab® (SSG) retained good efficiency after rework. CPV act very sufficient when added before the second compression step into the extra-granular phase. The loss of the disintegration efficiency was explained by the authors with the different structure of the disintegrants. CPV shows a sponge-like matrix (popcorn structure), whereas CCS consist of “spaghetti-like” fibrous being broken down by the first compaction process.

Similar effects might explain the loss in disintegration and prolonged dissolution of the compacts in this study, as the TSMG process applies high shear energy to the product, the use of kneading elements might result in a destruction of the disintegrants structure, resulting in a loss of their efficiency. The theory is supported by the results obtained from the compressibility studies. The formulations containing CPV in the extra-phase showed a lower SF (higher porosity) compared to the formulations containing CPV in the intra-granular phase. This might be explained by a change of the structure of CPV during granulation, negatively affecting its elastic recovery during tableting process and consequently the disintegration and the dissolution performance of the formulation.

Interestingly the lower SF of the formulation with CPV did not influence the TS of the tablets in a large extent. This can be explained with high plasticity of the melt granules [193], maintaining the bonding capacity of the formulation.
In contrast to CPV, the majority of the SSG particles might be unaffected by the granulation process, therefore most of the enormous swelling capacity is maintained after the granulation process. Moreover a positive effect on the TS of the formulations containing high concentrations of SSG intra-granular was observed. The higher TS did not negatively influence the dissolution performance of the tablets.
However, it was postulated that the heat exposure during the melt granulation process, might result in an unwanted loss of disintegration efficiency, especially when using starch-based disintegrants. A pregelatinization might occur, negatively affecting the disintegration performance [194]. In contrast to native starches, the used SSG was not influenced by the melt granulation process (T_{max}: 95°C and absence of water) and maintained its disintegration capacity.

7.8 Conclusion

The current study showed that, especially extra-granular addition of superdisintegrant revealed fast disintegrating tablets with subsequently short $Q_{80\%}$. At the same time the benefits of tablets from TSMG like excellent tensile strength and friability could be remained even in combination with a high drug load (> 80% (w/w)). The rank order in efficiency for extra-granular addition was CPV > CCS > SSG. For SSG higher concentrations of (>6 % (w/w)) were needed, whereas already 4% (w/w) achieved acceptable results for CPV and CCS. Intra-granular addition showed mainly negative effects on the disintegration performance. This effect was very pronounced, when CPV was added into the granulation process and to a lesser extent for CCS. In contrast, SSGs disintegration efficiency was unaffected by the granulation process. The results are of fundamental importance, when using TSMG in a continuous processing line and additional mixing steps after granulation should be avoided.

7.9 Acknowledgments

The authors thank Romaco Kilian and Medelpharm for providing the Styl'One classic single-punch compression simulator.

7.10 List of Symbols and Abbrevations

API	active pharmaceutical ingredient	
BCS	biopharmaceutical classification system	
CCS	croscarmellose sodium	
CPV	crospovidone	
L/D	length/diameter	
MCC	microcrystalline cellulose	
MGST	magnesium stearate	
PCM	paracetamol	
PEG	polyethylene glycole	
Ph. Eur.	European Pharmacopoeia	
PM	physical mixture	
SDO	colloidal silicium dioxide	
SEM	scanning electron microscope	
SF	solid fraction	
SSG	sodium starch glycolate	
TS	tensile strength	[N/mm²]
TSMG	twin-screw melt granulation	
USP	United States Pharmacopeia	

8 Summary and outlook

This work investigated melt granulation to enhance tabletability, compactibility and compressibility of poorly compactable and especially brittle materials with drug loads up to 95% (w/w). The direct comparison of granules and their respective physical mixtures demonstrated that the improved behavior of the granules was mainly attributed to a more homogenous distribution of the binder in the tablets. A new method was established to quantify the binder distribution by means of image analysis of energy-dispersive X-ray maps. This method might be also applicable for the characterization of APIs in tablets or other dosage forms, if an X-ray sensitive element is present in the formulation. The quantitative analysis procedure might be further applicable to other imaging-based methods like Raman-mapping, too.

The influence of filler particle size used for melt granulation was systematically evaluated (chapter 3 and chapter 4). Dependent on the particle size, different granulation mechanisms were observed. While fine-grade fillers agglomerated via an immersion mechanism, the distribution mechanism was found for coarse particles. In the case of fine-grade fillers, produced granules showed superior tabletability, whereas coarse particles maintained larger quantity of their material properties after granulation. In the case a very small particle size was used, the addition of more binding material, to achieve a similar effect on tabletability, was required. Moreover, colloidal silicon dioxide was needed as adjuvant to enable feeding of the fine mixture into the extruder. These results might be transferable to blends, where a fine API grade is added. In contrast, coarse grade of API/filler are preferable, if a “melt coating” is required e.g. if taste masking is in focus, rather than enhanced tabletability.

Compressibility studies revealed an increase in plastic deformation due to granulation (chapter 4). This enhancement was described via the plasticity performance factor. This factor is a relative value of Heckel’s yield pressure. It describes the YP in relation to the YP of the neat filler material and was calculated for the physical mixtures and melt granules. The compression analyses showed that the melt granulation strongly increased plastic deformation of the melt granulated material compared to simple binary mixtures, even when the binder content was low (5-15 % w/w). A correlation

between the enhancement in plasticity and the primary filler particle size used in the melt granulation process, was found. Additionally, the plasticity performance factor was similar among all physical mixtures (independent of the fillers particle size) and thus, it might be a new approach for the description of binary mixtures.
Consequently, the initial particle size of the material to be agglomerated and the required level of melt binder should be closely regarded in formulation and process development, as these substantially impact the product performance.
Nevertheless, the impact of shear stress (screw speed and screw configuration), mean-residence time (e.g. throughput), melt viscosity of the binder, which also includes granulation temperature, and material attributes of the filler (e.g. brittle or plastic deformation behavior) needs to be further investigated. These parameters likely influence the granules critical quality attributes. Moreover, the influence of different particle size fractions of the granules at similar binder contents needs to be investigated, as it might affect hardness and solid fraction of the tablet. Additionally, due to a different pore size distribution in the tablet, disintegration and dissolution might be influenced by using different granules size as intermediate product during tablet production.

Regarding different granulation techniques, the two prominent high-shear melt granulation processing methods, namely high-shear granulation (HSG) and twin-screw melt granulation (TSG), were compared (Chapter 5). The influence of granulation throughput and screw speed were investigated by using the model formulation DI-CAFOS A12 and Kolliphor P407 15% (w/w). Granules produced via TSG achieved a narrower particle size distribution (PSD) and a higher yield than the HSG granules. Overall, the extrusion granulation was found to be more robust and variation of the extrusion parameters (throughput and screw speed) had only a minor impact on the PSD and yield. The HSG granules were less porous and more spherical in shape, which explained the slightly better flowability and higher density of these granules. However, the tablets made of the TSG granules achieved a higher compactibility, which was traced back to a more homogenous binder distribution and a higher available binder content on the tablet surface structure (detected by energy dispersive X-ray analysis). Overall, as a results of process adjustments, similar granule quality can be achieved either by HSG or by TSG.

However, when changing from batch (HSG) to a continuous process (TSG), a slightly different tablet quality (e.g. solid fraction, tensile strength, disintegration, dissolution) is likely, which is mainly attributed to a different shape, PSD, porosity and binder distribution in the granules. This change in granules properties requires a fine-tuning of the production process but it might not hinder the change in production mode (batch to continuous).

To enhance wettability and dissolution of a poorly soluble model API (carbamazepine), melt granulation proved its capability by employing functional polymers as melt binder (chapter 6). This technique enables significant drug loads up to 90% (w/w), if the polymer serves as both, a binder and dissolution enhancer. In contrast to the often desired ASD (amorphous solid dispersion), the high API content in this case leads to drug particles, which remained in their crystalline state. This study showed that with the choice of the binder and its concentration, dissolution performance of the granules is controllable. Therefore, binder and its concentration should be selected according to the required dissolution profile.
To enhance the dissolution of a poorly soluble APIs, several functional polymers, like polyvinylpyrrolidone or hydroxypropylcellulose, could be tested for their potential.

A decrease of the obtained granules particle size as a function of increased granulation temperature was also observed (chapter 6). This aspect should be further investigated, as it might be a function of binder's viscosity. This is especially interesting for continuous production, if additional milling steps should be avoided. However, results also indicated that temperature related degradation or polymorphic transitions due to drug-polymer interaction might occur, which can limit the process application. Stability studies, also for long-term storage of the products are therefore of fundamental importance. Additionally, due to the solvent-free nature of the process, the potential to protect hygroscopic drugs from moisture absorption, resulting in an improved shelf life, might be tested.

When a superdisintegrant is added, dissolution studies revealed that the melt granulation process is suitable to produce immediate-release dosage forms (chapter 7). Extra-granular incorporation of the superdisintegrants croscarmellose sodium (CCS), crospovidone (CPV) and sodium starch glycolate (SSG) (> 6% (w/w)) resulted in a fast disintegration of the tablet, consisting of the highly soluble model drug paracetamol. Intra-granular addition had negative effects on the disintegration performance. This effect was major, when CPV was used. In contrast, SSGs disintegration efficiency was unaffected by the granulation process. These results are of fundamental importance, when using TSMG in a continuous processing line, if additional mixing steps after granulation should be avoided.
Disintegration efficiency strongly depends on the formulation (soluble or insoluble compounds). Therefore, this study should be repeated with poorly soluble APIs and different functional polymers to investigate, if the performance of the disintegrants after granulation is also transferable to other formulations.
Dissolution studies without disintegrant addition indicated the applicability of melt granulation for producing controlled release profiles. This is especially of great importance when a high-drug load formulation is required. Due to the very homogenous distribution of the binder/ polymer used, the incorporation of a very high-drug load and a controlled-release profile at the same time might be feasible.

Overall melt granulation was identified as valuable and versatile granulation strategy, with the potential to run on a continuous processing line. The process offers a high flexibility, due to the large set of polymers that can be applied as melt binder. This flexibility offers a great scope of dissolution profiles than can be achieved, while producing formulations with a very high drug load. However, this large set of available binders demonstrates also the need for further research in melt granulation as alternative granulation strategy. In the future scale-up and transfer to a continuous processing line will be of fundamental importance to prove, if this versatile and advantageous process can be implemented in pharmaceutical production.

9 Publications

Parts of this work are already published as:

Articles:

Steffens, Kristina E., and Karl G. Wagner. "Improvement of tabletability via twin-screw melt granulation: Focus on binder distribution." International journal of pharmaceutics 570 (2019): 118649.
DOI:10.1016/j.ijpharm.2019.118649

Steffens, Kristina E., and Karl G. Wagner. "Compression behaviour of granules produced via twin-screw melt granulation: Effect of initial particle size on granulation efficiency." *Powder Technology* 374 (2020): 430-442.
DOI: 10.1016/j.powtec.2020.07.037

Steffens, Kristina E., et al. "Melt granulation: A comparison of granules produced via high-shear mixing and twin-screw granulation." *International Journal of Pharmaceutics* 591 (2020): 119941.
DOI: 10.1016/j.ijpharm.2020.119941.

Steffens, Kristina E., and Karl G. Wagner. "Dissolution enhancement of carbamazepine using twin-screw melt granulation." *European Journal of Pharmaceutics and Biopharmaceutics* 148 (2020): 77-87.
DOI: 10.1016/j.ejpb.2020.01.006

Steffens, Kristina E., and Karl G. Wagner. “Immediate-Release Formulations Produced via Twin-Screw Melt Granulation: Systematic Evaluation of the Addition of Disintegrants.” *AAPS PharmSciTech* 22, 183 (2021).
DOI: 10.1208/s12249-021-02056-0

Abstracts (Conference participation):

Steffens, Kristina E., and Karl G. Wagner. “Improvement of the tabletability of brittle material via twin-screw melt extrusion.” 11th PBP World Meeting, Granada, Spain, March 2018 (poster presentation)

Steffens, Kristina E., and Karl G. Wagner. “Enhancement of tabletability via twin-screw melt granulation: Focus on Binder distribution.” 9th Granulation Conference, Lausanne, Switzerland, June 2019 (oral presentation)

10 References

[1] K.A. Mehta, G.S. Rekhi, D.M. Parikh, Handbook of Pharmaceutical Granulation Technology, CRC Press, 2005. doi:10.1201/9780849354953.ch17.

[2] J.P. Lakshman, J. Kowalski, M. Vasanthavada, W.Q. Tong, Y.M. Joshi, A.T.M. Serajuddin, Application of melt granulation technology to enhance tabletting properties of poorly compactible high-dose drugs, J. Pharm. Sci. 100 (2011) 1553–1565. doi:10.1002/jps.22369.

[3] A. Royce, J. Suryawanshi, U. Shah, K. Vishnupad, Alternative granulation technique: Melt granulation, Drug Dev. Ind. Pharm. 22 (1996) 917–924. doi:10.3109/03639049609065921.

[4] M. Vasanthavada, Y. Wang, T. Haefele, J.P. Lakshman, M. Mone, W. Tong, Y.M. Joshi, A.T.M. Serajuddin, Application of Melt Granulation Technology Using Twin-screw Extruder in Development of High-dose Modified-Release Tablet Formulation, J. Pharm. Sci. 100 (2011) 1923–1934. doi:10.1002/JPS.22411.

[5] T. Schaefer, P. Holm, H.G. Kristensen, Melt granulation in a laboratory scale high shear mixer, Drug Dev. Ind. Pharm. 16 (1990) 1249–1277. doi:10.3109/03639049009115960.

[6] N. Passerini, B. Albertini, M.L. González-Rodríguez, C. Cavallari, L. Rodriguez, Preparation and characterisation of ibuprofen-poloxamer 188 granules obtained by melt granulation, Eur. J. Pharm. Sci. 15 (2002) 71–78. doi:10.1016/S0928-0987(01)00210-X.

[7] D. Yang, R. Kulkarni, R.J. Behme, P.N. Kotiyan, Effect of the melt granulation technique on the dissolution characteristics of griseofulvin, Int. J. Pharm. 329 (2007) 72–80. doi:10.1016/j.ijpharm.2006.08.029.

[8] L. Rodriguez, C. Cavallari, N. Passerini, B. Albertini, M.L. González-Rodríguez, A. Fini, Preparation and characterization by morphological analysis of diclofenac/PEG 4000 granules obtained using three different techniques, Int. J. Pharm. 242 (2002) 285–289. doi:10.1016/s0378-5173(02)00189-8.

[9] B. Perissutti, F. Rubessa, M. Moneghini, D. Voinovich, Formulation design of carbamazepine fast-release tablets prepared by melt granulation technique, Int. J. Pharm. 256 (2003) 53–63. doi:10.1016/S0378-5173(03)00062-0.

[10] P. Flanders, G.A. Dyer, D. Jordan, The Control of Drug Release from Conventional Melt Granulation Matrices, Drug Dev. Ind. Pharm. 9045 (1987)

1001–1022. doi:10.3109/03639048709068366.

[11] L. Ochoa, M. Igartua, R. Hernández, A.R. Gascón, J.L. Pedraz, Preparation of sustained release hydrophilic matrices by melt granulation in a high-shear mixer ., J. Pharm. Pharm. Sci. 8 (2005) 132–140.

[12] D. Voinovich, M. Moneghini, B. Perissutti, E. Franceschinis, Melt pelletization in high shear mixer using a hydrophobic melt binder : influence of some apparatus and process variables, Eur. J. Pharm. Biopharm. 52 (2001) 305–313. doi:10.1016/s0939-6411(01)00196-5.

[13] D. Voinovich, M. Moneghini, B. Perissutti, J. Filipovic-Grcic, I. Grabnar, Preparation in high-shear mixer of sustained-release pellets by melt pelletisation, Int. J. Pharm. 203 (2000) 235–244. doi:10.1016/s0378-5173(00)00455-5.

[14] Y. Zhang, J.B. Schwartz, Melt Granulation and Heat Treatment for Wax Matrix-Controlled Drug Release, Drug Dev. Ind. Pharm. 29 (2003) 131–138. doi:10.1081/ddc-120016720.

[15] C. Mangwandi, M.J. Adams, M.J. Hounslow, A.D. Salman, Effect of batch size on mechanical properties of granules in high shear granulation, Powder Technol. 206 (2011) 44–52. doi:10.1016/j.powtec.2010.05.025.

[16] T. Schaefer, C. Mathiesen, Melt pelletization in a high shear mixer. IX. Effects of binder particle size, Int. J. Pharm. 139 (1996) 139–148. doi:10.1016/0378-5173(96)04548-6.

[17] R. Thies, P. Kleinebudde, Melt pelletisation of a hygroscopic drug in a high shear mixer Part 1 . Influence of process variables, Int. J. Pharm. 188 (1999) 131–143. doi:10.1016/S0378-5173(99)00214-8.

[18] T. Schæfer, B. Taagegaard, L.J. Thomsen, H. Gjelstrup Kristensen, Melt pelletization in a high shear mixer. V. Effects of apparatus variables, Eur. J. Pharm. Sci. 1 (1993) 133–141. doi:10.1016/0928-0987(93)90003-S.

[19] E.I. Keleb, A. Vermeire, C. Vervaet, J.P. Remon, Continuous twin screw extrusion for the wet granulation of lactose, Int. J. Pharm. 239 (2002) 69–80. doi:10.1016/S0378-5173(02)00052-2.

[20] S.B. Tiwari, T.K. Murthy, M. Raveendra Pai, P.R. Mehta, P.B. Chowdary, Controlled release formulation of tramadol hydrochloride using hydrophilic and hydrophobic matrix system, AAPS PharmSciTech. 4 (2003) 18–23. doi:10.1208/pt040331.

[21] B. Mu, M.R. Thompson, Examining the mechanics of granulation with a hot melt binder in a twin-screw extruder, Chem. Eng. Sci. 81 (2012) 46–56. doi:10.1016/j.ces.2012.06.057.

[22] M.J. Gamlen, C. Eardley, Continuous Extrusion Using a Raker Perkins MP50 (Multipurpose) Extruder, Drug Dev. Ind. Pharm. 12 (1986) 1701–1713. doi:10.3109/03639048609042604.

[23] B. Van Melkebeke, B. Vermeulen, C. Vervaet, J.P. Remon, Melt granulation using a twin-screw extruder: A case study, Int. J. Pharm. 326 (2006) 89–93. doi:10.1016/j.ijpharm.2006.07.005.

[24] S. Weatherley, B. Mu, M.R. Thompson, P.J. Sheskey, K.P. O'Donnell, Hot-melt granulation in a twin screw extruder: Effects of processing on formulations with caffeine and ibuprofen, J. Pharm. Sci. 102 (2013) 4330–4336. doi:10.1002/jps.23739.

[25] H. Leuenberger, New trends in the production of pharmaceutical granules : the classical batch concept and the problem of scale-up, Eur. J. Pharm. Biopharm. 52 (2001) 279–288. doi:10.1016/S0939-6411(01)00200-4.

[26] D.E. Zecevic, R.C. Evans, K. Paulsen, K.G. Wagner, From benchtop to pilot scale – experimental study and computational assessment of a hot-melt extrusion scale-up of a solid dispersion of dipyridamole and copovidone, Int. J. Pharm. 537 (2018) 132–139. doi:10.1016/j.ijpharm.2017.12.033.

[27] J. Van Renterghem, S. Van De Steene, T. Digkas, M. Richter, Assessment of volumetric scale-up law for processing of a sustained release formulation on co-rotating hot-melt extruders Assessment of volumetric scale-up law for processing of a sustained release formulation on co-rotating hot-melt extruders, Int. J. Pharm. 569 (2019) 118587. doi:10.1016/j.ijpharm.2019.118587.

[28] C. Vervaet, J.P. Remon, Continuous granulation in the pharmaceutical industry, Chem. Eng. Sci. 60 (2005) 3949–3957. doi:10.1016/j.ces.2005.02.028.

[29] E.I. Keleb, A. Vermeire, C. Vervaet, J.P. Remon, Twin screw granulation as a simple and efficient tool for continuous wet granulation, Int. J. Pharm. 273 (2004) 183–194. doi:10.1016/j.ijpharm.2004.01.001.

[30] M.R. Thompson, J. Sun, Wet Granulation in a Twin-Screw Extruder : Implications of Screw Design, J. Pharm. Sci. 99 (2010) 2090–2103. doi:10.1002/jps.

[31] D. Djuric, B. Van Melkebeke, P. Kleinebudde, J.P. Remon, C. Vervaet,

Comparison of two twin-screw extruders for continuous granulation, Eur. J. Pharm. Biopharm. 71 (2009) 155–160. doi:10.1016/j.ejpb.2008.06.033.

[32] R. Meier, K.P. Moll, M. Krumme, P. Kleinebudde, Impact of fill-level in twin-screw granulation on critical quality attributes of granules and tablets, Eur. J. Pharm. Biopharm. 115 (2017) 102–112. doi:10.1016/j.ejpb.2017.02.010.

[33] R. Meier, M. Thommes, N. Rasenack, K.P. Moll, M. Krumme, P. Kleinebudde, Granule size distributions after twin-screw granulation – Do not forget the feeding systems, Eur. J. Pharm. Biopharm. 106 (2016) 59–69. doi:10.1016/j.ejpb.2016.05.011.

[34] A.S. El Hagrasy, J.R. Hennenkamp, M.D. Burke, J.J. Cartwright, J.D. Litster, Twin screw wet granulation: Influence of formulation parameters on granule properties and growth behavior, Powder Technol. 238 (2013) 108–115. doi:10.1016/j.powtec.2012.04.035.

[35] B. Van Melkebeke, C. Vervaet, J.P. Remon, Validation of a continuous granulation process using a twin-screw extruder, Int. J. Pharm. 356 (2008) 224–230. doi:10.1016/j.ijpharm.2008.01.012.

[36] A. Batra, D. Desai, A.T.M. Serajuddin, Investigating the Use of Polymeric Binders in Twin Screw Melt Granulation Process for Improving Compactibility of Drugs, J. Pharm. Sci. 106 (2017) 140–150. doi:10.1016/j.xphs.2016.07.014.

[37] W. Grymonpré, G. Verstraete, V. Vanhoorne, J.P. Remon, T. De Beer, C. Vervaet, Downstream processing from melt granulation towards tablets: In-depth analysis of a continuous twin-screw melt granulation process using polymeric binders, Eur. J. Pharm. Biopharm. 124 (2018) 43–54. doi:10.1016/j.ejpb.2017.12.005.

[38] E.S. Bochmann, E.E. Üstüner, A. Gryczke, K.G. Wagner, Predicting melt rheology for hot-melt extrusion by means of a simple Tg-measurement, Eur. J. Pharm. Biopharm. 119 (2017) 47–55. doi:10.1016/j.ejpb.2017.05.010.

[39] J.M. Keen, C.J. Foley, J.R. Hughey, R.C. Bennett, V. Jannin, Y. Rosiaux, D. Marchaud, J.W. McGinity, Continuous twin screw melt granulation of glyceryl behenate: Development of controlled release tramadol hydrochloride tablets for improved safety, Int. J. Pharm. 487 (2015) 72–80. doi:10.1016/j.ijpharm.2015.03.058.

[40] M. Jivraj, L.G. Martini, C.M. Thomson, An overview of the different excipients

useful for the direct compression of tablets, Pharm. Sci. Technol. Today. 3 (2000) 58–63. doi:10.1016/S1461-5347(99)00237-0.

[41] S. Patel, A.M. Kaushal, A.K. Bansal, Compression Physics in the Formulation Development of Tablets, Crit. Rev. Ther. Drug Carr. Syst. 23 (2006) 1–65. doi:10.1615/critrevtherdrugcarriersyst.v23.i1.10.

[42] C. Nyström, G. Alderborn, M. Duberg, P.G. Karehill, Bonding Surface area and Bonding Mechanism- Two Important Factors fir the Understanding of Powder Comparability, Drug Dev. Ind. Pharm. 19 (1993) 2143–2196. doi:10.3109/03639049309047189.

[43] R.W. Heckel, Density-Pressure Relationships in Powder Compaction, Trans. Metall. Soc. AIME. 221 (1961) 671–675.

[44] M. Krumme, L. Schwabe, K. Fro, Development of computerised procedures for the characterisation of the tableting properties with eccentric machines : extended Heckel analysis q, i (2000) 275–286.

[45] R.J. Roberts, R.C. Rowe, Brittle/ductile behaviour in pharmaceutical materials used in tabletting, Int. J. Pharm. 36 (1987) 205–209. doi:10.1016/0378-5173(87)90157-8.

[46] L.W. Wong, N. Pilpel, The effect of particle shape on the mechanical properties of powders, Int. J. Pharm. 59 (1990) 145–154. doi:10.1016/0378-5173(90)90089-M.

[47] P. York, Particle slippage and rearrangement during compression of pharmaceutical powders, J. Pharm. Pharm. Sci. 30 (1978) 6–10.

[48] K. Kawakita, K.-H. Lüdde, Some Considerations on Powder Compression Equations, Powder Technol. 4 (1971) 61–68. doi:10.1016/0032-5910(71)80001-3.

[49] F. Nicklasson, G. Alderborn, Analysis of the Compression Mechanics of Pharmaceutical Agglomerates of Different Porosity and Composition Using the Adams and Kawakita Equations, Pharm. Res. 17 (2000) 949–954. doi:10.1023/A:1007575120817.

[50] P.J. Denny, Compaction equations: A comparison of the Heckel and Kawakita equations, Powder Technol. 127 (2002) 162–172. doi:10.1016/S0032-5910(02)00111-0.

[51] L. V Allen, N.G. Popovich, H.C. Ansel, Ansel’s Pharmaceutical Dosage Forms

and Drug Delivery Systems, 9th ed., Wolters Kluw; Lippincott Williams & Wilkins, 2011.

[52] J. Swarbrick, N. Carolina, L.L. Augsburger, H.G. Brittain, A.J. Hickey, C. Hill, N. Carolina, Generic Drug Product Development, (2005).

[53] D. Markl, J.A. Zeitler, A Review of Disintegration Mechanisms and Measurement Techniques, Pharm. Res. 34 (2017) 890–917. doi:10.1007/s11095-017-2129-z.

[54] A. Kumar Gupta, M. Dalal, A. Kumar, D. Mishra, S. Kumar Singh, True MDTs : Mouth disintegrating tablets or mouth dissolving tablets , a comparative study, Pharma Res. J. 6 (2011) 1–11.

[55] M. Kidokoro, Y. Haramiishi, S. Sagasaki, T. Shimizu, Y. Yamamoto, Application of Fluidized Hot-Melt Granulation (FHMG) for the Preparation of Granules for Tableting ; Properties of Granules and Tablets Prepared by FHMG, Drug Dev. Ind. Pharm. 28 (2002) 67–76. doi:10.1081/DDC-120001487.

[56] G.L. Amidon, H. Lennernäs, V.P. Shah, J.R. Crison, A Theoretical Basis for a Biopharmaceutic Drug Classification, Pharm. Res. 12 (1995) 413–420. doi:10.1023/A:1016212804288.

[57] INTERNATIONAL COUNCIL FOR HARMONISATION OF TECHNICAL REQUIREMENTS FOR PHARMACEUTICALS FOR HUMAN USE, (2018).

[58] T. Schæfer, Growth mechanisms in melt agglomeration in high shear mixers, Powder Technol. 117 (2001) 68–82. doi:10.1016/S0032-5910(01)00315-1.

[59] J. Kowalski, O. Kalb, Y.M. Joshi, A.T.M. Serajuddin, Application of melt granulation technology to enhance stability of a moisture sensitive immediate-release drug product, Int. J. Pharm. 381 (2009) 56–61. doi:10.1016/j.ijpharm.2009.05.043.

[60] T. Monteyne, J. Vancoillie, J.P. Remon, C. Vervaet, T. De Beer, Continuous melt granulation: Influence of process and formulation parameters upon granule and tablet properties, Eur. J. Pharm. Biopharm. 107 (2016) 249–262. doi:10.1016/j.ejpb.2016.07.021.

[61] P.C. Schmidt, R. Herzog, Calcium phosphates in pharmaceutical tableting, Pharm. World Sci. 15 (1993) 116–122. doi:10.1007/BF02113939.

[62] M. Schöller, A. Emrich, S. John, Two types of Dicalcium phosphate anhydrous for controlling the size of tablets, (2010) Poster.

[63] BASF, Kolliphor ® P Grades, Tech. Doc. (2013) 1–8.

[64] J.T. Fell, J.M. Newton, Determination of tablet strength by the diametral compression test, J. Pharm. Sci. 59 (1970) 688–691. doi:10.1002/jps.2600590523.

[65] H. Egermann, P. Frank, Novel Approach to Estimate Quality of Binary Random Powder Mixtures : Samples of Constant Volume . I : Derivation of Equation, J. Pharm. Sci. 81 (1992) 551–555. doi:10.1002/jps.2600810617.

[66] H. Leuenberger, B.D. Rohera, C. Haas, Percolation theory - a novel approach to solid dosage form design, Int. J. Pharm. 38 (1987) 109–115. doi:10.1016/0378-5173(87)90105-0.

[67] Chemische Fabrik Budenheim KG, Pharma Portfolio for Solid dosage forms, Tech. Doc. (2017).

[68] M.G. Herting, P. Kleinebudde, Roll compaction/dry granulation: Effect of raw material particle size on granule and tablet properties, Int. J. Pharm. 338 (2007) 110–118. doi:10.1016/j.ijpharm.2007.01.035.

[69] M. Eriksson; G. Alderborn, The effect of particle fragmentation and deformation on the interparticulate bond formation process during powder compaction, Pharm. Res. 12 (1995) 1031–1039. doi:10.1023/a:1016214616042.

[70] C. Nyström, J. Mazur, J. Sjögren, Studies on direct compression of tablets II. The influence of the particle size of a dry binder on the mechanical strength of tablets, Int. J. Pharm. 10 (1982) 209–218. doi:10.1016/0378-5173(82)90071-0.

[71] I. Caraballo, M. Millan, A.M. Rabasco, Relationship between drug percolation threshold and particle size in matrix tablets, Pharm. Res. 13 (1996) 387–390. doi:10.1023/A:1016088424993.

[72] F.A.A. Mohamed, M. Roberts, L. Seton, J.L. Ford, M. Levina, A.R. Rajabi-Siahboomi, The effect of HPMC particle size on the drug release rate and the percolation threshold in extended-release mini-tablets, Drug Dev. Ind. Pharm. 41 (2015) 70–78. doi:10.3109/03639045.2013.845843.

[73] D. Blattner, M. Kolb, H. Leuenberger, Percolation Theory and Compactibility of Binary Powder Systems, Pharm. Res. 7 (1990) 113–117. doi:10.1023/A:1015864415693.

[74] M. Millan, I. Caraballo, A.M. Rabasco, The Role of the Drug/Excipient Particle Size Ratio in the Percolation Model for Tablets, Pharm. Res. 15 (1998) 216–220. doi:10.1023/A:1011906416291.

[75] M. Wikberg, G. Alderborn, Compression Characteristics of Granulated Materials. VII. The Effect of Intragranular Binder Distribution on the Compactibility of Some Lactose Granulations, Pharm. Res. An Off. J. Am. Assoc. Pharm. Sci. 10 (1993) 88–94. doi:10.1023/A:1018929214629.

[76] T. Vilhelmsen, H. Eliasen, T. Schæfer, Effect of a melt agglomeration process on agglomerates containing solid dispersions, Int. J. Pharm. 303 (2005) 132–142. doi:10.1016/j.ijpharm.2005.07.012.

[77] F. Liu, R. Lizio, U.J. Schneider, H.U. Petereit, P. Blakey, A.W. Basit, SEM/EDX and confocal microscopy analysis of novel and conventional enteric-coated systems, Int. J. Pharm. 369 (2009) 72–78. doi:10.1016/j.ijpharm.2008.10.035.

[78] N. Scoutaris, K. Vithani, I. Slipper, B. Chowdhry, D. Douroumis, SEM/EDX and confocal Raman microscopy as complementary tools for the characterization of pharmaceutical tablets, Int. J. Pharm. 470 (2014) 88–98. doi:10.1016/j.ijpharm.2014.05.007.

[79] P. Katewongsa, K. Terada, T. Phaechamud, Spatial distributing lubricants from Raman mapping and scanning electron microscopy–energy dispersive X-ray spectroscopy on cetirizine dihydrochloride fast disintegrating tablet properties, J. Pharm. Investig. 47 (2017) 249–262. doi:10.1007/s40005-016-0283-7.

[80] K.E. Steffens, K.G. Wagner, Dissolution Enhancement of Carbamazepine using Twin-screw Melt Granulation, Eur. J. Pharm. Biopharm. 148 (2020) 77–87. doi:10.1016/j.ejpb.2020.01.006.

[81] K.E. Steffens, K.G. Wagner, Improvement of tabletability via twin-screw melt granulation : Focus on binder distribution, Int. J. Pharm. 570 (2019). doi:10.1016/j.ijpharm.2019.118649.

[82] P. Paronen, Heckel plots as indicators of elastic properties of pharmaceuticals, Drug Dev. Ind. Pharm. 12 (1986) 1903–1912. doi:10.3109/03639048609042616.

[83] G. Alderborn, P.O. Lang, A. Sageström, A. Kristensen, Compression characteristics of granulated materials . I . Fragmentation propensity and compactibility of some granulations of a high dosage drug, Int. J. Pharm. 37 (1987) 155–161. doi:https://doi.org/10.1016/0378-5173(87)90020-2.

[84] M. Šantl, I. Ilić, F. Vrečer, S. Baumgartner, A compressibility and compactibility study of real tableting mixtures: The impact of wet and dry granulation versus a direct tableting mixture, Int. J. Pharm. 414 (2011) 131–139.

doi:10.1016/j.ijpharm.2011.05.025.

[85] H. Murakami, T. Yoneyama, K. Nakajima, M. Kobayashi, Correlation between loose density and compactibility of granules prepared by various granulation methods, Int. J. Pharm. 216 (2001) 159–164. doi:10.1016/s0378-5173(01)00575-0.

[86] M.G. Herting, P. Kleinebudde, Studies on the reduction of tensile strength of tablets after roll compaction / dry granulation, Eur. J. Pharm. Sci. 70 (2008) 372–379. doi:10.1016/j.ejpb.2008.04.003.

[87] F. Freitag, J. Runge, P. Kleinebudde, Coprocessing of Powdered Cellulose and Magnesium Carbonate : Direct Tableting Versus Tableting After Roll Compaction /Dry Granulation, Pharm. Dev. Technol. 10 (2005) 353–362. doi:10.1081/PDT-65667.

[88] A.L.L. Soares, G.G. Ortega, P.R. Petrovick, P.C. Schmidt, Dry Granulation and Compression of Spray-Dried Plant Extracts, AAPS PharmSciTech. 6 (2005) 359–366. doi:10.1208/pt060345.

[89] A.-S. Persson, J. Nordström, G. Frenning, G. Alderborn, Compression analysis for assessment of pellet plasticity: identification of reactant pores and comparison between Heckel, Kawakita, and Adams equations, Chem. Eng. Res. Des. 110 (2016) 183–191. doi:10.1016/j.cherd.2016.01.028.

[90] S. Paul, C.C. Sun, The suitability of common compressibility equations for characterizing plasticity of diverse powders, Int. J. Pharm. 532 (2017) 124–130. doi:10.1016/j.ijpharm.2017.08.096.

[91] R. Schmidtke, D. Schröder, J. Menth, A. Staab, M. Braun, K.G. Wagner, Prediction of solid fraction from powder mixtures based on single component compression analysis, Int. J. Pharm. 523 (2017) 366–375. doi:10.1016/j.ijpharm.2017.03.054.

[92] I. Ilić, B. Govedarica, R. Sibanc, R. Dreu, S. Srčič, Deformation properties of pharmaceutical excipients determined using an in-die and out-die method ˇ, Int. J. Pharm. 446 (2013) 6–15. doi:10.1016/j.ijpharm.2013.02.001.

[93] J.A. Hersey, J.E. Rees, Deformation of Particles during Briquetting, Nat. Phys. Sci. 230 (1971) 96.

[94] P. York, Crystal engineering and particle design for the powder compaction process, Drug Dev. Ind. Pharm. 18 (1992) 677–721.

doi:10.3109/03639049209058558.

[95] G. Frenning, J. Nordström, G. Alderborn, Effective Kawakita parameters for binary mixtures, Powder Technol. 189 (2009) 270–275. doi:10.1016/j.powtec.2008.04.016.

[96] H. Olsson, S. Mattsson, C. Nyström, Evaluation of the effect of addition of polyethylene glycols of differing molecular weights on the mechanical strength of sodium chloride and sodium bicarbonate tablets, Int. J. Pharm. 171 (1998) 31–44. doi:10.1016/S0378-5173(98)00164-1.

[97] S. Mattsson, C. Nyström, Evaluation of strength-enhancing factors of a ductile binder in direct compression of sodium bicarbonate and calcium carbonate powders, Eur. J. Pharm. Sci. 10 (2000) 53–66. doi:10.1016/S0928-0987(99)00088-3.

[98] S. Mattsson, C. Nyström, Evaluation of Critical Binder Properties Affecting the Compactibility of Binary Mixtures, Drug Dev. Ind. Pharm. 27 (2001) 181–194. doi:10.1081/DDC-100000236.

[99] B. Van Veen, K. Van Der Voort Maarschalk, G.K. Bolhuis, K. Zuurman, H.W. Frijlink, Tensile strength of tablets containing two materials with a different compaction behaviour, Int. J. Pharm. 203 (2000) 71–79. doi:10.1016/S0378-5173(00)00450-6.

[100] J. Ilkka, P. Paronen, Prediction of the compression behaviour of powder mixtures by the Heckel equation, Int. J. Pharm. 94 (1993) 181–187. doi:10.1016/0378-5173(93)90022-8.

[101] M. Grassi, D. Voinovich, M. Moneghini, E. Franceschinis, B. Perissutti, J. Filipovic-Grcic, Preparation and evaluation of a melt pelletised paracetamol/stearic acid sustained release delivery system, J. Control. Release. 88 (2003) 381–391. doi:10.1016/S0168-3659(03)00011-7.

[102] L. Ochoa, M. Igartua, R.M. Hernández, M.Á. Solinís, A.R. Gascón, J.L. Pedraz, In vivo evaluation of two new sustained release formulations elaborated by one-step melt granulation: Level A in vitro-in vivo correlation, Eur. J. Pharm. Biopharm. 75 (2010) 232–237. doi:10.1016/j.ejpb.2010.02.008.

[103] J. Hamdani, A.J. Moës, K. Amighi, Development and evaluation of prolonged release pellets obtained by the melt pelletization process, Int. J. Pharm. 245 (2002) 167–177. doi:10.1016/S0378-5173(02)00348-4.

[104] N. Passerini, G. Calogerà, B. Albertini, L. Rodriguez, Melt granulation of pharmaceutical powders: A comparison of high-shear mixer and fluidised bed processes, Int. J. Pharm. 391 (2010) 177–186. doi:10.1016/j.ijpharm.2010.03.013.

[105] N. Kittikunakorn, J.J. Koleng, T. Listro, C.C. Sun, F. Zhang, Effects of thermal binders on chemical stabilities and tabletability of gabapentin granules prepared by twin-screw melt granulation, Int. J. Pharm. 559 (2019) 37–47. doi:10.1016/j.ijpharm.2019.01.014.

[106] N. Kittikunakorn, C.C. Sun, F. Zhang, Effect of screw profile and processing conditions on physical transformation and chemical degradation of gabapentin during twin-screw melt granulation, Eur. J. Pharm. Sci. 131 (2019) 243–253. doi:10.1016/J.EJPS.2019.02.024.

[107] Y. Miyazaki, V. Lenhart, P. Kleinebudde, Switch of tablet manufacturing from high shear granulation to twin-screw granulation using quality by design approach, Int. J. Pharm. 579 (2020) 119139. doi:10.1016/j.ijpharm.2020.119139.

[108] E.I. Keleb, A. Vermeire, C. Vervaet, J.P. Remon, Extrusion granulation and high shear granulation of different grades of lactose and highly dosed drugs: A comparative study, Drug Dev. Ind. Pharm. 30 (2004) 679–691. doi:10.1081/DDC-120039338.

[109] K.T. Lee, A. Ingram, N.A. Rowson, Comparison of granule properties produced using Twin Screw Extruder and High Shear Mixer: A step towards understanding the mechanism of twin screw wet granulation, Powder Technol. 238 (2013) 91–98. doi:10.1016/j.powtec.2012.05.031.

[110] P. Beer, D. Wilson, Z. Huang, M.D.E. Matas, Transfer from High-Shear Batch to Continuous Twin Screw Wet Granulation : A Case Study in Understanding the Relationship, (2014) 3075–3082. doi:10.1002/jps.24078.

[111] T. Schæfer, Melt pelletization in a high shear mixer. X. Agglomeration of binary mixtures, Int. J. Pharm. 139 (1996) 149–159. doi:10.1016/0378-5173(96)04615-7.

[112] T. Schæfer, D. Johnsen, A. Johansen, Effects of powder particle size and binder viscosity on intergranular and intragranular particle size heterogeneity during high shear granulation, Eur. J. Pharm. Sci. 21 (2004) 525–531.

doi:10.1016/j.ejps.2003.12.002.

[113] B. Campisi, D. Vojnovic, D. Chicco, R. Phan-Tan-Luu, Melt granulation in a high shear mixer: Optimization of mixture and process variables using a combined experimental design, Chemom. Intell. Lab. Syst. 48 (1999) 59–70. doi:10.1016/S0169-7439(99)00008-8.

[114] D. Voinovich, B. Campisi, M. Moneghini, C. Vincenzi, R. Phan-Tan-Luu, Screening of high shear mixer melt granulation process variables using an asymmetrical factorial design, Int. J. Pharm. 190 (1999) 73–81. doi:10.1016/s0378-5173(99)00278-1.

[115] C.A. Lipinski, F. Lombardo, B.W. Dominy, P.J. Feeney, Experimental and computational approaches to estimate solubility and permeability in drug discovery and development settings, Adv. Drug Deliv. Rev. 64 (2012) 4–17. doi:10.1016/j.addr.2012.09.019.

[116] D.T. Friesen, R. Shanker, M. Crew, D.T. Smithey, W.J. Curatolo, J.A.S. Nightingale, Hydroxypropyl Methylcellulose Acetate Succinate-Based Spray-Dried Dispersions: An Overview, Mol. Pharm. 5 (2008) 1003–1019. doi:10.1021/mp8000793.

[117] B. Perissutti, J.M. Newton, F. Podczeck, F. Rubessa, Preparation of extruded carbamazepine and PEG 4000 as a potential rapid release dosage form, Eur. J. Pharm. Biopharm. 53 (2002) 125–132. doi:10.1016/S0939-6411(01)00209-0.

[118] L.G. Jensen, F.B. Skautrup, A. Müllertz, B. Abrahamsson, T. Rades, A. Priemel, Petra, Amorphous is not always better—A dissolution study on solid state forms of carbamazepine, Int. J. Pharm. 522 (2017) 74–79. doi:10.1016/j.ijpharm.2017.02.062.

[119] Y. Kobayashi, S. Ito, S. Itai, K. Yamamoto, Physicochemical properties and bioavailability of carbamazepine polymorphs and dihydrate, Int. J. Pharm. 193 (2000) 137–146. doi:10.1016/S0378-5173(99)00315-4.

[120] K. Ueda, K. Higashi, K. Yamamoto, K. Moribe, The effect of HPMCAS functional groups on drug crystallization from the supersaturated state and dissolution improvement, Int. J. Pharm. 464 (2014) 205–213. doi:10.1016/j.ijpharm.2014.01.005.

[121] A.D. Gift, P.E. Luner, L. Luedeman, L.S. Taylor, Influence of Polymeric Excipients on Crystal Hydrate Formation Kinetics in Aqueous Slurries, J. Pharm.

Sci. 97 (2008) 5198–5211. doi:10.1002/jps.

[122] F. Tian, D.J. Saville, K.C. Gordon, C.J. Strachan, J.A. Zeitler, N. Sandler, T. Rades, The influence of various excipients on the conversion kinetics of carbamazepine polymorphs in aqueous suspension, J. Pharm. Pharmacol. 59 (2007) 193–201. doi:10.1211/jpp.59.2.0006.

[123] A.D. Gift, J.A. Hettenbaugh, R.A. Quandahl, M. Mapes, Inhibition of the Solid State Transformation of Carbamazepine in Aqueous Solution: Impact of Polymeric Properties, Pharm. Dev. Technol. 23 (2018) 933–940. doi:10.1080/10837450.2017.1395038.

[124] F.U. Krahn, J.B. Mielck, Effect of type and extent of crystalline order on chemical and physical stability of carbamazepine, Int. J. Pharm. 53 (1989) 25–34. doi:10.1016/0378-5173(89)90357-8.

[125] M.M.J. Lowes, M.R. Caira, A.P. Lötter, J.G. van der Watt, Physicochemical Properties and X-ray Structural Studies of the Trigonal Polymorph of Carbamazepine, J. Pharm. Sci. 76 (1987) 744–752. doi:10.1002/jps.2600760914.

[126] M. Lang, J.W. Kampf, A.J. Matzger, Form IV of Carbamazepine, J. Pharm. Sci. 91 (2002) 1186–1190. doi:10.1002/jps.10093.

[127] E. Laine, V. Tuominen, P. Ilvessalo, P. Kahela, Formation of dihydrate from carbamazepine anhydrate in aqueous conditions, Int. J. Pharm. 20 (1984) 307–314. doi:10.1016/0378-5173(84)90177-7.

[128] P. Kahela, R. Aaltonen, E. Lewing, M. Anttila, E. Kristoffersson, Pharmacokinetics and dissolution of two crystalline forms of carbamazepine, Int. J. Pharm. 14 (1983) 103–112. doi:10.1016/0378-5173(83)90118-7.

[129] F. Tian, N. Sandler, J. Aaltonen, C. Lang, D.J. Saville, K.C. Gordon, C.J. Strachan, J. Rantanen, T. Rades, Influence of Polymorphic Form , Morphology , and Excipient Interactions on the Dissolution of Carbamazepine Compacts, J. Pharm. Sci. 96 (2007) 584–594. doi:10.1002/jps.

[130] A.L. Grzesiak, M. Lang, K. Kim, A.J. Matzger, Comparison of the Four Anhydrous Polymorphs of Carbamazepine and the Crystal Structure of Form I, J. Pharm. Sci. 92 (2003) 2260–2271. doi:10.1002/jps.10455.

[131] C. Rustichelli, G. Gamberini, V. Ferioli, M.C. Gamberini, R. Ficarra, S. Tommasini, Solid-state study of polymorphic drugs: Carbamazepine, J. Pharm.

Biomed. Anal. 23 (2000) 41–54. doi:10.1016/S0731-7085(00)00262-4.

[132] A.G. K. Kolter, M.Karl, Hot-Melt Extrusion with BASF Pharma Polymers, 2nd Editio, BASF Pharma ingredients & Service, Ludwigshafen, Germany, 2012.

[133] Carl Roth GmbH +Co KG, Safety data sheet, (2015).

[134] W.W.L. Young, R. Suryanarayanan, Kinetics of transition of anhydrous carbamazepine to carbamazepine dihydrate in aqueous suspensions, J. Pharm. Sci. 80 (1991) 496–500. doi:10.1002/jps.2600800519.

[135] K. Kachrimanis, U.J. Griesser, Dehydration Kinetics and Crystal Water Dynamics of Carbamzepine Dihydrate, Pharm. Res. 29 (2012) 1143–1157. doi:10.1007/s11095-012-0698-4.

[136] D. Murphy, F. Rodríguez-Cintrón, B. Langevin, R.C. Kelly, N. Rodríguez-Hornedo, Solution-mediated phase transformation of anhydrous to dihydrate carbamazepine and the effect of lattice disorder, Int. J. Pharm. 246 (2002) 121–134. doi:10.1016/S0378-5173(02)00358-7.

[137] L.X. Yu, A.S. Carlin, G.L. Amidon, A.S. Hussain, Feasibility studies of utilizing disk intrinsic dissolution rate to classify drugs, Int. J. Pharm. 270 (2004) 221–227. doi:10.1016/j.ijpharm.2003.10.016.

[138] P. Zakeri-Milani, M. Barzegar-Jalali, M. Azimi, H. Valizadeh, Biopharmaceutical classification of drugs using intrinsic dissolution rate (IDR) and rat intestinal permeability, Eur. J. Pharm. Biopharm. 73 (2009) 102–106. doi:10.1016/j.ejpb.2009.04.015.

[139] F. Flicker, V.A. Eberle, G. Betz, Variability in commercial carbamazepine samples – Impact on drug release, Int. J. Pharm. 410 (2011) 99–106. doi:10.1016/j.ijpharm.2011.03.032.

[140] S. Šehić, G. Betz, Š. Hadžidedić, S.K. El-Arini, H. Leuenberger, Investigation of intrinsic dissolution behavior of different carbamazepine samples ˇ, Int. J. Pharm. 386 (2010) 77–90. doi:10.1016/j.ijpharm.2009.10.051.

[141] N. Zerrouk, S. Toscani, J.-M. Gines-Dorado, C. Chemtob, R. Ceólin, J. Dugué, Interactions between carbamazepine and polyethylene glycol (PEG) 6000 : characterisations of the physical , solid dispersed and eutectic mixtures, Eur. J. Pharm. Sci. 12 (2001) 395–404. doi:10.1016/S0928-0987(00)00168-8.

[142] J. Djuris, I. Nikolakakis, S. Ibric, Z. Djuric, K. Kachrimanis, Preparation of carbamazepine – Soluplus solid dispersions by hot-melt extrusion , and

prediction of drug – polymer miscibility by thermodynamic model fitting, Eur. J. Pharm. Sci. 84 (2013) 228–237. doi:10.1016/j.ejpb.2012.12.018.

[143] J. Djuris, N. Ioannis, S. Ibric, Z. Djuric, K. Kachrimanis, Effect of composition in the development of carbamazepine hot-melt extruded solid dispersions, (2013) 232–243. doi:10.1111/jphp.12199.

[144] W. Ali, A.A. Badawi, M.A. Mahdy, H.M. El-Nahas, FORMULATION AND EVALUATION OF CARBAMAZEPINE 200MG IMMEDIATE RELEASE TABLETS USING POLYETHYLENE GLYCOL 6000, Int. J. Pharm. Pharm. Sci. 5 (2013) 114–119.

[145] D.P. Medarevic, K. Kachrimanis, M. Mitric, J. Djuris, Z. Djuric, S. Ibric, Dissolution rate enhancement and physicochemical characterization of carbamazepine-poloxamer solid dispersions, Pharm. Dev. Technol. 21 (2016) 268–276. doi:10.3109/10837450.2014.996899.

[146] D.D. Sun, P.I. Lee, Evolution of Supersaturation of Amorphous Pharmaceuticals: The Effect of Rate of Supersaturation Generation, Mol. Pharm. 10 (2013) 4330–4346. doi:10.1021/mp400439q.

[147] F. Tian, N. Sandler, K.C. Gordon, C.M. McGoverin, A. Reay, C.J. Strachan, D.J. Saville, T. Rades, Visualizing the conversion of carbamazepine in aqueous suspension with and without the presence of excipients: A single crystal study using SEM and Raman microscopy, Eur. J. Pharm. Biopharm. 64 (2006) 326–335. doi:10.1016/j.ejpb.2006.05.014.

[148] J.R. Hughey, J.M. Keen, D.A. Miller, K. Kolter, N. Langley, J.W. McGinity, The use of inorganic salts to improve the dissolution characteristics of tablets containing Soluplus®-based solid dispersions, Eur. J. Pharm. Sci. 48 (2013) 758–766. doi:10.1016/j.ejps.2013.01.004.

[149] S. Kukec, R. Dreu, T. Vrbanec, S. Srčič, F. Vrečer, Characterization of agglomerated carvedilol by hot-melt processes in a fluid bed and high shear granulator, Int. J. Pharm. 430 (2012) 74–85. doi:10.1016/j.ijpharm.2012.03.041.

[150] K.E. Steffens, M.B. Brenner, M.U. Hartig, M. Monschke, K.G. Wagner, Melt granulation : A comparison of granules produced via high-shear mixing and twin-screw granulation, Int. J. Pharm. 591 (2020) 119941. doi:10.1016/j.ijpharm.2020.119941.

[151] S. Schiermeier, P.C. Schmidt, Fast dispersible ibuprofen tablets, Eur. J. Pharm.

Sci. 15 (2002) 295–305. doi:10.1016/s0928-0987(02)00011-8.

[152] P.M. Desai, P.X.H. Er, C.V. Liew, P.W.S. Heng, Functionality of Disintegrants and Their Mixtures in Enabling Fast Disintegration of Tablets by a Quality by Design Approach, AAPS PharmSciTech. 15 (2014) 1093–1104. doi:10.1208/s12249-014-0137-4.

[153] E.M. Rudnic, J.L. Kanig, C.T. Rhodes, The Effect of Molecular Structure on the Function of Sodium Starch Glycolate in wet Granulated Systems, Drug Dev. Ind. Pharm. 9 (1983) 303–320. doi:10.3109/03639048309044676.

[154] E.M. Rudnic, J.L. Kanig, C.T. Rhodes, Effect of Molecular Structure Variation on the Disintegrant Action of Sodium Starch Glycolate, J. Pharm. Sci. 74 (1985) 647–650. doi:10.1002/jps.2600740613.

[155] U. Shah, L. Augsburger, Evaluation of the Functional Equivalence of Crospovidone NF from Different Sources . II . Standard Performance Test, Pharm. Dev. Technol. 6 (2001) 419–430. doi:10.1081/PDT-100002250.

[156] E. Shotton, G.S. Leonard, The effect of intra- and extragranular maize starch on the disintegration of compressed tablets, J. Pharm. Pharm. Sci. 24 (1972) 798–803. doi:10.1111/j.2042-7158.1972.tb08886.x.

[157] E. Shotton, G.S. Leonard, Effect of Intragranular and Extragranular Disintegrating Agents on Particle Size of Disintegrated Tablets, J. Pharm. Sci. 65 (1976) 1170–1174. doi:10.1002/jps.2600650810.

[158] M. Gordon, B. Chatterjee, Z.T. Chowhan, Effect of the Mode of Croscarmellose Sodium Incorporation on Tablet Dissolution and Friability, J. Pharm. Sci. 79 (1990) 43–47. doi:10.1002/jps.2600790111.

[159] M. Gordon, V.S. Rudraraju, K. Dani, Z.T. Chowhan, Effect of the Mode of Super Disintegrant Incorporation on Dissolution in Wet Granulated Tablets, J. Pharm. Sci. 82 (1993) 220–226. doi:10.1002/jps.2600820222.

[160] L. Kalantzi, C. Reppas, J.B. Dressman, G.L. Amidon, H.E. Junginger, K.K. Midha, V.P. Shah, S.A. Stavchansky, D.M. Barends, Biowaiver Monographs for Immediate Release Solid Oral Dosage Forms: Acetaminophen (Paracetamol), J. Pharm. Sci. 95 (2006) 4–14. doi:10.1002/jps.20477.

[161] European Directorate for the Quality of Medicines and Health Care (EDQM), European Pharmacopoeia 8.0, Straßbourg, 2010.

[162] European Directorate for the Quality of Medicines and Health Care (EDQM),

EUROPEAN PHARMACOPOEIA 8.0, Straßbourg, 2011.

[163] United States Pharmacopeial Convention, C. of Experts, THE UNITED STATES PHARMACOPEIA 41, 2018.

[164] P.L. Gould, S.B. Tan, The Effect of Recompression on Disintegrant Efficiency in Tablets Prepared by wet Granulation, Drug Dev. Ind. Pharm. 11 (1985) 441–460. doi:10.3109/03639048509056880.

[165] M.S. Gordon, V.S. Rudraraju, J.K. Rhie, Z.T. Chowhan, The effect of aging on the dissolution of wet granulated tablets containing super disintegrants, Int. J. Pharm. 97 (1993) 119–131. doi:10.1016/0378-5173(93)90132-Y.

[166] C. Caramella, F. Ferrari, M.C. Bonferoni, M. Ronchi, Disintegrants in Solid Dosage Forms, Drug Dev. Ind. Pharm. 16 (1990) 2561–2577. doi:10.3109/03639049009058547.

[167] N. Zhao, L.L. Augsburger, Functionality Comparison of 3 Classes of Superdisintegrants in Promoting Aspirin Tablet Disintegration and Dissolution, AAPS PharmSciTech. 6 (2005) 634–640. doi:10.1208/pt060479.

[168] J. Rojas, S. Guisao, V. Ruge, Functional Assessment of Four Types of Disintegrants and their Effect on the Spironolactone Release Properties, AAPS PharmSciTech. 13 (2012) 1054–1062. doi:10.1208/s12249-012-9835.

[169] D. Gissinger, A. Stamm, A Comparative Evaluation of the Properties of some Tablet Disintegrants, Drug Dev. Ind. Pharm. 6 (1980) 511–536. doi:10.3109/03639048009068720.

[170] N. Zhao, L.L. Augsburger, The Influence of Swelling Capacity of Superdisintegrants in Different pH Media on the Dissolution of Hydrochlorothiazide From Directly Compressed Tablets, AAPS PharmSciTech. 6 (2005) 120–126. doi:10.1208/pt060119.

[171] U. Shah, L. Augsburger, Multiple Sources of Sodium Starch Glycolate , NF : Evaluation of Functional Equivalence and Development of Standard Performance Tests, Pharm. Dev. Technol. 7 (2002) 345–359. doi:10.1081/PDT-120005731.

[172] E.M. Rudnic, C.T. Rhodes, S. Welch, P. Bernardo, Evaluations of the Mechanism of Disintegrant Action, Drug Dev. Ind. Pharm. 8 (1982) 87–109. doi:10.3109/03639048209052562.

[173] U. Shah, L. Augsburger, Evaluation of the Functional Equivalence of

Crospovidone NF from Different Sources . I . Physical Characterization, Pharm. Dev. Technol. 6 (2001) 39–51. doi:10.1081/PDT-100000012.

[174] N. Zhao, L.L. Augsburger, The Influence of Product Brand-to-Brand Variability on Superdisintegrant Performance A Case Study with Croscarmellose Sodium, Pharm. Dev. Technol. 11 (2006) 179–185. doi:10.1080/10837450600561281.

[175] P.M. Desai, C.V. Liew, P.W.S. Heng, Review of Disintegrants and the Disintegration Phenomena, J. Pharm. Sci. 105 (2016) 2545–2555. doi:10.1016/j.xphs.2015.12.019.

[176] J. Quodbach, P. Kleinebudde, A critical review on tablet disintegration, Pharm. Dev. Technol. 21 (2016) 763–774. doi:10.3109/10837450.2015.1045618.

[177] C.F. Lerk, G.K. Bolhuis, A.H. de Boer, Effect of Microcrystalline Cellulose on Liquid Penetration in and Disintegration of Directly Compressed Tablets, J. Pharm. Sci. 68 (1979) 205–211. doi:10.1002/jps.2600680222.

[178] P.C. Schmidt, S. Lang, Pharmazeutische Hilfsstoffe : Eigenschaften, Anwendung und Handelsprodukte, Govi-Verlag, Eschborn, 2013. http://search.ebscohost.com/login.aspx?direct=true&db=nlebk&AN=1333977&site=ehost-live&scope=site.

[179] P.M. Desai, C.V. Liew, P.W.S. Heng, Understanding Disintegrant Action by Visualization, J. Pharm. Sci. 101 (2012) 2155–2164. doi:10.1002/jps.

[180] J. Quodbach, A. Moussavi, R. Tammer, J. Frahm, P. Kleinebudde, Tablet Disintegration Studied by High-Resolution Real-Time Magnetic Resonance Imaging, J. Pharm. Sci. 103 (2014) 249–255. doi:10.1002/jps.23789.

[181] A. Berardi, L. Bisharat, A. Blaibleh, L. Pavoni, M. Cespi, A Simple and Inexpensive Image Analysis Technique to Study the Effect of Disintegrants Concentration and Diluents Type on Disintegration, J. Pharm. Sci. 107 (2018) 2643–2652. doi:10.1016/j.xphs.2018.06.008.

[182] K.A. Khan, D.J. Rooke, Effect of disintegrant type upon the relationship between compressional pressure and dissolution efficiency, J. Pharm. Pharm. Sci. 28 (1976) 633–636. doi:10.1111/j.2042-7158.1976.tb02816.x.

[183] Y.X. Bi, H. Sunada, Y. Yonezawa, K. Danjo, Evaluation of Rapidly Disintegrating Tablets Prepared by a Direct Compression Method, Drug Dev. Ind. Pharm. 25 (1999) 571–581. doi:10.1081/DDC-100102211.

[184] J. Ringard, A.M. Guyot-Hermann, Calculation of Disintegrant Critical

Concentration in Order to Optimize Tablets Disintegration, Drug Dev. Ind. Pharm. 14 (1988) 2321–2339. doi:10.3109/03639048809152018.

[185] C. Ferrero, N. Munoz, M. V Velasco, A. Munoz-Ruiz, R. Jiménez-Castellanos, Disintegrating efficiency of croscarmellose sodium in a direct compression formulation, Int. J. Pharm. 147 (1997) 11–21. doi:10.1016/S0378-5173(96)04784-9.

[186] I. Khateeb, A. Menon, A. Sakr, Effect of Mode of Incorporation of Disintegrants on the Characteristics of Fluid-bed Wet-granulated Tablets, J. Pharm. Pharmacol. 45 (1993) 687–691. doi:10.1111/j.2042-7158.1993.tb07089.x.

[187] H.V. van Kamp, G.K. Bolhuis, C.F. Lerk, Improvement by super disintegrants of the properties of tablets containing lactose , prepared by wet granulation, Pharm. Weekbl. Sci. Ed. 5 (1983) 65–71. doi:10.1007/bf01961475.

[188] J.R. Johnson, L.-H. Wang, M.S. Gordon, Z.T. Chowhan, Effect of Formulation Solubility and Hygroscopicity on Disintegrant Efficiency in Tablets Prepared by Wet Granulation , in Terms of Dissolution, J. Pharm. Sci. 80 (1991) 469–471. doi:10.1002/jps.2600800514.

[189] M.S. Gordon, Z.T. Chowhan, Effect of Tablet Solubility and Hygroscopicity on Disintegrant Efficiency in Direct Compression Tablets in Terms of Dissolution, J. Pharm. Sci. 76 (1987) 907–909. doi:10.1002/jps.2600761213.

[190] J.H. Proost, G.K. Bolhuis, C.F. Lerk, The effect of the swelling capacity of disintegrants on the in vitro and in vivo availability of diazepam tablets , containing magnesium stearate as a lubricant, Int. J. Pharm. 13 (1983) 287–296. doi:10.1016/0378-5173(83)90077-7.

[191] G.K. Bolhuis, A.J. Smallenbroek, C.F. Lerk, Interaction of Tablet Disintegrants and Magnesium Stearate during Mixing I : Effect on Tablet Disintegration, J. Pharm. Sci. 70 (1981) 1328–1330. doi:10.1002/jps.2600701210.

[192] N. Zhao, L.L. Augsburger, The Influence of Granulation on Super Disintegrant Performance, Pharm. Dev. Technol. 11 (2006) 47–53. doi:10.1080/10837450500463828.

[193] K.E. Steffens, K.G. Wagner, Compression behaviour of granules produced via twin-screw melt granulation : Effect of initial particle size on granulation efficiency, Powder Technol. 374 (2020) 430–442. doi:10.1016/j.powtec.2020.07.037.

[194] L.L. Augsburger, S.W. Hoag, PHARMACEUTICAL DOSAGE FORMS : TABLETS; Rational Design and Formulation, Informa Healthcare USA, Inc, 2008.